Exploring Proton Structure using Lattice QCD

by

Dru Bryant Renner

Submitted to the Department of Physics
in partial fulfillment of the requirements for the degree of

Doctor of Philosophy

at the

MASSACHUSETTS INSTITUTE OF TECHNOLOGY

June 2004

Author .....
Department of Physics
April 30, 2004

Certified by .....
John W. Negele
William A. Coolidge Professor of Physics
Thesis Supervisor

Accepted by .....
Thomas J. Greytak
Associate Department Head for Education

Exploring Proton Structure using Lattice QCD

by

Dru Bryant Renner

Submitted to the Department of Physics
on April 30, 2004, in partial fulfillment of the
requirements for the degree of
Doctor of Philosophy

Abstract

We calculate moments of the generalized parton distributions of the nucleon using lattice QCD. The generalized parton distributions determine the angular momentum decomposition of the nucleon and the transverse distributions of partons within the nucleon. Additionally, the generalized parton distributions reduce to the elastic form factors and ordinary parton distributions in particular kinematic limits. Thus by calculating moments of the generalized parton distributions in lattice QCD we can explore many facets of the structure of the nucleon. In this effort, we have developed the *building block* method to determine all the lattice correlation functions which contribute to the off forward matrix elements of the twist two operators. These matrix elements determine the generalized form factors of the nucleon which in turn give the moments of the generalized parton distributions. Thus we use our building block method to calculate all the matrix elements of the lowest twist two operators. Furthermore, we use our method to construct an overdetermined set of matrix elements allowing a more accurate calculation of the generalized form factors.

Thesis Supervisor: John W. Negele
Title: William A. Coolidge Professor of Physics

Acknowledgments

First, I thank my family. My mother, my father, my brother, and my two sisters have never been anywhere other than by my side and in my heart. To my friends in the CTP, I say thanks for the beers and the fun and yes, even for the physics conversations. Certainly, I thank my fiancee Ali for all her love and all her patience, which I have reason to believe is infinite since I've done my best to test it and have never found it faltering. I must thank my collaborators; there are many, but I am most indebted to Wolfram Schroers, Philipp Hägler, and Andrew Pochinsky. Most of all, I must thank John. John Negele has been my teacher, my mentor, and my friend. From him, I have learned physics, but by his example, I have learned to do it. For all this, I say thank you.

Contents

List of Figures

List of Tables

Chapter 1

Introduction

Understanding hadronic structure, particularly that of the nucleon, remains an outstanding challenge for QCD. As the theory of the strong interactions, QCD purports to describe the structure and interactions of hadrons as a consequence of quarks and gluons and the interactions thereof. This picture has had considerable success in describing the shortest distances probed in experiments to date, yet our view of the mechanisms responsible for the construction of the proton, neutron, and other hadrons remains obscured. We are left with the vague notion that some complicated and rich dynamics of quarks and gluons culminates in the hadronic physics observed in the detectors of nuclear and particle experiments daily and more generally in the world around us. It is this hadronic engineering that we want to understand. That is, we want to know how to build a hadron, especially the proton and neutron, from the quarks and gluons of QCD.

As a step in this direction, in this thesis we explore the generalized parton distributions of the nucleon. In particular, we calculate the generalized form factors for the lowest three vector and axial vector twist two operators. The generalized parton distributions and generalized form factors are equivalent languages which encompass a variety of nucleon matrix elements. These include those matrix elements that determine the elastic form factors, ordinary parton distributions, nucleon spin decomposition, and transverse parton distributions.

The excitement surrounding generalized parton distributions was initiated by the

discovery [22] that the generalized parton distributions resolve the nucleon spin into three separately gauge invariant contributions: quark helicity, quark orbital, and total gluon angular momentum contributions. The quark helicity, or simply quark spin, contribution to the nucleon spin is determined by the unpolarized quark distributions and is known experimentally to be quite small. The remaining quark orbital and gluon contributions are determined by the appropriate generalized form factors which have yet to be measured. Thus the ability to measure and calculate the remaining contributions will reveal exactly how the quarks and gluons contrive to give the nucleon precisely spin one half.

The generalized parton distributions were promoted to a new level of understanding with the realization [5] that they encoded a three dimensional picture of a fast moving nucleon, extending the longitudinal momentum distributions, as described by ordinary parton distributions, into the transverse plane. This adds a new dimension, or two, to our ability to study the internal composition of the nucleon, by allowing us to construct the joint probability distribution to find, within the nucleon, a quark or gluon with some longitudinal momentum and some transverse displacement from the center of the nucleon. At this point, we can take the argument full circle and average over all longitudinal momenta to give simply the probability to find a quark at some transverse separation from the center of the nucleon. This line of reasoning breathes new life into the ordinary form factors as they are now rigorously, without relativistic corrections, related to the transverse charge distribution of the nucleon. Furthermore, the generalized form factors determine the transverse momentum distribution within the nucleon and generally the transverse distribution of the higher moments of parton distributions.

Calculation of nucleon matrix elements in lattice QCD is the only known method for determining these physical observables from the complete underlying theory. Perturbation theory fails to describe the low energy physics required to understand nucleon matrix elements. Models proffer valuable insight but at the expense of uncontrolled amputations of various aspects of the full quark and gluon dynamics of QCD. Effective field theories offer the ability to study QCD in corners of the quark mass

parameter space but suffer from the proliferation of low energy constants which still need to be calculated from QCD. Large N_c arguments provide a qualitative picture of QCD, but our world of three colors certainly differs in the details from a world with infinite colors. Given the unique position lattice QCD calculations possess, that is, the ability to establish a quantitative connection between low energy QCD and the natural world and, furthermore, the ability to exceed physical limitations and study insightful observables beyond the reach of experiments, we have undertaken the calculation of generalized parton distributions in lattice QCD.

In this thesis we calculate various generalized form factors of the nucleon. In turn the generalized form factors determine moments of the generalized parton distributions and, hence, we find ourselves limited by a familiar problem. We are able to calculate only a few low moments yet we want the complete distribution. This is a difficult problem for the lattice calculations of moments of ordinary parton distributions, but we have an alternative route to QCD physics. We can study the transverse distributions without the limitations of the moments. Therefore in this thesis we focus on those aspects of generalized parton distributions that do not require unravelling of all the moments. We present results for the nucleon spin decomposition and the transverse distribution of both unpolarized and polarized quarks, charge, and momentum within the nucleon as well as the transverse distributions of the higher moments of the quark distributions. In short, our lattice calculations of generalized form factors demonstrate that the quarks, even the heavy quarks of contemporary lattice calculations, contribute individually to the nucleon spin by way of their oribtal motion. Additionally, our calculations show that the transverse structure of the nucleon varies significantly with the longitudinal momentum fraction at which it is observed.

As a guide to the reader, we now outline the contents of this thesis. The basic results and interpretations of generalized parton distributions and generalized form factors are reviewed in Chapter 2. In particular we highlight their relationships with form factors, parton distributions, quark angular momenta, and transverse quark distributions. Given the prominence that the ideas of transverse structure have in this

thesis, we dedicate Chapter 3 to an expanded derivation of the transverse distributions of the moments of quark distributions. In Chapter 4, we provide the basic results required from lattice QCD, and in Chapters 5 through Chapter 8 we provide the details of our lattice calculation of the generalized form factors of the nucleon. Finally in Chapter 9, we share a few select results illustrating the physics of the nucleon spin decomposition and the transverse quark distributions. Aspects of this thesis work have been presented in several previous publications and conference proceedings [8, 11, 12, 13, 21, 27, 31, 33, 24, 28].

Chapter 2

Generalized Parton Distributions and Generalized Form Factors

Generalized parton distributions significantly expand our understanding of the quark and gluon composition of the nucleon. Using generalized parton distributions, we can construct a three dimensional picture of a fast moving nucleon which extends the ordinary parton distributions into the transverse plane, thus providing a joint distribution in longitudinal momentum and transverse position. Similarly, generalized parton distributions determine the transverse distribution of charge and momentum within the nucleon. Generalized parton distributions also resolve the nucleon spin into contributions from its quark and gluon constituents. In particular generalized parton distributions provide a decomposition of the nucleon spin into contributions from quark helicity, quark orbital motion, and gluons. Furthermore, generalized parton distributions unify these qualitatively new insights with the traditional tools for studying nucleon structure, form factors and parton distributions.

For the purposes of this thesis, generalized parton distributions should be understood in terms of the physical quantities they determine: form factors, parton distributions, the nucleon spin decomposition, and transverse parton distributions. Still, there are other ways to appreciate generalized parton distributions. For example, generalized parton distributions parameterize a variety of scattering experiments. In particular, generalized parton distributions determine the hadronic contributions

to cross sections for a range of experiments from deep inelastic scattering, to a variety of high energy exclusive processes like deeply virtual Compton scattering, to elastic lepton nucleon scattering. Generalized parton distributions can also be understood at the partonic level as a variety of quark and gluon amplitudes in the nucleon. Additionally, generalized parton distributions can be constructed in terms of light cone wave functions where light cone quantization is used to create a Fock space decomposition of quarks and gluons. Such a framework provides the formal ground work for the quark and gluon interpretations of the ordinary and transverse parton distributions.

Generalized form factors are an equivalent description of all that generalized parton distributions encompass. As we show shortly, generalized parton distributions parameterize nucleon matrix elements of the light cone operators commonly probed in high energy scattering experiments. Generalized form factors, on the other hand, parameterize nucleon matrix elements of the corresponding twist two operators. Quite naturally, the operator product expansion provides the formal translation between the languages of generalized parton distributions and generalized form factors. This proves beneficial as some physical observables are more naturally expressed in one language or the other. However, the language of generalized form factors, as we show later, is particularly well suited to describe lattice QCD calculations.[1] Therefore, those physical quantities that are most easily represented by generalized form factors are correspondingly simplest to calculate on the lattice.

In this chapter we provide the basic definitions for the generalized parton distributions and generalized form factors. After which, we demonstrate the equivalence of these two descriptions. Then in turn we illustrate the connection of generalized parton distributions and generalized form factors to parton distributions, form factors, quark angular momenta, and transverse quark distributions, including transverse charge and momentum distributions. There are several reviews of generalized parton

[1]We present generalized parton distributions and generalized form factors on equal footing and only favor generalized form factors when describing lattice calculations. However, the literature seems to favor the use of generalized parton distributions over generalized form factors.

distributions [23, 30, 16, 10],[2] and all formulas not explicitly cited can be found in or derived from those in [23] and [10].

2.1 Definition of Generalized Parton Distributions

Generalized parton distributions parameterize matrix elements of the light cone operators described shortly. There are eight generalized parton distributions for each quark.[3] There are two unpolarized distributions H^q and E^q. There are two helicity distributions $\tilde{H}^q$ and $\tilde{E}^q$. And there are four transversity distributions H_T^q, $\tilde{H}_T^q$, E_T^q and $\tilde{E}_T^q$. There are also another eight analogous gluon distributions H^g, E^g, $\tilde{H}^g$, $\tilde{E}^g$, H_T^g, $\tilde{H}_T^g$, E_T^g, and $\tilde{E}_T^g$.

Generalized parton distributions for each quark are defined as form factors of light cone operators of the form

$$\frac{1}{2}\int\frac{d\lambda}{2\pi}\,e^{ix\overline{P}\cdot\lambda n}\,\overline{q}(-\lambda n/2)\,\Gamma\,\mathcal{P}e^{-ig\int_{\lambda n/2}^{-\lambda n/2}dz\,n\cdot A(z)}\,q(\lambda n/2) \tag{2.1}$$

where $\Gamma = n_\mu\gamma^\mu$, $n_\mu\gamma^\mu\gamma^5$, or $in_\mu\sigma^{\mu\nu}$ and n is a light like vector conventionally chosen to be $(1,0,0,-1)/\sqrt{2}$. We have also written $\overline{P} = (P' + P)/2$ in anticipation of matrix elements of the form $\langle P', S'|O_\Gamma(x)|P, S\rangle$ where $O_\Gamma(x)$ indicates one of the light cone operators above and $|P, S\rangle$ labels the states of the nucleon. We include the path ordered exponential connecting the point $\lambda n/2$ to the point $-\lambda n/2$ to ensure gauge invariance, though the light cone operators are usually written in light cone coordinates and light cone gauge. In light cone coordinates, given by

$$z^\pm = \frac{z^0 \pm z^3}{\sqrt{2}} \quad \text{and} \quad \vec{z}_\perp = (z^1, z^2),$$

[2]The earliest review by Ji [23] provides an excellent starting point, while the most recent review by Diehl [10] is the most comprehensive.

[3]For simplicity all nucleon observables will be defined for the proton only. The corresponding neutron observables have analogous definitions.

the operators become

$$\frac{1}{2}\int\frac{dz^-}{2\pi}\,e^{ix\overline{P}^+z^-}\,\overline{q}(-z/2)\,\Gamma\,\mathcal{P}\,e^{-ig\int_{z/2}^{-z/2}dz\,A^+(z)}\,q(z/2)\Big|_{z^+=0,\vec{z}_\perp=0}$$

where now $\Gamma = \gamma^+$, $\gamma^+\gamma^5$, or $i\sigma^{+i}$. Additionally fixing to light cone gauge, given by $A^+ = 0$, gives

$$\frac{1}{2}\int\frac{dz^-}{2\pi}\,e^{ix\overline{P}^+z^-}\,\overline{q}(-z/2)\,\Gamma\,q(z/2)\,|_{z^+=0,\vec{z}_\perp=0}\,. \tag{2.2}$$

The generalized parton distributions are the invariant functions in the form factor decomposition of $\langle P', S'|O_\Gamma(x)|P, S\rangle$. The structure of the decomposition depends on Γ, but the Lorentz invariants that can appear as arguments to the generalized parton distributions do not. There are three linearly independent four vectors, $\overline{P}$, $\Delta = P' - P$, and n. There are three constraints, $P^2 = m^2$, $P'^2 = m^2$, and $n^2 = -1$ where m denotes the nucleon mass. Thus there are only three independent kinematic variables, $t = \Delta^2$, $\Delta\cdot n$, and $\overline{P}\cdot n$. Additionally, it can be shown that matrix elements of the form $\langle P', S'|O_\Gamma(x)|P, S\rangle$ depend only on the ratio of $\Delta\cdot n$ and $\overline{P}\cdot n$, thus it is convention to choose the independent kinematic variables to be t and ξ given by

$$\xi = \frac{\Delta\cdot n}{2\overline{P}\cdot n} = \frac{\Delta^+}{2\overline{P}^+}.$$

The variable ξ is half the longitudinal momentum transfer normalized by the average longitudinal momentum. Furthermore, the light cone operators themselves depend on x, therefore each generalized parton distribution is parameterized by x, ξ, and t.

The two unpolarized generalized parton distributions for each quark, $H^q(x,\xi,t)$ and $E^q(x,\xi,t)$, are defined by the matrix elements of the light cone operator in Equation 2.2 with $\Gamma = \gamma^+$,

$$\begin{aligned}\frac{1}{2}\int\frac{dz^-}{2\pi}\,e^{ix\overline{P}^+z^-}\,\langle P', S'|\,\overline{q}(-z/2)\,\gamma^+\,q(z/2)\,|P, S\rangle\,\Big|_{z^+=0,\vec{z}_\perp=0} = \\ \frac{1}{2\overline{P}^+}\,\overline{U}(P', S')\left[H^q(x,\xi,t)\,\gamma^+ + E^q(x,\xi,t)\,\frac{i\sigma^{+\mu}\Delta_\mu}{2m}\right]U(P, S),\end{aligned} \tag{2.3}$$

where $U(P, S)$ is an on-shell nucleon spinor. The above Dirac structures are complete

and independent. Given that the operator is of the form $\overline{q}\gamma^{\mu}q$, it is reasonable that the relevant spin structures are $\overline{U}\gamma^{\mu}U$ and $\overline{U}\sigma^{\mu\nu}\Delta_{\nu}U$ as we would expect from the vector current. As shown in later sections, the generalized parton distributions H^q and E^q determine the vector form factors F_1 and F_2, the unpolarized quark distribution $q(x)$, the quark angular momentum contribution to the nucleon J_q, and the unpolarized transverse quark distribution $q(x,\vec{b}_{\perp})$. Additionally, they give the integrated transverse quark distribution, $q(\vec{b}_{\perp})$, and the transverse charge and momentum distributions.

There are also two polarized generalized parton distributions, or generalized helicity distributions, for each quark flavor, $\tilde{H}^q(x,\xi,t)$ and $\tilde{E}^q(x,\xi,t)$. These generalized parton distributions parameterize the matrix elements of the light cone operator in Equation 2.2 with $\Gamma = \gamma^+\gamma^5$.

$$\frac{1}{2}\int\frac{dz^-}{2\pi}\,e^{ix\overline{P}^+z^-}\,\langle P',S'|\,\overline{q}(-z/2)\,\gamma^+\gamma^5\,q(z/2)\,|P,S\rangle\,\Big|_{z^+=0,\vec{z}_{\perp}=0} = \frac{1}{2\overline{P}^+}\,\overline{U}(P',S')\left[\tilde{H}^q(x,\xi,t)\,\gamma^+\gamma^5 + \tilde{E}^q(x,\xi,t)\,\frac{\gamma^5\Delta^+}{2m}\right]U(P,S) \tag{2.4}$$

The above spin structures are also complete and independent. Again it is reasonable, given that the operator is of the form $\overline{q}\gamma^{\mu}\gamma^5 q$, that the relevant Dirac structures are $\overline{U}\gamma^{\mu}\gamma^5 U$ and $\overline{U}\Delta^{\mu}\gamma^5 U$ as we would have for the axial vector current. We show later that the generalized parton distributions $\tilde{H}^q$ and $\tilde{E}^q$ determine the axial form factors G_A and G_P, the polarized quark distribution $\Delta q(x)$, the quark spin contribution to the nucleon $\Delta\Sigma_q$, and the polarized transverse quark distribution $\Delta q(x,\vec{b}_{\perp})$. Furthermore, they give the momentum independent polarized transverse quark distribution, $\Delta q(\vec{b}_{\perp})$, and the polarized transverse charge and momentum distributions.

Additionally, there are four transverse generalized parton distributions, or generalized transversity distributions, for each quark, $H_T^q(x,\xi,t)$, $\tilde{H}_T^q(x,\xi,t)$, $E_T^q(x,\xi,t)$, and $\tilde{E}_T^q(x,\xi,t)$. They are the form factors for the nucleon matrix elements of the light

cone operator given in Equation 2.2 with $\Gamma = i\sigma^{+i}$.

$$\frac{1}{2}\int\frac{dz^-}{2\pi}\,e^{ix\overline{P}^+z^-}\,\langle P',S'|\,\overline{q}(-z/2)\,i\sigma^{+i}\,q(z/2)\,|P,S\rangle\,\Big|_{z^+=0,\vec{z}_\perp=0} = \tag{2.5}$$

$$\frac{1}{2\overline{P}^+}\,\overline{U}(P',S')\left[H_T^q(x,\xi,t)\,i\sigma^{+i} + \tilde{H}_T^q(x,\xi,t)\,\frac{\overline{P}^+\Delta^i - \Delta^+\overline{P}^i}{m^2}\right.$$

$$\left.+E_T^q(x,\xi,t)\,\frac{\gamma^+\Delta^i - \Delta^+\gamma^i}{2m} + \tilde{E}_T^q(x,\xi,t)\,\frac{\gamma^+\overline{P}^i - \overline{P}^+\gamma^i}{m}\right]U(P,S)$$

Again, the above is a complete and independent decomposition. The generalized parton distribution H_T^q gives the ordinary transversity distribution $\delta q(x)$. Apart from that, the phenomenological significance of the transverse generalized parton distributions is less well understood. Consequently, we have not calculated these distributions in our initial work, but it is a straightforward extension of our methods to do so, and we note the above formula for future use.

There is a corresponding set of eight generalized gluon distributions H^g, E^g, $\tilde{H}^g$, $\tilde{E}^g$, H_T^g, $\tilde{H}_T^g$, E_T^g, $\tilde{E}_T^g$ all functions of x, ξ, and t. The generalized gluon distributions give rise to similar physical observables. We have strong interest in examining these distributions as well, but attempts to calculate even the ordinary gluon distributions within lattice QCD have faced significant difficulties [15] and may likely require novel techniques. Particular observables of interest are the gluon contribution to the nucleon spin J^g. As described later, a lattice calculation of J^g would allow us to test, rather than assume, the continuum sum rule. Furthermore, only the sum of the gluon and total quark contributions to the transverse momentum distribution is independent of the renormalization scale, and hence a gluon calculation would enhance the corresponding quark calculation we describe in this thesis.

$O_q^{\mu_1\cdots\mu_n}$	$n+1$
$\tilde{O}_q^{\mu_1\cdots\mu_n}$	$2[\frac{n}{2}]+2$
$O_{Tq}^{\mu_1\cdots\mu_n}$	$2[\frac{n}{2}]+n+3$

Table 2.1: Number of Generalized Form Factors

2.2 Definition of Generalized Form Factors

For each light cone operator in Equation 2.2 in the previous section, there is a tower of twist two operators.[4] The generalized form factors are defined as form factors of these twist two operators. For each tower of twist two operators there are several sets of generalized form factors resulting in altogether nine sets of generalized form factors for each quark. There are three sets of unpolarized generalized form factors A_{ni}^q, B_{ni}^q, and C_n^q, two sets of polarized generalized form factors $\tilde{A}_{ni}^q$ and $\tilde{B}_{ni}^q$, and four sets of transverse generalized form factors A_{Tni}^q, $\tilde{A}_{Tni}^q$, B_{Tni}^q, and $\tilde{B}_{Tni}^q$.

The operator product expansion relates the light cone operators in Equation 2.2 to the twist two operators given here.

$$\begin{aligned} O_q^{\mu_1\cdots\mu_n} &= \bar{q}\, iD^{(\mu_1}\cdots iD^{\mu_{n-1}}\gamma^{\mu_n)}\, q \\ \tilde{O}_q^{\mu_1\cdots\mu_n} &= \bar{q}\, iD^{(\mu_1}\cdots iD^{\mu_{n-1}}\gamma^{\mu_n)}\gamma^5\, q \\ O_{Tq}^{\mu_1\cdots\mu_n\alpha} &= \bar{q}\, iD^{(\mu_1}\cdots iD^{\mu_{n-1}}\sigma^{\mu_n)\alpha}\, q \end{aligned} \tag{2.6}$$

The sets of operators $O_q^{\mu_1\cdots\mu_n}$, $\tilde{O}_q^{\mu_1\cdots\mu_n}$, and $O_{Tq}^{\mu_1\cdots\mu_n\alpha}$ correspond to the light cone operators in Equation 2.2 with $\Gamma = \gamma^+$, $\gamma^+\gamma^5$, and $i\sigma^{+i}$ respectively. The parenthesis denote symmetrization and subtraction of traces for all enclosed and uncontracted indices.[5] Additionally, the derivatives are symmetrized, $D = (\vec{D} - \overleftarrow{D})/2$. In the following we define δ^n_{even} to be 1 if n is even and 0 if n is odd, and we use the stair function $[x]$ to give the largest integer less than or equal to x.

The form factor decomposition for the vector twist two operators, $O_q^{\mu_1\cdots\mu_n}$, defines the generalized form factors A_{ni}^q, B_{ni}^q, and C_n^q. For each n there are $n+1$ generalized

[4] In Appendix M, we include a brief sketch of the light cone expansion relating the light cone operators in Equation 2.2 to the twist two operators in Equation 2.6.

[5] The restriction to uncontracted indices is relevant for Equation 2.7.

$O_q^{\mu_1 \cdots \mu_n}$	$A_{ni}^q,\ B_{ni}^q$
$\tilde{O}_q^{\mu_1 \cdots \mu_n}$	$\tilde{A}_{ni}^q,\ \tilde{B}_{ni}^q$
$O_{Tq}^{\mu_1 \cdots \mu_n}$	$A_{Tni}^q,\ \tilde{A}_{Tni}^q,\ B_{Tni}^q,\ \tilde{B}_{Tni}^q$

Table 2.2: Names of Generalized Form Factors

form factors. There are $[(n+1)/2]$ generalized form factors of the type A_{ni}^q and $[(n+1)/2]$ generalized form factors of the type B_{ni}^q. In addition, for n even there is one C_n^q generalized form factor, while for n odd there is no additional C_n^q. The A_{ni}^q and B_{ni}^q are defined for all i that are even integers in the range $[0, n)$. The generalized form factors A_{ni}^q, B_{ni}^q, and C_n^q parameterize the nucleon matrix elements of the twist two operators $O_q^{\mu_1 \cdots \mu_n}$ as follows.[6]

$$\begin{aligned}
&\langle P', S' | \, O_q^{\mu_1 \cdots \mu_n} \, | P, S \rangle = \qquad (2.7)\\
&\overline{U}(P', S') \left[\sum_{\substack{i=0 \\ \text{even}}}^{n-1} A_{ni}^q(t) \; \gamma^{(\mu_1} \Delta^{\mu_2} \cdots \Delta^{\mu_{i+1}} \overline{P}^{\mu_{i+2}} \cdots \overline{P}^{\mu_n)} \right.\\
&+ \sum_{\substack{i=0 \\ \text{even}}}^{n-1} B_{ni}^q(t) \; \frac{i\sigma^{(\mu_1 \alpha} \Delta_\alpha}{2m} \Delta^{\mu_2} \cdots \Delta^{\mu_{i+1}} \overline{P}^{\mu_{i+2}} \cdots \overline{P}^{\mu_n)}\\
&\left. + \delta^n_{\text{even}} \; C_n^q(t) \, \frac{1}{m} \Delta^{(\mu_1} \cdots \Delta^{\mu_n)} \right] U(P, S)
\end{aligned}$$

Notice the similarity to the ordinary form factor decomposition of the vector current, $O_1^\mu = \overline{q} \gamma^\mu q$. The spinor structures $\overline{U}(P') \gamma^\mu U(P)$ and $\overline{U}(P') i\sigma^{\mu\nu} \Delta_\nu U(P)$ are present just as for the ordinary vector form factors. The additional structure $\overline{U}(P) \Delta^\mu U(P)$, which is excluded by current conservation for the vector current, is present for n even only. As we show in the following section, the generalized form factors A_{ni}^q, B_{ni}^q, and C_n^q are an equivalent description of the generalized parton distributions H^q and E^q. In particular, the generalized form factors determine the moments of the ordinary

[6]The sums used in the following equations are occasionally written in another form as follows.

$$\sum_{\substack{i=0 \\ \text{even}}}^{n-1} f_i = \sum_{i}^{[\frac{n-1}{2}]} f_{2i} \qquad \sum_{\substack{i=0 \\ \text{odd}}}^{n-1} f_i = \sum_{i}^{[\frac{n}{2}-1]} f_{2i+1}$$

To be clear, the last sum has no contributions for $n = 1$.

quark distribution $q(x)$ and the transverse quark distribution $q(x,\vec{b}_\perp)$. They also give the moments of the integrated transverse quark distribution $q(\vec{b}_\perp)$ and the transverse charge and momentum distributions as well. Additionally, they give the vector form factors F_1 and F_2.

The polarized generalized form factors $\tilde{A}^q_{ni}$ and $\tilde{B}^q_{ni}$ are defined by the form factor decomposition of the axial vector twist two operators, $\tilde{O}^{\mu_1\cdots\mu_n}_q$. There are $2\,[(n+1)/2]$ generalized form factors for each n. There are $[(n+1)/2]$ $\tilde{A}^q_{ni}$ and $[n/2+1]$ $\tilde{B}^q_{ni}$ generalized form factors. As above, the $\tilde{A}^q_{ni}$ and $\tilde{B}^q_{ni}$ are defined for all i that are even integers in the range $[0,n)$. As above, the form factors $\tilde{A}^q_{ni}$ and $\tilde{B}^q_{ni}$ are defined by the following.

$$\begin{aligned}&\langle P',S'|\,\tilde{O}^{\mu_1\cdots\mu_n}_q\,|P,S\rangle = \\ &\quad\overline{U}(P',S')\left[\sum_{\substack{i=0\\ \text{even}}}^{n-1} A^q_{ni}(t)\;\gamma^{(\mu_1}\Delta^{\mu_2}\cdots\Delta^{\mu_{i+1}}\overline{P}^{\mu_{i+2}}\cdots\overline{P}^{\mu_n)}\gamma^5+\right. \\ &\quad\left.\sum_{\substack{i=0\\ \text{even}}}^{n-1} B^q_{ni}(t)\;\frac{\Delta^{(\mu_1}}{2m}\Delta^{\mu_2}\cdots\Delta^{\mu_{i+1}}\overline{P}^{\mu_{i+2}}\cdots\overline{P}^{\mu_n)}\gamma^5\right]U(P)\end{aligned} \tag{2.8}$$

Notice the usual spinor structures $\overline{U}(P')\gamma^\mu\gamma^5U(P)$ and $\overline{U}(P')\Delta^\mu\gamma^5U(P)$ present for the form factor decomposition of the axial vector current, $\tilde{O}^1_q=\overline{q}\gamma^\mu\gamma^5 q$. Unlike the vector case, there are no additional structures beyond those for $n=1$. The $\tilde{A}^q_{ni}$ and $\tilde{B}^q_{ni}$ generalized form factors are an alternative parametrization of the $\tilde{H}^q$ and $\tilde{E}^q$ generalized quark distributions. In particular, $\tilde{A}^q_{ni}$ and $\tilde{B}^q_{ni}$ give the moments of the polarized quark distribution $\Delta q(x)$ and the transverse counterpart $\Delta q(x,\vec{b}_\perp)$. Furthermore they determine the axial form factors G_A and G_P, the moments of the momentum independent polarized transverse quark distribution, $\Delta q(\vec{b}_\perp)$, and the moments of the polarized transverse charge and momentum distributions.

The transverse generalized form factors A^q_{Tni}, $\tilde{A}^q_{Tni}$, B^q_{Tni}, and $\tilde{B}^q_{Tni}$ parameterize the nucleon matrix elements of the tensor twist two operators, $O^{\mu_1\cdots\mu_n\alpha}_{Tq}$. There are $3\,[(n+1)/2]+[n/2]$ generalized form factors for each n. There are $[(n+1)/2]$ A^q_{Tni}, $\tilde{A}^q_{Tni}$, and B^q_{Tni} generalized form factors with i any even integer in the range $[0,n)$.

There are $[n/2]$ $\tilde{B}^q_{Tni}$ generalized form factors where i is any odd integer in the range $[0, n)$. The defining relations for A^q_{Tni}, $\tilde{A}^q_{Tni}$, B^q_{Tni}, and $\tilde{B}^q_{Tni}$ are given in [20]. These generalized form factors have not been calculated in this thesis, but the methods outlined here are easily extended to calculate the transverse generalized form factors.

There are additional towers of twist two operators for the gluons with corresponding generalized form factors. As discussed in Section 2.1, there are several illuminating gluon observables determined by the generalized gluon distributions, in particular the gluon contributions to the nucleon spin or transverse momentum distribution. Hence calculating the gluon generalized form factors would offer additional insight into nucleon structure but pose a real challenge to current lattice techniques and as such are not included in this thesis.

2.3 Equivalence of Generalized Parton Distributions and Generalized Form Factors

The generalized form factors and generalized parton distributions are equivalent descriptions of the same physics. Granted, some observables, transverse parton distributions and of course ordinary parton distributions, are more naturally expressed in the generalized parton distribution language. Other observables, such as elastic form factors and nucleon spin contributions, are more easily stated in the generalized form factor language. Despite the relative convenience of one language over the other, each observable can be equally represented in both frameworks. As shown below, the moments in x, often called Mellin moments, of generalized parton distributions are given by linearly independent combinations of generalized form factors. Therefore the generalized form factors can be determined from the generalized parton distributions. Conversely, the generalized parton distributions can be constructed from the generalized form factors by the inverse Mellin transform. The explicit relationships for the moments of generalized parton distributions in terms of generalized form factors are

given here.

$$
\begin{aligned}
\int_{-1}^{1} dx\, x^{n-1} H^q(x,\xi,t) &= \sum_{\substack{i=0 \\ \text{even}}}^{n-1} A^q_{ni}(t)(-2\xi)^i + \delta^n_{\text{even}} C^q_n(t)(-2\xi)^n \qquad (2.9)\\
\int_{-1}^{1} dx\, x^{n-1} E^q(x,\xi,t) &= \sum_{\substack{i=0 \\ \text{even}}}^{n-1} B^q_{ni}(t)(-2\xi)^i - \delta^n_{\text{even}} C^q_n(t)(-2\xi)^n \\
\int_{-1}^{1} dx\, x^{n-1} \tilde{H}^q(x,\xi,t) &= \sum_{\substack{i=0 \\ \text{even}}}^{n-1} \tilde{A}^q_{ni}(t)(-2\xi)^i \\
\int_{-1}^{1} dx\, x^{n-1} \tilde{E}^q(x,\xi,t) &= \sum_{\substack{i=0 \\ \text{even}}}^{n-1} \tilde{B}^q_{ni}(t)(-2\xi)^i \\
\int_{-1}^{1} dx\, x^{n-1} H^q_T(x,\xi,t) &= \sum_{\substack{i=0 \\ \text{even}}}^{n-1} A^q_{Tni}(t)(-2\xi)^i \\
\int_{-1}^{1} dx\, x^{n-1} \tilde{H}^q_T(x,\xi,t) &= \sum_{\substack{i=0 \\ \text{even}}}^{n-1} \tilde{A}^q_{Tni}(t)(-2\xi)^i \\
\int_{-1}^{1} dx\, x^{n-1} E^q_T(x,\xi,t) &= \sum_{\substack{i=0 \\ \text{even}}}^{n-1} B^q_{Tni}(t)(-2\xi)^i \\
\int_{-1}^{1} dx\, x^{n-1} \tilde{E}^q_T(x,\xi,t) &= \sum_{\substack{i=0 \\ \text{odd}}}^{n-1} \tilde{B}^q_{Tni}(t)(-2\xi)^i
\end{aligned}
$$

Notice that the right hand sides of each of the above equations are polynomials in ξ. Furthermore, all moments, except those for $\tilde{E}^q_T(x,\xi,t)$, contain only even powers of ξ while the moments for $\tilde{E}^q_T(x,\xi,t)$ contain only odd powers of ξ. Therefore all generalized parton distributions are even in ξ except for $\tilde{E}^q_T$ which is odd in ξ. Additionally, notice that the lowest moment, $n = 1$, is independent of ξ for all generalized parton distributions.

All of the results presented in Chapter 9 require $\xi = 0$ only.[7] The above moment relations are particularly simple in this situation and are given here explicitly for later

[7] We do, however, calculate all the generalized form factors for each twist two operator considered.

convenience.

$$\begin{aligned}
\int_{-1}^{1} dx\, x^{n-1} H^q(x,0,t) &= A^q_{n0}(t) \\
\int_{-1}^{1} dx\, x^{n-1} E^q(x,0,t) &= B^q_{n0}(t) \\
\int_{-1}^{1} dx\, x^{n-1} \tilde{H}^q(x,0,t) &= \tilde{A}^q_{n0}(t) \\
\int_{-1}^{1} dx\, x^{n-1} \tilde{E}^q(x,0,t) &= \tilde{B}^q_{n0}(t) \\
\int_{-1}^{1} dx\, x^{n-1} H^q_T(x,0,t) &= A^q_{Tn0}(t) \\
\int_{-1}^{1} dx\, x^{n-1} \tilde{H}^q_T(x,0,t) &= \tilde{A}^q_{Tn0}(t) \\
\int_{-1}^{1} dx\, x^{n-1} E^q_T(x,0,t) &= B^q_{Tn0}(t) \\
\int_{-1}^{1} dx\, x^{n-1} \tilde{E}^q_T(x,0,t) &= 0
\end{aligned} \tag{2.10}$$

Though generalized parton distributions and generalized form factors provide equivalent languages to describe the same physics, there is a significant practical difference: generalized form factors are directly accessible to lattice QCD calculations. Generalized parton distributions are form factors of the non-local light cone operators, whereas generalized form factors are form factors of the local twist two operators. This distinction is significant as lattice QCD calculations are performed in Euclidean space. Local operators in Minkowski space are simply related to local operators in Euclidean space.[8] The non-local light cone operators in Minkowski space require analytic continuation into Euclidean space and hence are extremely difficult to evaluate. This distinction between light cone operators and local operators already exists for the lattice calculations of ordinary parton distributions and is the reason that only moments of parton distributions can be calculated in lattice QCD. This complication persists for the lattice calculations of generalized parton distributions, though there is a distinct advantage in this case. As we discuss in Section 2.7,

[8] Actually, the operators only have to be local in time to allow a simple mapping from Minkowski space to Euclidean space.

the lowest two moments of the generalized parton distributions $H^q(x, \xi \to 0, t)$ and $\tilde{H}^q(x, \xi \to 0, t)$ are given by generalized form factors and hence have a calculable t dependence which is related by a Fourier transform to the transverse quark, charge, and momentum distributions. Furthermore, the transverse distribution of higher moments of H^q and $\tilde{H}^q$ are also calculable in terms of generalized form factors and are hence within the reach of lattice calculations.

2.4 Connection to Form Factors

The electromagnetic form factors of the nucleon, F_1 and F_2, are the archetypical probe of nucleon structure. Unfortunately though, the expectation that the form factors are simply related to the Fourier transforms of charge and current densities is spoiled by relativistic corrections. As we discuss in Section 2.7, the relativistic corrections can be eliminated by considering the charge distribution in the transverse plane for a fast moving nucleon. Despite the inability to simply interpret the form factors in terms of three dimensional densities, the form factors are sensitive to the internal dynamics of the nucleon and provide a challenge to any framework attempting to calculate the non-perturbative dynamics of QCD. An extensive experimental program has examined the electromagnetic form factors for fifty years and new techniques such as recoil polarization measurements have rejuvenated the experimental effort. This requires a commensurate effort to calculate the form factors from lattice QCD. Additionally, the neutral current weak interaction couples to a combination of vector and axial vector currents and provides experimental access to the axial form factors, G_A and G_P as well.

The vector and axial vector form factors are defined by the following equations.

$$\langle P', S' | \, \overline{q} \, \gamma^\mu \, q \, | P, S \rangle = \overline{U}(P', S') \left[F_1^q(t) \, \gamma^\mu + F_2^q(t) \, \frac{i \sigma^{\mu\nu} \Delta_\nu}{2m} \right] U(P, S) \quad (2.11)$$

$$\langle P', S' | \, \overline{q} \, \gamma^\mu \gamma^5 \, q \, | P, S \rangle = \overline{U}(P', S') \left[G_A^q(t) \, \gamma^\mu \gamma^5 + G_P^q(t) \, \frac{\Delta^\mu \gamma^5}{2m} \right] U(P, S)$$

By comparing these equations with the defining Equation 2.7 for A_{ni}^q and B_{ni}^q and

remembering that the lowest vector twist two operator is $O_1^\mu = \overline{q}\gamma^\mu q$, we can relate the F_1 and F_2 form factors to the generalized form factors as follows

$$\begin{aligned} F_1^q(t) &= A_{10}^q(t) = \int_{-1}^{1} dx\, H^q(x,\xi,t) \\ F_2^q(t) &= B_{10}^q(t) = \int_{-1}^{1} dx\, E^q(x,\xi,t) \end{aligned}$$

where we use Equation 2.9 to express the results as moments of generalized parton distributions. Similarly, by comparing Equation 2.11 for G_A and G_P above with Equation 2.8 for $\tilde{A}_{ni}^q$ and $\tilde{B}_{ni}^q$ and noting that $\tilde{O}_q^1 = \overline{q}\gamma^\mu\gamma^5 q$, we have

$$\begin{aligned} G_A^q(t) &= \tilde{A}_{10}^q(t) = \int_{-1}^{1} dx\, \tilde{H}^q(x,\xi,t) \\ G_P^q(t) &= \tilde{B}_{10}^q(t) = \int_{-1}^{1} dx\, \tilde{E}^q(x,\xi,t) \end{aligned}$$

where again we use the moment relations in Equation 2.9. Notice, as discussed in Section 2.3, the ξ dependence drops out for the lowest moments of generalized parton distributions, and hence we can study the ordinary form factors in the limiting case $\xi = 0$. Also note that the vector and axial vector form factors are more simply related to the generalized form factors than the generalized parton distributions.

For the vector form factors, typically one is interested in the flavor combinations that are probed in lepton scattering. These are

$$\begin{aligned} F_i^p(t) &= \frac{2}{3} F_i^u(t) - \frac{1}{3} F_i^d(t) \\ F_i^n(t) &= -\frac{1}{3} F_i^u(t) + \frac{2}{3} F_i^d(t) \end{aligned}$$

where $i = 1$ or 2. The nature of lattice calculations, in particular the problems with disconnected diagrams discussed in Section 8.2, instead favors consideration of the isospin combinations

$$\begin{aligned} F_i^{I=0}(t) &= F_i^u(t) + F_i^d(t) \\ F_i^{I=1}(t) &= F_i^u(t) - F_i^d(t) \end{aligned}$$

where again $i = 1$ or 2. However, for the axial currents, the natural flavor combination is the isovector component, so we only concentrate on the $I = 0$ and 1 parts,

$$\begin{aligned} G_i^{I=0}(t) &= G_i^u(t) + G_i^d(t) \\ G_i^{I=1}(t) &= G_i^u(t) - G_i^d(t), \end{aligned}$$

where $i = A$ or P.

2.5 Connection to Parton Distributions

The quark distributions $q(x)$, $\Delta q(x)$, and $\delta q(x)$ probe the quark content of the nucleon directly. They are probability densities for the longitudinal momentum fraction in the infinite momentum frame. This peculiar feature of defining parton distributions in the infinite momentum frame is an essential part of nucleon structure for the simple reason that only in such a frame can we construct a Fock space of quarks and gluons. As we see in Chapter 3, even the form factors can profitably be discussed in the infinite momentum frame. The parton distributions determine not only the longitudinal momentum distribution but also shed light on the spin structure of the nucleon. The fraction of the nucleon spin carried by the spin of the quarks is $\Delta\Sigma_q/2$ as determined by the lowest moment of $\Delta q(x)$. As we discuss in Sections 2.6 and 2.7, the generalized parton distributions enhance both of these insights by expanding our understanding of the distribution of quarks and gluons within the nucleon into the transverse plane and by complementing the quark spin contribution to the nucleon spin with the additional contributions from quark orbital motion and gluons.

The usual parton distributions are defined by the forward matrix elements of the

light cone operators in Equation 2.2 and are given here

$$
\begin{aligned}
& q(x)\,\frac{1}{2P^+}\,\overline{U}(P,S')\,\gamma^+\,U(P,S) = \qquad (2.12)\\
&\quad = \frac{1}{2}\int\frac{dz^-}{2\pi}\;e^{ixP^+z^-}\;\langle P,S'|\,\overline{q}(-z/2)\,\gamma^+\,q(z/2)\,|P,S\rangle\,\Big|_{z^+=0,\vec{z}_\perp=0}\\
& \Delta q(x)\,\frac{1}{2P^+}\,\overline{U}(P,S')\,\gamma^+\gamma^5\,U(P,S) =\\
&\quad = \frac{1}{2}\int\frac{dz^-}{2\pi}\;e^{ixP^+z^-}\;\langle P,S'|\,\overline{q}(-z/2)\,\gamma^+\gamma^5\,q(z/2)\,|P,S\rangle\,\Big|_{z^+=0,\vec{z}_\perp=0}\\
& \delta q(x)\,\frac{1}{2P^+}\,\overline{U}(P,S')\,i\sigma^{+i}\,U(P,S) =\\
&\quad = \frac{1}{2}\int\frac{dz^-}{2\pi}\;e^{ixP^+z^-}\;\langle P,S'|\,\overline{q}(-z/2)\,i\sigma^{+i}\,q(z/2)\,|P,S\rangle\,\Big|_{z^+=0,\vec{z}_\perp=0}
\end{aligned}
$$

where we include the spin structures for future convenience. The ordinary parton distributions are defined for $-1 \le x \le 1$ with the interpretation that particle distributions are $q(x)$, $\Delta q(x)$, and $\delta q(x)$ for $x \ge 0$ and the anti-particle distributions are $\overline{q}(x) = -q(-x)$, $\Delta\overline{q}(x) = \Delta q(-x)$, and $\delta\overline{q}(x) = \delta q(-x)$ again for $x \ge 0$. By comparing the above equations for $q(x)$, $\Delta q(x)$, and $\delta q(x)$ with the Equations 2.3, 2.4, and 2.5 defining H^q, $\tilde{H}^q$, and H_T^q and furthermore taking the forward limit, $t \to 0$ and $\xi \to 0$, we find the following relations between ordinary and generalized quark distributions.

$$
\begin{aligned}
q(x) &= H^q(x,0,0)\\
\Delta q(x) &= \tilde{H}^q(x,0,0)\\
\delta q(x) &= H_T^q(x,0,0)
\end{aligned}
$$

Equivalently, using the moment relations in Equation 2.10, the moments of the quark distributions are given by the A^q_{n0}, $\tilde{A}^q_{n0}$, and A^q_{Tn0} generalized form factors in the

forward limit.

$$\begin{aligned}
\langle x^{n-1}\rangle_q &= \int_{-1}^{1} dx\, x^{n-1}\, q(x) &&= \int_0^1 dx\, x^{n-1}\,(q(x)+(-1)^n\overline{q}(x)) &&= A^q_{n0}(0)\\
\langle x^{n-1}\rangle_{\Delta q} &= \int_{-1}^{1} dx\, x^{n-1}\Delta q(x) &&= \int_0^1 dx\, x^{n-1}\,(\Delta q(x)-(-1)^n\Delta\overline{q}(x)) &&= \tilde{A}^q_{n0}(0)\\
\langle x^{n-1}\rangle_{\delta q} &= \int_{-1}^{1} dx\, x^{n-1}\,\delta q(x) &&= \int_0^1 dx\, x^{n-1}\,(\delta q(x)-(-1)^n\delta\overline{q}(x)) &&= A^q_{Tn0}(0)
\end{aligned}$$

Particularly interesting moments are the momentum fraction $\langle x\rangle_q = A^q_{20}(0)$ and the spin fraction $\langle 1\rangle_{\Delta q} = \tilde{A}^q_{10}(0)$.

2.6 Connection to Quark Angular Momenta

Lorentz symmetry demands that all spins are either integers or half integers. Therefore we know that the nucleon has spin 1/2 and not, say, 0.5001, but symmetry considerations do not determine how the precise value of 1/2 is constructed from the quark and gluon constituents of the nucleon. Generalized parton distributions provide insight into this very construction. The nucleon spin can be decomposed into three separately gauge invariant pieces [22] as

$$\frac{1}{2} = J_q + J_g = \frac{1}{2}\Delta\Sigma_q + L_q + J_g. \tag{2.13}$$

The spin fraction, $\Delta\Sigma_q/2$, can be determined from the quark helicity distribution, $\Delta q(x)$, as discussed in the previous section, and determines the contribution of the quarks' spin to the nucleon's spin. The experimental determination of this quantity reveals that $\Delta\Sigma$ is quite small. However, the spin fraction would be 1 in the naive quark model, and hence the experimental result indicates a striking departure from such simple ideas. The quantities J_q and J_g can be determined from generalized parton distributions, thus allowing determination of the total contribution of quarks and gluons to be separately determined.[9] Having determined J_q and $\Delta\Sigma_q/2$, the

[9]Note these quantities separately do depend on the renormalization scale, hence what is counted as a quark or a gluon contribution at one scale may contribute differently at another scale. It is only the total contribution that is indeed renormalization scale independent.

difference gives us the contribution to the nucleon spin due to the orbital motion of the quarks L_q. This quantity probes different aspects of the dynamics of the nucleon than the spin fraction because it is sensitive to the motion of the quarks within the nucleon and not just the spin orientation of the quarks.

The quark contribution to the nucleon spin is given by the generalized parton distributions and generalized form factors as

$$J^q = \frac{1}{2}\int_{-1}^{1} dx\, x\, (H^q(x,0,0) + E^q(x,0,0)) = \frac{1}{2}\,(A^q_{20}(0) + B^q_{20}(0)) \tag{2.14}$$

and the spin fraction is given as

$$\frac{1}{2}\Delta\Sigma^q = \int_{-1}^{1} dx\, \tilde{H}^q(x,0,0) = \tilde{A}^q_{10}(0). \tag{2.15}$$

Therefore the contribution from the orbital motion of the quarks is given by

$$L^q = J^q - \frac{1}{2}\Delta\Sigma^q = \frac{1}{2}A^q_{20}(0) + \frac{1}{2}B^q_{20}(0) - \tilde{A}^q_{10}(0). \tag{2.16}$$

The orbital contribution, L_q, can also be expressed in terms of the generalized parton distributions by using Equations 2.14 and 2.15.

2.7 Connection to Transverse Quark Distributions

The ordinary parton distributions provide a view of the nucleon that is restricted to the longitudinal direction. Furthermore, they describe the momentum of partons rather than their position. The transverse parton distributions [5, 6] extend this picture into the transverse coordinates, giving the joint probability distribution in both longitudinal momentum and transverse displacement. Thus transverse parton distributions paint a three dimensional picture of the nucleon in this mixed representation of momentum and position. In this section we state the results and interpretations relevant to the various transverse distributions we study in this thesis. Given the emphasis we place on these results, we provide in Chapter 3 sketches of the derivations

for the results discussed in this section.

The transverse quark distributions $q(x, \vec{b}_\perp)$ and $\Delta q(x, \vec{b}_\perp)$ are related to the generalized quark distributions H^q and $\tilde{H}^q$ by

$$\begin{aligned} q(x, \vec{b}_\perp) &= \int \frac{d^2\Delta_\perp}{(2\pi)^2} e^{-i\vec{b}_\perp \cdot \Delta_\perp} H^q(x, 0, -\vec{\Delta}_\perp^2) \\ \Delta q(x, \vec{b}_\perp) &= \int \frac{d^2\Delta_\perp}{(2\pi)^2} e^{-i\vec{b}_\perp \cdot \Delta_\perp} \tilde{H}^q(x, 0, -\vec{\Delta}_\perp^2). \end{aligned} \tag{2.17}$$

Notice that this result is analogous to the canonical definition of the rest frame charge distribution in terms of the Fourier transform of the electric form factor. However, as discussed in Chapter 3, the results in Equation 2.17 for transverse quark distributions are rigorous statements free from the relativistic corrections which plague the construction of a rest frame charge distribution. Using the results of Equation 2.10, relating the moments of generalized parton distributions to the generalized form factors, gives the corresponding moments of the transverse quark distributions in terms of the generalized form factors as

$$\begin{aligned} \int_{-1}^{1} dx\, x^{n-1} q(x, \vec{b}_\perp) &= \int \frac{d^2\Delta_\perp}{(2\pi)^2} e^{-i\vec{b}_\perp \cdot \Delta_\perp} A^q_{n0}(-\vec{\Delta}_\perp^2) \\ \int_{-1}^{1} dx\, x^{n-1} \Delta q(x, \vec{b}_\perp) &= \int \frac{d^2\Delta_\perp}{(2\pi)^2} e^{-i\vec{b}_\perp \cdot \Delta_\perp} \tilde{A}^q_{n0}(-\vec{\Delta}_\perp^2). \end{aligned} \tag{2.18}$$

The lowest moment, $n = 1$, for the unpolarized and polarized distributions,

$$q(\vec{b}_\perp) = \int_{-1}^{1} dx\, q(x, \vec{b}_\perp) = \int \frac{d^2\Delta_\perp}{(2\pi)^2}\, , e^{-i\vec{b}_\perp \cdot \Delta_\perp} A^q_{n0}(-\vec{\Delta}_\perp^2) \tag{2.19}$$

and

$$\Delta q(\vec{b}_\perp) = \int_{-1}^{1} dx\, \Delta q(x, \vec{b}_\perp) = \int \frac{d^2\Delta_\perp}{(2\pi)^2}\, , e^{-i\vec{b}_\perp \cdot \Delta_\perp} \tilde{A}^q_{n0}(-\vec{\Delta}_\perp^2) \tag{2.20}$$

simply give the probability to find a quark, unpolarized and polarized respectively, at some displacement $\vec{b}_\perp$ from the center of the nucleon. When clarity is required we refer to $q(\vec{b}_\perp)$ and $\Delta q(\vec{b}_\perp)$ as integrated or momentum independent transverse distributions. Notice that these distributions in $\vec{b}_\perp$ can be calculated from a single moment of the

generalized parton distributions. This is significant because lattice calculations are limited to several of the lowest moments of generalized parton distributions, and hence any observable that follows from a single moment can be unambiguously calculated on the lattice without the need to attempt a truncated inverse Mellin transform.

The transverse quark distributions can also be used to construct a transverse charge distribution. These are simple flavor combinations of the transverse quark distributions $q(\vec{b}_\perp)$ above, but that fact that these charge distributions have a rigorous interpretation as distributions in the transverse plane of a fast moving nucleon is reason enough to consider them separately. The transverse charge distribution for the proton is

$$\begin{aligned} \rho^p(\vec{b}_\perp) &= \int_{-1}^{1} dx \left(\frac{2}{3}u(x,\vec{b}_\perp) - \frac{1}{3}d(x,\vec{b}_\perp)\right) \\ &= \int \frac{d^2\Delta_\perp}{(2\pi)^2} e^{-i\vec{b}_\perp\cdot\Delta_\perp} \left(\frac{2}{3}A^u_{10}(-\vec{\Delta}^2_\perp) - \frac{1}{3}A^d_{10}(-\vec{\Delta}^2_\perp)\right) \\ &= \int \frac{d^2\Delta_\perp}{(2\pi)^2} e^{-i\vec{b}_\perp\cdot\Delta_\perp} F_1^p(-\vec{\Delta}^2_\perp) \end{aligned} \tag{2.21}$$

and for the neutron[10] is

$$\begin{aligned} \rho^n(\vec{b}_\perp) &= \int_{-1}^{1} dx \left(-\frac{1}{3}u(x,\vec{b}_\perp) + \frac{2}{3}d(x,\vec{b}_\perp)\right) \\ &= \int \frac{d^2\Delta_\perp}{(2\pi)^2} e^{-i\vec{b}_\perp\cdot\Delta_\perp} \left(-\frac{1}{3}A^u_{10}(-\vec{\Delta}^2_\perp) + \frac{2}{3}A^d_{10}(-\vec{\Delta}^2_\perp)\right) \\ &= \int \frac{d^2\Delta_\perp}{(2\pi)^2} e^{-i\vec{b}_\perp\cdot\Delta_\perp} F_1^n(-\vec{\Delta}^2_\perp). \end{aligned} \tag{2.22}$$

Notice that it is F_1 and not G_E that occurs as the Fourier transform of the transverse charge distribution. Remember, the relationship between the two is

$$G_E(q^2) = F_1(q^2) + \frac{q^2}{4m^2}F_2(q^2).$$

The argument that G_E is the Fourier transform of the charge distribution is a non-

[10]We assume isospin symmetry and relate the proton-proton matrix elements to the neutron-neutron matrix elements by a simple isospin rotation: $u \to d$ and $d \to u$. Remember that we write all generalized parton distributions, and other observables, explicitly for the proton.

relativistic argument. That is, it assumes $q^2 \ll m^2$. In this limit there is no difference between G_E and F_1, and there really is no reason to choose G_E over F_1 to be the Fourier transform of the three dimensional charge distribution. In fact this quantity has relativistic corrections of the size $\langle r^2 \rangle / m^2$ where $\langle r^2 \rangle$ is any reasonable definition of the charge radius, hence the inclusion or omission of the F_2 term is within this ambiguity.[11] It is important to repeat that relativistic corrections muddle the interpretation of F_1 or G_E as Fourier transforms of the three dimensional charge distribution but that the infinite momentum frame results in Equations 2.21 and 2.22 for the two dimensional charge distribution in the transverse plane are free from such relativistic corrections.

The second moment of the transverse quark distribution can also be naturally interpreted as the distribution of momentum in the transverse plane.

$$\varepsilon^q(\vec{b}_\perp) = \int_{-1}^{1} dx\, x\, q(x, \vec{b}_\perp) = \int \frac{d^2\Delta_\perp}{(2\pi)^2}\, e^{-i\vec{b}_\perp \cdot \Delta_\perp} A^q_{20}(-\vec{\Delta}^2_\perp) \tag{2.23}$$

The first equality in the above equation clearly indicates that $\varepsilon^q(\vec{b}_\perp)$ is the average momentum carried by the quark q at a distance $b_\perp$ from the center of the nucleon. As for the integrated transverse quark distribution or the transverse charge distribution, the transverse momentum distribution is given by a single low moment and hence can be directly calculated on the lattice without resorting to an inverse Mellin transform. Unfortunately, the higher moments do not admit such simple interpretations, but nonetheless represent the transverse distribution of that moment. Comparing the transverse extent of each of the low moments of the quark distributions is a crucial tool to understand the transverse structure of the nucleon as revealed by our calculations.

[11] The Breit frame arguments lead to the conclusion that G_E and G_M are Fourier transforms of charge and current densities, but we remind the reader that there is no fixed Breit frame. The Breit frame depends on the resulting momentum transfer in any given scattering event and hence changes from event to event. Thus such arguments only provide a prescription for fixing the $\langle r^2 \rangle / m^2$ ambiguity induced by recoil effects.

Chapter 3

Transverse Quark, Charge, and Momentum Distributions

In this chapter we elaborate and extend the discussion of transverse distributions initiated in [5] and [6]. There it is shown that the generalized parton distributions are related to three dimensional distributions of the quarks and gluons within the nucleon. The three dimensions happen to correspond to a mixed representation of position and momentum providing a joint description of the longitudinal momentum and transverse position of the constituents of the nucleon. The moments of these transverse quark distributions are determined by the Fourier transforms of the generalized form factors. In this chapter we present an alternative derivation of these results starting from the matrix elements of twist two operators in wave packet states of the nucleon. By examining the appropriate infinite momentum and transverse localization limits, these matrix elements reduce to the transverse distributions of the corresponding moments of quark distributions. In particular, we present a detailed derivation of the integrated transverse quark and transverse charge distributions previously given in [5] and then give a similar derivation of the transverse momentum distribution. In addition, we extend these derivations to all the higher moments of the transverse quark distributions, both unpolarized and polarized.

In Section 3.1 we present a general discussion of the wave packet construction and corresponding infinite momentum and transverse localization limits. The details

are provided in Appendix O.1. Then in Section 3.2 we use these results to derive the integrated transverse quark and transverse charge distributions. In Section 3.3 we give a similar argument for the transverse momentum distribution. Finally in Section 3.4, we generalize these results to all the higher moments of the unpolarized and polarized transverse quark distributions.

3.1 Infinite Momentum and Transverse Localization Limits

The transverse distributions are all defined in the limit of a fast moving nucleon, in other words, in the *infinite momentum frame*. To carefully derive these distributions we start with a nucleon with finite momentum and take the infinite momentum limit. The state for such a nucleon is

$$|\psi, s\rangle = \int \frac{d^3p}{\sqrt{(2\pi)^3}} \frac{\psi(\vec{p})}{\sqrt{2E_{\vec{p}}}} |\vec{p}, s\rangle \tag{3.1}$$

where $|\vec{p}, s\rangle$ is a single nucleon state with momentum $\vec{p}$ and spin polarization $s = \pm 1$ in the z direction and where use relativistic normalization for $|\vec{p}, s\rangle$,

$$\langle \vec{p}', s' | \vec{p}, s\rangle = (2\pi)^3 \, 2E_{\vec{p}} \, \delta_{s's} \, \delta^3(\vec{p}' - \vec{p}).$$

As shown in Equation O.1, the normalization condition $\langle \psi, s | \psi, s\rangle = 1$ implies the usual normalization condition for the wave function $\psi(\vec{p})$,

$$\int d^3p \, |\psi(\vec{p})|^2 = 1.$$

We are interested in matrix elements in the above wave packet for the operators corresponding to the momentum independent quark distribution, the charge and momentum distributions, and additionally, the higher moments of quark distributions. These operators are the vector currents $J^\mu_q(\vec{x})$ for the quark distribution, the elec-

tromagnetic current $J^{\mu}(\vec{x})$ for the charge distribution, the energy-momentum tensor $T^{\mu\nu}(\vec{x})$ for the momentum distribution, and the twist two operators $O_q^{\mu_1\cdots\mu_n}(\vec{x})$ and $\tilde{O}_q^{\mu_1\cdots\mu_n}(\vec{x})$ from Equation 2.6 for the corresponding higher moments of the quark distributions. Furthermore, we are interested in the limit in which the wave packet corresponds to a nucleon moving with large momentum in the z, or longitudinal, direction yet localized in the x and y, or transverse, directions. We will examine the effect of such a limit for a generic operator $O(\vec{x})$ in this section and substitute the appropriate operators in the following sections.

To localize the nucleon in the transverse coordinates and yet give it a well defined momentum in the longitudinal direction, we choose a wave packet that factorizes,

$$\psi(\vec{p}) = \psi_{\perp}(\vec{p}_{\perp})\,\psi_z(p_z),$$

where $\vec{p} = (\vec{p}_{\perp}, p_z)$ and each of $\psi_{\perp}$ and ψ_z is normalized as

$$\int d^2p_{\perp}\ |\psi_{\perp}(\vec{p}_{\perp})|^2 = 1 \quad \text{and} \quad \int dp_z\ |\psi_z(p_z)|^2 = 1.$$

To give the nucleon a large momentum in the longitudinal direction, we take $\psi_z(p_z)$ to be sharply peaked about $p_z = K_z$ and take the limit $K_z \to \infty$, and to localize the nucleon in the transverse directions, we take $\psi_{\perp}(\vec{p}_{\perp})$ to be broad in $\vec{p}_{\perp}$. We are ultimately interested in the Fourier transform in the transverse coordinates of distributions of the form $\langle\psi, s|O(\vec{x})|\psi, s\rangle$, so we examine

$$\int d^3x\ e^{i\vec{q}\cdot\vec{x}}\,\langle\psi, s|\,O(\vec{x})\,|\psi, s\rangle$$

where $\vec{q} = (\vec{q}_{\perp}, 0)$ is restricted to transverse momentum transfers.

Properly, the above is the Fourier transform of the distribution of $O(\vec{x})$ in the specific wave packet $|\psi, s>$. To isolate the intrinsic distribution of the nucleon we will take the limits in which K_z becomes large and $\psi_{\perp}$ becomes broad. First we consider simply the limit in which $\psi_z(p_z)$ becomes sharply peaked about $p_z = K_z$.

Inserting the wave packets into the equation above gives

$$\int \frac{d^3p'}{\sqrt{(2\pi)^3}} \frac{\psi^*(\vec{p}')}{\sqrt{2E_{\vec{p}'}}} \int \frac{d^3p}{\sqrt{(2\pi)^3}} \frac{\psi(\vec{p})}{\sqrt{2E_{\vec{p}}}} \int d^3x \; e^{i\vec{q}\cdot\vec{x}} \langle \psi, s| \, O(\vec{x}) \, |\psi, s\rangle.$$

Now we use translational covariance, $O(\vec{x}) = e^{-i\vec{P}\cdot\vec{x}} O(\vec{0}) \, e^{i\vec{P}\cdot\vec{x}}$, where $\vec{P}$ is the momentum operator. The result is

$$\int d^3p \; \frac{\psi^*(\vec{p}') \, \psi(\vec{p})}{2\sqrt{E_{\vec{p}'} E_{\vec{p}}}} \langle \vec{p}', s| \, O(\vec{0}) \, |\vec{p}, s\rangle$$

where now $\vec{p}' = \vec{p} + \vec{q}$ is no longer an independent variable. It is more symmetric and convenient to change variables to the following,

$$\vec{p}' = \vec{k} + \frac{1}{2}\vec{q} \quad \text{and} \quad \vec{p} = \vec{k} - \frac{1}{2}\vec{q}.$$

This gives

$$\int d^3k \; \frac{\psi^*(\vec{k} + \frac{1}{2}\vec{q}) \, \psi(\vec{k} - \frac{1}{2}\vec{q})}{2\sqrt{E'E}} \langle \vec{k} + \frac{1}{2}\vec{q}, s| \, O(\vec{0}) \, |\vec{k} - \frac{1}{2}\vec{q}, s\rangle$$

where $E' = E_{\vec{k}+\frac{1}{2}\vec{q}}$ and $E = E_{\vec{k}-\frac{1}{2}\vec{q}}$. Next we introduce the factorized wave function and split the integral into longitudinal and transverse pieces.

$$\int dk_z \; \psi_z^*(k_z) \, \psi_z(k_z)$$
$$\int d^2k_\perp \; \frac{\psi_\perp^*(\vec{k}_\perp + \frac{1}{2}\vec{q}_\perp) \, \psi_\perp(\vec{k}_\perp - \frac{1}{2}\vec{q}_\perp)}{2\sqrt{E'E}} \langle \vec{k}_\perp + \frac{1}{2}\vec{q}_\perp, k_z, s| \, O(\vec{0}) \, |\vec{k}_\perp - \frac{1}{2}\vec{q}_\perp, k_z, s\rangle$$

In the above we use the assumption that $q_z = 0$. Next we take $\psi_z(p_z)$ to be sharply peaked at K_z, thus we evaluate the integrand at $k_z = K_z$. The result is

$$\int dk_z \; \psi^*(k_z) \, \psi(k_z)$$
$$\int d^2k_\perp \; \frac{\psi_\perp^*(\vec{k}_\perp + \frac{1}{2}\vec{q}_\perp) \, \psi_\perp(\vec{k}_\perp - \frac{1}{2}\vec{q}_\perp)}{2\sqrt{E'E}} \langle \vec{k}_\perp + \frac{1}{2}\vec{q}_\perp, K_z, s| \, O(\vec{0}) \, |\vec{k}_\perp - \frac{1}{2}\vec{q}_\perp, K_z, s\rangle$$

where E' and E are explicitly evaluated at $k_z = K_z$. Now the dk_z integral simply

follows from the normalization of the ψ_z wave function. The result is

$$\int d^2k_\perp \frac{\psi_\perp^*(\vec{k}_\perp + \frac{1}{2}\vec{q}_\perp)\,\psi_\perp(\vec{k}_\perp - \frac{1}{2}\vec{q}_\perp)}{2\sqrt{E'\overline{E}}} \langle \vec{k}_\perp + \frac{1}{2}\vec{q}_\perp, K_z, s|\, O(\vec{0})\, |\vec{k}_\perp - \frac{1}{2}\vec{q}_\perp, K_z, s\rangle.$$

To be clear, the above result follows from simply taking a wave packet with a well defined momentum K_z in the longitudinal direction.

At this point we take the transverse limit in the infinite momentum frame. Note that there is an issue with the order of limits. The infinite momentum limit clearly requires K_z to be large, but additionally the localization limit in the transverse coordinates introduces contributions from the integration region $k_\perp < 1/\sigma_\perp$ where $\sigma_\perp$ is a measure of the transverse localization of the nucleon wave packet which should be small. Thus there are two large scales in the problem, K_z and $1/\sigma_\perp$, which provide a potential difficulty. There are at least two ways to take the transverse limit in the infinite momentum frame and still suppress relativistic corrections. One, we can simply choose to take $K_z \to \infty$ first and then $\sigma_\perp \to 0$ second. Or, we can take a simultaneous limit in which $\sigma \to 1/K_z \to 0$ and $K_z \to \infty$ together. In our explicit manipulations in Appendix O.1, we proceed in such a way that both limits are enforced. For illustration purposes, we proceed in this chapter with the infinite momentum limit before the transverse localization limit. Therefore the resulting integral for our arbitrary operator O is

$$\begin{aligned} &\int d^3x\; e^{i\vec{q}\cdot\vec{x}} \langle \psi, s|\, O(\vec{x})\, |\psi, s\rangle = \\ &= \int d^2k_\perp\; \psi_\perp^*(\vec{k}_\perp + \frac{1}{2}\vec{q}_\perp)\,\psi_\perp(\vec{k}_\perp - \frac{1}{2}\vec{q}_\perp) \\ &\quad \lim_{K_z\to\infty} \frac{1}{2\sqrt{E'\overline{E}}} \langle \vec{k}_\perp + \frac{1}{2}\vec{q}_\perp, K_z, s|\, O(\vec{0})\, |\vec{k}_\perp - \frac{1}{2}\vec{q}_\perp, K_z, s\rangle. \end{aligned} \tag{3.2}$$

The various types of operators we are interested in, the vector and electromagnetic currents, the energy-momentum tensor, and the twist two operators, all have form factor decompositions. For each case, the above matrix element has the form of a sum of terms each a product of a form factor and a spinor matrix element. In each case, the form factor is independent of K_z and the spinor matrix element reduces to

a particularly simple form. These matrix elements are evaluated in Appendix O.1. We now consider each case separately in the following sections.

3.2 Transverse Quark and Charge Distributions

In this section we consider the transverse distributions of quarks and charge in the nucleon. The quark and charge distributions correspond to simply different flavor combinations of the vector currents. The vector currents $J^\mu_q = \overline{q}\gamma^\mu q$ for $\mu = 0$ count the number of quarks, and the electromagnetic current $J^\mu = \sum_q e_q J^\mu_q$ for $\mu = 0$ counts the net charge. The manipulations in this section apply equally well to either case, but for simplicity we explicitly describe the derivation of the transverse charge distribution and note that the corresponding results for the quark distribution are implicitly determined.

For the transverse charge distribution, the electromagnetic current matrix element is given in Equation 2.11 as

$$\langle \vec{k}_\perp + \frac{1}{2}\vec{q}_\perp, K_z, s|J^\mu(0)|\vec{k}_\perp - \frac{1}{2}\vec{q}_\perp, K_z, s\rangle = \overline{U}(P', S')\left[F_1(t)\gamma^\mu + F_2(t)\frac{i\sigma^{\mu\nu}\Delta_\nu}{2m}\right]U(P, S).$$

Using the results of Appendix O.1, in particular Equations O.8 and O.14, the spinor matrix elements in the above equation simplify in the infinite momentum limit as follows,

$$\lim_{K_z\to\infty} \frac{1}{2E}\,\overline{U}(\vec{p}', s)\,\gamma^\mu\,U(\vec{p}, s) = n^\mu_+$$

$$\lim_{K_z\to\infty} \frac{1}{2E}\,\overline{U}(\vec{p}', s)\,\sigma^{\mu\nu}\,U(\vec{p}, s) = 0,$$

where $n_+ = (1, 0, 0, 1)$ is a light like vector which reappears throughout the following sections. Furthermore, we note that in the infinite momentum and transverse localization limits we have

$$\lim_{K_z\to\infty} t = -\vec{q}^{\,2}_\perp$$

where we use $t = (E' - E)^2 - \vec{q}^{\,2}$ and $\vec{q} = (\vec{q}_\perp, 0)$. Therefore the matrix element of

the electromagnetic current satisfies

$$\lim_{K_z\to\infty} \frac{1}{2E} \langle \vec{k}_\perp + \frac{1}{2}\vec{q}_\perp, K_z, s| \, J^\mu(0) \, |\vec{k}_\perp - \frac{1}{2}\vec{q}_\perp, K_z, s\rangle = F_1(-\vec{q}_\perp^{\,2})\, n_+^\mu.$$

In particular note that only F_1 contributes because the tensor matrix element vanishes in the limits we consider. Inserting the above result into the right hand side of the wave packet expression in Equation 3.2, gives

$$\int d^2k_\perp \; \psi_\perp^*(\vec{k}_\perp + \frac{1}{2}\vec{q}_\perp)\, \psi_\perp(\vec{k}_\perp - \frac{1}{2}\vec{q}_\perp)\, F_1(-\vec{q}_\perp^{\,2})\, n_+^\mu = \int d^2k_\perp \; |\psi_\perp(\vec{k}_\perp)|^2 \, F_1(-\vec{q}_\perp^{\,2})\, n_+^\mu$$

where we assume that $\psi_\perp$ is sufficiently broad to ignore the $\vec{q}_\perp$ dependence in the wave functions relative to that in the F_1 form factor. Using the normalization condition for $\psi_\perp$ gives the final result for J^μ,

$$\int d^3x \; e^{i\vec{q}\cdot\vec{x}} \, \langle \psi, s| \, J^\mu(\vec{x}) \, |\psi, s\rangle = F_1(-\vec{q}_\perp^{\,2})\, n_+^\mu.$$

Note that $\mu = 0$ gives rise to the charge operator and $\mu = i$ is the corresponding spatial current. Therefore we find the very sensible result that the current distribution in the infinite momentum frame corresponds to a speed of $n_+^0/n_+^3 = 1$ in the longitudinal direction. In particular, the transverse charge distribution, $\mu = 0$, is given by

$$\int d^3x \; e^{i\vec{q}\cdot\vec{x}} \, \langle \psi, s| \, J^0(\vec{x}) \, |\psi, s\rangle = F_1(-\vec{q}_\perp^{\,2}). \tag{3.3}$$

This demonstrates that F_1, and not G_E, is the Fourier transform of the transverse charge distribution for a fast moving nucleon.

3.3 Transverse Momentum Distribution

Now we consider the transverse momentum distribution. The form factor decomposition of the energy-momentum tensor $T^{\mu\nu}$ is given in Equation 2.7 as

$$\langle \vec{k}_\perp + \frac{1}{2}\vec{q}_\perp, K_z, s| \, T^{\mu\nu}(0) \, |\vec{k}_\perp - \frac{1}{2}\vec{q}_\perp, K_z, s\rangle = \\ \overline{U}(P', S') \left[A_{20}(t) \, \gamma^{(\mu} \overline{P}^{\nu)} + B_{20}(t) \, \frac{i\sigma^{(\mu\alpha}\Delta_\alpha \overline{P}^{\nu)}}{2m} + C_2(t) \, \frac{1}{m} \right] U(P, S)$$

where we implicitly take the symmetric traceless piece of $T^{\mu\nu}$, in other words we replace $T^{\mu\nu}$ with $T^{(\mu\nu)} = \sum_q O_q^{\mu\nu}$. The trace piece will not be needed in this argument, hence we will ignore it from the start. As the name clearly indicates, the total momentum of the nucleon is infinite in the infinite momentum frame, and hence we must study the momentum fraction. Therefore we are interested in matrix elements of $T^{\mu\nu}/K_z$. Using the results for spinor matrix elements from Appendix O.1, especially Equation O.3, we have

$$\lim_{K_z \to \infty} \frac{1}{2E} \, \overline{U}(\vec{p}', s) \, U(\vec{p}, s) = 0$$

in addition to the results for the vector and tensor matrix elements given in Section 3.2 above or in Equations O.8 and O.14. Furthermore, we note that in the infinite momentum and transverse localization limits we have

$$\lim_{K_z \to \infty} \frac{\overline{P}}{K_z} = n_+ \quad \text{and} \quad \lim_{K_z \to \infty} \frac{\Delta}{K_z} = 0$$

where we use $\overline{P} = ((E' + E)/2, \vec{k}_\perp, K_z)$ and $\Delta = (E' - E, \vec{q}_\perp, 0)$. Using these results, the limit of the matrix element of $T^{\mu\nu}/K_z$ is

$$\lim_{K_z \to \infty} \frac{1}{2E} \frac{1}{K_z} \langle \vec{k}_\perp + \frac{1}{2}\vec{q}_\perp, K_z, s| \, T^{\mu\nu}(0) \, |\vec{k}_\perp - \frac{1}{2}\vec{q}_\perp, K_z, s\rangle = A_{20}(-\vec{q}_\perp^{\,2}) \, n_+^\mu n_+^\nu.$$

We note that including the factor of $1/K_z$ is essential, otherwise the large factor of $\overline{P}$ in the B_{20} term overwhelms the small tensor matrix element leading to the erroneous inclusion of B_{20} in the result above. Just as for the case of the electromagnetic current,

we insert the above matrix element into the right hand side of the wave packet matrix element in Equation 3.2 and find

$$\int d^2k_\perp \, \psi_\perp^*(\vec{k}_\perp + \frac{1}{2}\vec{q}_\perp) \, \psi_\perp(\vec{k}_\perp - \frac{1}{2}\vec{q}_\perp) \, A_{20}(-\vec{q}_\perp^2) \, n_+^\mu n_+^\nu = \int d^2k_\perp \, |\psi_\perp(\vec{k}_\perp)|^2 \, A_{20}(-\vec{q}_\perp^2) \, n_+^\mu n_+^\nu$$

where we assume the localization limit, that is $\psi_\perp(\vec{k} \pm \vec{q}_\perp/2) = \psi_\perp(\vec{k})$. The resulting integral is simply the normalization condition for $\psi_\perp$, therefore the final result for $T^{\mu\nu}$ is

$$\int d^3x \; e^{i\vec{q}\cdot\vec{x}} \, \langle \psi, s | \, \frac{1}{K_z} T^{\mu\nu}(\vec{x}) \, | \psi, s \rangle = A_{20}(-\vec{q}_\perp^2) \, n_+^\mu n_+^\nu .$$

We find the tensor structure $n_+^\mu n_+^\nu$ which is symmetric and traceless as it must be. (It is traceless because $n_+ \cdot n_+ = 0$ for $n_+ = (1, 0, 0, 1)$). The longitudinal momentum distribution in particular is determined by $\mu = 0$ and $\nu = 3$ giving

$$\int d^3x \; e^{i\vec{q}\cdot\vec{x}} \, \langle \psi, s | \, \frac{1}{K_z} T^{03}(\vec{x}) \, | \psi, s \rangle = A_{20}(-\vec{q}_\perp^2). \tag{3.4}$$

Therefore we see that the A_{20} generalized form factor is the Fourier transform of the transverse momentum distribution in the infinite momentum frame. We note that the $\mu = 0$ and $\nu = 3$ component does not involve the trace of $T^{\mu\nu}$, so we are indeed justified in dropping the trace contributions as we did by replacing $T^{\mu\nu}$ with $T^{(\mu\nu)}$.

3.4 Transverse Distributions of Higher Moments

At this point we have all the ingredients to examine the remaining twist two operators. Unfortunately, the interpretations of these operators is not as clear as for the quark, charge, or momentum distributions, but, as we show shortly, they do lead to the transverse distribution of higher moments of the transverse quark distributions $q(x, \vec{b}_\perp)$ and $\Delta q(x, \vec{b}_\perp)$. The only new feature is the continued addition of extra factors of $1/K_z$. We do this to keep the matrix elements finite and dimensionless, otherwise the matrix elements would scale as positive powers of K_z as $K_z \to \infty$.

We consider both the unpolarized and polarized twist two operators, $O_q^{\mu_1 \cdots \mu_n}$ and

$\tilde{O}_q^{\mu_1\cdots\mu_n}$, at once. The matrix elements of the vector and axial vector twist two operators are given in Equations 2.7 and 2.8 respectively. The form factor decomposition of the vector operators contains only the vector, tensor, and scalar spinor matrix elements discussed in Sections 3.2 and 3.3 above or in Equations O.8, O.14, and O.3. On the other hand, the form factors of the axial vector operators contain only the axial vector and pseudo scalar spinor matrix elements given in Appendix O.1 in Equations O.11 and O.5 and written here.

$$\lim_{K_z\to\infty} \frac{1}{2E}\,\overline{U}(\vec{p}',s)\,\gamma^5\,U(\vec{p},s) = 0.$$

$$\lim_{K_z\to\infty} \frac{1}{2E}\,\overline{U}(\vec{p}',s)\,\gamma^\mu\gamma^5\,U(\vec{p},s) = n_+^\mu$$

For each higher moment n for the operators $O_q^{\mu_1\cdots\mu_n}$ and $\tilde{O}_q^{\mu_1\cdots\mu_n}$, there is at most one extra power of $\overline{P}$ in the form factor decompositions in Equations 2.7 and 2.8 which we cancel with an extra factor of K_z for each moment. Including the required additional powers of K_z, the results for the infinite momentum limit and transverse localization limit for both vector and axial vector twist two operators are

$$\lim_{K_z\to\infty} \frac{1}{2E}\,\frac{1}{K_z^{n-1}}\,\langle \vec{k}_\perp + \frac{1}{2}\vec{q}_\perp, K_z, s|\, O_q^{\mu_1\cdots\mu_n}(\vec{x})\, |\vec{k}_\perp - \frac{1}{2}\vec{q}_\perp, K_z, s\rangle = A_{n0}(-\vec{q}_\perp^{\,2})\, n_+^{\mu_1}\cdots n_+^{\mu_n}$$

and

$$\lim_{K_z\to\infty} \frac{1}{2E}\,\frac{1}{K_z^{n-1}}\,\langle \vec{k}_\perp + \frac{1}{2}\vec{q}_\perp, K_z, s|\, \tilde{O}_q^{\mu_1\cdots\mu_n}(\vec{x})\, |\vec{k}_\perp - \frac{1}{2}\vec{q}_\perp, K_z, s\rangle = \tilde{A}_{n0}(-\vec{q}_\perp^{\,2})\, n_+^{\mu_1}\cdots n_+^{\mu_n}.$$

Notice we find the only symmetric traceless combination of n_+ possible, and the corresponding coefficient is a single generalized form factor, A_{n0} or $\tilde{A}_{n0}$. With these results, the final expressions for the Fourier transform of $O_q^{\mu_1\cdots\mu_n}(\vec{x})$ and $\tilde{O}_q^{\mu_1\cdots\mu_n}(\vec{x})$ are

$$\int d^3x\; e^{i\vec{q}\cdot\vec{x}}\,\langle\psi,s|\,\frac{1}{K_z^{n-1}} O_q^{\mu_1\cdots\mu_n}(\vec{x})\,|\psi,s\rangle = A_{n0}(-\vec{q}_\perp^{\,2})\, n_+^{\mu_1}\cdots n_+^{\mu_n}$$

and

$$\int d^3x\; e^{i\vec{q}\cdot\vec{x}}\,\langle\psi,s|\,\frac{1}{K_z^{n-1}} \tilde{O}_q^{\mu_1\cdots\mu_n}(\vec{x})\,|\psi,s\rangle = \tilde{A}_{n0}(-\vec{q}_\perp^{\,2})\, n_+^{\mu_1}\cdots n_+^{\mu_n}.$$

In particular, we recover our previous results for $J^\mu = O^\mu$ and $T^{(\mu\nu)} = O^{\mu\nu}$. The final conclusion is that the generalized form factors A_{n0} and $\tilde{A}_{n0}$ give the Fourier transform of the transverse distribution of the n^{th} moments of the quark distributions $q(x, \vec{b}_\perp)$ and $\Delta q(x, \vec{b}_\perp)$ respectively.

Chapter 4

Lattice QCD Basics

In this chapter we collect the basic lattice field theory results required and establish our conventions. We review how fermion and gauge fields are represented on the lattice. We record the quark and gluon actions used in our calculations and the corresponding functional integrals. We briefly illustrate the use of the transfer matrix to determine hadronic masses and matrix elements. And we sketch the renormalization of lattice calculations. The details of our calculations are discussed in Chapters 5 through 8. All other details are left to any of several lattice field theory text books [7, 26, 32, 34] and the references therein.

4.1 Quark and Gluon Fields

The fundamental degrees of freedom of QCD are quarks and gluons. Thus any lattice QCD framework must specify precisely how the quark and gauge fields are constructed for the lattice. Gauge fields are represented on the lattice as group elements belonging to the group $SU(N_c)$ where $N_c = 3$ is the number of colors. This is distinctly different than the continuum formulation of gauge theories in which gauge fields are represented by the algebra $su(N_c)$ instead. Representing the gauge fields by the group rather than the algebra allows for the construction of lattice Yang Mills actions that have an exact local gauge symmetry for non-zero lattice spacing. Without such a symmetry it is not known how to ensure that the full continuum gauge symmetry is restored in the

continuum limit.

For each edge of the lattice there is a group element, $U_\mu(x)$, where x denotes the points of the lattice and $\mu = 1, \ldots, D$ denotes the directions in a $D = 4$ dimensional Euclidean space. The gauge links transform in the adjoint representation of $\mathrm{SU(N_c)}$, so explicitly we have $U_\mu^{ab}(x)$ where $a, b = 1, \ldots, \mathrm{N_c}$ are color indices. Our convention is to take $U_\mu^\dagger(x)$ to be the link directed *away* from the site x in the positive μ^{th} direction. It is natural to extend this convention to include the negative directions as well by defining the backward link as the inverse of the corresponding forward link.

$$U_{-\mu}^\dagger(x) = \left(U_\mu^\dagger(x-\mu)\right)^{-1} = U_\mu(x-\mu) \tag{4.1}$$

For a lattice with spatial volume V and time extent T, we have $D \cdot V \cdot T$ independent gauge links $U_\mu(x)$. We refer to the gauge field collectively as U_μ.

Quark fields are represented on the lattice as Grassmann variables at each point of the lattice. In QCD quarks belong to the fundamental representation of $\mathrm{SU(N_c)}$, so for each quark flavor q we have $q_\alpha^a(x)$ and $\overline{q}_\alpha^a(x)$ where $a = 1, \ldots, \mathrm{N_c}$ are color indices, $\alpha = 1, \ldots, \mathrm{N_d}$ are spinor indices, and $\mathrm{N_d} = 4$ is the dimension of the Dirac matrices. We are explicitly considering Wilson like fermions which have all $\mathrm{N_d}$ spin components at each site as opposed to Kogut-Susskind like fermions which do not. As required for fermion degrees of freedom, all components of the quark field anti-commute. In other words, there are $2 \cdot \mathrm{N_c} \cdot \mathrm{N_d} \cdot V \cdot T$ Grassmann generators. We refer to all quark flavors collectively as ψ and $\overline{\psi}$.

Gauge transformations are implemented by $\mathrm{SU(N_c)}$ matrices in the adjoint representation at each lattice point x. Explicitly we have $g^{ab}(x)$ where $a, b = 1, \ldots, \mathrm{N_c}$ are color indices. The gauge transformations act on the quark and gauge fields as follows.

$$\begin{aligned}
q_\alpha(x) &\rightarrow {}^g q_\alpha(x) &&= g(x)\, q_\alpha(x) \\
\overline{q}_\alpha(x) &\rightarrow {}^g \overline{q}_\alpha(x) &&= \overline{q}_\alpha(x)\, g^\dagger(x) \\
U_\mu^\dagger(x) &\rightarrow {}^g U_\mu^\dagger(x) &&= g(x+\mu)\, U_\mu^\dagger(x)\, g^\dagger(x) \\
U_\mu(x) &\rightarrow {}^g U_\mu(x) &&= g(x)\, U_\mu(x)\, g^\dagger(x+\mu)
\end{aligned} \tag{4.2}$$

Though the second equation follows from the first and the fourth from the third, it is useful to record them separately. Also note that the definition of the backward link fields in Equation 4.1 is consistent with the above gauge transformations and consequently the transformations in Equation 4.2 are valid for $\mu = 1, \ldots, D$ as well as $-1, \ldots, -D$.

The gauge transformations in Equation 4.2 have a geometric interpretation in terms of parallel propagation. The concept of parallel propagation is necessary to construct the lattice actions in Section 4.2 as well as the covariant derivatives required to calculate twist two operators. It also illustrates the conventions above. To compare a quark field at the point x to a quark field at the point $x + \mu$ we must parallel propagate $q(x)$ along the μ^{th} link. The field resulting from such a parallel propagation one lattice unit in the μ^{th} direction is

$$U_\mu^\dagger(x - \mu)\, q(x - \mu) \tag{4.3}$$

where again the definition of gauge fields for the backward links in Equation 4.1 is such that the above equation holds for negative μ as well as positive. Applying the gauge transformations in Equation 4.2 we see that the combination above transforms identically as the quark fields at x under a local gauge transformation.

$$\begin{aligned} & U_\mu^\dagger(x - \mu)\, q(x - \mu) \rightarrow \\ & \quad \rightarrow \quad g(x)\, U_\mu^\dagger(x - \mu)\, g^\dagger(x - \mu)\, g(x - \mu)\, q(x - \mu) \\ & \quad = \quad g(x)\, U_\mu^\dagger(x - \mu)\, q(x - \mu) \end{aligned}$$

Therefore to construct a gauge invariant lattice action, as we do in Section 4.2, or a gauge invariant lattice operator we use combinations of gauge fields and quark fields similar to the combination in Equation 4.3.

4.2 Lattice Actions

Using the quark and gauge fields introduced in Section 4.1, we construct the lattice QCD actions used in this thesis. The gauge action we use is the original lattice action as introduced by Wilson [37, 36]. The basic component of the Wilson gauge action is the plaquette defined as

$$P_{\mu\nu}(x) = \mathrm{tr}\left(U^{\dagger}_{-\nu}(x+\nu)U^{\dagger}_{-\mu}(x+\mu+\nu)U^{\dagger}_{\nu}(x+\mu)U^{\dagger}_{\mu}(x)\right).$$

This is simply the trace of the Wilson line around the smallest closed loop on a lattice, a square in the μ-ν plane with sides one lattice spacing in length. The trace in the above equation ensures that the plaquette is gauge invariant, as can be shown using the gauge transformation in Equation 4.2. In terms of the plaquette, the Wilson gauge action is

$$S_G[U] = \beta \sum_x \sum_{1\le\mu<\nu\le D} \left(1 - \frac{1}{\mathrm{N_c}} \mathrm{Re}\, P_{\mu\nu}\right) \tag{4.4}$$

where

$$\beta = \frac{2\mathrm{N_c}}{g^2}$$

and g is the *bare* gauge coupling on the lattice.

The continuum gauge fields $A_\mu(x)$ can be related to the lattice fields $U_\mu(x)$ by

$$U_\mu(x) = e^{iagA_\mu(x+\mu/2)} \tag{4.5}$$

where a is the lattice spacing. As described in Section 4.6, the lattice spacing a and the bare lattice coupling g are not independent quantities. For pure gauge theory a single renormalization condition must be fixed, after which g becomes a function of a chosen such that the renormalization condition holds for all a. Using the relationship between $U_\mu(x)$ and $A_\mu(x)$ given in Equation 4.5, it can be shown that $S_G^{\mathrm{lat}} = S_G^{\mathrm{con}} + \mathrm{O}(a^2)$ in the classical continuum limit, where the superscript "lat" denotes the lattice action in Equation 4.4 and "con" denotes the continuum QCD gauge action. Additionally, the classical continuum limit is defined by taking $a \to 0$ assuming $A_\mu(x)$ is a smooth

field.

It is interesting to note that even though the momentum modes of the $A_\mu(x)$ vector fields are restricted to a single Brillouin zone, the theory retains a local gauge invariance. This is surprising because a gauge theory with a strict cutoff breaks gauge invariance. However the lattice action above is not a strict cutoff in the vector fields $A_\mu(x)$ but only in the link fields $U_\mu(x)$. Hence the Wilson action contains interactions with arbitrarily high powers of the continuum gauge fields $A_\mu(x)$ with coefficients arranged in just such a way to maintain a residual local gauge invariance.

The fermion action for a single quark flavor q is

$$\begin{aligned} & S_F[\,q,\bar{q}\,] = \\ & = \; a^4 \sum_x \left(m_q\, \bar{q}(x)\, q(x) + \sum_{\mu=1}^{D} \bar{q}(x)\, \gamma_\mu D_\mu\, q(x) - \frac{ar}{2} \sum_{\mu=1}^{D} \bar{q}(x)\, D_\mu D_\mu\, q(x) \right) \end{aligned} \tag{4.6}$$

where the covariant derivative D_μ is defined by

$$(D_\mu q)(x) = \frac{1}{2a} \left(U^\dagger_{-\mu}(x+\mu)\, q(x+\mu) - U^\dagger_\mu(x-\mu)\, q(x-\mu) \right),$$

m_q is the *bare* lattice quark mass, and $r = 1$ is the Wilson parameter described shortly. Notice in the covariant derivative the use of Equation 4.3 to properly parallel propagate the quark fields from the points $x + \mu$ and $x - \mu$ to a common point x before taking the difference. The above action is a simple discretization of the continuum QCD action except for the term proportional to r. This is the Wilson term which is added to decouple the *doublers*, thus ensuring the action describes one fermion flavor in the continuum limit. The consequence of the Wilson term is that the Wilson quark action breaks the chiral symmetries that would be present in the continuum for $m_q = 0$. Without chiral symmetry the quark masses are not multiplicatively renormalized, and hence, we must non-perturbatively determine the bare quark mass which corresponds to the chiral limit. This is discussed briefly in Section 4.6. Despite the lack of chiral symmetry, the Wilson quark action in Equation 4.6 is a correct description of the long distance physics of QCD. Replacing

$U_\mu(x)$ by $A_\mu(x)$ as indicated in Equation 4.5, it can be shown that $S_F^{\rm lat} = S_F^{\rm con} + \mathrm{O}(a)$ in the classical continuum limit. Notice that while the gauge action was accurate to $O(a^2)$, the leading errors in the fermion action are $O(a)$.

By expanding the second derivative in the Wilson term, we can caste the action into the form

$$a^4 \sum_x \left(\left(m_q + \frac{4r}{a} \right) \overline{q}(x)\, q(x) - \frac{1}{2a} \sum_{\mu=\pm 1}^{\pm D} \overline{q}(x)\ (r + \gamma_\mu)\ U_\mu^\dagger(x-\mu)\, q(x-\mu) \right)$$

where we define the backward Dirac matrices

$$\gamma_{-\mu} = -\gamma_\mu .$$

It is useful to introduce a matrix notation for the above by defining the Wilson-Dirac matrix M_q as

$$\begin{aligned} & M_{\alpha\alpha'}^{aa'}(x,x';q) = \\ & = \left(m_q + \frac{4r}{a} \right) \delta_{\alpha\alpha'}^{aa'}\, \delta(x-x') - \frac{1}{2a} \sum_{\mu=\pm 1}^{\pm D} (r+\gamma_\mu)_{\alpha\alpha'}\, U_\mu^{\dagger aa'}(x-\mu)\, \delta(x-(x'+\mu)) \end{aligned} \tag{4.7}$$

where we use the short hand $\delta_{\alpha\alpha'}^{aa'} = \delta^{aa'}\delta_{\alpha\alpha'}$. Using this notation, the quark action is

$$S_F[\,q,\overline{q}\,] = a^4 \sum_{aa'} \sum_{\alpha\alpha'} \sum_{xx'} \overline{q}_\alpha^a(x)\, M_{\alpha\alpha'}^{aa'}(x,x';q)\, q_{\alpha'}^{a'}(x') = a^4\, \overline{q}\, M_q\, q .$$

We further generalize the matrix notation to include all the quark flavors by defining M as the appropriate block diagonal matrix implied below.

$$S_F[\,\psi,\overline{\psi}\,] = \sum_q S_F[\,q,\overline{q}\,] = a^4\, \overline{\psi}\, M\, \psi \tag{4.8}$$

In the above equation $\psi = (u,d)$ and $M = \mathrm{diag}(M_u, M_d)$.

It is a common but unfortunate practice to rescale the quark fields by $m_q + \frac{4r}{a}$.

Defining the hopping parameter κ_q by

$$\kappa_q = \frac{1}{2a}\left(m_q + \frac{4r}{a}\right) = \frac{1}{8r + 2m_q a}$$

gives the resulting rescaled fermion action

$$a^4 \sum_x \left(\overline{q}(x)\, q(x) - \frac{1}{\kappa_q} \sum_{\mu=\pm 1}^{\pm D} \overline{q}(x)\, (r + \gamma_\mu)\; U_\mu^\dagger(x-\mu)\, q(x-\mu) \right)$$

and the resulting Wilson-Dirac matrix

$$\begin{aligned} & M_{\alpha\alpha'}^{aa'}(x, x'; q) = \\ & = \delta_{\alpha\alpha'}^{aa'}\, \delta(x - x') - \frac{1}{\kappa_q} \sum_{\mu=\pm 1}^{\pm D} (r + \gamma_\mu)_{\alpha\alpha'}\, U_\mu^{\dagger aa'}(x-\mu)\, \delta(x - (x' + \mu)). \end{aligned} \tag{4.9}$$

We note that use of the rescaled quark fields implies factors of κ in various results for correlation functions in later chapters. Therefore, though we occasionally use the rescaled action in Equation 4.9 above, we record all results for correlation functions assuming the canonical normalization used in Equation 4.7.

4.3 Correlation Functions and Functional Integrals

The starting point of most lattice calculations is the evaluation of a variety of lattice correlation functions. We discuss in detail the two point correlation functions in Chapter 7 and the three point correlation functions in Chapter 8. In this section we examine the features common to the calculation of any correlation function. Lattice correlation functions are of the form

$$\begin{aligned} & \langle\, \psi_1 \cdots \psi_N\, \overline{\psi}_N \cdots \overline{\psi}_1\, U_1 \cdots U_M \,\rangle = \\ & \quad \int DU_\mu\; e^{-S_G[U_\mu]} \int D\psi D\overline{\psi}\; e^{-S_F[\psi,\overline{\psi},U_\mu]}\; \psi_1 \cdots \psi_N\, \overline{\psi}_N \cdots \overline{\psi}_1\, U_1 \cdots U_M \end{aligned}$$

where $\psi_i = \psi^{a_i}_{f_i\alpha_i}(x_i)$, $\overline{\psi}_i = \overline{\psi}^{b_i}_{g_i\beta_i}(y_i)$, and $U_i = U^{c_i d_i}_{\mu_i}(z_i)$, and the integration measures are

$$DU_\mu = \prod_{x,\mu} dU_\mu(x) \tag{4.10}$$

where x runs over all lattice points, $\mu = 1, \ldots, D$, and $dU_\mu(x)$ is the invariant group measure for $\mathrm{SU(N_c)}$ and

$$D\psi D\overline{\psi} = \prod_f \prod_{x,a,\alpha} d\psi^a_{f\alpha}\, d\overline{\psi}^a_{f\alpha} \tag{4.11}$$

where $f = 1, \ldots, \mathrm{N_f}$, $a = 1, \ldots, \mathrm{N_c}$, $\alpha = 1, \ldots, \mathrm{N_d}$, and $d\psi^a_{f\alpha}$ and $\overline{\psi}^a_{f\alpha}$ are Grassmann integrations. Note that all other integrals with unequal numbers of ψ and $\overline{\psi}$ fields vanish. Furthermore, gauge symmetry ensures that only the gauge singlet portions of the integrand contribute to the correlation function.

The fermion action is quadratic and hence the fermion integrals can be performed analytically. The result is

$$\begin{aligned} &\langle\, \psi_1 \cdots \psi_N\, \overline{\psi}_N \cdots \overline{\psi}_1\, U_1 \cdots U_M \,\rangle = \\ &= \int DU_\mu\, e^{-S_G[U_\mu]}\, \det(M[U_\mu])\, U_1 \cdots U_M \sum_\pi (-1)^\pi M[U_\mu]^{-1}_{1\pi_1} \cdots M[U_\mu]^{-1}_{N\pi_N} \end{aligned} \tag{4.12}$$

where $M[U_\mu]^{-1}_{i\pi_i} = (M^{-1})^{a_i b_{\pi_i}}_{\alpha_i \beta_{\pi_i}}[x_i, y_{\pi_i}; f_i]\, \delta_{f_i g_{\pi_i}}$, the sum is over all permutations π of $1, \ldots, N$, and $(-1)^\pi$ is the sign of that permutation. The sum over all permutations gives the usual Wick contractions, and the block diagonal structure of M as given in Equation 4.8 ensures that only contractions between quark fields of the same flavor occur. Also the determinant of M gives the usual fermion determinants for each quark.

$$\det(M[U_\mu]) = \prod_f \det(M^f[U_\mu])$$

As Equation 4.12 shows, after performing the fermion functional integrals, the correlation functions are reduced to functional integrals over the gauge fields whose integrands are implicitly defined functions of U_μ.

The gauge action and fermion determinants are common to all correlation func-

tions and are collectively referred to as the effective action defined below.

$$e^{-S_{\text{eff}}[U_\mu]} = e^{-S_G[U_\mu]} \prod_f \det(M^f[U_\mu])$$

The effective action is real for the case of two degenerate up and down quarks pursued in our calculations. The addition of a strange quark or the introduction of a mass splitting between the up and down quarks gives rise to a complex effective action. We also note that in past and even some current calculations the fermion determinant has been neglected. This is referred to as the quenched approximation and is used to avoid the large computational resources required to include the fermion determinant. Using the definition of the effective action above, the resulting expression for the correlation functions is

$$\begin{aligned} &\langle \psi_1 \cdots \psi_N \overline{\psi}_N \cdots \overline{\psi}_1 U_1 \cdots U_M \rangle = \\ &= \int DU_\mu \, e^{-S_{\text{eff}}[U_\mu]} \, U_1 \cdots U_M \sum_\pi (-1)^\pi M[U_\mu]^{-1}_{1\pi_1} \cdots M[U_\mu]^{-1}_{N\pi_N}. \end{aligned} \tag{4.13}$$

We note that, though our calculations do include the fermion determinant, the expression above holds in the quenched approximation as well with the understanding that $S_{\text{eff}} \rightarrow S_G$.

We note that for non-zero lattice spacing and finite volume the integral in Equation 4.13 is a product of a finite number of $\mathrm{SU(N_c)}$ integrals. Each group integral is over a compact domain, and since there are only a finite number of such integrals, the entire functional integral is simply a high dimensional integral over some unspecified compact domain. As long as the integrand is continuous and defined on the whole domain the integral will converge. In distinction to the perturbative approach to functional integration it is not necessary to fix a gauge to achieve a finite integral.[1]

Finally we are left with a well defined but extremely difficult integral. Integrals of this form are evaluated by the methods of stochastic integration. These are simply well defined numerical algorithms for evaluating an integral to a given precision. We

[1]Gauge fixing can still be performed on the lattice and is needed in order to calculation quark or gluon correlation functions as opposed to gauge invariant hadronic correlation functions.

leave the details to the lattice text books cited earlier and simply state the generic form for such algorithms. The integrals in Equation 4.13 for the correlation functions are of the form

$$\int DU_\mu \; e^{-S_{\rm eff}[U_\mu]} \; F[U_\mu]$$

where $F[U_\mu]$ represents the appropriate combination of gauge fields and inverses of the Wilson-Dirac matrix. The above integral is replaced by the average of $F[U_\mu]$ over an appropriately chosen ensemble of gauge fields. This set of gauge fields is chosen according to the probability distribution given by

$$\rho[U_\mu] = e^{-S_{\rm eff}[U_\mu]}.$$

The resulting form for the integrals is

$$\int DU_\mu \; e^{-S_{\rm eff}[U_\mu]} \; F[U_\mu] = \frac{1}{N} \sum_i F[U_\mu^{(i)}] \pm \frac{\sigma_F}{\sqrt{N}} \tag{4.14}$$

where the value of σ_F depends on the integrand $F[U_\mu]$ and can only be determined after performing the integral. This integration formula can be compared to more standard integration formulas often used for low dimensional integrals. The generic form for such methods is

$$\int dx \, f(x) = \sum_i f(x_i) \, \Delta_i \pm \frac{f^{(n)}}{N^n}$$

where $f^{(n)}$ is evaluated at some unknown point. Again, the accuracy is unknown until you do the calculation and examine the behavior as a function of N. Therefore conceptually the methods are very similar. The basic distinction is a practical matter, that is, the computer resources required to numerically evaluate a functional integral to a given accuracy is significantly larger than the resources required to evaluate a simple integral to the same accuracy.

We apply the above integration methods to the lattice correlation functions in our

calculations. The result is

$$\int DU_\mu \, e^{-S_{\rm eff}[U_\mu]} \, U_1 \cdots U_M \sum_\pi (-1)^\pi M[U_\mu]^{-1}_{1\pi_1} \cdots M[U_\mu]^{-1}_{N\pi_N} = \tag{4.15}$$
$$\frac{1}{N} \sum_i U_1^{(i)} \cdots U_M^{(i)} \sum_\pi (-1)^\pi M[U_\mu^{(i)}]^{-1}_{1\pi_1} \cdots M[U_\mu^{(i)}]^{-1}_{N\pi_N} \pm \frac{\sigma}{\sqrt{N}}$$

where σ again depends on the correlation function in the integrand. Determining an appropriate ensemble to use in the above method is the most computationally demanding aspect of lattice QCD calculations. (This is however not true for a quenched lattice calculation.) The advantage of choosing such algorithms is that once an ensemble of gauge fields is constructed, any correlation function can be evaluated. The only issue is whether the value of σ for a given correlation function is small enough to allow for a sufficiently accurate calculation for the number N of gauge fields in the ensemble.

We note that in Equation 4.15 above, the inverse of the very large matrix M appears. This inverse is the quark propagator in a classical gauge field background. Calculating this inverse is a computationally demanding task that amounts to solving Dirac's equation for an arbitrary gauge field on the lattice. As it turns out, the methods for constructing ensembles of gauge fields to use in Equation 4.15 also require inverting M. Therefore the calculation of M^{-1} is a pervasive aspect of nearly all lattice QCD calculations. The numerical methods commonly used to evaluate M^{-1} are described in the lattice text books mentioned earlier. A common feature of the known algorithms for calculating the inverse of M is that all such algorithms become less efficient for smaller quark masses. Other problems also plague lattice calculations for light quark masses. As a result, lattice QCD calculations are always performed for quark masses that are heavier than those in the natural world. Consequently, comparing lattice calculations to experimental measurements requires an extrapolation of lattice observables as a function of quark mass.

4.4 Transfer Matrix

For the simplest actions, including the Wilson actions used in our calculations, a transfer matrix exists for finite lattice spacing. The transfer matrix acts as e^{-Ha} and we denote it as such. The defining property of the transfer matrix is that a Hilbert space exists with a Hamiltonian H that is bounded from below and satisfies the following property relating correlation functions to quantum mechanical matrix elements.

$$\frac{\langle O_N(x_N)\cdots O_1(x_1)\rangle}{\mathcal{Z}} = \frac{\mathrm{Tr}\left(e^{-HT}\,\mathcal{T}\left\{O_N^H(x_N)\cdots O_1^H(x_1)\right\}\right)}{\mathrm{Tr}\left(e^{-HT}\right)} \tag{4.16}$$

where $\mathcal{Z} = \langle 1\rangle$, $\mathcal{T}$ denotes time ordering, and $O_i^H(x_i)$ denotes the Heisenberg operator corresponding to the field $O_i(x_i)$. The corresponding Schrödinger operator is $O_i^S(\vec{x}_i) = e^{Hx_i^0}O_i^H(x_i)e^{-Hx_1^0}$. In the remainder of this thesis we drop the labels H and S, and the nature of the symbol is determined by the context. It will be clear whether the operator (in a quantum mechanical sense) or a field (in the functional integral sense) is implied. Additionally, if the argument is a space-time coordinate x or a space coordinate $\vec{x}$, then the Heisenberg or Schrödinger operator is respectively assumed.

Now change the Heisenberg operators to Schrödinger operators in the above equation. To keep things simple we assume $x_N^0 > x_{N-1}^0 > \cdots x_2^0 > x_1^0$. The result is

$$\begin{aligned}\frac{\langle O_N(x_N)\cdots O_1(x_1)\rangle}{\mathcal{Z}} &= \\ &= \mathrm{Tr}\Big(e^{-H(T-x_N^0)}\,O_N(\vec{x}_N)\,e^{-H(x_N^0-x_{N-1}^0)}\,O_{N-1}(\vec{x}_{N-1})\cdots \\ &\qquad O_2(\vec{x}_2)\,e^{-H(x_2^0-x_1^0)}\,O_1(\vec{x}_1)\,e^{-Hx_1^0}\Big)\,/\,\mathrm{Tr}\left(e^{-HT}\right).\end{aligned}$$

Next evaluate the trace using a complete set of eigenstates of the Hamiltonian $|H,n\rangle$ where $n = 0, 1, \ldots$ label the states. The energies of the states $|H,n\rangle$ are given by $H|H,n\rangle = E_n|H,n\rangle$, and the resulting expression is

$$\frac{\langle O_N(x_N)\cdots O_1(x_1)\rangle}{\mathcal{Z}} =$$

$$= \left(\sum_{n=0} e^{-E_n(T-x_N^0)} \langle H,n| O_N(\vec{x}_N)\, e^{-H(x_N^0-x_{N-1}^0)}\, O_{N-1}(\vec{x}_{N-1}) \cdots \right.$$
$$\left. O_2(\vec{x}_2)\, e^{-H(x_2^0-x_1^0)}\, O_1(\vec{x}_1)\, |H,n\rangle\, e^{-E_n x_1^0} \right) / \sum_{n=0} e^{-E_n T}.$$

The vacuum state is $|\Omega\rangle = |H,0\rangle$ with energy E_0. Now extract a common factor of $e^{-E_0 T}$ from the numerator and denominator. This has the effect of replacing E_n with $E_n - E_0$ and H with $H - E_0$. This is equivalent to assuming $E_0 = 0$ from the start, which we now assume.

The limit $T \to \infty$ extracts the leading term from the numerator and denominator. The contributions to the trace from all other states are suppressed in this limit. The resulting equation is

$$\lim_{T\to\infty} \frac{\langle O_N(x_N) \cdots O_1(x_1) \rangle}{\mathcal{Z}} = \tag{4.17}$$
$$= \langle \Omega|\, O_N(\vec{x}_N)\, e^{-H(x_N^0-x_{N-1}^0)}\, O_{N-1}(\vec{x}_{N-1}) \cdots O_2(\vec{x}_2)\, e^{-H(x_2^0-x_1^0)}\, O_1(\vec{x}_1)\, |\Omega\rangle.$$

This is the basic expression relating lattice correlation functions to quantum mechanical matrix elements. This result holds for non-zero lattice spacing in lattice theories with a transfer matrix; otherwise, it is expected to hold in the continuum limit. The construction of a Hilbert space ensures that correlation functions have the correct positivity properties as expected in the continuum. In particular, the above result is the formal basis for the spectral representation that is used in Chapters 7 and 8 to interpret the nucleon two and three point correlation functions. Furthermore, the introduction of a Hilbert space allows us to use the conventional description of symmetries in quantum mechanics. Of course the symmetries are different for a lattice calculation, but they are still implemented by unitary or anti-unitary operators as usual.

The result from Equation 4.17 above will be applied to the calculations in this thesis without taking the limit $T \to \infty$. The canonical rule many calculations follow is to choose $T \geq 2L$ where L is the linear extent of the spatial volume. The logic is as follows. The finite volume effects are controlled by $e^{-m_\pi L}$ for sufficiently large L. In order to avoid substantial finite volume effects, the common rule is to choose

$m_\pi L \geq 4$. Also m_π controls the leading corrections to the $T \to \infty$ limit given by $e^{-m_\pi T}$. We then have $m_\pi L \geq 8$. This assures that the leading correction to the limit $T \to \infty$ is significantly lower than the leading correction to the infinite volume limit.

We note that Equation 4.17 holds for calculations employing anti-periodic boundary conditions in the time direction for the fermion fields. However, our calculations use Dirichlet boundary conditions for the fermions in the time direction. The effect of such boundary conditions is to introduce boundary terms into Equation 4.16 giving

$$\frac{\langle O_N(x_N) \cdots O_1(x_1) \rangle}{\mathcal{Z}} = \frac{\mathrm{Tr}\left(e^{-HT} B_1 \mathcal{T} \left\{ O_N^H(x_N) \cdots O_1^H(x_1) \right\} B_2 \right)}{\mathrm{Tr}\left(e^{-HT} \right)}$$

where we have written two arbitrary boundary terms B_1 and B_2 to allow for any appropriate boundary conditions. It can be shown that as long as $\langle \Omega | B_i | \Omega \rangle \neq 0$, the essential conclusion in Equation 4.17 is unchanged. The final result in such a case is

$$\begin{aligned} &\lim_{T\to\infty} \frac{\langle O_N(x_N) \cdots O_1(x_1) \rangle}{\mathcal{Z}} = \\ &= \langle \Omega | \, O_N(\vec{x}_N) \, e^{-H(x_N^0 - x_{N-1}^0)} \, O_{N-1}(\vec{x}_{N-1}) \cdots O_2(\vec{x}_2) \, e^{-H(x_2^0 - x_1^0)} \, O_1(\vec{x}_1) \, | \Omega \rangle \\ &\quad \langle \Omega | \, B_1 \, | \Omega \rangle \, \langle \Omega | \, B_2 \, | \Omega \rangle. \end{aligned}$$

The additional factors of $\langle \Omega | B_1 | \Omega \rangle$ and $\langle \Omega | B_2 | \Omega \rangle$ can be removed by taking ratios of correlation functions which is always done in lattice calculations to remove a variety of other normalization factors as well.

4.5 Hadronic Masses and Matrix Elements

Ultimately the observables of interest are quantum mechanical matrix elements not correlation functions. Both hadronic masses and the traditional hadronic matrix elements can be expressed as quantum mechanical matrix elements of various operators. Hadronic masses are the expectation values of the QCD Hamiltonian in the corresponding hadronic state, whereas, the traditional hadronic matrix elements are matrix elements of well defined and simple operators composed of quark and gluon

fields. The details of our calculations of the nucleon mass and nucleon matrix elements are given in Chapters 5 through 8. Therefore in this section we provide only an introductory sketch of the lattice calculation of masses and matrix elements.

To calculate a hadron-hadron matrix element we must be able to obtain the appropriate hadronic state. Naively this seems to require solving for the eigenstates of the QCD Hamiltonian, however, the nature of a Euclidean space calculation provides an alternative method. To see this, choose an operator $\hat{H}$ with the quantum numbers of the hadron of interest and act with it on the vacuum state $|\Omega\rangle$. Now consider the Euclidean time evolution of this state, $\hat{H}|\Omega\rangle$. The time evolution in Euclidean space is generated by e^{-Ht} as

$$\begin{aligned} & e^{-Ht}\,\hat{H}\,|\Omega\rangle = \\ & = \sum_n e^{-E_n t}\,|H,n\rangle\,\langle H,n|\,\hat{H}\,|\Omega\rangle \\ & \rightarrow e^{-E_0 t}\,|H,0\rangle\,\langle H,0|\,\hat{H}\,|\Omega\rangle \end{aligned}$$

where in the last step we take the asymptotic limit $t \rightarrow \infty$ and $|H,n\rangle$ labels the spectrum of states in the appropriate hadronic channel with $|H,0\rangle$ denoting the ground state hadron. We see that, barring a miraculous choice of hadronic operator such that $\langle H,0|\hat{H}|\Omega\rangle = 0$, the hadron ground state dominates the asymptotic limit $t \rightarrow \infty$. Thus we find the rather curious result that we can obtain the hadron ground state of interest without ever explicitly constructing it. There is, however, a practical limitation. All lattice calculations are done with only a finite time extent. Hence we can not wait for asymptotically long Euclidean times to examine the hadron, but instead we must attempt to make $\langle H,n|\hat{H}|\Omega\rangle$ for $n > 0$ as small as possible to allow the ground state to dominate as early as possible.

Using the method described above to ferret out the hadronic ground state, we now proceed to calculate the various matrix elements of interest. First we consider the hadron mass which is simply the hadron-hadron matrix element of the QCD Hamiltonian. For these particular matrix elements there is a special technique that uses the two point hadronic correlation function. The time dependence of such a

correlation function is determined here,

$$\begin{aligned}
&\langle\, H(t)\, H(0)\,\rangle = \\
&\quad = \langle\Omega|\, \hat{H}\, e^{-Ht}\, \hat{H}\, |\Omega\rangle \\
&\quad = \sum_n \langle\Omega|\, \hat{H}\, |H,n\rangle\, e^{-E_n t}\, \langle H,n|\, \hat{H}\, |\Omega\rangle \\
&\quad \rightarrow \langle\Omega|\, \hat{H}\, |H,0\rangle\, \langle H,0|\, \hat{H}\, |\Omega\rangle\, e^{-E_0 t}
\end{aligned}$$

where in the last line we again consider the asymptotic limit $t \rightarrow \infty$. This result clearly demonstrates that we can determine the energy of the hadronic ground state, hence its mass, from the asymptotic time dependence of the corresponding two point correlation function.

The method for calculating hadronic masses sketched above capitalizes on the fact that the QCD Hamiltonian determines the Euclidean time evolution of states. To calculate the matrix elements of other operators, however, we must explicitly include these operators in the correlation functions we calculate. We do this by calculating three point correlation functions in which the additional field corresponds to the desired operator. As above, we examine the asymptotic time dependence of such correlation functions to isolate the contribution from the ground state hadron. The following sequence of steps illustrates the basic method.

$$\begin{aligned}
&\langle\, H(t)\, O(\tau)\, H(0)\,\rangle = \\
&\quad = \langle\Omega|\, \hat{H}\, e^{-H(t-\tau)}\, \hat{O}\, e^{-H\tau}\, \hat{H}\, |\Omega\rangle \\
&\quad = \sum_{n,m} \langle\Omega|\, \hat{H}\, |H,n\rangle\, e^{-E_n(t-\tau)}\, \langle H,n|\, \hat{O}\, |H,m\rangle\, e^{-E_m\tau}\, \langle H,m|\, \hat{H}\, |\Omega\rangle \\
&\quad \rightarrow \langle\Omega|\, \hat{H}\, |H,0\rangle\, \langle H,0|\, \hat{H}\, |\Omega\rangle\, e^{-E_0 t}\, \langle H,0|\, \hat{O}\, |H,0\rangle
\end{aligned}$$

In the last line we take two asymptotic limits, $(t-\tau) \rightarrow \infty$ and $\tau \rightarrow \infty$. We find that the three point correlation function reduces to the matrix element we want, $\langle H,0|\, \hat{O}\, |H,0\rangle$, times precisely the same combination of factors as found in the asymptotic limit of the two point correlation function above. Thus by taking ratios of three

point to two point correlation functions we can determine the quantum mechanical matrix elements for ground state hadrons.

4.6 Renormalization and Continuum Limit

Now that we understand how to calculate masses and matrix elements for a fixed lattice spacing, as described in Section 4.5, we must renormalize and take the continuum limit. To renormalize our lattice calculations we must not only renormalize the bare coupling and mass, g and m discussed in Section 4.2, but also each of the many operators whose matrix elements we calculate. The bare paramcters must be renormalized to ensure that the correct continuum limit is achieved as the lattice spacing $a \to 0$. Schematically, this is accomplished by determining $g(a)$ and $m(a)$ as functions of a such that two appropriate renormalization conditions are satisfied for all a. We illustrate such a scheme below. Additionally, we must renormalize the operators to account for the short distance physics that is excluded by the presence of a minimum length scale a, and, to compare our calculations to experimental results, we must match the operators in lattice QCD to the operators in perturbative QCD that are ultimately measured in high energy scattering experiments.

The nature of a lattice calculation leads to a slightly different strategy. There is no formula that gives g and m as functions of a. We must calculate at several values of g and m thereby numerically evaluating points of the $g(a)$ and $m(a)$ curves. To do this we start at some fixed bare coupling g_{fix}, calculate the pion and nucleon masses m_π^{lat} and m_N^{lat} at several values of m, and determine the value of the bare quark mass m_{fix} at which $m_\pi^{\text{lat}}/\, m_N^{\text{lat}} = m_\pi^{\text{phy}}/\, m_N^{\text{phy}}$. (The superscript "lat" denotes dimensionless lattice observables; "phy" denotes physical masses; and "fix" denotes the *fixed* bare parameters.) Now we determine the lattice spacing a_{fix} such that the nucleon mass attains the correct physical value $m_N^{\text{lat}} = a_{\text{fix}}\, m_N^{\text{phy}}$. At this point we have fixed the bare parameters; that is, we have determined a_{fix} and m_{fix} at a fixed value of the bare coupling g_{fix}. Consequently, we have implicitly determined a point on each curve $g(a)$ and $m(a)$ at which $g(a_{\text{fix}}) = g_{\text{fix}}$ and $m(a_{\text{fix}}) = m_{\text{fix}}$. Having renormalized the

action at one lattice spacing, we approach the continuum limit by reducing g_{fix} and repeating the calculation. In this, we rely on asymptotic freedom to ensure that the limit $g_{\text{fix}} \to 0$ implies the limit $a_{\text{fix}} \to 0$.

Now that we have renormalized the bare parameters in the lattice action, we must renormalize and match the lattice operators to the continuum $\overline{\text{MS}}$ scheme. In principle, operator renormalization and matching to the $\overline{\text{MS}}$ scheme are conceptually distinct efforts. However, in practice, all experimental measurements are reported in the $\overline{\text{MS}}$ scheme, and hence there is essentially no reason to calculate lattice observables in any other scheme. Therefore the methods of renormalization and matching are commonly applied in one step. The basic idea is to calculate quark and gluon matrix elements of an operator in both lattice QCD and perturbative QCD. Then for a fixed external state $|q\rangle$ containing a combination of quarks and gluons we determine the matching coefficient Z_O for the operator O by demanding that $\langle q|O|q\rangle^{\text{lat}} Z_O = \langle q|O|q\rangle^{\overline{\text{MS}}}$. (For illustration purposes we ignore the question of operator mixing.) Furthermore, the gauge coupling and quark masses must be matched. Using the notation from the previous paragraph, the lattice calculation should be performed with a_{fix}, g_{fix}, and m_{fix} while the continuum calculation should be performed with $\mu = a_{\text{fix}}^{-1}$, $g^{\overline{\text{MS}}}(\mu)$, and $m^{\overline{\text{MS}}}(\mu)$. Having calculated the matching coefficient Z_O for one fixed external state, we can now renormalize all other matrix elements of the same operator O with the same coefficient Z_O. For example, this allows us to report our lattice calculations of nucleon matrix elements of the same operator O in the $\overline{\text{MS}}$ scheme and to compare these results directly with experimental measurements.

Chapter 5

Nucleon Fields

To determine the nucleon mass or nucleon matrix elements as sketched in Section 4.5 we need to construct a nucleon field. We then use this nucleon field in the calculation of the two point and three point correlation functions described in Chapters 7 and 8 respectively. In this chapter we consider a broad class of nucleon fields. We examine the symmetry properties of these fields and discuss a method of parity projection that reduces the computational cost of correlation functions by half. We also record the particular choice of nucleon field used in the calculations presented in Chapter 9.

There are three requirements for a nucleon field. First it must have the correct quantum numbers to act on the vacuum and produce a nucleon state. Therefore it must have the correct baryon number, isospin, spin, and parity. Additionally, we choose a gauge invariant nucleon field to avoid gauge fixing.[1] In principle this is sufficient because the large Euclidean time limit of correlation functions calculated with such a nucleon field will asymptotically be dominated by the nucleon ground state. However, there is a practical difficulty. Lattice calculations are performed for finite Euclidean time extent. Therefore we require that the nucleon state dominate correlation functions within the Euclidean times accessible to our calculations. Thus our second requirement is that the nucleon field couple sufficiently strongly to the nucleon ground state that the ground state dominates our two and three point cor-

[1] As discussed in Section 4.3, lattice QCD calculations do not require a fixed gauge. Additionally, problems with Gribov copies [17] make fixing a gauge problematic and hence worth avoiding if possible.

relation functions by modestly short Euclidean times. (This aspect is discussed more fully in Chapter 6.) The third requirement is again a practical requirement. The nucleon field must be sufficiently simple that our lattice calculations can be performed with the computational resources at our disposal. This requirement precludes the use of nucleon fields containing quark anti-quark excitations and hence limits us to nucleon fields in the three quark sector. In particular, we use the product field described shortly.

5.1 General Form

The calculations in this thesis use the proton field given later in Equation 5.9, but many results are independent of any particular choice of nucleon field and are more clearly stated for a general form. For this purpose we introduce the following form for the proton field.

$$P_\alpha(x) = f_{\alpha\beta\gamma\delta}\,\epsilon_{bcd}\,U^b_\beta(x)\,U^c_\gamma(x)\,D^d_\delta(x) \tag{5.1}$$

The corresponding neutron field is determined in Appendix O.2. The result from Equation O.15 is

$$N_\alpha(x) = -f_{\alpha\beta\gamma\delta}\,\epsilon_{bcd}\,D^b_\beta(x)\,D^c_\gamma(x)\,U^d_\delta(x). \tag{5.2}$$

The fields $U(x)$ and $D(x)$ are extended quark fields. These are extended objects containing contributions from gluons as well as quarks and are described in Chapter 6. The details of the extended quark fields are not required at this point. We only require that U and D have the same gauge, translation, rotation, parity, charge conjugation, time reversal, and isospin properties as point quarks u and d. The symmetry properties of point quarks are discussed in Appendix K and in particular Section K.1. Extended quark fields with these properties are constructed in Chapter 6.

The proton field given above in Equation 5.1 is the general form for a field that is constrained to be a product of extended quark fields with coefficients that do not depend on $U_\mu(x)$. We expect the physical nucleon to consist not only of three u

and *d valence* quarks but also quark anti-quark pairs as well as gluons. The field in Equation 5.1 does contain gluon contributions as described in Chapter 6, but, due to the computational difficulties involved with disconnected diagrams, we can not easily study nucleon fields with quark anti-quark contributions.

The adjoint of the nucleon field is required for two point and three point correlation functions. The details are given in Section O.3 in Equations O.16, O.17, and O.18. The result is

$$\overline{P}_\alpha(x) = \overline{D}^d_\delta(x)\,\overline{U}^c_\gamma(x)\,\overline{U}^b_\beta(x)\,\overline{\epsilon}_{dcb}\,\overline{f}_{\delta\gamma\beta\alpha} \tag{5.3}$$

where

$$\overline{f}_{\delta\gamma\beta\alpha} = \gamma^0_{\delta\delta'}\,\gamma^0_{\gamma\gamma'}\,\gamma^0_{\beta\beta'}\,f^*_{\alpha'\beta'\gamma'\delta'}\,\gamma^0_{\alpha'\alpha} \tag{5.4}$$

and

$$\overline{\epsilon}_{dcb} = \epsilon_{bcd}. \tag{5.5}$$

Notice the order of indices in Equations 5.1, 5.2, and 5.3. In particular the order of indices of f and ϵ or $\overline{f}$ and $\overline{\epsilon}$ match the order of the corresponding quark fields. This order and furthermore the choice of index labels is chosen for convenience when calculating two point and three point correlation functions in Chapters 7 and 8.

5.2 Symmetry Properties

In this section, we determine several constraints on $f_{\alpha\beta\gamma\delta}$ such that the nucleon field $P_\alpha(x)$ given in Equation 5.1 satisfies the expected symmetry properties. In particular, we examine the behavior of $P_\alpha(x)$ under translations, Lorentz transformations, Euclidean rotations, parity, Minkowski and Euclidean time reversals, charge conjugation, isospin, and gauge transformations. The responses of quarks and gluons to each of these symmetries is described in Appendix K, and the corresponding symmetry properties of extended quarks are described in Chapter 6.

First we require the nucleon field to transform as a Dirac fermion under rotations.

As described in Equation K.2 this gives

$$M_{\alpha\alpha'}(R)\, U(R)\, P_{\alpha'}(x)\, U^{\dagger}(R) = P_{\alpha}(Rx).$$

The resulting constraint is derived in Equation O.20 and given here.

$$M_{\alpha'\alpha}(R)\, f_{\alpha\beta\gamma\delta}\, M^{\dagger}_{\beta\beta'}(R)\, M^{\dagger}_{\gamma\gamma'}(R)\, M^{\dagger}_{\delta\delta'}(R) = f_{\alpha'\beta'\gamma'\delta'} \tag{5.6}$$

We also require the nucleon field to have the correct parity transform. The parity transformation for a quark is given in Equation K.4 and is stated here for a nucleon.

$$\gamma^{0}_{\alpha\alpha'}\, U(P)\, P_{\alpha'}(x)\, U^{\dagger}(P) = P_{\alpha}(Px)$$

The constraint that follows is determined in Equation O.21 and written here.

$$\gamma^{0}_{\alpha'\alpha}\, f_{\alpha\beta\gamma\delta}\, \gamma^{0}_{\beta\beta'}\, \gamma^{0}_{\gamma\gamma'}\, \gamma^{0}_{\delta\delta'} = f_{\alpha'\beta'\gamma'\delta'} \tag{5.7}$$

The proper charge conjugation behavior, given for quarks in Equation K.5, is written below for a nucleon.

$$C_{\alpha\alpha'} U(C)\, P^{a}_{\alpha'}(x)\, U^{\dagger}(C) = \overline{P}^{a}_{\alpha}(x)$$

The resulting constraint, worked out in Equation O.22, is

$$C_{\alpha'\alpha}\, f_{\alpha\beta\gamma\delta}\, C_{\beta\beta'}\, C_{\gamma\gamma'}\, C_{\delta\delta'} = \overline{f}_{\delta'\gamma'\beta'\alpha'}. \tag{5.8}$$

We also require that the nucleon field is gauge invariant.

$${}^{g}P_{\alpha}(x) = P_{\alpha}(x)$$

This requirement is manifestly satisfied, as shown in Equation O.23, and provides no constraint on $f_{\alpha\beta\gamma\delta}$. Additionally we require the proper translational behavior for the

nucleon field.

$$U(\Delta)P_\alpha(x)U^\dagger(\Delta) = P_\alpha(x+\Delta)$$

As demonstrated in Equation O.19, the nucleon field automatically satisfies this condition.

5.3 Parity Projection

The nucleon field $P_\alpha(x)$ has the same behavior under parity as does any Dirac field. This implies that the nucleon field creates both positive and negative parity states. For the case of the nucleon, the negative parity state, in other words, the nucleon parity partner, is heavier than the ground state nucleon and can be treated as an excited state that is suppressed at large Euclidean times.[2] Better yet, we can parity project the nucleon field into a definite positive parity state and explicitly exclude the parity partner. We can accomplish this in two ways. We can parity project the nucleon field as a whole or parity project each quark field individually within the nucleon field. There is a practical advantage to the second option. By parity projecting the quarks we can eliminate half of the computation. Either option gives rise to a field which still satisfies the constraints discussed in the previous section.

First consider parity projection at the hadronic level. Take $P_\alpha(x)$ to be a nucleon field as given in Equation 5.1. The corresponding parity projected field is

$$P^\pm_\alpha(x) = P^\pm_{\alpha\alpha'}P_{\alpha'}(x)$$

where the parity projection is accomplished by

$$P^\pm_{\alpha\alpha'} = \left(\frac{1 \pm \gamma^0}{2}\right)_{\alpha\alpha'}.$$

[2]The ground state in the $I(J^P) = \frac{1}{2}(\frac{1}{2}^+)$ channel is, of course, the proton $N(940)$, whereas the ground state in the $I(J^P) = \frac{1}{2}(\frac{1}{2}^-)$ channel is, the parity partner, $N(1535)$ [19].

For such a field the effect of a parity transformation is

$$U(P)\, P^{\pm}_{\alpha}(x)\, U^{\dagger}(P) = \pm\, P^{\pm}_{\alpha}(Px)$$

as is shown in Equation O.24. Additionally notice that $P^{+}_{\alpha}(x) = 0$ for $\alpha = 3$ and 4 and that $P^{-}_{\alpha}(x) = 0$ for $\alpha = 1$ and 2. Hence for each $P^{+}_{\alpha}(x)$ and $P^{-}_{\alpha}(x)$, we have a two component spinor with definite parity $+1$ or -1 respectively.

Now consider parity projection at the quark level. Again take $P_{\alpha}(x)$ to be a proton field as given in Equation 5.1 with the corresponding parity projected field given by

$$P^{\pm}_{\alpha}(x) = f_{\alpha\beta\gamma\delta}\, \epsilon_{bcd}\, P^{\pm}_{\beta\beta'}\, U^{b}_{\beta'}(x)\, P^{\pm}_{\gamma\gamma'}\, U^{c}_{\gamma'}(x)\, P^{\pm}_{\delta\delta'}\, D^{d}_{\delta'}(x).$$

We show in Equation O.25 that this field too has the following parity behavior

$$U(P)\, P^{\pm}_{\alpha}(x)\, U^{\dagger}(P) = \pm\, P^{\pm}_{\alpha}(Px)$$

with the same conclusion that $P^{\pm}_{\alpha}(x)$ are both two component spinors with definite parity ± 1. Additionally the nucleon field $P^{+}_{\alpha}(x)$ depends only on the $\alpha = 1$ and 2 components of the U and D fields, and $P^{-}_{\alpha}(x)$ depends only on the $\alpha = 3$ and 4 components. This fact is the reason that calculations using a proton field with parity projected quarks are half as computationally demanding as calculations which simply parity project the overall nucleon field. We demonstrate this explicitly in Section 7.4 for the two point correlation functions and in Section 8.4 for the three point correlation functions.

5.4 Common Form

There are two particular nucleon fields that we draw attention to. A common form used in lattice calculations is

$$P_{\alpha}(x) = U^{a}_{\alpha}(x)\, U^{b}_{\beta}(x)\, \left(C\gamma^{5}\right)_{\beta\gamma}\, D^{c}_{\gamma}(x)\, \epsilon_{abc}$$

where $C = i\gamma^2\gamma^0$ is the charge conjugation matrix. This is of the general form given in Equation 5.1 with the choice

$$f_{\alpha\beta\gamma\delta} = \delta_{\alpha\beta}\left(C\gamma^5\right)_{\gamma\delta}.$$

Therefore all the statements in Section 5.1 apply equally well to this particular choice.

The form we use in our lattice calculations follows from the above by parity projection of the quarks as described in Section 5.3, in other words, by substituting $U \to \frac{1}{2}(1+\gamma^0)U$ and $D \to \frac{1}{2}(1+\gamma^0)D$. The resulting proton field is

$$P_\alpha(x) = \left(\frac{1+\gamma^0}{2}\right)_{\alpha\alpha'} U^a_{\alpha'}(x)\, U^b_\beta(x) \left(\left(\frac{1+\gamma^0}{2}\right) C\gamma^5 \left(\frac{1+\gamma^0}{2}\right)\right)_{\beta\gamma} D^c_\gamma(x)\, \epsilon_{abc}. \quad (5.9)$$

This field is also of the general form in Equation 5.1 with the choice

$$f_{\alpha\beta\gamma\delta} = \left(\frac{1+\gamma^0}{2}\right)_{\alpha\beta} \left(\left(\frac{1+\gamma^0}{2}\right) C\gamma^5 \left(\frac{1+\gamma^0}{2}\right)\right)_{\gamma\delta}.$$

As above, this choice for a nucleon field satisfies all the properties described in Section 5.1. Furthermore, given that quarks have each been projected onto definite positive parity, this nucleon field also satisfies all statements in Section 5.3.

Chapter 6

Extended Quark Fields

The physical nucleon is expected to be an extended object. Additionally, we expect to find gluons and quark anti-quark pairs in abundance within the nucleon. These expectations should hold for a lattice calculation as well. Therefore, to enhance the coupling of our nucleon field to the nucleon state in our lattice calculations we construct an extended nucleon field. Typical calculations involving an extended nucleon field require evaluation of additional quark propagators and are significantly more computationally demanding.[1] (In such a scenario the number of extra quark propagators is given by the number of lattice points covered by the extent of the nucleon field.) However, we can avoid this limitation by retaining a nucleon field that factorizes into a product of quark like fields.

To create an extended nucleon field yet retain a simple product form, we introduce extended quark fields, $U(x)$ and $D(x)$. Then a proton field with the extended quark content UUD, as opposed to the point quark content uud, has additional structure that we can adjust to more accurately resemble the proton state in our lattice calculation. As we show shortly, to maintain gauge invariance we must make the extended quark fields depend on the gauge field, and hence this construction will introduce a gluon component to the nucleon field; however, introducing quark anti-quark pairs into the nucleon field is complicated by the occurrence of disconnected diagrams and

[1] Such calculations are however pursued, for example calculations of the excited nucleon or pentaquark spectrums.

will not be considered in this thesis.

In Section 6.1 we discuss the construction of both gauge fixed and gauge invariant extended quark fields in both Minkowski and Euclidean space-time. After which, in Section 6.2 we present and generalize the iterative methods commonly used in lattice calculations. Additionally in that section we record the explicit method of smearing used in this thesis.

6.1 General Construction

In this section we consider several general forms for extended quarks. In particular, we examine both gauge fixed and gauge invariant smearing. Additionally, we discuss Lorentz invariant smearing in Minkowski space-time and rotation invariant smearing in Euclidean space. First we consider gauge fixed smearing in Minkowski space-time. The general form for the corresponding extended quarks is

$$Q^a_\alpha(x) = \int d^4y \; f((x-y)^2)\, q^a_\alpha(y). \tag{6.1}$$

In a non-local object like the above it is impossible to maintain gauge covariance without introducing factors of the gauge field. Hence to consider such smearing, we must fix gauge. In Equation 6.1, we take f to be a Lorentz invariant function. As a result the extended quark field above has the same Lorentz transformation properties as a point quark. Equation K.2 gives the Lorentz transformation of a point quark as

$$M_{\alpha\beta}(\Lambda)\, U(\Lambda)\, q^a_\beta(x)\, U^\dagger(\Lambda) = q^a_\alpha(\Lambda x),$$

and in Equation O.26, we demonstrate that the extended quark field in Equation 6.1 does indeed have the same Lorentz transformation as a point quark.

Next we consider the construction of gauge covariant extended quark fields while remaining in Minkowski space-time momentarily. We first consider a simple concrete example; then we introduce a general form. We want to maintain gauge covariance, in other words, we want the extended quark $Q^a_\alpha(x)$ to gauge transform in the same

way as the point quark $q^a_\alpha(x)$. The gauge transformation of point quarks is given in Equation 4.2 as

$$^g q_\alpha(x) = g(x)\, q_\alpha(x).$$

A simple example of a quark field which satisfies the above requirement is

$$Q^a_\alpha(x) = \int d^4y\; U^{ab}(x,y)\, q^b_\alpha(y)\, f((x-y)^2) \tag{6.2}$$

where $U^{ab}(x,y)$ is the Wilson path ordered line integral for the straight line path from the point y to the point x. (We carefully define this shortly.) This Wilson line is shown to be a scalar functional of each argument in Equation O.28, $U(\Lambda)U(x,y)U^\dagger(\Lambda) = U(\Lambda x, \Lambda y)$. Using this result, in Equation O.30 we verify that the quark field in Equation 6.2 above gauge transforms like a point quark at x, and in Equation O.27 we also verify that this quark field Lorentz transforms like a point quark as well. Therefore the extended quark field in Equation 6.2 has the same gauge and Lorentz transformation properties as a point quark. The example in Equation 6.2 illustrates the basic structure required to build a gauge covariant quark field; that is, the contributions from all quarks must first be parallel propagated to a common point x and then, and only then, summed.

We now generalize the above example to include all possible Wilson paths from the point x to y. To maintain the Lorentz transformation of the quark field, every Lorentz transform of each path must occur with the same weight. The general form for our extended quark fields is given by

$$Q^a_\alpha(x) = \int Dz(\tau)_{z(0)=x}\; F[z(\tau)]\, U^{ab}[z(\tau)]\, q^b_\alpha(z(1)) \tag{6.3}$$

where $\int Dz(\tau)_{z(0)=x}$ is a functional integral over all paths in space-time $z(\tau)$ with $\tau \in [0,1]$ and $z(0) = x$. Additionally, the Wilson path $U^{ab}[z(\tau)]$ is defined by

$$U[z(\tau)] = \mathcal{P} e^{i \int_{z(0)}^{z(1)} A^a_\mu(z) \lambda^a dz^\mu}, \tag{6.4}$$

and in Equation K.13 it is shown that $U[z(\tau)]$ is a scalar functional, i.e. the Lorentz transformation of $U[z(\tau)]$ is

$$U(\Lambda)\, U[z(\tau)]\, U^{\dagger}(\Lambda) = U[\Lambda z(\tau)].$$

Furthermore, to maintain Lorentz covariance we assume $F[\Lambda z(\tau)] = F[z(\tau)]$. We do not make an effort to properly define the measure $Dz(\tau)$, since the only situation in which we implement Equation 6.3 above is on the lattice and the details of the measure are clear there. (On the lattice $Dz(\tau)$ simply becomes a sum over all discrete paths along the edges of the lattice.) We only assume the formal property $D(\Lambda z(\tau)) = Dz(\tau)$. The gauge covariance of the these extended quarks is demonstrated in Equation O.31, and the Lorentz covariance is shown in Equation O.29. Therefore the general form for an extended quark field given in Equation 6.3 above has the correct gauge and Lorentz transformation properties. Additionally, the example given earlier in Equation 6.2 is a specific case of the general form in which $U(x, y)$ is the Wilson line along the path $z(\tau) = (1 - \tau)x + \tau y$ and $F[z(\tau)]$ is restricted to simple straight line paths only.

Thus far we have considered smearing in space-time only. We find that we can maintain the Lorentz and gauge transformation properties of the quarks, but we will have difficulty identifying the contributions of distinct intermediates states in correlation functions constructed from such smeared quarks. (The role of correlation functions in lattice calculations is briefly discussed in Section 4.5 and thoroughly described in Chapters 7 and 8). The difficulty is due to the fact that there are, potentially, contributions in the extended quarks from every possible time. This prevents us from using the spectral representations discussed in Sections 7.6 and 8.7 to interpret the two point and three point correlation functions in terms of nucleon observables. Therefore we now consider smearing the quarks at a single time only.[2] This clearly ruins the transformation properties that involve Lorentz boosts, but we can still maintain the correct rotational symmetries.

[2]Though we do not discuss it here, we have considered the use of quark fields smeared over a small number of time slices in such a way that the spectral representation is not significantly altered.

First we reconsider the gauge fixed smearing in Equation 6.1. Restricting the support of the function $f((x-y)^2)$ to space-like arguments only gives

$$Q^a_\alpha(\vec{x},t) = \int d^3\vec{y}\; f(|\vec{x}-\vec{y}|)\, q^a_\alpha(\vec{y},t). \tag{6.5}$$

The result in Equation O.26 still applies for rotations of the above extended quark and hence implies that this quark field still maintains the correct rotational covariance of a point quark but fails to be properly Lorentz covariant. Similarly, we also reconsider the gauge covariant extended quarks in Equation 6.3. By restricting the measure $Dz(\tau)$ to spatial paths only or by requiring $F[z]$ to vanish for all paths not restricted to a spatial plane we find

$$Q^a_\alpha(t,\vec{x}) = \int D\vec{z}(\tau)_{\vec{z}(0)=\vec{x}}\; F[\vec{z}(\tau)]\, U^{ab}[(t,\vec{z}(\tau))]\, q^b_\alpha(t,\vec{z}(1)). \tag{6.6}$$

This is the final form for extended quarks that we consider in the remainder of this thesis. The argument in Equation O.31 still ensures that these extended quarks are properly gauge covariant. Furthermore, the result in Equation O.29 still implies that the extended quark fields in Equation 6.6 above have the correct rotational properties. However, Lorentz covariance is lost.

Before proceeding to describe the algorithm for constructing extended quarks, we introduce a convenient matrix notation which applies to the continuum description above as well as our lattice calculation. We write the general form for extended quarks in Equation 6.6 as

$$Q^a_\alpha(x) = S^{aa'}_{\alpha\alpha'}(x,x')\, q^{a'}_{\alpha'}(x') \tag{6.7}$$

where a', α', and x' are all summed over. This is simply a statement of the fact that the extended quark field is a linear combination of point quark fields, and $S^{aa'}_{\alpha\alpha'}(x,x')$ are the appropriate coefficients. Note that $S^{aa'}_{\alpha\alpha'}(x,x')$ are certainly functions of the gauge field U_μ even though we often suppress this dependence. We now treat color, spin, and position indices collectively as a single matrix index and write the above as

the following matrix equation.

$$Q = S\,q \tag{6.8}$$

The adjoint of an extended quark field is required to evaluate correlation functions in Chapters 7 and 8 and is worked out in Equation O.32. The result is

$$\overline{Q}^{a}_{\alpha}(x) = \overline{q}^{a'}_{\alpha'}(x')\overline{S}^{a'a}_{\alpha'\alpha}(x', x) \tag{6.9}$$

where

$$\overline{S}^{a'a}_{\alpha'\alpha}(x', x) = \gamma^{0}_{\alpha'\beta'}\, S^{aa'*}_{\beta\beta'}(x, x')\, \gamma^{0}_{\beta\alpha}.$$

Again it is useful to introduce a matrix formulation in which

$$\overline{Q} = \overline{q}\,\overline{S} \tag{6.10}$$

and

$$\overline{S} = \gamma^{0}\, S^{\dagger}\, \gamma^{0}.$$

For the explicit calculations described in this thesis, the smearing matrix S is diagonal in the Dirac indices.[3] Therefore the above equation simplifies to $\overline{S} = S^{\dagger}$.

6.2 Iterative Algorithm

The general form for an extended quark given in Equation 6.6 is computationally expensive to achieve. However, there is a simple iterative algorithm [18] which achieves a significant reduction of excited states without too much effort. A single iteration is given by

$$Q^{(n)} = Q^{(n-1)} + \alpha \sum_{\mu=\pm 1}^{\pm D} U^{\dagger}_{\mu}(x-\mu)\, Q^{(n-1)}(x-\mu) \tag{6.11}$$

where α is a free parameter and $Q^{(i)}$ denotes the i^{th} iteration of this algorithm. Note that we have suppressed all color and Dirac indices. This iteration is applied to a

[3] We have considered the possibility of a non-trivial Dirac structure in the smearing matrix S, though we do not present this effort in this thesis.

point quark N times. After N such iterations we have contributions of the form $U^\dagger_{\mu_N} \cdots U^\dagger_{\mu_1} q(x + \mu_1 + \cdots + \mu_N)$ for all paths with length less than or equal to N lattice steps. This algorithm is parameterized by only two parameters, N and α, and it clearly does not encompass the full definition in Equation 6.6, yet it is found to be rather efficient at suppressing excited states.

There is a natural generalization of this technique. The next step would be to use the following iteration

$$\begin{aligned} Q^{(n)} &= Q^{(n-1)} + \alpha \sum_{\mu=\pm 1}^{\pm D} U^\dagger_\mu(x-\mu)\, Q^{(n-1)}(x-\mu) \\ &\quad + \beta \sum_{\mu\neq\nu=\pm 1}^{\pm D} U^\dagger_\nu(x-\mu)\, U^\dagger_\mu(x-\mu)\, Q^{(n-1)}(x-\mu-\nu). \end{aligned}$$

This iteration contains one additional free parameter β which provides additional control over the relative weights of paths that enter the smeared quark in Equation 6.6. By proceeding along these lines, that is, by adding more link patterns, with adjustable coefficients, to the iteration step, we can approach the general construction given in Equation 6.6. Certainly there is a limit in which a single iteration includes all paths and by iterating only once we would achieve the general form. (Actually there are paths of arbitrary length in the general form, so the above argument only works in an asymptotic sense.) Nonetheless, given that the simple iterative method in Equation 6.11 works surprisingly well, it would be interesting to pursue the generalizations described above.

Chapter 7

Two Point Correlation Functions

In this chapter we consider both the calculation and interpretation of nucleon two point correlation functions using the nucleon fields presented in Chapter 5. Nucleon two point functions are used to determine the nucleon mass and are essential to the calculation of nucleon matrix elements discussed in Chapter 8. We define the two point functions in position space in Section 7.1 and evaluate the fermion functional integrals in Section 7.2. We explain how to calculate the resulting quark contractions by introducing the concept of forward propagators for smeared quarks in Section 7.3. In that section we also discuss how to formulate these propagators as solutions to linear systems. We then examine parity projection and momentum projection in Sections 7.4 and 7.5 respectively. Then in Section 7.6 we evaluate the spectral representation after which we illustrate the determination of the nucleon mass in Section 7.7.

7.1 Position Space Definition

The proton two point correlation function in position space is

$$\langle\, P'_{\alpha'}(x')\,\overline{P}_{\alpha}(x)\,\rangle = \int DU_{\mu}\; e^{-S_G[U_\mu]} \int D\psi D\overline{\psi}\; e^{-S_F[\psi,\overline{\psi},U_\mu]}\; P'_{\alpha'}(x')\,\overline{P}_{\alpha}(x) \qquad (7.1)$$

where the nucleon fields,

$$\begin{aligned} P'_{\alpha'}(x') &= f_{\alpha'\beta'\gamma'\delta'}\,\epsilon_{b'c'd'}\,U'^{b'}_{\beta'}(x)\,U'^{c'}_{\gamma'}(x)\,D'^{d'}_{\delta'}(x) \\ \overline{P}_{\alpha}(x) &= \overline{D}^{d}_{\delta}(x)\,\overline{U}^{c}_{\gamma}(x)\,\overline{U}^{b}_{\beta}(x)\,\overline{\epsilon}_{dcb}\,\overline{f}_{\delta\gamma\beta\alpha}, \end{aligned}$$

are given in Equations 5.1 and 5.3 and the symbols $\overline{f}_{\delta\gamma\beta\alpha}$ and $\overline{\epsilon}_{dcb}$ are defined in Equations 5.4 and 5.5. As explained in Chapter 6, U, D, U', and D' are extended or smeared quark fields. We distinguish U from U' and D from D' to allow for different extended quarks in the proton *source* $\overline{P}_{\alpha}(x)$ or *sink* $P'_{\alpha'}(x')$.[1] We do, however, insist that (U, D) and (U', D') transform as isospin one-half doublets. Otherwise, we can not ensure that our nucleon fields similarly transform as isospin one-half doublets, and our nucleon fields would likely couple to the $J^P = \frac{1}{2}^+$ excited states of the isospin three-halves Δ^+ and Δ^0 as well.

Notice that the above integrals are well defined finite integrals on a finite volume lattice where the integration measures DU_μ and $D\psi D\overline{\psi}$ are defined in Equations 4.10 and 4.11 and the Euclidean space-time points x and x' are restricted to lattice points. The above equation also holds as a formal definition in a Euclidean or Minkowski continuum theory. This two point function can be thought of as a proton propagator, though with the understanding that since the nucleon is not a fundamental particle the choice of nucleon field is not unique.

Due to the extended nature of the quark fields U, D, U', and D', the two point function actually involves fields at numerous points on the lattice. Substituting the explicit forms for the proton fields into the expression for the two point correlation function gives

$$\begin{aligned} &\langle\, P'_{\alpha'}(x')\,\overline{P}_{\alpha}(x)\,\rangle = \\ &\quad \int DU_\mu\; e^{-S_G[U_\mu]} \int D\psi D\overline{\psi}\; e^{-S_F[\psi,\overline{\psi},U_\mu]}\; f_{\alpha'\beta'\gamma'\delta'}\,\overline{f}_{\delta\gamma\beta\alpha}\,\epsilon_{b'c'd'}\,\overline{\epsilon}_{dcb} \\ &\quad U'^{b'}_{\beta'}(x')\,U'^{c'}_{\gamma'}(x')\,D'^{d'}_{\delta'}(x')\,\overline{D}^{d}_{\delta}(x)\,\overline{U}^{c}_{\gamma}(x)\,\overline{U}^{b}_{\beta}(x). \end{aligned} \tag{7.2}$$

[1] Note that $\overline{P}_{\alpha}(x)$ creates a proton, whereas $P'_{\alpha'}(x')$ annihilates a proton. Hence the names source and sink.

The expression, in Equation 6.7, for the extended quark fields reveals that the above really is a multi point function in terms of quarks and gluons, yet we still refer to it as a two point function because all quark and gauge fields are localized near one of the two points x and x'. The distribution of quark and gluon fields about x or x' is controlled by the smearing of the quarks and is adjusted to matched the typical length scales in the nucleon which remain finite in the continuum limit.

7.2 Quark Contractions

We analytically evaluate the fermion functional integral for the nucleon two point correlation function in Equation 7.2. In Appendix L and in particular Equation L.1 we generalize Wick's theorem and show how to evaluate such fermion integrals. In short, if the quark fields in the above integrand where point quarks, in other words if we replace U and U' with u and D and D' with d, the fermion integral would simply give the contractions of the quark fields as indicated by Wick's theorem. However, the smeared quarks U, U', D, and D' are linear in the point quarks u and d, and hence the integral reduces to a sum of integrals involving point quarks. As shown in Equation L.1, this gives rise to a sum of quark contractions which can be organized into a form analogous to the case for point quarks. The result is

$$\int DU_\mu \; e^{-S_{\text{eff}}[U_\mu]} \; f_{\alpha'\beta'\gamma'\delta'} \overline{f}_{\delta\gamma\beta\alpha} \epsilon_{b'c'd'} \overline{\epsilon}_{dcb} \langle D'^{d'}_{\delta'}(x') \overline{D}^{d}_{\delta}(x) \rangle_{U_\mu} \tag{7.3}$$
$$\left(\langle U'^{b'}_{\beta'}(x') \overline{U}^{b}_{\beta}(x) \rangle_{U_\mu} \langle U'^{c'}_{\gamma'}(x') \overline{U}^{c}_{\gamma}(x) \rangle_{U_\mu} - \langle U'^{b'}_{\beta'}(x') \overline{U}^{c}_{\gamma}(x) \rangle_{U_\mu} \langle U'^{c'}_{\gamma'}(x') \overline{U}^{b}_{\beta}(x) \rangle_{U_\mu} \right)$$

where $\langle O[\psi, \overline{\psi}, U_\mu] \rangle_{U_\mu}$ denotes the expectation of $O[\psi, \overline{\psi}, U_\mu]$ for a fixed gauge field background U_μ given by

$$\langle O[\psi, \overline{\psi}, U_\mu] \rangle_{U_\mu} = \frac{\int D\psi D\overline{\psi} e^{-S_F[\psi, \overline{\psi}, U_\mu]} O[\psi, \overline{\psi}, U_\mu]}{\int D\psi D\overline{\psi} e^{-S_F[\psi, \overline{\psi}, U_\mu]}}. \tag{7.4}$$

This result is simply a generalization of Wick's theorem for extended quarks.

The final result in Equation 7.3 is commonly expressed as the sum of Feynman

Figure 7-1: Diagrams for the Two Point Function

diagrams shown in Figure 7-1. In such diagrams the flow of Euclidean time is from right to left. This is intended to mirror the time ordering of the quark fields in Equation 7.2. Note that the diagrams are drawn such that the sign of each diagram is correctly given by the number of fermion line interchanges. The ovals represent the factors of $\overline{f}$ and $\overline{\epsilon}$ for the source (right) and f and ϵ for the sink (left) and additionally represent the smearing used to construct each extended quark. Lastly, the lines represent the appropriate factors of extended quark propagators, $\langle Q'^{a'}_{\alpha'}(x')\overline{Q}^{a}_{\alpha}(x)\rangle_{U_\mu}$.

Now we use the result from Equation 4.14 to evaluate the functional integral as an average over an appropriate ensemble of gauge fields. The result is

$$\langle P'_{\alpha'}(x')\overline{P}_{\alpha}(x)\rangle = \frac{1}{N}\sum_{U^{(i)}_\mu} f_{\alpha'\beta'\gamma'\delta'}\overline{f}_{\delta\gamma\beta\alpha}\epsilon_{b'c'd'}\overline{\epsilon}_{dcb}\langle D'^{d'}_{\delta'}(x')\overline{D}^{d}_{\delta}(x)\rangle_{U^{(i)}_\mu}$$
$$\Big(\langle U'^{b'}_{\beta'}(x')\overline{U}^{b}_{\beta}(x)\rangle_{U^{(i)}_\mu}\langle U'^{c'}_{\gamma'}(x')\overline{U}^{c}_{\gamma}(x)\rangle_{U^{(i)}_\mu}$$
$$-\langle U'^{b'}_{\beta'}(x')\overline{U}^{c}_{\gamma}(x)\rangle_{U^{(i)}_\mu}\langle U'^{c'}_{\gamma'}(x')\overline{U}^{b}_{\beta}(x)\rangle_{U^{(i)}_\mu}\Big) \pm \frac{\sigma}{\sqrt{N}}$$

where σ implicitly depends on the integrand of the functional integral above. In particular it depends on the arguments of the nucleon fields. Thus the integration error is a function of $t' - t$. The above expression makes it clear that the diagrams in Figure 7-1 represent the quark propagation for a fixed gauge field background and must be evaluated for each gauge field $U^{(i)}_\mu$ in the ensemble.

Notice that we require two things to calculate the nucleon two point correlation function. First, we must construct an ensemble of gauge fields $U^{(i)}_\mu$. This aspect of the calculation is ubiquitous and the same ensemble can be used to calculate many different correlation functions. Second, we must evaluate the extended or smeared quark propagators, $\langle U^{a'}_{\alpha'}(x')\overline{U}^{a}_{\alpha}(x)\rangle_{U^{(i)}_\mu}$ and $\langle D^{a'}_{\alpha'}(x')\overline{D}^{a}_{\alpha}(x)\rangle_{U^{(i)}_\mu}$, in each of the gauge

field backgrounds $U_\mu^{(i)}$. We show how to do this in the next section.

7.3 Forward Propagators

In this section we introduce the concept of a *forward propagator*. The forward propagators are defined by

$$F^{a'a}_{\alpha'\alpha}(x', x; Q', Q, U_\mu) = \frac{\int D\psi D\overline{\psi}\; e^{-S_F[\psi,\overline{\psi},U_\mu]}\, Q'^{a'}_{\alpha'}(x')\, \overline{Q}^{a}_{\alpha}(x)}{\int D\psi D\overline{\psi}\; e^{-S_F[\psi,\overline{\psi},U_\mu]}} \tag{7.5}$$

which is precisely the extended quark propagator required to evaluate the proton two point function in Equation 7.3. The distinction between Q' and Q simply allows for different smearings to be used for each of the extended quarks in the above definition. We often suppress the dependence on the gauge field U_μ and simply write $F^{a'a}_{\alpha'\alpha}(x', x; Q', Q)$. We also introduce a matrix notation where (a, α) and (a', α') are collectively treated as matrix indices. In such a case we write $F_{Q'Q}(x', x)$. Additionally, we extend this matrix notation and consider (a, α, x) and (a', α', x') as matrix indices and simply write $F_{Q'Q}$. In Section 8.2 we explicitly need the situation in which Q or Q' is a point quark. In such cases we replace Q or Q' as appropriate with q in the above symbols.[2]

Using this notation, we can write the nucleon two point correlation function as follows.

$$\begin{aligned}
&\langle\, P'_{\alpha'}(x')\, \overline{P}_{\alpha}(x)\,\rangle = \\
&= \int DU_\mu\; e^{-S_G[U_\mu]}\, \det{}^{\mathrm{N_f}}(M[U_\mu])\, f_{\alpha'\beta'\gamma'\delta'}\, \overline{f}_{\delta\gamma\beta\alpha}\, \epsilon_{b'c'd'}\, \epsilon_{dcb} \\
&\quad F^{d'd}_{\delta'\delta}(x', x; D', D, U_\mu)\, \Big(F^{b'b}_{\beta'\beta}(x', x; U', U, U_\mu)\, F^{c'c}_{\gamma'\gamma}(x', x; U', U, U_\mu) \\
&\qquad - F^{b'c}_{\beta'\gamma}(x', x; U', U, U_\mu)\, F^{c'b}_{\gamma'\beta}(x', x; U', U, U_\mu) \Big)
\end{aligned} \tag{7.6}$$

We now show how to calculate the various forward propagators required above in terms of M_q^{-1} where M_q is the Wilson-Dirac matrix introduced in Equation 4.9. First

[2] It is common to call $F_{Q'Q}$ a *smeared-to-smeared* propagator, F_{Qq} a *point-to-smeared* propagator, F_{qQ} a *smeared-to-point* propagator, and F_{qq} a *point-to-point* propagator.

consider the point-to-point propagator F_{qq}. Using Equation 7.5 above, the point-to-point propagator is

$$F^{a'a}_{\alpha'\alpha}(x', x; q, q, U_\mu) = \frac{\int D\psi D\overline{\psi}\; e^{-S_F[\psi,\overline{\psi},U_\mu]}\; q^{a'}_{\alpha'}(x')\; \overline{q}^{a}_{\alpha}(x)}{\int D\psi D\overline{\psi}\; e^{-S_F[\psi,\overline{\psi},U_\mu]}}. \tag{7.7}$$

The fermion action is given in Equation 4.8 as

$$S_F[\psi, \overline{\psi}, U_\mu] = \sum_q \overline{q}\, M_q\, q.$$

Given that the fermion action is quadratic, the integrals in Equation 7.7 are given in terms of $\det(M_q)$ and M_q^{-1}. The result is

$$F^{a'a}_{\alpha'\alpha}(x', x; q, q, U_\mu) = \frac{\prod_f \det(M_f) \left(M_q^{-1}\right)^{a'a}_{\alpha'\alpha}(x', x)}{\prod_f \det(M_f)} = \left(M_q^{-1}\right)^{a'a}_{\alpha'\alpha}(x', x). \tag{7.8}$$

Using a matrix notation, this result can be written compactly as

$$F_{qq} = M_q^{-1}.$$

Therefore the point-to-point forward propagator is simply the inverse of the Wilson-Dirac matrix. In the next paragraph we discuss the evaluation of M_q^{-1}, and then in the following paragraph we return to the calculation of the complete smeared-to-smeared propagator.

The matrix M_q is an $N \times N$ matrix where $N = N_c \cdot N_d \cdot L^3 \cdot T$ is typically of the order of several million for contemporary lattice QCD calculations. The matrix, though extremely large, is sparse, but still there is no known technique to evaluate all the components of M_q^{-1} in a reasonable, or even unreasonable, amount of time, and even storing all the components within the memory of a computer would be an extreme task.[3] The strategy is to arrange that only a few columns or rows of M_q^{-1}

[3]This situation is not likely to change significantly even though computational power continues to grow. It will be more advantageous to use the additional computer resources in the future to perform calculations with smaller a, larger V, and lighter m_q. Thus most lattice QCD calculations will proceed to saturate computational resources for at least the near future.

are needed. For example, if we keep x fixed in the nucleon two point function in Equation 7.6 and consider point quarks, we need $F^{a'a}_{\alpha'\alpha}(x', x; q, q)$ for all a', α', and x' and for each a and α but only for a single fixed x. This corresponds to $N_c \cdot N_d$ columns of M_q^{-1}; that is, a column of M_q^{-1} for each a and α. Each column can be expressed as a solution of a linear equation. The columns of M_q^{-1} that we need are of the form $P^a_\alpha(x) = F^{ab}_{\alpha\beta}(x, y; q, q) = \left(M_q^{-1}\right)^{ab}_{\alpha\beta}(x, y)$ where we envision b, β, and y as held fixed. Similarly we introduce another column vector $S^{a'}_{\alpha'}(x') = \delta^{a'b}_{\alpha'\beta}\delta(x' - y)$ in which we again take b, β, and y as fixed. The resulting equation for the column of M_q^{-1} we want is

$$(M_q)^{a'a}_{\alpha'\alpha}(x', x) P^a_\alpha(x) = S^{a'}_{\alpha'}(x')$$

or in matrix notation

$$M_q\, P = S.$$

The above equation is a rather generic form. It is common to call any P that satisfies such an equation a *propagator* and to call the corresponding S the *source*. In the situation in which $S = 0$, the above equation is merely Dirac's equation in Euclidean space on a lattice. In the situation described above, when S vanishes everywhere except at a single point, P is the Green's function for the Dirac equation in Euclidean space, and S is referred to as a *point source*. Other choices for S will be considered shortly, and in such a case, P is simply the corresponding Green's function.

Now we express the general smeared-to-smeared propagator in terms of a solution to a similar linear system. The extended quarks fields Q' and $\overline{Q}$ are given in Equations 6.7 and 6.9.

$$\begin{aligned} Q'^a_\alpha(x) &= S'^{ab}_{\alpha\beta}(x, y)\; q^b_\beta(y) \\ \overline{Q}^a_\alpha(x) &= \overline{q}^b_\beta(y)\; \overline{S}^{ba}_{\beta\alpha}(y, x). \end{aligned}$$

We can evaluate the forward propagators in terms of the smearing matrices S' and S

and the inverse Wilson-Dirac matrix M^{-1} as follows.

$$\begin{aligned} F^{a'a}_{\alpha'\alpha}(x',x;Q',Q,U_\mu) &= \\ &= \frac{\int D\psi D\overline{\psi} e^{-S_F[\psi,\overline{\psi},U_\mu]} S'^{a'b'}_{\alpha'\beta'}(x',y') q'^{b'}_{\beta'}(y') \overline{q}^{b}_{\beta}(y) \overline{S}^{ba}_{\beta\alpha}(y,x)}{\int D\psi D\overline{\psi} e^{-S_F[\psi,\overline{\psi},U_\mu]}} \\ &= S'^{a'b'}_{\alpha'\beta'}(x',y') M^{-1}{}^{b'b}_{\beta'\beta}(y',y) \overline{S}^{ba}_{\beta\alpha}(y,x) \end{aligned} \tag{7.9}$$

Note that S' and $\overline{S}$ can depend on the gauge field U_μ yet still can be simply moved through the fermion integral as we do above. It is natural to express this result as a multiplication of matrices.

$$F_{Q'Q} = S' M_q^{-1} \overline{S} \tag{7.10}$$

where color, spin, and position indices are collectively treated as matrix indices. Using a previous result, $F_{qq} = M_q^{-1}$, we can write the above equation as

$$F_{Q'Q} = S' F_{qq} \overline{S}.$$

This last expression indicates how to calculate $F_{Q'Q}$ from F_{qq}, but, as before, computational capabilities limit us to the consideration of only a few columns of $F_{Q'Q}$. To understand how we accomplish this, first consider a point sink, i.e. the situation in which Q' is simply a point quark q. This corresponds to the case above with $S' = 1$, and therefore the smeared-to-point propagator is

$$F_{qQ} = M_q^{-1} S \tag{7.11}$$

and satisfies

$$M_q F_{qQ} = S. \tag{7.12}$$

Hence, columns of the smeared-to-point propagator can also be calculated as solutions to a linear system where now we must choose the appropriate smeared source S. Furthermore, the smeared-to-smeared propagator is given by the smeared-to-point

propagator as follows.

$$F_{Q'Q} = S' F_{qQ} \tag{7.13}$$

Notice that the above equation requires F_{qQ} for all sink indices but only a fixed choice of source indices. To see this more explicitly we rewrite the equation with all the indices expressed.

$$F^{ab}_{\alpha\beta}(x, y; Q', Q, U_\mu) = S'^{aa'}_{\alpha\alpha'}(x, x') F^{a'b}_{\alpha'\beta}(x', y; U_\mu)$$

Therefore to calculate $F^{ab}_{\alpha\beta}(x, y; Q', Q, U_\mu)$ for all a, α, and x and a fixed choice of b, β, and y, we need $F^{a'b}_{\alpha'\beta}(x', y; q, Q, U_\mu)$ for all a', α', and x' and only the *same* fixed b, β, and y. Therefore a column of the complete smeared-to-smeared propagator $F_{Q'Q}$ can be calculated by solving a linear system for the corresponding column of F_{qQ} and multiplying this column by the smearing matrix S'.

With the ability to calculate forward propagators, we return to the discussion of the nucleon two point function given in Equations 7.1 and 7.6. Translational invariance implies that

$$\langle P'_{\alpha'}(x') \overline{P}_\alpha(x) \rangle = \langle P'_{\alpha'}(x' - x) \overline{P}_\alpha(0) \rangle.$$

Therefore, without loss of generality, we can calculate the complete nucleon two point correlation function with a fixed choice of x, and hence we require the forward smeared-to-smeared propagators at all a', α', and x' and all a and α but only at a single fixed x. As discussed above, this implies that we only need to solve $\mathrm{N_c} \cdot \mathrm{N_d}$ appropriate linear equations for each gauge field in the ensemble $U^{(i)}_\mu$.

7.4 Parity Projection

At this point we consider a technical point raised in Section 5.3. It is stated in that section that parity projection at the level of the quarks reduces the computational effort required for our calculation by half. As we show in that section, parity projec-

tion of the quarks creates a nucleon field with $f_{\alpha\beta\gamma\delta}$ that vanishes if any index, α, β, γ, or δ, takes values of 3 or 4. (Our convention is that Dirac indices take values 1, 2, 3, and 4.) By examining the integrand in Equation 7.6 for the proton two point function, we find that the Dirac indices appear in the combination

$$f_{\alpha'\beta'\gamma'\delta'}\,\overline{f}_{\delta\gamma\beta\alpha}\,F_{\delta'\delta}\,(F_{\beta'\beta}\,F_{\gamma'\gamma}-F_{\beta'\gamma}\,F_{\gamma'\beta})$$

where we suppress all color and lattice indices and retain only the portion of the integrand involving the Dirac indices explicitly. Therefore we only need $F^{a'a}_{\alpha'\alpha}(x',x,Q',Q)$ for $\alpha=1$ and 2 and not for $\alpha=3$ and 4. Consequently, we need to solve the linear system in Equation 7.12 for each a but only for $\alpha=1$ and 2. The net result is a reduction, by half, of the number of forward propagators required to calculate the nucleon two point correlation function. We show a similar effect for the three point function in Section 8.4.

7.5 Momentum Projection

The states of a quantum field theory are labelled by momenta not position, hence, as discussed in Section 7.6 on spectral representations, it is ultimately more fruitful to consider the nucleon two point correlation function in momentum space not position space. Given the position space definition for the two point function $\langle\, P'_{\alpha'}(x')\,\overline{P}_{\alpha}(x)\,\rangle$ in Equation 7.1, the momentum space two point correlation function is simply

$$\langle\, P'_{\alpha'}(t',\vec{p}')\,\overline{P}_{\alpha}(t,\vec{p})\,\rangle=\int d^3\vec{x}'\int d^3\vec{x}\;e^{-i\vec{p}'\cdot\vec{x}'}\,e^{i\vec{p}\cdot\vec{x}}\,\langle\, P'_{\alpha'}(t',\vec{x}')\,\overline{P}_{\alpha}(t,\vec{x})\,\rangle \qquad (7.14)$$

where we introduce the momentum projected proton field $P_{\alpha}(t,\vec{p})$ given by

$$P_{\alpha}(t,\vec{p})=\int d^3\vec{x}\;e^{-i\vec{p}\cdot\vec{x}}\,P_{\alpha}(t,\vec{x}).$$

There is, of course, the corresponding definition for $\overline{P}_\alpha(t,\vec{p})$,

$$\overline{P}_\alpha(t,\vec{p}) = \int d^3\vec{x}\; e^{i\vec{p}\cdot\vec{x}}\,\overline{P}_\alpha(t,\vec{x}).$$

In particular, the signs of $\vec{p}'$ and $\vec{p}$ in Equation 7.14 above are correctly accounted for by the proper definitions of $P_\alpha(t,\vec{p})$ and $\overline{P}_\alpha(t,\vec{p})$.

Translation invariance ensures momentum conservation in the momentum space two point function in Equation 7.14.[4] The consequences of momentum conservation for this two point function are determined in Appendix O.14. The result from Equation O.35 in that appendix is

$$\langle\, P'_{\alpha'}(t',\vec{p}')\,\overline{P}_\alpha(t,\vec{p})\,\rangle = (2\pi)^3\,\delta^3\,(\vec{p}'-\vec{p})\;\langle\, P'_{\alpha'}(t',\vec{p}')\,\overline{P}_\alpha(t,\vec{x}=\vec{0})\,\rangle \tag{7.15}$$

which relates the *momentum-momentum* two point correlation function to the *momentum-position* two point function. The momentum conserving δ function is merely a kinematical consequence of translation invariance, whereas all dynamical content is encoded in the mixed momentum and position correlation function

$$\begin{aligned} C^{(2)}_{\alpha'\alpha}(t',\vec{p}';t,\vec{x}) &= \\ &= \langle\, P'_{\alpha'}(t',\vec{p}')\,\overline{P}_\alpha(t,\vec{x})\,\rangle \\ &= \int d^3\vec{x}'\; e^{-i\vec{p}'\cdot\vec{x}'}\,\langle\, P_{\alpha'}(t',\vec{x}')\,\overline{P}_\alpha(t,\vec{x})\,\rangle. \end{aligned} \tag{7.16}$$

Therefore in the remainder of this thesis we consider solely this mixed representation correlation function which we simply call the momentum projected two point function.

7.6 Spectral Representation

To determine the hadronic content of the momentum projected two point correlation function defined in Equation 7.16, we examine the corresponding spectral representation. It is convient to calculate a basis independent correlation function by contracting

[4] This is not strictly true for Dirichlet boundary conditions.

Γ	$\mathrm{tr}\left(\Gamma\left(p\cdot\gamma+m_N\right)\right)$
1	$4m_N$
$\left(\frac{1+\gamma^5 s\cdot\gamma}{2}\right)$	$2m_N$
$\left(\frac{1+\gamma^0}{2}\right)\left(\frac{1+\gamma^5 s\cdot\gamma}{2}\right)\left(\frac{1+\gamma^0}{2}\right)$	$E_{\vec{p}}^N+m_N$

Table 7.1: Traces for Two Point Functions

the Dirac indices α and α' in Equation 7.16 with a spin matrix Γ. Therefore we define

$$C_\Gamma^{(2)}(t',\vec{p}';t,\vec{x}) = \Gamma^{\alpha\alpha'} C_{\alpha'\alpha}^{(2)}(t',\vec{p}';t,\vec{x}). \tag{7.17}$$

The spectral representations for $C_{\alpha'\alpha}^{(2)}$ and $C_\Gamma^{(2)}$ are determined in Appendix O.15. The results from Equations O.36 and O.37 are

$$C_{\alpha'\alpha}^{(2)}(t',\vec{p}';t,\vec{x}) = \sum_N \frac{|Z_N|^2}{2E_{\vec{p}'}^N} e^{-E_{\vec{p}'}^N(t'-t)} e^{-i\vec{p}'\cdot\vec{x}} \left(p'_N\cdot\gamma+m_N\right)_{\alpha'\alpha} \tag{7.18}$$

and

$$C_\Gamma^{(2)}(t',\vec{p}';t,\vec{x}) = \sum_N \frac{|Z_N|^2}{2E_{\vec{p}'}^N} e^{-E_{\vec{p}'}^N(t'-t)} e^{-i\vec{p}'\cdot\vec{x}} \,\mathrm{tr}\left(\Gamma\left(p'_N\cdot\gamma+m_N\right)\right) \tag{7.19}$$

where we explicitly assume $t' > t$. Additionally, N labels the states with the quantum numbers of the proton and p_N is the on-shell four momentum for the N^{th} state, $p_N^2 = m_N^2$. There are several common choices for Γ. The resulting traces are collected in Table 7.1. The spectral representations in either Equations 7.18 or 7.19 are used to determine the nucleon mass in the next section.

7.7 Nucleon Mass

The mass spectrum of the nucleon is calculated using the proton two point correlation functions given in Equation 7.17. In this thesis we are only interested in the ground state nucleon, hence this discussion is limited to just that case.[5] The simplest strategy

[5]However, the determination of the excited state spectrum is a challenging and illuminating calculation of its own.

to calculate the proton mass is to study the correlation function for large Euclidean times. Using the spectral representation for $C_\Gamma^{(2)}$ given in Equation 7.19, the large Euclidean time limit is

$$\lim_{t'\to\infty} C_\Gamma^{(2)}(t',\vec{p}';t,\vec{x}) = \frac{|Z|^2}{2E_{\vec{p}'}}\, e^{-E_{\vec{p}'}(t'-t)}\, e^{-i\vec{p}'\cdot\vec{x}}\, \mathrm{tr}\left(\Gamma\left(p'\cdot\gamma + m\right)\right) \tag{7.20}$$

where the quantities in the above equation all refer to the nucleon ground state and thus the label N has been dropped. Additionally, the equal sign in the above expression implies equality only asymptotically[6] because clearly the right hand side of Equation 7.20 vanishes for $t' \to \infty$. This suggests studying the effective energy defined by

$$E_{\vec{p}'}^{\mathrm{eff}}(t') = \ln\left(\frac{C_\Gamma^{(2)}(t',\vec{p}';t,\vec{x})}{C_\Gamma^{(2)}(t'+1,\vec{p}';t,\vec{x})}\right).$$

Using the result from Equation 7.20, it is straight forward to show that

$$\lim_{t'\to\infty} E_{\vec{p}'}^{\mathrm{eff}}(t') = E_{\vec{p}'}$$

where $E_{\vec{p}'}$ is the ground state nucleon energy at the momentum $\vec{p}'$. For the particular choice $\vec{p}' = \vec{0}$, the effective energy defined above is usually referred to as the effective mass and written as

$$m^{\mathrm{eff}}(t') = E_{\vec{p}'=\vec{0}}^{\mathrm{eff}}(t')$$

and has the limit

$$\lim_{t'\to\infty} m^{\mathrm{eff}}(t') = m$$

where m is the ground state nucleon mass.

There are two difficulties with this strategy. Lattice calculations are performed with a finite time extent T which prevents the formal evaluation of this limit. More important is that the fractional error in the numerical calculation of the correlation

[6]Two expressions, $A(t)$ and $B(t)$, are asymptotically equal for $t \to \infty$ if

$$\lim_{t\to\infty} \frac{A(t)}{B(t)} = 1.$$

function grows with the time separation, $t' - t$. This reduces the practically accessible time extent of a lattice calculation. This limitation suggests considering a technique which can utilize the two point correlation function at shorter distances where the fractional errors are smallest. However, this is precisely the regime in which excited states are most prominent. Thus, even though we only need to determine the ground state mass, we allow for excited states to capitalize on the smaller fractional errors of the correlation function at shorter time separations. The ground state for the nucleon is a discrete state and the lowest excited states are narrow. This suggests fitting the two point correlation function to the functional form given by the spectral representation in Equation 7.19 but only including a few discrete states rather than the complete spectrum. The resulting functional form is

$$C_{\Gamma}^{(2)}(t', \vec{p}'; t, \vec{x}) = \sum_{N} A_{\Gamma}^{N}(\vec{p}', \vec{x}) e^{-E_{\vec{p}'}^{N}(t'-t)}$$

where the summation over N is restricted to a small number of excited states. The nucleon masses calculated this way are collected in Table 9.1.

Chapter 8

Three Point Correlation Functions

Three point correlation functions are used to determine nucleon matrix elements as sketched in Section 4.5. In this thesis we calculate the nucleon matrix elements of the twist two operators in order to evaluate the generalized form factors for the nucleon. The physical observables that are determined by the generalized form factors are discussed in Chapter 2, and correspondingly a selection of our results is presented in Chapter 9. In this chapter we consider an arbitrary two quark operator and present the details of our calculations of the three point functions and the corresponding nucleon matrix elements.

In Section 8.1 we define the three point functions in position space. Then in Section 8.2 we evaluate the fermion functional integrals. The resulting quark contractions are expressed in terms of the so-called backward propagators in Section 8.3. Next we examine parity and momentum projection in Sections 8.4 and 8.5 respectively. Then in Section 8.6 we define the basic correlation functions used in our calculations which we call the *building blocks*. Finally we introduce the spectral representation in Section 8.7 and use it to determine the nucleon matrix elements in Section 8.8.

8.1 Position Space Definition

The proton three point correlation function[1] in position space is

$$\begin{aligned} &\langle\, P'_{\alpha'}(x')\,\overline{q}^{e}_{\epsilon}(y)\,O^{ee'}_{\epsilon\epsilon'}(y,y')\,q^{e'}_{\epsilon'}(y')\,\overline{P}_{\alpha}(x)\,\rangle = \\ &= \int DU_\mu\; e^{-S_G[U_\mu]} \int D\psi D\overline{\psi}\; e^{-S_F[\psi,\overline{\psi},U_\mu]}\; P'_{\alpha'}(x')\,\overline{q}^{e}_{\epsilon}(y)\,O^{ee'}_{\epsilon\epsilon'}(y,y')\,q^{e'}_{\epsilon'}(y')\,\overline{P}_{\alpha}(x) \end{aligned} \tag{8.1}$$

where the nucleon fields are given in Equations 5.1 and 5.3 as

$$\begin{aligned} P'_{\alpha'}(x') &= f_{\alpha'\beta'\gamma'\delta'}\,\epsilon_{b'c'd'}\,U'^{b'}_{\beta'}(x')\,U'^{c'}_{\gamma'}(x')\,D'^{d'}_{\delta'}(x') \\ \overline{P}_{\alpha}(x) &= \overline{D}^{d}_{\delta}(x)\,\overline{U}^{c}_{\gamma}(x)\,\overline{U}^{b}_{\beta}(x)\,\overline{\epsilon}_{dcb}\,\overline{f}_{\delta\gamma\beta\alpha}, \end{aligned}$$

and the operator is determined by $O^{ee'}_{\epsilon\epsilon'}(y,y')$ which is of the form

$$O^{ee'}_{\epsilon\epsilon'}(y,y') = \Gamma_{\epsilon\epsilon'}\left(U^{\dagger}_{\mu_n}(y'+\mu_1+\cdots+\mu_{n-1})\cdots U^{\dagger}_{\mu_2}(y'+\mu_1)\,U^{\dagger}_{\mu_1}(y')\right)^{ee'} \tag{8.2}$$

where $y = y'+\mu_1+\cdots+\mu_n$ and Γ is an arbitrary $\mathrm{N_d}\times\mathrm{N_d}$ spin matrix. Additionally, in the operator $q = u$ or d are point quarks. The string of gauge links $U^{\dagger}_{\mu_i}$ forms a Wilson line starting at y', traversing a path determined by $\mu_1, \ldots, \mu_n$, and terminating at y. This Wilson line ensures that the operator is gauge invariant.

The fields, U, U', D, and D', appearing in the proton source and sink are extended quark fields as described in Chapter 6, whereas the fields in the operator, u and d, are point quark fields. Remember we have significant freedom in constructing the nucleon fields. The only constraint is that P' and $\overline{P}$ couple sufficiently well to the proton state. However, the operators must eventually be renormalized and matched to continuum operators usually in the $\overline{MS}$ scheme. There still is flexibility in constructing operators, but given the complications involved in calculating the matching coefficients we use the simplest operators with the correct continuum limit

[1] We commonly refer to the correlation function in Equation 8.1 as the proton or nucleon three point function; however this is a slight misnomer. Only two of the three fields in this correlation function are protons. The third is always a two quark operator of some kind.

and with sufficient symmetry to avoid mixing with lower dimensional operators.[2] It is worth repeating that the above functional integrals are lattice regulated finite integrals, the integration measures DU_μ and $D\psi D\overline{\psi}$ are given in Equations 4.10 and 4.11 respectively, and x, x', y, and y' are restricted to lattice points. As written, the above equation is also a formal relationship in continuum QCD for both Euclidean and Minkowski space-times.

The operator $\overline{q}^e_\epsilon(y)\, O^{ee'}_{\epsilon\epsilon'}(y,y')\, q^{e'}_{\epsilon'}(y')$ contains quark and gluon fields separated by a number of lattice spacings, and the proton fields additionally contained quark and gluon fields distributed within the smeared quarks, yet we refer to Equation 8.1 as a three point function. We discuss the extended nature of P' and $\overline{P}$ in Section 7.2. There we note that the relevant length scales for the nucleon fields are controlled by typical hadronic length scales and remain finite in the continuum limit. In contrast, the fields in the operators extend over a fixed number of lattice spacings only, and hence these operators reduce to point operators in the continuum limit. Therefore the quark and gluon fields in Equation 8.1 cluster around any of three points, and hence we call these correlation functions three point functions.

Now substitute the expressions for the nucleon fields, P' and $\overline{P}$. The resulting three point correlation function is

$$\begin{aligned} &\langle\, P'_{\alpha'}(x')\, \overline{q}^e_\epsilon(y)\, O^{ee'}_{\epsilon\epsilon'}(y,y')\, q^{e'}_{\epsilon'}(y')\, \overline{P}_\alpha(x)\,\rangle = \qquad (8.3)\\ &= \int DU_\mu\; e^{-S_G[U_\mu]} \int D\psi D\overline{\psi}\; e^{-S_F[\psi,\overline{\psi},U_\mu]}\; f_{\alpha'\beta'\gamma'\delta'}\, \overline{f}_{\delta\gamma\beta\alpha}\, \epsilon_{b'c'd'}\, \overline{\epsilon}_{dcb}\, O^{ee'}_{\epsilon\epsilon'}(y,y') \\ &\quad U'^{b'}_{\beta'}(x')\, U'^{c'}_{\gamma'}(x')\, D'^{d'}_{\delta'}(x')\, \overline{q}^e_\epsilon(y)\, q^{e'}_{\epsilon'}(y')\, \overline{D}^d_\delta(x)\, \overline{U}^c_\gamma(x)\, \overline{U}^b_\beta(x). \end{aligned}$$

Notice in particular that $O^{ee'}_{\epsilon\epsilon'}(y,y')$ can be taken outside of the quark integral, and hence the choice of $O^{ee'}_{\epsilon\epsilon'}(y,y')$ does not affect the evaluation of the quark functional integral. As we show in the next two sections, this observation allows us to calculate all non-singlet two quark operators in terms of a basic set of correlation functions

[2]The flexibility in constructing operators is used when creating improved operators. As our calculations currently use the unimproved Wilson action we do not discuss improved operators.

which we call the building blocks.[3] In particular, the incremental computational effort required to calculate one additional operator is a small fraction of the effort necessary to calculate the first operator.

8.2 Quark Contractions

The fermion functional integral in Equation 8.3 for the three point function can be evaluated analytically. Given that the fermion action is quadratic, if we replaced each extended quark in Equation 8.3 with the corresponding point quark then we could calculate the fermion functional integral using Wick's theorem. The result would be the sum of all possible quark contractions. However, the quark fields in P' and $\overline{P}$ are extended quark fields. In Appendix L, we generalize Wick's theorem to account for extended quarks as well as point quarks. The resulting generalized Wick's theorem is given in Equation L.1 and simply states that Wick's theorem continues to hold for smeared quarks with the one requirement that all quark propagators must be replaced with the appropriate smeared-to-smeared forward propagators discussed in Section 7.3.

Therefore in the remainder of this section we determine the quark contractions which contribute to the three point functions in Equation 8.3. The contractions differ for operators of the form $\overline{d}^e_\epsilon(y)\, d^{e'}_{\epsilon'}(y')$ and $\overline{u}^e_\epsilon(y)\, u^{e'}_{\epsilon'}(y')$, so we discuss each separately in the following two subsections.[4]

8.2.1 U Quark Contractions

The proton three point function for operators of the form $\overline{u}^e_\epsilon(y)\, O^{ee'}_{\epsilon\epsilon'}(y,y')\, u^{e'}_{\epsilon'}(y')$ is given by Equation 8.3 with the replacement $q \rightarrow u$. The resulting correlation function

[3] Actually we can calculate the *connected* contributions to all two quark operators in terms of the building blocks. However it is only the non-singlet operators for which the *disconnected* diagrams do not contribute. (Connected and disconnected contributions are explained in the Section 8.2.)

[4] Even though we present the u quark contractions before the d quark contractions, it may be easier to understand the d quark case first.

is given below.

$$\langle\, P'_{\alpha'}(x')\,\overline{u}^{e}_{\epsilon}(y)\,O^{ee'}_{\epsilon\epsilon'}(y,y')\,u^{e'}_{\epsilon'}(y')\,\overline{P}_{\alpha}(x)\,\rangle = \tag{8.4}$$

$$= \int DU_\mu\; e^{-S_G[U_\mu]} \int D\psi D\overline{\psi}\; e^{-S_F[\psi,\overline{\psi},U_\mu]}\; f_{\alpha'\beta'\gamma'\delta'}\,\overline{f}_{\delta\gamma\beta\alpha}\,\epsilon_{b'c'd'}\,\overline{\epsilon}_{dcb}\,O^{ee'}_{\epsilon\epsilon'}(y,y')$$

$$U'^{b'}_{\beta'}(x')\,U'^{c'}_{\gamma'}(x')\,D'^{d'}_{\delta'}(x')\,\overline{u}^{e}_{\epsilon}(y)\,u^{e'}_{\epsilon'}(y')\,\overline{D}^{d}_{\delta}(x)\,\overline{U}^{c}_{\gamma}(x)\,\overline{U}^{b}_{\beta}(x)$$

As discussed in the beginning of this section, the fermion functional integrals can be evaluated using the generalized Wick's theorem in Equation L.1. The result is

$$\int DU_\mu\; e^{-S_{\rm eff}[U_\mu]}\; f_{\alpha'\beta'\gamma'\delta'}\,\overline{f}_{\delta\gamma\beta\alpha}\,\epsilon_{b'c'd'}\,\overline{\epsilon}_{dcb}\,O^{ee'}_{\epsilon\epsilon'}(y,y')\,\langle\, D'^{d'}_{\delta'}(x')\,\overline{D}^{d}_{\delta}(x)\,\rangle_{U_\mu} \tag{8.5}$$

$$\Big[\langle\, u^{e'}_{\epsilon'}(y')\,\overline{U}^{c}_{\gamma}(x)\,\rangle_{U_\mu}\langle\, U'^{c'}_{\gamma'}(x')\,\overline{u}^{e}_{\epsilon}(y)\,\rangle_{U_\mu}\langle\, U'^{b'}_{\beta'}(x')\,\overline{U}^{b}_{\beta}(x)\,\rangle_{U_\mu}$$

$$-\langle\, u^{e'}_{\epsilon'}(y')\,\overline{U}^{c}_{\gamma}(x)\,\rangle_{U_\mu}\langle\, U'^{c'}_{\gamma'}(x')\,\overline{U}^{b}_{\beta}(x)\,\rangle_{U_\mu}\langle\, U'^{b'}_{\beta'}(x')\,\overline{u}^{e}_{\epsilon}(y)\,\rangle_{U_\mu}$$

$$-\langle\, u^{e'}_{\epsilon'}(y')\,\overline{U}^{b}_{\beta}(x)\,\rangle_{U_\mu}\langle\, U'^{c'}_{\gamma'}(x')\,\overline{u}^{e}_{\epsilon}(y)\,\rangle_{U_\mu}\langle\, U'^{b'}_{\beta'}(x')\,\overline{U}^{c}_{\gamma}(x)\,\rangle_{U_\mu}$$

$$+\langle\, u^{e'}_{\epsilon'}(y')\,\overline{U}^{b}_{\beta}(x)\,\rangle_{U_\mu}\langle\, U'^{c'}_{\gamma'}(x')\,\overline{U}^{c}_{\gamma}(x)\,\rangle_{U_\mu}\langle\, U'^{b'}_{\beta'}(x')\,\overline{u}^{e}_{\epsilon}(y)\,\rangle_{U_\mu}$$

$$-\langle\, u^{e'}_{\epsilon'}(y')\,\overline{u}^{e}_{\epsilon}(y)\,\rangle_{U_\mu}\langle\, U'^{c'}_{\gamma'}(x')\,\overline{U}^{c}_{\gamma}(x)\,\rangle_{U_\mu}\langle\, U'^{b'}_{\beta'}(x')\,\overline{U}^{b}_{\beta}(x)\,\rangle_{U_\mu}$$

$$+\langle\, u^{e'}_{\epsilon'}(y')\,\overline{u}^{e}_{\epsilon}(y)\,\rangle_{U_\mu}\langle\, U'^{c'}_{\gamma'}(x')\,\overline{U}^{b}_{\beta}(x)\,\rangle_{U_\mu}\langle\, U'^{b'}_{\beta'}(x')\,\overline{U}^{c}_{\gamma}(x)\,\rangle_{U_\mu}\Big]$$

where we use the notation $\langle O[\psi,\overline{\psi},U_\mu]\rangle_{U_\mu}$ from Equation 7.4 and each pair of quark fields within brackets denotes the appropriate forward propagator. Notice that all four types of forward propagators appear in Equation 8.5: smeared-to-smeared, smeared-to-point, point-to-smeared, and point-to-point. We can express this result as the sum of Feynman diagrams shown in Figures 8-1 and 8-2. Note that the diagrams are drawn such that the sign of each diagram is correctly given by the number of fermion line interchanges and the number of closed fermion loops. The diagrams in Figure 8-1 are called connected diagrams by which we mean that the u and $\overline{u}$ quark fields in the operator are each contracted with quark fields in the nucleon source or sink. These four diagrams, as read from right to left and from top to bottom, correspond to the

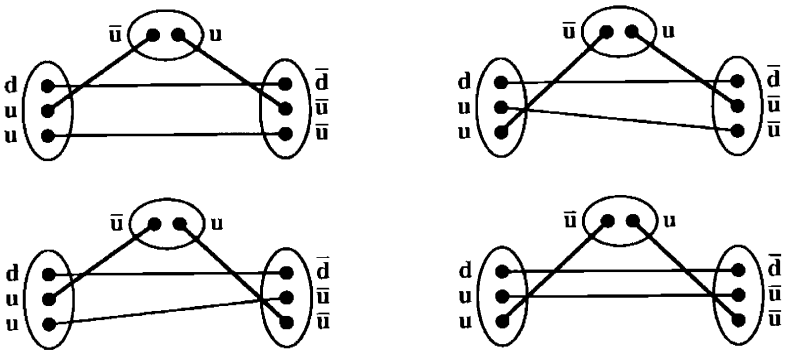

Figure 8-1: Connected U Quark Diagrams for the Three Point Function

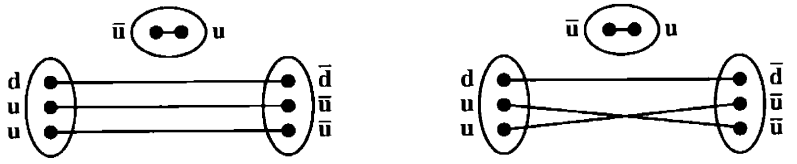

Figure 8-2: Disconnected U Quark Diagrams for the Three Point Function

first four terms in Equation 8.5. The diagrams in Figure 8-2 are called disconnected diagrams. By this we mean that the u and $\overline{u}$ fields in the operator contract with each other. These two diagrams, again as read from right to left, correspond to the last two terms in Equation 8.5. Remember that these diagrams are quark diagrams in a fixed gauge field background, and that the phrases connected or disconnected refer to the quark lines only because the functional integral of the gauge field generates all gluon interactions which, perturbatively speaking, dresses the quark diagrams with gluons connecting the quark lines in all possible ways.

In Section 8.3 we describe an algorithmic trick to efficiently calculate the connected diagrams. However, no such similar method exists for the disconnected diagrams, and furthermore, the direct evaluation of the disconnected diagrams is practically impossible. There are other methods for evaluating the disconnected contributions: stochastic estimators, wall source techniques, or eigenvalue methods, but the determination of the disconnected diagrams remains a difficult problem. Fortunately, the disconnected contributions cancel for non-singlet flavor combinations of observables. Hence we now separate the quark contractions in Equation 8.5 into the quark connected piece

labelled "qc" and the quark disconnected piece labelled "qd". The connected part of the three point function in Equation 8.5 is

$$\langle\, P'_{\alpha'}(x')\,\overline{u}^{e}_{\epsilon}(y)\,O^{ee'}_{\epsilon\epsilon'}(y,y')\,u^{e'}_{\epsilon'}(y')\,\overline{P}_{\alpha}(x)\,\rangle_{\rm qc} = \tag{8.6}$$

$$\int DU_\mu\; e^{-S_{\rm eff}[U_\mu]}\; f_{\alpha'\beta'\gamma'\delta'}\,\overline{f}_{\delta\gamma\beta\alpha}\,\epsilon_{b'c'd'}\,\overline{\epsilon}_{dcb}\,O^{ee'}_{\epsilon\epsilon'}(y,y')\,\langle\, D'^{d'}_{\delta'}(x')\,\overline{D}^{d}_{\delta}(x)\,\rangle_{U^{(i)}_\mu}$$

$$\Big[\langle\, u^{e'}_{\epsilon'}(y')\,\overline{U}^{c}_{\gamma}(x)\,\rangle_{U_\mu}\langle\, U'^{c'}_{\gamma'}(x')\,\overline{u}^{e}_{\epsilon}(y)\,\rangle_{U_\mu}\langle\, U'^{b'}_{\beta'}(x')\,\overline{U}^{b}_{\beta}(x)\,\rangle_{U_\mu}$$

$$-\langle\, u^{e'}_{\epsilon'}(y')\,\overline{U}^{c}_{\gamma}(x)\,\rangle_{U_\mu}\langle\, U'^{c'}_{\gamma'}(x')\,\overline{U}^{b}_{\beta}(x)\,\rangle_{U_\mu}\langle\, U'^{b'}_{\beta'}(x')\,\overline{u}^{e}_{\epsilon}(y)\,\rangle_{U_\mu}$$

$$-\langle\, u^{e'}_{\epsilon'}(y')\,\overline{U}^{b}_{\beta}(x)\,\rangle_{U_\mu}\langle\, U'^{c'}_{\gamma'}(x')\,\overline{u}^{e}_{\epsilon}(y)\,\rangle_{U_\mu}\langle\, U'^{b'}_{\beta'}(x')\,\overline{U}^{c}_{\gamma}(x)\,\rangle_{U_\mu}$$

$$+\langle\, u^{e'}_{\epsilon'}(y')\,\overline{U}^{b}_{\beta}(x)\,\rangle_{U_\mu}\langle\, U'^{c'}_{\gamma'}(x')\,\overline{U}^{c}_{\gamma}(x)\,\rangle_{U_\mu}\langle\, U'^{b'}_{\beta'}(x')\,\overline{u}^{e}_{\epsilon}(y)\,\rangle_{U_\mu}\Big]\,,$$

and the disconnected part of the three point function is

$$\langle\, P'_{\alpha'}(x')\,\overline{u}^{e}_{\epsilon}(y)\,O^{ee'}_{\epsilon\epsilon'}(y,y')\,u^{e'}_{\epsilon'}(y')\,\overline{P}_{\alpha}(x)\,\rangle_{\rm qd} = \tag{8.7}$$

$$\int DU_\mu\; e^{-S_{\rm eff}[U_\mu]}\; f_{\alpha'\beta'\gamma'\delta'}\,\overline{f}_{\delta\gamma\beta\alpha}\,\epsilon_{b'c'd'}\,\overline{\epsilon}_{dcb}\,O^{ee'}_{\epsilon\epsilon'}(y,y')\,\langle\, D'^{d'}_{\delta'}(x')\,\overline{D}^{d}_{\delta}(x)\,\rangle_{U^{(i)}_\mu}$$

$$\Big[-\langle\, u^{e'}_{\epsilon'}(y')\,\overline{u}^{e}_{\epsilon}(y)\,\rangle_{U_\mu}\langle\, U'^{c'}_{\gamma'}(x')\,\overline{U}^{c}_{\gamma}(x)\,\rangle_{U_\mu}\langle\, U'^{b'}_{\beta'}(x')\,\overline{U}^{b}_{\beta}(x)\,\rangle_{U_\mu}$$

$$+\langle\, u^{e'}_{\epsilon'}(y')\,\overline{u}^{e}_{\epsilon}(y)\,\rangle_{U_\mu}\langle\, U'^{c'}_{\gamma'}(x')\,\overline{U}^{b}_{\beta}(x)\,\rangle_{U_\mu}\langle\, U'^{b'}_{\beta'}(x')\,\overline{U}^{c}_{\gamma}(x)\,\rangle_{U_\mu}\Big]\,.$$

8.2.2 D Quark Contractions

We repeat the previous calculation in Section 8.2.1 now for the case of the d quark. In the following we present only the results and refer to Section 8.2.1 for the detailed explanations. The proton three point function corresponding to operators of the form $\overline{d}^{e}_{\epsilon}(y)\,O^{ee'}_{\epsilon\epsilon'}(y,y')\,d^{e'}_{\epsilon'}(y')$ is given by

$$\langle\, P'_{\alpha'}(x')\,\overline{d}^{e}_{\epsilon}(y)\,O^{ee'}_{\epsilon\epsilon'}(y,y')\,d^{e'}_{\epsilon'}(y')\,\overline{P}_{\alpha}(x)\,\rangle = \tag{8.8}$$

$$= \int DU_\mu\; e^{-S_G[U_\mu]}\int D\psi D\overline{\psi}\; e^{-S_F[\psi,\overline{\psi},U_\mu]}\; f_{\alpha'\beta'\gamma'\delta'}\,\overline{f}_{\delta\gamma\beta\alpha}\,\epsilon_{b'c'd'}\,\overline{\epsilon}_{dcb}\,O^{ee'}_{\epsilon\epsilon'}(y,y')$$

$$U'^{b'}_{\beta'}(x')\,U'^{c'}_{\gamma'}(x')\,D'^{d'}_{\delta'}(x')\,\overline{d}^{e}_{\epsilon}(y)\,d^{e'}_{\epsilon'}(y')\,\overline{D}^{d}_{\delta}(x)\,\overline{U}^{c}_{\gamma}(x)\,\overline{U}^{b}_{\beta}(x)$$

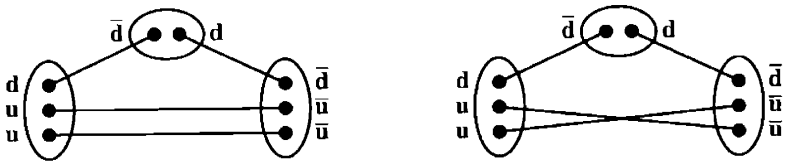

Figure 8-3: Connected D Quark Diagrams for the Three Point Function

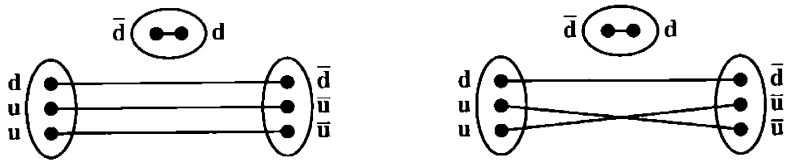

Figure 8-4: Disconnected D Quark Diagrams for the Three Point Function

where we use Equation 8.3 in which we replace q with d. As described in the beginning of this section, the quark integrals in Equation 8.8 above can be evaluated using our generalization of Wick's theorem which is stated in Equation L.1 and gives

$$\int DU_\mu \; e^{-S_{\text{eff}}[U_\mu]} \; f_{\alpha'\beta'\gamma'\delta'} \, \overline{f}_{\delta\gamma\beta\alpha} \, \epsilon_{b'c'd'} \, \overline{\epsilon}_{dcb} \, O^{ee'}_{\epsilon\epsilon'}(y,y') \tag{8.9}$$

$$\Big[\langle D'^{d'}_{\delta'}(x') \, \overline{d}^{e}_{\epsilon}(y) \rangle_{U_\mu} \langle d^{e'}_{\epsilon'}(y') \, \overline{D}^{d}_{\delta}(x) \rangle_{U_\mu} \langle U'^{b'}_{\beta'}(x') \, \overline{U}^{b}_{\beta}(x) \rangle_{U_\mu} \langle U'^{c'}_{\gamma'}(x') \, \overline{U}^{c}_{\gamma}(x) \rangle_{U_\mu}$$

$$- \langle D'^{d'}_{\delta'}(x') \, \overline{d}^{e}_{\epsilon}(y) \rangle_{U_\mu} \langle d^{e'}_{\epsilon'}(y') \, \overline{D}^{d}_{\delta}(x) \rangle_{U_\mu} \langle U'^{b'}_{\beta'}(x') \, \overline{U}^{c}_{\gamma}(x) \rangle_{U_\mu} \langle U'^{c'}_{\gamma'}(x') \, \overline{U}^{b}_{\beta}(x) \rangle_{U_\mu}$$

$$- \langle D'^{d'}_{\delta'}(x') \, \overline{D}^{d}_{\delta}(x) \rangle_{U_\mu} \langle d^{e'}_{\epsilon'}(y') \, \overline{d}^{e}_{\epsilon}(y) \rangle_{U_\mu} \langle U'^{b'}_{\beta'}(x') \, \overline{U}^{b}_{\beta}(x) \rangle_{U_\mu} \langle U'^{c'}_{\gamma'}(x') \, \overline{U}^{c}_{\gamma}(x) \rangle_{U_\mu}$$

$$+ \langle D'^{d'}_{\delta'}(x') \, \overline{D}^{d}_{\delta}(x) \rangle_{U_\mu} \langle d^{e'}_{\epsilon'}(y') \, \overline{d}^{e}_{\epsilon}(y) \rangle_{U_\mu} \langle U'^{b'}_{\beta'}(x') \, \overline{U}^{c}_{\gamma}(x) \rangle_{U_\mu} \langle U'^{c'}_{\gamma'}(x') \, \overline{U}^{b}_{\beta}(x) \rangle_{U_\mu} \Big]$$

where the notation $\langle O[\psi, \overline{\psi}, U_\mu] \rangle_{U_\mu}$ is given in Equation 7.4 and the bracketed pairs of quark fields indicate the corresponding forward propagators. This result is represented as the sum of Feynman diagrams given in Figures 8-3 and 8-4. As before, each diagram is drawn such that the sign of the diagram is given by the numbers of fermion line interchanges and closed fermion loops. The connected diagrams are given in Figure 8-3, and the disconnected diagrams are shown in Figure 8-4. The diagrams in Figure 8-3, reading from right to left, correspond to the first two terms in Equation 8.9, and the diagrams in Figure 8-4, again reading from right to left, correspond to the last two

terms in Equation 8.9. As discussed in Section 8.2.1, we calculate only the connected diagrams, and hence we now split the three point correlation function in Equation 8.8 into quark connected and quark disconnected pieces. The connected piece of the three point function is

$$\langle\, P'_{\alpha'}(x')\,\overline{d}^{e}_{\epsilon}(y)\,O^{ee'}_{\epsilon\epsilon'}(y,y')\,d^{e'}_{\epsilon'}(y')\,\overline{P}_{\alpha}(x)\,\rangle_{\rm qc} = \tag{8.10}$$

$$\int DU_\mu\; e^{-S_{\rm eff}[U_\mu]}\; f_{\alpha'\beta'\gamma'\delta'}\,\overline{f}_{\delta\gamma\beta\alpha}\,\epsilon_{b'c'd'}\,\overline{\epsilon}_{dcb}\,O^{ee'}_{\epsilon\epsilon'}(y,y')\,\langle\, D'^{d'}_{\delta'}(x')\,\overline{d}^{e}_{\epsilon}(y)\,\rangle_{U_\mu}\langle\, d^{e'}_{\epsilon'}(y')\,\overline{D}^{d}_{\delta}(x)\,\rangle_{U_\mu}$$

$$\Big[\langle\, U'^{b'}_{\beta'}(x')\,\overline{U}^{b}_{\beta}(x)\,\rangle_{U_\mu}\langle\, U'^{c'}_{\gamma'}(x')\,\overline{U}^{c}_{\gamma}(x)\,\rangle_{U_\mu} - \langle\, U'^{b'}_{\beta'}(x')\,\overline{U}^{c}_{\gamma}(x)\,\rangle_{U_\mu}\langle\, U'^{c'}_{\gamma'}(x')\,\overline{U}^{b}_{\beta}(x)\,\rangle_{U_\mu}\Big]\,,$$

and the disconnected part of the three point function in Equation 8.8 is

$$\langle\, P'_{\alpha'}(x')\,\overline{d}^{e}_{\epsilon}(y)\,O^{ee'}_{\epsilon\epsilon'}(y,y')\,d^{e'}_{\epsilon'}(y')\,\overline{P}_{\alpha}(x)\,\rangle_{\rm qd} = \tag{8.11}$$

$$\int DU_\mu\; e^{-S_{\rm eff}[U_\mu]}\; f_{\alpha'\beta'\gamma'\delta'}\,\overline{f}_{\delta\gamma\beta\alpha}\,\epsilon_{b'c'd'}\,\overline{\epsilon}_{dcb}\,O^{ee'}_{\epsilon\epsilon'}(y,y')\,\langle\, D'^{d'}_{\delta'}(x')\,\overline{D}^{d}_{\delta}(x)\,\rangle_{U_\mu}\langle\, d^{e'}_{\epsilon'}(y')\,\overline{d}^{e}_{\epsilon}(y)\,\rangle_{U_\mu}$$

$$\Big[\langle\, U'^{b'}_{\beta'}(x')\,\overline{U}^{c}_{\gamma}(x)\,\rangle_{U_\mu}\langle\, U'^{c'}_{\gamma'}(x')\,\overline{U}^{b}_{\beta}(x)\,\rangle_{U_\mu} - \langle\, U'^{b'}_{\beta'}(x')\,\overline{U}^{b}_{\beta}(x)\,\rangle_{U_\mu}\langle\, U'^{c'}_{\gamma'}(x')\,\overline{U}^{c}_{\gamma}(x)\,\rangle_{U_\mu}\Big]\,.$$

8.3 Backward Propagators

In this section we explain an algorithm [2] designed to exploit the nature of the connected quark contractions for the three point function in Equation 8.1. By examining Equations 8.6 and 8.10 for the connected contributions to the u and d three point functions, or more easily by looking at the corresponding Feynman diagrams in Figures 8-1 and 8-3, we find in each case that the operator $O^{ee'}_{\epsilon\epsilon'}(y,y')$ is contracted with two distinct quark lines. The fact the quark lines connecting to the operator $O^{ee'}_{\epsilon\epsilon'}(y,y')$ are different lines is essential to understanding how the algorithm described in this section works. In short, by using the γ^5 Hermiticity of forward propagators as described in Appendix O.13 we can arrange that the indices of $O^{ee'}_{\epsilon\epsilon'}(y,y')$ are contracted with the *free* ends of forward or backward quark propagators. (The backward quark propagators are defined for the u and d quarks shortly.) By the free end of a quark propagator we mean the end which solves Dirac's equation as described in Section 7.3, and hence the end for which all combinations of color, Dirac, and position indices are

solved for. Therefore, since all indices in $O^{ee'}_{\epsilon\epsilon'}(y,y')$ are contracted with the free ends of either forward or backward quark propagators we can easily decouple the operator from the surrounding quark lines. As we show in the following two sections, this leads to significant simplifications in the calculation of connected diagrams.

One the other hand, by examining the disconnected contributions in Equations 8.7 and 8.11 or the disconnected diagrams in Figures 8-2 and 8-4, we notice that, unlike the case for the connected diagrams above, the operator $O^{ee'}_{\epsilon\epsilon'}(y,y')$ is contracted to both ends of the same quark line. Therefore we can no longer use the γ^5 Hermiticity of forward propagators to associate all indices of $O^{ee'}_{\epsilon\epsilon'}(y,y')$ with the free ends of quark lines, and consequently we can not decouple the operator from the remaining quark propagators. As a result, the algorithm described in this section can not be applied to the calculation of disconnected diagrams.

In the rest of this section we implement the above described algorithm for the connected contributions to the u and d quark operators. The basic idea is essentially the same for both u and d quark correlation functions, but the details differ for each, and hence we examine each case separately.[5] We note that the following two sections are a little detailed.

8.3.1 Backward U Quark Propagator

As described in the beginning of this section, we want to isolate the particular quark propagators in Equation 8.6 which contract with the operator $O^{ee'}_{\epsilon\epsilon'}(y,y')$. First we rewrite the connected contribution to the u quark three point function in Equation 8.6 using the forward propagators as given in Section 7.3.

$$\langle\, P'_{\alpha'}(x')\, \overline{u}^{e}_{\epsilon}(y)\, O^{ee'}_{\epsilon\epsilon'}(y,y')\, u^{e'}_{\epsilon'}(y')\, \overline{P}_{\alpha}(x)\,\rangle_{\rm qc} =$$

$$\int DU_\mu\; e^{-S_{\rm eff}[U_\mu]}\; f_{\alpha'\beta'\gamma'\delta'}\, \overline{f}_{\delta\gamma\beta\alpha}\, \epsilon_{b'c'd'}\, \overline{\epsilon}_{dcb}\, O^{ee'}_{\epsilon\epsilon'}(y,y')\, F^{d'd}_{\delta'\delta}(x',x;D',D,U_\mu)$$

$$\Big[\, F^{e'c}_{\epsilon'\gamma}(y',x;u,U,U_\mu)\, F^{c'e}_{\gamma'\epsilon}(x',y,U',u,U_\mu)\, F^{b'b}_{\beta'\beta}(x',x,U',U,U_\mu)$$

[5] We calculate the backward propagator for the u quark first and the d quark second, but it may, instead, be easier to read the section for the d quark first.

$$-F^{e'c}_{\epsilon'\gamma}(y',x;u,U,U_\mu)\,F^{c'b}_{\gamma'\beta}(x',x;U',U,U_\mu)\,F^{b'e}_{\beta'\epsilon}(x',y,U',u,U_\mu)$$

$$-F^{e'b}_{\epsilon'\beta}(y',x;u,U,U_\mu)\,F^{c'e}_{\gamma'\epsilon}(x',y,U,u,U_\mu)\,F^{b'c}_{\beta'\gamma}(x',x;U',U,U_\mu)$$

$$+F^{e'b}_{\epsilon'\beta}(y',x;u,U,U_\mu)\,F^{c'c}_{\gamma'\gamma}(x',x;U',U,U_\mu)\,F^{b'e}_{\beta'\epsilon}(x',y;U,u,U_\mu)\Big]$$

Now we simply reorganize the terms above. In each term we move the propagator with a y argument to the right and the propagator with a y' argument to the left.

$$\int DU_\mu\; e^{-S_{\rm eff}[U_\mu]}\; f_{\alpha'\beta'\gamma'\delta'}\,\overline{f}_{\delta\gamma\beta\alpha}\,\epsilon_{b'c'd'}\,\overline{\epsilon}_{dcb}\,O^{ee'}_{\epsilon\epsilon'}(y,y')\,F^{d'd}_{\delta'\delta}(x',x;D',D,U_\mu)$$

$$\Big[F^{e'c}_{\epsilon'\gamma}(y',x;u,U,U_\mu)\,F^{b'b}_{\beta'\beta}(x',x,U',U,U_\mu)\,F^{c'e}_{\gamma'\epsilon}(x',y,U',u,U_\mu)$$

$$-F^{e'c}_{\epsilon'\gamma}(y',x;u,U,U_\mu)\,F^{c'b}_{\gamma'\beta}(x',x;U',U,U_\mu)\,F^{b'e}_{\beta'\epsilon}(x',y,U',u,U_\mu)$$

$$-F^{e'b}_{\epsilon'\beta}(y',x;u,U,U_\mu)\,F^{b'c}_{\beta'\gamma}(x',x;U',U,U_\mu)\,F^{c'e}_{\gamma'\epsilon}(x',y,U,u,U_\mu)$$

$$+F^{e'b}_{\epsilon'\beta}(y',x;u,U,U_\mu)\,F^{c'c}_{\gamma'\gamma}(x',x;U',U,U_\mu)\,F^{b'e}_{\beta'\epsilon}(x',y;U,u,U_\mu)\Big]$$

Now isolate the e, ϵ, and y pieces.

$$\int DU_\mu\; e^{-S_{\rm eff}[U_\mu]}\; f_{\alpha'\beta'\gamma'\delta'}\,\overline{f}_{\delta\gamma\beta\alpha}\,\epsilon_{b'c'd'}\,\overline{\epsilon}_{dcb}\,F^{d'd}_{\delta'\delta}(x',x;D',D,U_\mu)$$

$$\Big[F^{e'c}_{\epsilon'\gamma}(y',x;u,U,U_\mu)\,F^{b'b}_{\beta'\beta}(x',x,U',U,U_\mu)\,\delta^{c'f'}_{\gamma'\zeta'}$$

$$-F^{e'c}_{\epsilon'\gamma}(y',x;u,U,U_\mu)\,F^{c'b}_{\gamma'\beta}(x',x;U',U,U_\mu)\,\delta^{b'f'}_{\beta'\zeta'}$$

$$-F^{e'b}_{\epsilon'\beta}(y',x;u,U,U_\mu)\,F^{b'c}_{\beta'\gamma}(x',x;U',U,U_\mu)\,\delta^{c'f'}_{\gamma'\zeta'}$$

$$+F^{e'b}_{\epsilon'\beta}(y',x;u,U,U_\mu)\,F^{c'c}_{\gamma'\gamma}(x',x;U',U,U_\mu)\,\delta^{b'f'}_{\beta'\zeta'}\Big]$$

$$F^{f'e}_{\zeta'\epsilon}(x',y;U,u,U_\mu)\,O^{ee'}_{\epsilon\epsilon'}(y,y')$$

Next isolate the ϵ', ϵ', and y' pieces.

$$\int DU_\mu\; e^{-S_{\rm eff}[U_\mu]}\; f_{\alpha'\beta'\gamma'\delta'}\,\overline{f}_{\delta\gamma\beta\alpha}\,\epsilon_{b'c'd'}\,\overline{\epsilon}_{dcb}\,O^{ee'}_{\epsilon\epsilon'}(y,y')\,F^{d'd}_{\delta'\delta}(x',x;D',D,U_\mu)$$

$$\Big[\delta^{fc}_{\zeta\gamma}\,F^{b'b}_{\beta'\beta}(x',x,U',U,U_\mu)\,\delta^{c'f'}_{\gamma'\zeta'}$$

$$-\delta^{fc}_{\zeta\gamma}\, F^{c'b}_{\gamma'\beta}(x', x; U', U, U_\mu)\, \delta^{b'f'}_{\beta'\zeta'}$$

$$-\delta^{fb}_{\zeta\beta}\, F^{b'c}_{\beta'\gamma}(x', x; U', U, U_\mu)\, \delta^{c'f'}_{\gamma'\zeta'}$$

$$\delta^{fb}_{\zeta\beta}\, F^{c'c}_{\gamma'\gamma}(x', x; U', U, U_\mu)\, \delta^{b'f'}_{\beta'\zeta'} \Big]$$

$$F^{f'e}_{\zeta'\epsilon}(x', y; U, u, U_\mu)\, O^{ee'}_{\epsilon\epsilon'}(y, y')\, F^{e'f}_{\epsilon'\zeta}(y', x; u, U, U_\mu)$$

Now collect the part of the integrand, excluding the effective action, which does not depend on the operator or the two quark propagators which contract with it. The result is

$$\int DU_\mu\; e^{-S_{\rm eff}[U_\mu]}\; C^{ff'}_{\zeta\zeta'}(x, x'; \alpha, \alpha', u)\, F^{f'e}_{\zeta'\epsilon}(x', y; U, u, U_\mu)\, O^{ee'}_{\epsilon\epsilon'}(y, y')\, F^{e'f}_{\epsilon'\zeta}(y', x; u, U, U_\mu) \tag{8.12}$$

where

$$C^{ff'}_{\zeta\zeta'}(x, x'; \alpha, \alpha', u) =$$

$$f_{\alpha'\beta'\gamma'\delta'}\, \overline{f}_{\delta\gamma\beta\alpha}\, \epsilon_{b'c'd'}\, \overline{\epsilon}_{dcb}\, F^{d'd}_{\delta'\delta}(x', x; D', D, U_\mu)$$

$$\Big[\delta^{fc}_{\zeta\gamma}\, F^{b'b}_{\beta'\beta}(x', x, U', U, U_\mu)\, \delta^{c'f'}_{\gamma'\zeta'}$$

$$-\delta^{fc}_{\zeta\gamma}\, F^{c'b}_{\gamma'\beta}(x', x; U', U, U_\mu)\, \delta^{b'f'}_{\beta'\zeta'}$$

$$-\delta^{fb}_{\zeta\beta}\, F^{b'c}_{\beta'\gamma}(x', x; U', U, U_\mu)\, \delta^{c'f'}_{\gamma'\zeta'}$$

$$\delta^{fb}_{\zeta\beta}\, F^{c'c}_{\gamma'\gamma}(x', x; U', U, U_\mu)\, \delta^{b'f'}_{\beta'\zeta'} \Big] .$$

Notice that the integrand in Equation 8.12 has the form of a trace in color and spin indices. Writing Equation 8.12 in matrix form gives

$$\int DU_\mu\; e^{-S_{\rm eff}[U_\mu]}\; {\rm tr}\,(\, C_u(x, x'; \alpha, \alpha')\, F_{Uu}(x', y)\, O(y, y')\, F_{uU}(y', x)\,) \tag{8.13}$$

where the trace is over color and Dirac indices only and each of C_u, F_{Uu}, O, and F_{uU} implicitly depend on the gauge field U_μ.

At this point a few lines of linear algebra shows how to express the combination $C_u F_{Uu}$ as a solution to the Wilson-Dirac equation. Using $F_{Uu} M_u = S_U$ from Equa-

tion 7.11 where S_U is the smearing matrix, we have $(C_u F_{Uu})\, M_u = C_u S_U$. Taking the adjoint of the previous equation gives $M_u^\dagger\, (C_u F_{Uu})^\dagger = S_U^\dagger C_u^\dagger$. Now we use the γ^5 Hermiticity of M, $\gamma^5 M_u^\dagger \gamma^5 = M$, from Equation 0.33 to give $M_u \gamma^5\, (C_u F_{Uu})^\dagger = \gamma^5 S_U^\dagger C_u^\dagger$. Lastly, we define the backward propagator $B_u = \gamma^5\, (C_u F_{Uu})^\dagger$ and the backward source $S_u^B = \gamma^5 S_U^\dagger C_u^\dagger$ such that $M_u B_u = S_u^B$ and $C_u F_{Uu} = B_u^\dagger \gamma^5$.

Finally, using the backward propagator defined just above and the result from Equation 8.13 gives the final result for the connected contribution to the u quark three point function as

$$\begin{aligned} &\langle\, P'_{\alpha'}(x')\, \overline{u}^e_\epsilon(y)\, O^{ee'}_{\epsilon\epsilon'}(y,y')\, u^{e'}_{\epsilon'}(y')\, \overline{P}_\alpha(x)\,\rangle_{\rm qc} = \\ &\quad = \int DU_\mu\; e^{-S_{\rm eff}[U_\mu]}\; {\rm tr}\left(\, B_u^\dagger(y;x,x',\alpha,\alpha')\, \gamma^5\, O(y,y')\, F_{uU}(y',x)\,\right) \end{aligned} \tag{8.14}$$

where both the backward propagator $B_u(y;x,x',\alpha,\alpha')$ and the forward propagator $F_{uU}(y',x)$ depend on the gauge field U_μ as well as the operator $O(y,y')$. Additionally, we note again that the trace is over color and Dirac indices only.

8.3.2 Backward D Quark Propagator

As in the previous section, we want to isolate the quark propagators which contract with the operator $O^{ee'}_{\epsilon\epsilon'}(y,y')$ in Equation 8.10 for the connected contribution to the d quark three point function. As in Section 8.3.1, we first rewrite the connected three point function in Equation 8.10 using the forward propagators defined in Section 7.3. The result is

$$\langle\, P'_{\alpha'}(x')\, \overline{d}^e_\epsilon(y)\, O^{ee'}_{\epsilon\epsilon'}(y,y')\, d^{e'}_{\epsilon'}(y')\, \overline{P}_\alpha(x)\,\rangle_{\rm qc} =$$

$$\int DU_\mu\; e^{-S_{\rm eff}[U_\mu]}\; f_{\alpha'\beta'\gamma'\delta'}\, \overline{f}_{\delta\gamma\beta\alpha}\, \epsilon_{b'c'd'}\, \overline{\epsilon}_{dcb}\, O^{ee'}_{\epsilon\epsilon'}(y,y')$$

$$F^{d'e}_{\delta'\epsilon}(x',y;D',d,U_\mu)\, F^{e'd}_{\epsilon'\delta}(y',x;d,D,U_\mu)$$

$$\Big[F^{b'b}_{\beta'\beta}(x',x;U',U,U_\mu)\, F^{c'c}_{\gamma'\gamma}(x',x;U',U,U_\mu)$$

$$-F^{b'c}_{\beta'\gamma}(x',x;U',U,U_\mu)\, F^{c'b}_{\gamma'\beta}(x',x;U',U,U_\mu)\Big]\,.$$

The above expression is already written in the correct form with the appropriate quark propagators isolated. Next we just collect the factors in the integrand that do not involve the operator or the two quark propagators contracted with it. The result is

$$\int DU_\mu \; e^{-S_{\rm eff}[U_\mu]} \; C^{dd'}_{\delta\delta'}(x,x';\alpha,\alpha') \, F^{d'e}_{\delta' c}(x',y;D',d,U_\mu) \, O^{ee'}_{\epsilon\epsilon'}(y,y') \, F^{e'd}_{\epsilon'\delta}(y',x;d,D,U_\mu) \tag{8.15}$$

where

$$C^{dd'}_{\delta\delta'}(x,x';\alpha,\alpha',d) =$$

$$f_{\alpha'\beta'\gamma'\delta'} \, \overline{f}_{\delta\gamma\beta\alpha} \, \epsilon_{b'c'd'} \, \overline{\epsilon}_{dcb} \, \left(F^{b'b}_{\beta'\beta}(x',x) F^{c'c}_{\gamma'\gamma}(x',x) - F^{b'c}_{\beta'\gamma}(x',x) F^{c'b}_{\gamma'\beta}(x',x) \right).$$

At this point we note that Equation 8.15 above has the same structure as Equation 8.12 for the u quark. In particular, the integrand of Equation 8.15 above has the form of a trace over color and Dirac indices. Thus the remaining argument is identical to that given in Section 8.3.1, and we borrow the appropriate results. In particular, the backward d quark propagator B_d satisfies $M_d B_d = S^B_d$ where the backward source S^B_d is given by $S^B_d = \gamma^5 S^\dagger_D C^\dagger_d$ in which S_D is the smearing matrix. Additionally, we can use the result in Equation 8.14 to write the final expression for the connected contribution to the d quark three point function as

$$\begin{aligned} &\langle \, P'_{\alpha'}(x') \, \overline{d}^e_\epsilon(y) \, O^{ee'}_{\epsilon\epsilon'}(y,y') \, d^{e'}_{\epsilon'}(y') \, \overline{P}_\alpha(x) \, \rangle_{\rm qc} = \\ &= \int DU_\mu \; e^{-S_{\rm eff}[U_\mu]} \; {\rm tr} \left(\, B^\dagger_d(y;x,x',\alpha,\alpha') \, \gamma^5 \, O(y,y') \, F_{dD}(y',x) \, \right) \end{aligned} \tag{8.16}$$

where, as in Section 8.3.1, the trace is over color and Dirac indices only and the backward propagator $B_d(y;x,x',\alpha,\alpha')$, the forward propagator $F_{dD}(y',x)$, and the operator $O(y,y')$ all implicitly depend on the gauge field U_μ.

8.4 Parity Projection

Now we briefly revisit the question of parity projection raised in Section 5.3. The results for the connected contribution to the u and d quark three point correlation functions are given in Equations 8.14 and 8.16. Both results have the generic form given below

$$\begin{aligned} &\langle\, P'_{\alpha'}(x')\, \overline{q}^{e}_{\epsilon}(y)\, O^{ee'}_{\epsilon\epsilon'}(y,y')\, q^{e'}_{\epsilon'}(y')\, \overline{P}_{\alpha}(x)\,\rangle_{\rm qc} = \\ &\quad = \int DU_\mu\, e^{-S_{\rm eff}[U_\mu]}\, {\rm tr}\left(\, B^{\dagger}_{q}(y;x,x',\alpha,\alpha')\, \gamma^5\, O(y,y')\, F_{qQ}(y',x)\,\right) \end{aligned}$$

where the trace is over color and Dirac indices. For simplicity, we drop the arguments of B_q, O, and F_{qQ}, and furthermore, we write the color and Dirac indices explicitly. The result is

$$\begin{aligned} &\langle\, P'_{\alpha'}(x')\, \overline{q}^{e}_{\epsilon}(y)\, O^{ee'}_{\epsilon\epsilon'}(y,y')\, q^{e'}_{\epsilon'}(y')\, \overline{P}_{\alpha}(x)\,\rangle_{\rm qc} = \\ &\quad = \int DU_\mu\, e^{-S_{\rm eff}[U_\mu]}\, (B_q)^{ba\,*}_{\beta\alpha}\, \gamma^5_{\beta\beta'}\, O^{bc}_{\beta'\gamma}\, (F_{qQ})^{ca}_{\gamma\alpha}\,. \end{aligned}$$

As discussed in Sections 5.3 and 7.4, the smeared-to-point forward propagator $(F_{qQ})^{ca}_{\gamma\alpha}$ vanishes for $\alpha = 3$ and 4 when we parity project the quark fields in the proton field. Thus, by examining the equation above, we find that the backward propagator $(B_q)^{ba}_{\beta\alpha}$ only contributes to the three point function for $\alpha = 1$ and 2. Therefore, the number of required backward propagators is cut in half for a nucleon field in which the quarks have been parity projected as described in Section 5.3.

8.5 Momentum Projection

In Section 7.5, we discuss the momentum projection of the proton sink in the two point correlation functions of the form $\langle\, P'_{\alpha'}(x')\, \overline{P}_{\alpha}(x)\,\rangle$. In this section, we examine the same momentum projection but now for the connected contribution to the three point functions in Equation 8.1. The connected contributions to the u and d quark three point correlation functions are given in Equations 8.14 and 8.16 respectively.

Both the u and d quark results have the same form as follows

$$\begin{aligned} &\langle\, P'_{\alpha'}(x')\, \overline{q}^{e}_{\epsilon}(y)\, O^{ee'}_{\epsilon\epsilon'}(y,y')\, q^{e'}_{\epsilon'}(y')\, \overline{P}_{\alpha}(x)\,\rangle_{\rm qc} = \\ &= \int DU_\mu\; e^{-S_{\rm eff}[U_\mu]}\; {\rm tr}\Big(\, B^{\dagger}_{q}(y;x,x',\alpha,\alpha')\,\gamma^5\, O(y,y')\, F_{qQ}(y',x)\,\Big) \end{aligned} \tag{8.17}$$

where the backward propagator B_q satisfies the Wilson-Dirac equation

$$M_q\, B_q(x,x',\alpha,\alpha') = S^B_q(x,x',\alpha,\alpha') \tag{8.18}$$

and S^B_q is the corresponding backward source. Note that in this equation the argument y in $B_q(y;x,x',\alpha,\alpha')$ becomes part of the implied matrix index and is no longer explicitly written. The momentum projection of such a three point function is given by

$$\begin{aligned} &\langle\, P'_{\alpha'}(t',\vec{p}')\, \overline{q}^{e}_{\epsilon}(y)\, O^{ee'}_{\epsilon\epsilon'}(y,y')\, q^{e'}_{\epsilon'}(y')\, \overline{P}_{\alpha}(x)\,\rangle_{\rm qc} = \\ &= \int d^3\vec{x}'\; e^{-i\vec{p}'\cdot\vec{x}'}\,\langle\, P'_{\alpha'}(x')\, \overline{q}^{e}_{\epsilon}(y)\, O^{ee'}_{\epsilon\epsilon'}(y,y')\, q^{e'}_{\epsilon'}(y')\, \overline{P}_{\alpha}(x)\,\rangle_{\rm qc} \\ &= \int DU_\mu\; e^{-S_{\rm eff}[U_\mu]}\; {\rm tr}\Big(\, \int d^3\vec{x}'\; e^{-i\vec{p}'\cdot\vec{x}'}\, B^{\dagger}_{q}(y;x,x',\alpha,\alpha')\,\gamma^5\, O(y,y')\, F_{qQ}(y',x)\,\Big) \\ &= \int DU_\mu\; e^{-S_{\rm eff}[U_\mu]}\; {\rm tr}\Big(\, B^{\dagger}_{q}(y;x,(t',\vec{p}'),\alpha,\alpha')\,\gamma^5\, O(y,y')\, F_{qQ}(y',x)\,\Big) \end{aligned} \tag{8.19}$$

where we have introduced the momentum projected backward propagator defined by

$$B_q(y;x,(t',\vec{p}'),\alpha,\alpha') = \int d^3\vec{x}'\; e^{i\vec{p}'\cdot\vec{x}'}\; B_q(y;x,x',\alpha,\alpha'). \tag{8.20}$$

Note that the defining Equation 8.18 for the backward propagator $B_q(x,x',\alpha,\alpha')$ is linear. Therefore the momentum projected backward propagator satisfies a similar equation

$$M_q\, B_q(y;x,(t',\vec{p}'),\alpha,\alpha') = S^B_q(x,(t',\vec{p}'),\alpha,\alpha') \tag{8.21}$$

where the corresponding momentum projected backward source is defined by

$$S^B_q(x,(t',\vec{p}'),\alpha,\alpha') = \int d^3\vec{x}'\; e^{i\vec{p}'\cdot\vec{x}'}\; S^B_q(x,x',\alpha,\alpha'). \tag{8.22}$$

Thus the connected contribution to the momentum projected three point function, given in Equation 8.19 above, can be calculated using the backward propagator method as well.

8.6 Building Blocks

As we discuss in the next section, we need to momentum project the operators, as well as the proton sink, in the three point correlation functions in Equation 8.1. For convenience we rewrite the general result for the three point function in Equation 8.19 by simply interchanging e', ϵ', and y' with e, ϵ, and y. This gives the three point function with momentum projected sink as

$$\begin{aligned} &\langle\, P'_{\alpha'}(t',\vec{p}\,')\,\overline{q}^{e'}_{\epsilon'}(y')\,O^{e'e}_{\epsilon'\epsilon}(y',y)\,q^{e}_{\epsilon}(y)\,\overline{P}_{\alpha}(x)\,\rangle_{\rm qc} = \\ &= \int DU_\mu\; e^{-S_{\rm eff}[U_\mu]}\;\mathrm{tr}\left(\, B^{\dagger}_{q}(y';x,(t',\vec{p}\,'),\alpha,\alpha')\,\gamma^5\,O(y',y)\,F_{qQ}(y,x)\,\right). \end{aligned} \tag{8.23}$$

This result above is generally true for all two quark operators $\overline{q}^{e'}_{\epsilon'}(y')O^{e'e}_{\epsilon'\epsilon}(y',y)q^{e}_{\epsilon}(y)$, but now we specify to the operators described in Equation 8.2. Remembering to switch e', ϵ', and y' with e, ϵ, and y gives

$$O^{e'e}_{\epsilon'\epsilon}(y',y) = \Gamma_{\epsilon'\epsilon}\left(\, U^{\dagger}_{\mu_n}(y+\mu_1+\cdots+\mu_{n-1})\cdots U^{\dagger}_{\mu_1}(y)\,\right)^{e'e}$$

where $y' = y+\mu_1+\cdots+\mu_n$ and Γ is an arbitrary Dirac spin matrix. In particular we note that y' is completely fixed in terms of y and is not independent. When we need to make this point clear we use the notation $y'(y)$ to denote y' as the function of y given above.

Now, in analogy with the definition of $C^{(2)}_{\alpha'\alpha}$ given in Equation 7.16, we momentum project the operator and define the following

$$\begin{aligned} &C^{(3)}_{\alpha'\alpha}((t',\vec{p}\,');(\tau,\vec{q});x) = \\ &= \int d^3\vec{y}\; e^{i\vec{q}\,\vec{y}}\,\langle\, P'_{\alpha'}(t',\vec{p}\,')\,\overline{q}^{e'}_{\epsilon'}(y'(\tau,\vec{y}))\,O^{e'e}_{\epsilon'\epsilon}(y'(\tau,\vec{y}),(\tau,\vec{y}))\,q^{e}_{\epsilon}(\tau,\vec{y})\,\overline{P}_{\alpha}(x)\,\rangle_{\rm qc} \end{aligned} \tag{8.24}$$

where τ labels the time insertion of the operator and, as discussed above, $y'(\tau, \vec{y})$ is constrained by $(\tau, \vec{y})$. Using Equation 8.23 above, we can write $C^{(3)}$ as

$$C^{(3)}_{\alpha'\alpha}\left((t', \vec{p}'); (\tau, \vec{q}); x\right) = \int DU_\mu \; e^{-S_{\text{eff}}[U_\mu]} \; \mathcal{B}_q\left((t', \vec{p}'), \alpha'; (\tau, \vec{q}); x, \alpha\right) \tag{8.25}$$

where we introduce the building blocks $\mathcal{B}_q$ defined by

$$\begin{aligned} &\mathcal{B}_q\left((t', \vec{p}'), \alpha'; (\tau, \vec{q}); x, \alpha\right) = \\ &= \int d^3\vec{y} \; e^{i\vec{q}\cdot\vec{y}} \, \text{tr}\left(B^\dagger_q(y'(\tau, \vec{y}); x, (t', \vec{p}'), \alpha, \alpha') \, \gamma^5 \, O(y'(\tau, \vec{y}), (\tau, \vec{y})) \, F_{qQ}((\tau, \vec{y}), x) \right). \end{aligned} \tag{8.26}$$

Note that $(t', \vec{p}')$ and α' label the momentum projected proton sink, $(\tau, \vec{q})$ labels the momentum projected operator, and x and α label the proton source. Furthermore, the building blocks $\mathcal{B}_q$ implicitly depend on both the gauge field U_μ and the remaining details of the operator: the spin structure Γ and the link pattern $\mu_1, \ldots, \mu_n$. In any given calculation the proton source and sink are held fixed, thus a more meaningful set of arguments for the building blocks may be $\mathcal{B}_q\left((\tau, \vec{q}); \Gamma; \mu_1, \ldots, \mu_n; U_\mu\right)$. Applying the result in Equation 4.14, which describes the numerical evaluation of the gauge integral, to Equation 8.25 above gives the final expression for our calculation of the three point correlation functions,

$$C^{(3)}_{\alpha'\alpha}\left((t', \vec{p}'); (\tau, \vec{q}); x\right) = \frac{1}{N} \sum_i \mathcal{B}_q\left((t', \vec{p}'), \alpha'; (\tau, \vec{q}); x, \alpha; U^{(i)}_\mu\right) \pm \frac{\sigma}{\sqrt{N}} \tag{8.27}$$

where the sum is over all the gauge fields $U^{(i)}_\mu$ in an ensemble and σ depends on the spin matrix Γ, the link pattern $\mu_1, \ldots, \mu_n$, the operator insertion point τ, and the operator momentum $\vec{q}$.

8.7 Spectral Representation

In this section we determine the spectral representation of the three point functions given in Equation 8.1. To construct a spectral representation we momentum project the proton sink and the operator in the three point correlation functions. This is

given by $C^{(3)}_{\alpha\alpha'}$ in Equation 8.24. Just as in Equation 7.17 for the two point function, it is convenient to contract the Dirac indices of the proton source and sink with a spin matrix Γ.[6] The resulting definition for $C^{(3)}_{\Gamma}$ is

$$C^{(3)}_{\Gamma}\left((t',\vec{p}\,');(\tau,\vec{q});x\right) = \Gamma^{\alpha\alpha'} C^{(3)}_{\alpha'\alpha}\left((t',\vec{p}\,');(\tau,\vec{q});x\right). \tag{8.28}$$

The spectral representations for $C^{(3)}_{\alpha'\alpha}$ and $C^{(3)}_{\Gamma}$ are determined in Equations O.38 and O.39. The results are

$$\begin{aligned} & C^{(3)}_{\alpha'\alpha}\left((t',\vec{p}\,');(\tau,\vec{q});x\right) = \\ &= \sum_{N',N} \frac{Z_{N'}}{2E^{N'}_{\vec{p}\,'}} \frac{Z^*_{N}}{2E^{N}_{\vec{p}}} e^{-E^{N'}_{\vec{p}\,'}(t'-\tau)} e^{-E^{N}_{\vec{p}}(\tau-t)} e^{-i\vec{p}\cdot\vec{x}} \\ &\quad \left(\left(p'_{N'}\cdot\gamma + m_{N'}\right)\mathcal{O}_{N'N}\left(p_N\cdot\gamma + m_N\right)\right)_{\alpha'\alpha} \end{aligned} \tag{8.29}$$

and

$$\begin{aligned} & C^{(3)}_{\Gamma}\left((t',\vec{p}\,');(\tau,\vec{q});x\right) = \\ &= \sum_{N',N} \frac{Z_{N'}}{2E^{N'}_{\vec{p}\,'}} \frac{Z^*_{N}}{2E^{N}_{\vec{p}}} e^{-E^{N'}_{\vec{p}\,'}(t'-\tau)} e^{-E^{N}_{\vec{p}}(\tau-t)} e^{-i\vec{p}\cdot\vec{x}} \\ &\quad \mathrm{tr}\left(\Gamma\left(p'_{N'}\cdot\gamma + m_{N'}\right)\mathcal{O}_{N'N}\left(p_N\cdot\gamma + m_N\right)\right) \end{aligned} \tag{8.30}$$

where $\vec{p} = \vec{p}\,' - \vec{q}$ and we explicitly assume $t' > \tau > t$. Furthermore, the labels N' and N denote the states with the quantum numbers of the proton, and the four momenta $p_{N'}$ and p_N are on-shell for the N'^{th} and N^{th} states, $p^2_{N'} = m^2_{N'}$ and $p^2_N = m^2_N$. Additionally, $\mathcal{O}_{N'N}$ is the form factor decomposition for the nucleon-nucleon matrix elements of O defined by

$$\langle N',s',\vec{p}\,'|\, O\,|N,s,\vec{p}\rangle = \overline{U}(p'_{N'},s')\,\mathcal{O}_{N'N}\,U(p_N,s).$$

[6] We use Γ to denote both the spin projection of the three point function and the spin structure of the operators. When the possibility for confusion arises, we use Γ_{op} to specifically denote the Γ matrix in the operator and Γ_{sp} to denote the Γ matrix for the spin projection.

8.8 Nucleon Matrix Elements

We now demonstrate how the nucleon matrix elements are extracted from the three point correlation functions $C_{\Gamma}^{(3)}\left((t',\vec{p}');(\tau,\vec{q});x\right)$ given in Equation 8.28. Using the spectral representation for $C_{\Gamma}^{(3)}$ given in Equation 8.30, we find that the asymptotic limit of large Euclidean time separations between each of the fields in the three point correlation function is given by

$$\begin{aligned}\lim_{(t'-\tau)\to\infty}\lim_{(t'-\tau)\to\infty} C_{\Gamma}^{(3)}\left((t',\vec{p}');(\tau,\vec{q});x\right) \to \\ = \frac{|Z|^2}{2E_{\vec{p}'}\,2E_{\vec{p}}}\, e^{-E_{\vec{p}'}(t'-\tau)}\, e^{-E_{\vec{p}}(\tau-t)}\, e^{-i\vec{p}\cdot\vec{x}} \\ \mathrm{tr}\left(\Gamma\left(p'\cdot\gamma+m\right)\mathcal{O}\left(p\cdot\gamma+m\right)\right)\end{aligned} \tag{8.31}$$

where all four momenta p and p', amplitudes Z, energies E, and form factors $\mathcal{O}$ refer specifically to the nucleon ground state and hence the labels N and M in Equation 8.30 have been suppressed. Additionally, both the limits $(t'-\tau)\to\infty$ and $(\tau-t)\to\infty$ are implied by $\to$ in this section.

Notice that Equation 8.31 above has a structure that is quite similar to that of Equation 7.20 for the asymptotic limit of the nucleon two point function. The only significant difference is, of course, the presence of the trace term depending on the operator O in Equation 8.31. This suggests that an appropriate ratio of $C_{\Gamma}^{(3)}$ to $C_{\Gamma}^{(2)}$ may eliminate the unwanted factors of Z and E as well as the exponentials. First, as an example, we pursue this suggestion in the forward limit, $\vec{p}'=\vec{p}$. In this limit the asymptotic three point function in Equation 8.31 becomes

$$\frac{|Z|^2}{2E_{\vec{p}'}\,2E_{\vec{p}'}}\, e^{-E_{\vec{p}'}(t'-t)}\, e^{-i\vec{p}'\cdot\vec{x}}\,\mathrm{tr}\left(\Gamma\left(p'\cdot\gamma+m\right)\mathcal{O}\left(p'\cdot\gamma+m\right)\right),$$

and the two point function from Equation 7.20 is

$$\frac{|Z|^2}{2E_{\vec{p}'}}\, e^{-E_{\vec{p}'}(t'-t)}\, e^{-i\vec{p}'\cdot\vec{x}}\,\mathrm{tr}\left(\Gamma\left(p'\cdot\gamma+m\right)\right).$$

Therefore, the asymptotic limit of $C_\Gamma^{(3)}/C_\Gamma^{(2)}$ is

$$\frac{C_\Gamma^{(3)}\left((t',\vec{p}');(\tau,\vec{0});x\right)}{C_\Gamma^{(2)}(t',\vec{p}';t,\vec{x})} \rightarrow \frac{\mathrm{tr}\left(\Gamma\left(p'\cdot\gamma+m\right)\mathcal{O}\left(p'\cdot\gamma+m\right)\right)}{2E_{\vec{p}'}\,\mathrm{tr}\left(\Gamma\left(p'\cdot\gamma+m\right)\right)}. \tag{8.32}$$

Thus we find that the simple ratio of $C_\Gamma^{(3)}$ to $C_\Gamma^{(2)}$ nearly eliminates all unwanted terms. In particular it eliminates any dependence on t', τ, t, and Z. The generalization of the ratio in Equation 8.32 above for off-forward matrix elements, that is $\vec{p}' \neq \vec{p}$, is given by

$$\frac{C_\Gamma^{(3)}\left((t',\vec{p}');(\tau,\vec{p}'-\vec{p});x\right)}{C_\Gamma^{(2)}(t',\vec{p}';t,\vec{x})}\sqrt{\frac{C_\Gamma^{(2)}(t'-\tau+t,\vec{p};t,\vec{x})}{C_\Gamma^{(2)}(t'-\tau+t,\vec{p}';t,\vec{x})}\frac{C_\Gamma^{(2)}(\tau,\vec{p}';t,\vec{x})}{C_\Gamma^{(2)}(\tau,\vec{p};t,\vec{x})}\frac{C_\Gamma^{(2)}(t',\vec{p}';t,\vec{x})}{C_\Gamma^{(2)}(t',\vec{p};t,\vec{x})}} \tag{8.33}$$

and has the asymptotic limit

$$\frac{\mathrm{tr}\left(\Gamma\left(p'\cdot\gamma+m\right)\mathcal{O}\left(p\cdot\gamma+m\right)\right)}{2\sqrt{E_{\vec{p}'}\,E_{\vec{p}}}\,\mathrm{tr}\left(\Gamma\left(p'\cdot\gamma+m\right)\right)\mathrm{tr}\left(\Gamma\left(p\cdot\gamma+m\right)\right)}\,e^{i\vec{x}\cdot(\vec{p}'-\vec{p})/2}.$$

As in the forward case, the dependence on t', τ, t, and Z has been removed by the ratio in Equation 8.33. Thus the nucleon form factors $\mathcal{O}$ corresponding to the nucleon matrix elements of the operator O can be determined from the appropriate ratios of three and two point correlation functions.

Chapter 9

Select Results

We present here a few select results to illustrate the calculations described in this thesis. As explained in Chapter 2, the physical observables we are interested in are all derived in one way or another from the generalized form factors. Using the techniques described in this work, we calculate all the generalized form factors for the vector, $O_q^{\mu_1 \cdots \mu_n}$, and axial vector, $\tilde{O}_q^{\mu_1 \cdots \mu_n}$, twist two operators for $n \leq 3$. The twist two operators are given in Equation 2.6, and the resulting *seventeen* generalized form factors are given in Equations 2.7 and 2.8. We calculate all these generalized form factors for each of three quark masses. Rather than present a deluge of plots, we focus on a few select results, in particular, those that are easiest and simplest to understand. In Section 9.1 we provide a guide to our calculations of the generalized form factors shown in Appendices B, C, D, and E as well as the corresponding forward moments and fits given in Appendices F, G, and H. In Section 9.2 we present the quark helicity and orbital angular momentum contributions to the nucleon spin. Then in Section 9.3 we examine the transverse quark structure of the nucleon implied directly by our calculation of generalized form factors by focusing on the slopes of the generalized form factors and the corresponding transverse radii. In particular, we study the mass, flavor, and spin dependence of the transverse quark structure in Sections 9.3.2, 9.3.3, and 9.3.4 respectively. Finally in Section 9.4 we discuss several aspects of the transverse quark distributions that follow from extending the observed dipole form for the generalized form factors to arbitrarily large momentum transfer. We study the

κ	a (fm)	a^{-1} (GeV)	$m_q^{\overline{\text{MS}}}$ (MeV)	m_π (MeV)	m_N (GeV)
0.1560	0.0982(5)	2.01(1)	123	895(8)	1.71(2)
0.1565	0.0949(5)	2.08(2)	101	835(13)	1.62(3)
0.1570	0.0914(4)	2.16(3)	79	753(15)	1.56(4)

Table 9.1: Lattice Spacing, Quark Mass at $\mu = 2$ GeV, Pion Mass, and Nucleon Mass

resulting transverse flavor structure in Section 9.4.1, the transverse spin structure in Section 9.4.2, the transverse charge distribution in Section 9.4.3, and the transverse momentum distribution in Section 9.4.4.

Our calculations use the gauge fields generated by the SESAM Collaboration [14]. These gauge fields were calculated using the Wilson gauge action in Equation 4.4 and the Wilson fermion action in Equation 4.6. The lattice dimensions are $L = 16$ and $T = 32$. The bare coupling for these calculations is given by $\beta = 5.6$, and the bare quark masses are given by $\kappa = 0.1560$, 0.1565, and 0.1570.[1] The corresponding lattice spacing for each quark mass is determined by the Sommer scale $r_0^{-1} = 394$ MeV and are given in Table 9.1 [1] along with the $\overline{\text{MS}}$ quark masses, the pion masses, and the nucleon masses.

As is true for contemporary full lattice QCD calculations, the pion is significantly heavier in our calculations than in the natural world.[2] Furthermore, any attempt to extrapolate to the chiral limit from such heavy pion masses is questionable. There is no belief that chiral perturbation theory converges for these quark masses, and there is no other sensible way to extrapolate physical observables as a function of the pion mass. Instead we interpret the following calculations as results in a would-be world with a heavy pion. As we show in the remaining sections of this chapter, there is, indeed, physical insight to be gained from our calculations in this hypothetical *heavy pion world.*

[1]The bare coupling g and bare quark masses in lattice units ma are discussed in Section 4.2 and are related to β and κ by $\beta = 2\text{N}_\text{c}/g^2$ and $\kappa = 1/(8 + 2ma)$.

[2]We are currently pursuing calculations with $m_\pi = 340$ MeV to 735 MeV to begin to study the chiral limit.

9.1 Generalized Form Factors

We calculate the seventeen generalized form factors corresponding to the nucleon matrix elements of the twist two operators $O_q^{\mu_1 \cdots \mu_n}$ and $\tilde{O}_q^{\mu_1 \cdots \mu_n}$ for $n \leq 3$. The generalized form factors for $O_q^{\mu_1 \cdots \mu_n}$ are A_{10} and B_{10} for $n = 1$, A_{20}, B_{20}, and C_2 for $n = 2$, and A_{30}, A_{32}, B_{30}, and B_{32} for $n = 3$. Additionally, the generalized form factors for $\tilde{O}_q^{\mu_1 \cdots \mu_n}$ are $\tilde{A}_{10}$ and $\tilde{B}_{10}$ for $n = 1$, $\tilde{A}_{20}$ and $\tilde{B}_{20}$ for $n = 2$, and $\tilde{A}_{30}$, $\tilde{A}_{32}$, $\tilde{B}_{30}$, and $\tilde{B}_{32}$ for $n = 3$. We calculate all of these generalized form factors for each of the three quark masses in Table 9.1.

In this chapter we examine the physical observables relating to the quark angular momentum contributions to the nucleon spin and the transverse quark distributions within the nucleon. As discussed in each of the appropriate following sections, we need A_{n0} and $\tilde{A}_{n0}$ for $n = 1$, 2, and 3 as well as B_{20} to examine the observables of interest. To illustrate the nature of our lattice results for the nucleon generalized form factors we provide a variety of examples. In Appendix B we show A_{10}^f for $f = u - d$ and $u + d$ and for each of the three quark masses. We do the same for A_{20} in Appendix C and for B_{20} in Appendix D. We also show $\tilde{A}_{10}$ in Appendix E for $f = u - d$ and $u + d$ but for the heaviest quark mass only.

The forward limits of A_{n0} and $\tilde{A}_{n0}$ can be directly calculated from the matrix elements of the twist two operators. The values of $A_{n0}(0)$ and $\tilde{A}_{n0}(0)$ correspond to the moments of the unpolarized and polarized parton distributions as described in Section 2.5. Our lattice calculations of these moments are given in Appendix F. The forward limits of the remaining generalized form factors must be determined by extrapolating our results for $t \neq 0$ to $t = 0$. Furthermore, to determine the slopes of the A_{n0} and $\tilde{A}_{n0}$ generalized form factors at $t = 0$ we must interpolate between $t = 0$ and the next non-zero value of t accessible to our lattice calculation. We resolve both of these issues by fitting the lattice results to functional forms as we now describe.

Each of the generalized form factors mentioned above, with the exception of B_{20}^{u+d}, are fit to a dipole functional form. The resulting best fit dipole is plotted along with the lattice calculations in each of the plots in Appendices B, C, and E. As indicated

in each of these figures, the dipole ansatz is a consistent description of the lattice results in the region of t examined in this thesis. The resulting best fit parameters for each of these generalized form factors are collected in the tables in Appendix G. As mentioned, B_{20}^{u+d} is not fit to a dipole functional form. The lattice results for B_{20}^{u+d} are small and the errors are large enough than no discernable dipole behavior can be realistically determined. In this case only, we fit the lattice results to a constant. The best fit results are shown with the lattice data in each of the plots in Appendix D, and the corresponding best fit parameters are given in the tables in Appendix H.

Using the fitting method described above, we can determine the forward limits as well as the slopes at $t = 0$ of all the generalized form factors. These results are mildly dependent on the dipole, or constant, behavior assumed for the generalized form factors. This dependence is essentially a finite volume effect as the first non-zero value of t accessible to lattice calculations is inversely proportional to the square of the physical size L of the box in which the calculation is performed. Thus the need to extrapolate or interpolate the lattice results to determine the value and slope of the generalized form factors at $t = 0$ is reduced for larger volumes.

Additionally, we can use the dipole fits described earlier to extend the generalized form factors beyond the range of t values within the reach of our lattice calculation. We take advantage of this idea to perform the Fourier transforms to convert the generalized form factors to various quark distributions in the transverse coordinates. However, this use of the dipole fits to the generalized form factors introduces a systematic dependence on the choice of extrapolation to large t values. In particular, the short distance behavior of the resulting transverse quark distributions is strongly dependent on the method of extrapolation to large t.

9.2 Quark Angular Momenta

The nucleon spin decomposition is discussed in Section 2.6. The continuum sum rule for the nucleon spin is given in Equation 2.13 as

$$\frac{1}{2} = J^{u+d} + J^g = \frac{1}{2}\Delta\Sigma^{u+d} + L^{u+d} + J^g.$$

The expressions for the quark helicity and total quark contributions to the nucleon spin are given in Equations 2.14 and 2.15.

$$\frac{1}{2}\Delta\Sigma^q = \frac{1}{2}\tilde{A}^q_{10}(0)$$

$$J^q = \frac{1}{2}\left[A^q_{20}(0) + B^q_{20}(0)\right]$$

The quark orbital contribution is the difference of the total quark and quark spin contributions,

$$L^q = J^q - \frac{1}{2}\Delta\Sigma^q,$$

and the gluon contribution can be determined by assuming the continuum spin sum rule above with the result

$$J^g = \frac{1}{2} - J^{u+d}.$$

As we see from the above expressions, the physical observables $\Delta\Sigma^q$, J^q, L^q, and J^g are determined by the forward limits of the $\tilde{A}^q_{10}$, A^q_{20}, and B^q_{20} generalized form factors. As discussed in Section 2.2, only the A^q_{n0} and $\tilde{A}^q_{n0}$ generalized form factors can be calculated in the forward limit. Thus $\tilde{A}^q_{10}(0)$ and $A^q_{20}(0)$ can both be measured directly. However, to determine $B^q_{20}(0)$, we calculate $B^q_{20}(t)$ for several values of t and extrapolate to the forward limit $t = 0$. Our results for the B^q_{20} form factors are shown in Section D for the flavor combinations $u - d$ and $u + d$ and for each quark mass in our calculation. As indicated in the Figures D-1, D-3, and D-5, the flavor combination $u - d$ is clearly consistent with a dipole functional form in the range of t values we have calculated. Shown in each of these figures are the lattice results for

f	$u-d$	$u+d$	u	d
$\Delta\Sigma^f$	1.19(2)	0.68(2)	0.94(2)	−0.25(1)
$2J^f$	0.80(6)	0.67(1)	0.73(3)	−0.07(3)
$2L^f$	−0.39(6)	−0.02(2)	−0.20(3)	0.19(3)

Table 9.2: $\Delta\Sigma^f$, J^f, and L^f for $f = u-d$, $u+d$, u, and d at $m_\pi = 895$ MeV

f	$u-d$	$u+d$	u	d
$\Delta\Sigma^f$	1.22(3)	0.73(3)	0.98(2)	−0.25(2)
$2J^f$	0.84(4)	0.66(1)	0.75(2)	−0.09(2)
$2L^f$	−0.38(5)	−0.07(3)	−0.22(3)	0.16(3)

Table 9.3: $\Delta\Sigma^f$, J^f, and L^f for $f = u-d$, $u+d$, u, and d at $m_\pi = 835$ MeV

B_{20}^{u-d} with a dipole fit, and the corresponding dipole parameters and errors are given in Table G.3. The independent flavor combination $u+d$ for each quark mass is shown in Figures D-2, D-4, and D-6. The B_{20}^{u+d} generalized form factor is consistent with a constant in this same range of t values, and hence, given in each of these figures are the results of our calculation for B_{20}^{u+d} and a fit to a constant. Additionally, the corresponding fit results and errors are given in Table H.1.

As mentioned above, the quantities $\tilde{A}_{10}^q(0)$ and $A_{20}^q(0)$ can be calculated directly without extrapolating in t. These quantities correspond to the spin fraction and momentum fraction respectively. The results of our calculations for $\tilde{A}_{10}^q(0)$ are given in Table F.3, and the results for $A_{20}^q(0)$ are given in Table F.2.

Given the results for $\tilde{A}_{10}^q$, A_{20}^q, and B_{20}^q, we tabulate our calculations of $\Delta\Sigma^q$, $2J^q$, and $2L^q$ for the flavor combinations $u-d$, $u+d$, u, and d in Tables 9.2, 9.3, and 9.4 for each quark mass respectively. Additionally, the corresponding results for $2J^g$ are collected in Table 9.5 for each quark mass. Notice that the quantities as written

f	$u-d$	$u+d$	u	d
$\Delta\Sigma^f$	1.09(3)	0.67(3)	0.88(2)	−0.21(2)
$2J^f$	0.84(14)	0.68(2)	0.76(7)	−0.08(7)
$2L^f$	−0.25(14)	0.01(4)	−0.12(7)	0.13(7)

Table 9.4: $\Delta\Sigma^f$, J^f, and L^f for $f = u-d$, $u+d$, u, and d at $m_\pi = 753$ MeV

m_π (MeV)	895	835	753
$2J^g$	0.335(10)	0.336(8)	0.324(22)

Table 9.5: J^g for $m_\pi = 895$, 835, and 753 MeV

with the peculiar factors of 2 are the fractional contributions to the nucleon spin.[3] Additionally, note that the $u - d$ combination is determined solely by the connected diagrams, and hence is unambiguously calculated. However, the other three flavor combinations require the calculation of disconnected diagrams. The disconnected diagrams are beyond the scope of this thesis, and hence we discuss only our results for the connected contributions to $u + d$, u, and d observables, and we point out those cases for which the disconnected diagrams may play a significant role.

First we discuss our results for the quantity L^{u-d}. As mentioned earlier, this quantity receives no contributions from disconnected diagrams and hence is unambiguously calculated at our fixed lattice parameters. Furthermore, it shows clearly that the quarks are contributing to the nucleon spin by way of their orbital motion. The results for the heaviest to lightest quark masses in our calculation are $L^{u-d} = -0.20(3)$, $-0.19(3)$, and $-0.13(7)$. In each case L^{u-d} is statistically different from zero, and for all but the lightest quark mass, L^{u-d} is several standard deviations from zero. Without regard to the value of L^{u+d}, this is a clear indication that one or both of the u and d quarks has sufficient orbital motion to contribute at least $L^q_{\text{min}} = L^{u-d}/2$ to the nucleon spin. This occurs at the point $L^u = -L^d$ which minimizes $\max(|L^u|, |L^d|)$ with the constraint $L^{u-d} = L^u - L^d$. Therefore a quark, u or d, in the nucleon makes a fractional contribution to the nucleon spin at least as large as L^{u-d} which is a ten to twenty percent effect for each of the quark masses studied in this thesis.

The other non-singlet matrix element discussed in this section is $\Delta\Sigma^{u-d}$. This matrix element is free from disconnected diagrams as well. The results of our calculations for the heaviest to lightest quark mass are $\Delta\Sigma^{u-d} = 1.19(2)$, 1.22(3), and 1.09(3). The quark masses used in these calculations are too heavy to attempt an

[3] $\Delta\Sigma$ is by definition the fractional contribution, so no factor of 2 is required.

extrapolation using only the leading order results from chiral perturbation theory, so a quantitative comparison with the experimental result is not justified. However, we do cite the experimentally measured value of $\Delta\Sigma^{u-d} = 1.27(14)$ for comparison [4]. Thus we find that the lattice results are already accurate at the ten percent level for the heavy quark masses used in our calculation. With regard to this, we note that the chiral extrapolation for the polarized moments of quark distributions is argued to be flatter than for the unpolarized moments [8], suggesting that the pion mass dependence of the spin fraction, being the lowest polarized moment, may, for example, be flatter than the corresponding mass dependence of the momentum fraction.

The values for the connected piece of the total quark orbital contribution are $L^{u+d} = -0.02(2)$, $-0.07(3)$, and $0.01(4)$. The fact that the connected piece of L^{u+d} seems to be consistent with zero for each quark mass we have studied is a curiosity in light of the clear statement above that at least one of L^u or L^d represents at least ten to twenty percent of the nucleon spin. Clearly this is an observable for which disconnected diagrams must be calculated because, quite simply in this case, the disconnected contribution appears to be the dominant, if not nearly sole, contribution to L^{u+d}.

The effect of disconnected diagrams on L^{u+d} is severe because the connected contribution is nearly zero. However, the connected contribution to J^{u+d} is not small and represents a sizeable fractional contribution to the nucleon spin. The total fractional quark contribution is $2J^{u+d} = 0.67(1)$, $0.66(1)$, and $0.68(2)$ percent for the heaviest to lightest quark mass. With a bit of caution, we use these results to calculate the corresponding estimates for the *connected* gluon contributions given by $2J^g = 0.34(1)$, $0.34(1)$, and $0.32(2)$. Though it is numerically possible for the disconnected contribution to J^{u+d} to account for the apparent gluon contribution, it would require a fifty percent effect to completely eliminate any contribution from the gluons. Thus it seems quite reasonable that, indeed, the gluons are contributing significantly to the nucleon spin for the quark masses in our calculation.

9.3 Transverse Quark Structure

This is the first of two sections in which we examine the transverse structure of the nucleon. In this section we discuss those features of the transverse quark distributions which are unambiguously determined by our lattice calculations. In the following section, Section 9.4, we examine the consequences of extending our lattice results to arbitrarily large t values by assuming a dipole ansatz for the generalized form factors. However, the assumption of a dipole behavior for the generalized form factors introduces a systematic dependence on the method used to extrapolate the lattice results to large t, and consequently, the short distance behavior of the resulting transverse quark distributions is particularly sensitive to the dipole assumption. Hence, in this section we rely on the dipole fit to the generalized form factors only as a means to determine the slope at $t = 0$, and, as discussed in Section 9.1, this is essentially a finite volume effect. Therefore the results we present in this section follow from our lattice results for the generalized form factors presented in Section 9.1 without any further assumptions. Thus in Section 9.3.1 below we discuss the momentum fraction dependence of the transverse quark distributions, and in Sections 9.3.2, 9.3.3, and 9.3.4 we discuss the mass, flavor, and spin dependence respectively of the transverse quark distributions of the nucleon.

9.3.1 Momentum Fraction Dependence

The generalized form factors give the moments of the transverse quark distributions as discussed in Section 2.7. The result is given here

$$\int_{-1}^{1} dx\, x^{n-1}\, q(x, \vec{b}_\perp) = \int \frac{d^2\Delta_\perp}{(2\pi)^2}\, e^{-i\vec{b}_\perp \cdot \vec{\Delta}_\perp} A^q_{n0}(-\vec{\Delta}^2_\perp). \tag{9.1}$$

As with the lattice calculation of the ordinary parton distributions, our lattice calculation is limited to the lowest few moments of the distribution. However, in calculating the transverse quark distributions we have an extra foot hold on the problem: we can examine the t behavior of the generalized form factors or equivalently the $\vec{b}_\perp$ behavior

of the transverse quark distributions. Additionally, the limit $x \to 1$ of the quark distribution $q(x, \vec{b}_\perp)$ can be understood. Qualitatively the argument is as follows. For $x \to 1$ a single quark carries all the longitudinal momentum of the nucleon. Furthermore, the center of the nucleon in transverse coordinates is defined as the center of longitudinal momentum,[4] thus a single fast moving quark with $x \to 1$ forms the center of the nucleon. Hence the distribution of this quark about the center must reduce to a delta function. Explicit calculations with light cone wave functions exhibit the same result [9], that is

$$\lim_{x \to 1} q(x, \vec{b}_\perp) = \delta^2(\vec{b}_\perp).$$

Now we note that the higher moments in Equation 9.1 above are dominated more and more by the contributions from x near 1. Thus we find the qualitative prediction that the Fourier transform of the generalized form factors for higher n should approach a delta function. Therefore the generalized form factors themselves should become flatter and flatter for higher moments.

There is one caveat in the argument above. The integral in Equation 9.1 for higher moments n is dominated by not only the contributions near $x = 1$ but also the contributions near $x = -1$. This effect can be removed but at the expense of explicitly keeping track of the particle and anti-particle distributions. That is, the odd moments measure the moments of $q(x) - \overline{q}(x)$ whereas the even moments give the moments of $q(x) + \overline{q}(x)$. Hence in the following, to ensure that we compare observables calculated in the same distribution we can only safely compare moments which differ by an even number.

We show our lattice results for the A_{n0}^{u-d} generalized form factors for $n = 1$, 2, and 3 in Figure 9-1. These are the generalized form factors for the heaviest quark mass considered in this thesis. Each of the generalized form factors have been normalized to unity at $t = 0$. Additionally, the lowest curve is A_{10}^{u-d}, the next curve up is A_{20}^{u-d}, and the highest curve is A_{30}^{u-d}. Therefore we find precisely the qualitative behavior we expect from the argument above. That is, the slopes of the generalized form factors

[4] This is the natural definition of the transverse center of a nucleon in the infinite momentum plane.

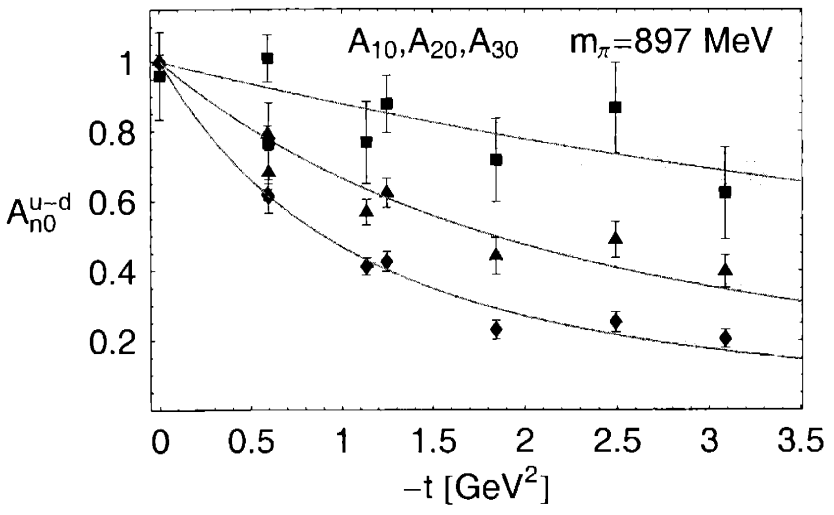

Figure 9-1: A_{n0}^{u-d} for $m_\pi = 897$ MeV

are decreasing for higher and higher moments.

Additionally, we can attempt a more quantitative description of the above result. The radius of the n^{th} moment of the transverse quark distribution is given by

$$\langle b_\perp^2 \rangle^{(n)} = \frac{\int d^2\vec{b}_\perp b_\perp^2 \int_{-1}^{1} dx\, x^{n-1}\, q(x, \vec{b}_\perp)}{\int d^2\vec{b}_\perp \int_{-1}^{1} dx\, x^{n-1}\, q(x, \vec{b}_\perp)} = \frac{4}{A_{n0}^q(0)} \frac{d}{dt} A_{n0}^q(0). \tag{9.2}$$

Therefore the properly normalized slopes of the generalized form factors determine the transverse radii of the moments of the transverse quark distributions. Applying Equation 9.2 above to the generalized form factors shown in Figure 9-1 gives the following root mean square (rms) radii $\sqrt{\langle b_\perp^2 \rangle_{u-d}^{(1)}} = 0.380(8)$ fm and $\sqrt{\langle b_\perp^2 \rangle_{u-d}^{(3)}} = 0.145(19)$ fm. Thus we find a 62 percent drop, from the first to the third moment, in the transverse size of the nucleon.

9.3.2 Quark Mass Dependence

We now repeat the discussion of the previous section for the results of the generalized form factors for the lightest quark mass studied in this thesis. The A_{n0}^{u-d} generalized form factors for $n = 1$, 2, and 3 are shown in Figure 9-2. As in Figure 9-1, the generalized form factors have all been normalized to unity, and additionally the curves

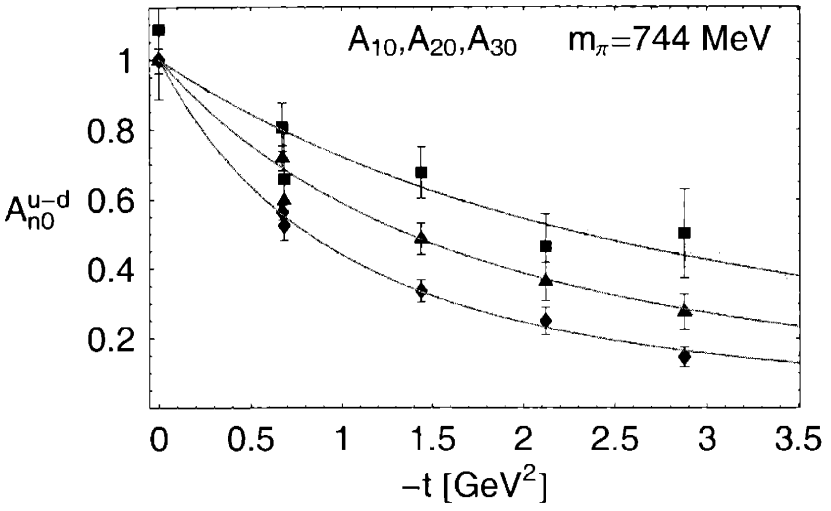

Figure 9-2: A_{n0}^{u-d} for $m_\pi = 744$ MeV

from the lowest to the highest correspond to A_{10}^{u-d}, A_{20}^{u-d}, and A_{30}^{u-d}. Therefore we find again that the qualitative expectation, as described in Section 9.3.1, that the slopes of the generalized form factors should be flatter and flatter for higher and higher moments holds for the lightest quark mass in our calculation as well as the heaviest. We can also use Equation 9.2 to determine the transverse rms radii of the moments of the transverse quark distribution. The results are $\sqrt{\langle b_\perp^2 \rangle_{u-d}^{(1)}} = 0.398(5)$ fm and $\sqrt{\langle b_\perp^2 \rangle_{u-d}^{(3)}} = 0.235(14)$ fm. Thus, as for the heavier quark mass, we find that the transverse quark distribution is dropping for larger momentum fractions x. However we note two differences. The transverse radii are larger for the lighter quark masses indicating that the nucleon is broader in the transverse coordinates for lighter quark masses. This certainly makes sense. The pion mass has dropped from $m_\pi = 895$ MeV to 753 MeV, thus we expect the pion cloud to be larger and hence the nucleon to be broader. Additionally, we note that the rate of fall off is down from 62 percent to 41 percent indicating that not only is the nucleon broader for lighter quark masses but also remains broader for higher momentum fractions x too.

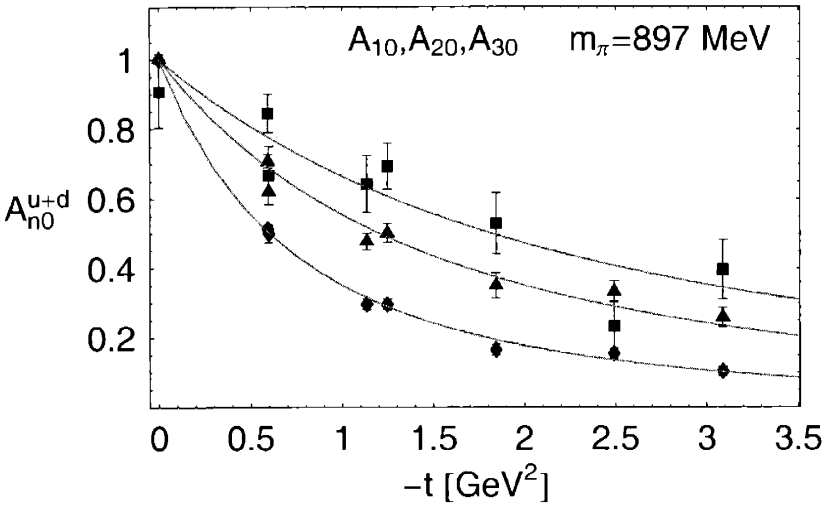

Figure 9-3: A_{n0}^{u+d} for $m_\pi = 897$ MeV

9.3.3 Flavor Dependence

Following Sections 9.3.1 and 9.3.2, we now consider the flavor structure of the transverse quark distributions. The A_{n0}^{u+d} generalized form factors for $n = 1$, 2, and 3 and for the heaviest quark mass considered in this thesis are shown in Figure 9-3. As in Sections 9.3.1 and 9.3.2, the curves in Figure 9-3 running from the lowest to the highest are A_{10}^{u+d}, A_{20}^{u+d}, and A_{30}^{u+d}. Again we find clearly the expected qualitative behavior, that is, the higher moments of the transverse quark distributions are successively flatter in t. The corresponding transverse radii, as calculated in Equation 9.2, are $\sqrt{\langle b_\perp^2 \rangle_{u-d}^{(1)}} = 0.463(5)$ fm and $\sqrt{\langle b_\perp^2 \rangle_{u-d}^{(3)}} = 0.266(19)$ fm, and the fall off between the first and third moment is 41 percent. For comparison the results from Section 9.3.1 for the $u - d$ distribution are $\sqrt{\langle b_\perp^2 \rangle_{u-d}^{(1)}} = 0.380(8)$ fm and $\sqrt{\langle b_\perp^2 \rangle_{u-d}^{(3)}} = 0.145(19)$ fm with a drop off of 62 percent from the first to third moment. Thus we find that the $u + d$ distribution is broader than the $u - d$ distribution, and additionally that the $u + d$ distribution has a flatter dependence on the momentum fraction x than the $u - d$ distribution.

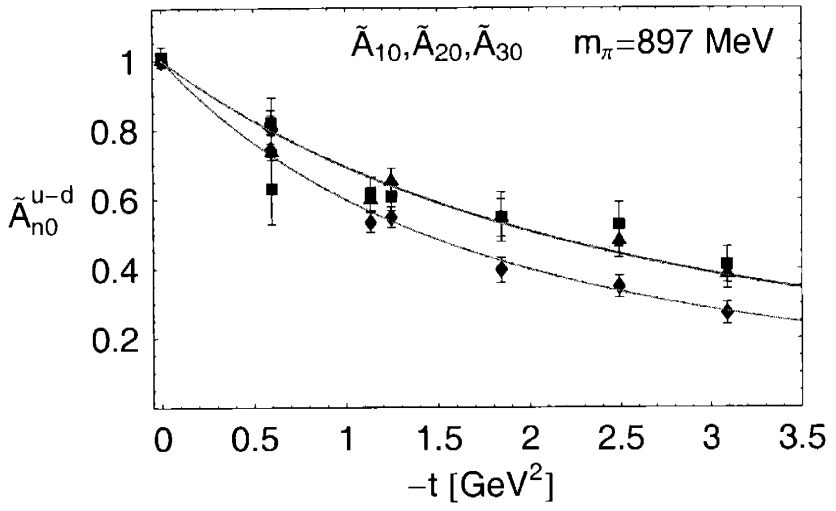

Figure 9-4: $\tilde{A}^{u-d}_{n0}$ for $m_\pi = 897$ MeV

9.3.4 Spin Dependence

Now we consider the spin structure of the transverse quark distributions. Again for the heaviest quark mass, the $\tilde{A}^{u-d}_{n0}$ generalized form factors for $n = 1$, 2, and 3 are shown in Figure 9-4. Notice that there are only two curves drawn. The lowest curve is $\tilde{A}^{u-d}_{10}$ and the highest curve is $\tilde{A}^{u-d}_{30}$. Therefore we find the ordering expected from the qualitative argument in Section 9.3.1. We also find an example of the caveat discussed in Section 9.3.1 that states that we can only safely compare moments which differ by an even number. As we see in the case of the polarized distributions, the $\tilde{A}^{u-d}_{20}$ generalized form factor does not lie in between the $\tilde{A}^{u-d}_{10}$ and $\tilde{A}^{u-d}_{30}$ generalized form factors. We suspect, though, that the $\tilde{A}^{u-d}_{40}$ generalized form factor should lie above $\tilde{A}^{u-d}_{20}$. Despite this subtlety, we can still compare the transverse rms radii of the first and third moments. The results following from Equation 9.2 are $\sqrt{\langle b_\perp^2 \rangle^{(1)}_{\Delta u - \Delta d}} = 0.302(5)$ fm and $\sqrt{\langle b_\perp^2 \rangle^{(3)}_{\Delta u - \Delta d}} = 0.250(10)$ fm which correspond to a drop of 17 percent from the first to the third moment. We can compare this with the transverse radii from the unpolarized distributions which are $\sqrt{\langle b_\perp^2 \rangle^{(1)}_{u-d}} = 0.380(8)$ fm and $\sqrt{\langle b_\perp^2 \rangle^{(3)}_{u-d}} = 0.145(19)$ fm with a corresponding drop of 62 percent. Thus we find a mixed result. The polarized distribution is narrower than the unpolarized distribution at low momentum fraction but is broader than the polarized distribution at higher momentum fraction.

Furthermore, the dependence of the transverse width on the momentum fraction is significantly weaker for the polarized distribution.

9.4 Transverse Quark Distributions from Dipole Fits

In this section we construct the $\vec{b}_\perp$ behavior of the transverse quark distributions as Fourier transforms of the generalized form factors, but we do this at the expense of assuming a dipole behavior for the generalized form factors for all t. Our calculations of the generalized form factors are clearly consistent with a dipole behavior, and additionally, we know that a dipole form factor is a reasonable phenomenological description of the elastic form factors as measured experimentally. Therefore in this section we assume that the dipole functional form for the generalized form factors observed for the range of t values in our calculations continues to hold for all t. Using this assumption in Section 9.4.1, we construct the unpolarized transverse quark distributions. Then in Sections 9.4.2, 9.4.3, and 9.4.4 we similarly determine the polarized transverse quark distributions, the transverse charge distributions, and the transverse momentum distributions respectively.

9.4.1 Unpolarized Transverse Quark Distributions

The unpolarized transverse quark distribution is determined by the A_{10} generalized form factor. The result from Equation 3.3 is

$$q(\vec{b}_\perp) = \int_{-1}^{1} dx\, q(x, \vec{b}_\perp) = \int \frac{d^2\Delta_\perp}{(2\pi)^2}\, e^{-i\vec{b}_\perp \cdot \vec{\Delta}_\perp} A^q_{10}(-\vec{\Delta}^2_\perp).$$

The transverse radii of these distributions are given by

$$\langle b^2_\perp \rangle^q = \frac{\int d^2b_\perp b^2_\perp q(\vec{b}_\perp)}{\int d^2b_\perp q(\vec{b}_\perp)} = \frac{4}{A^q_{10}(0)} \frac{d}{dt} A^q_{10}(0).$$

To examine the $\vec{b}_\perp$ dependence of the transverse quark distribution, we see from

m_π (MeV)	$\sqrt{\langle b_\perp^2 \rangle^{u-d}}$ (fm)	$\sqrt{\langle b_\perp^2 \rangle^{u+d}}$ (fm)	$\sqrt{\langle b_\perp^2 \rangle^{u}}$ (fm)	$\sqrt{\langle b_\perp^2 \rangle^{d}}$ (fm)
895	0.376(10)	0.451(7)	0.434(6)	0.485(10)
835	0.380(7)	0.451(8)	0.435(7)	0.483(11)
753	0.396(5)	0.479(10)	0.460(8)	0.515(14)

Table 9.6: Unpolarized Transverse Quark Radii

the above that we need the t dependence of $A_{10}^f(t)$. The results of our calculations for A_{10}^{u-d} and A_{10}^{u+d} are shown in Appendix B for each of the three quark masses in our calculation. The results are fit to a dipole form factor in each case. As seen it Figures B-1 through B-6, the dipole functional form consistently fits our results for A_{10}^f in the region of t consider in our calculations. The resulting fit parameters and errors are given in Table G.1. One the other hand, the transverse radius, $\langle b_\perp^2 \rangle^f$, requires only the normalization and slope of A_{10}^f. As described in Section 9.1, we can directly calculate the forward limit of A_{10}^f, and these results are tabulated in Table F.1. However, the slope of A_{10}^f requires an extrapolation for small t, for which we use the results of the dipole fits discussed above. Any small systematic error involved in the choice of the method to determine the slope of the form factors from discrete lattice results can be considered a finite volume effect as described in Section 9.1.

Using the results of our calculation described in the previous paragraph, we calculate the transverse radius for each flavor combination $u-d$, $u+d$, u, and d at each quark mass. These transverse radii are collected in Table 9.6. Note as usual, the $u-d$ combination is independent of the disconnected diagrams, whereas the $u+d$, u, and d combinations indicate the connected piece of these observables only. The transverse radii for all flavor combinations and quark masses lie in the range $0.38 - 0.52$ fm. Additionally, using the experimental results for the slopes of F_1^f for $f = u - d$, $u + d$, u, and d that we determine in Appendix I, the corresponding experimental values for the transverse radii are $\sqrt{\langle b_\perp^2 \rangle^{u-d}} = 0.644(7)$ fm, $\sqrt{\langle b_\perp^2 \rangle^{u+d}} = 1.14(1)$ fm, $\sqrt{\langle b_\perp^2 \rangle^{u}} = 0.654(6)$ fm, and $\sqrt{\langle b_\perp^2 \rangle^{d}} = 0.663(7)$ fm. Note that for all flavor combinations the lattice results are lower than the physical results. This is quite natural and expected. The quarks in our lattice calculation are more massive than those in the

natural world, and as a result the pion in our calculation is significantly heavier than the physical pion. This suppresses the pion cloud surrounding the nucleon and gives rise to a much more compact state than in the natural world.

For the quark masses considered in this thesis, the pion mass dependence of the transverse radii is very mild and essentially consistent with being flat. With caution, however, we note that the trend is in the correct direction. That is, the nucleon grows broader in the transverse coordinates as the pion mass decreases. Additionally, we note that the $u+d$ distribution is broader than the $u-d$ distribution and that the d distribution is broader than the u distribution, as is the case indicated by the physical values.

The transverse radii set the scales for the transverse distributions, and furthermore are essentially unambiguous calculations modulo disconnected diagrams. Now we go a bit further and attempt to calculate the transverse quark distributions as functions of $\vec{b}_\perp$. As Equation 3.3 indicates, this requires the Fourier transform of $A_{10}^f(t)$ and hence requires the complete t dependence of A_{10}^f. As seen in Figures B-1 through B-6, both A_{10}^{u-d} and the connected piece of A_{10}^{u+d} are consistently described by dipole form factors in the region of t accessible to our lattice calculations. For the purpose of developing an understanding of the shape of the $\vec{b}_\perp$ distributions, we now extend the dipole form factor to all t and evaluate the Fourier transform. It is clear that at this point we have introduced a model dependency into the calculation of $q(\vec{b}_\perp)$. It is conceivable that at some point lattice calculations will be performed with a sufficient range of t values that the Fourier transform can be evaluated numerically. As our calculations are not currently at that stage, we simple assume the dipole form. Note that the assumption of a dipole functional form is most questionable for the $t > 3$ GeV^2 region missing from our calculations. Therefore we expect that the systematic error due to this assumption is most significant for the region $b_\perp < 1/\sqrt{3 \text{ GeV}^2} \approx 0.11$ fm.

We offer two further comments with regard to the dipole assumption. First the resulting t^{-2} behavior for large t is consistent with the perturbative expectation for $A_{10}(t) = F_1(t)$, although the coefficient of this behavior is not known perturbatively. Additionally, as shown in Appendices N and O.17, the Fourier transform of a dipole

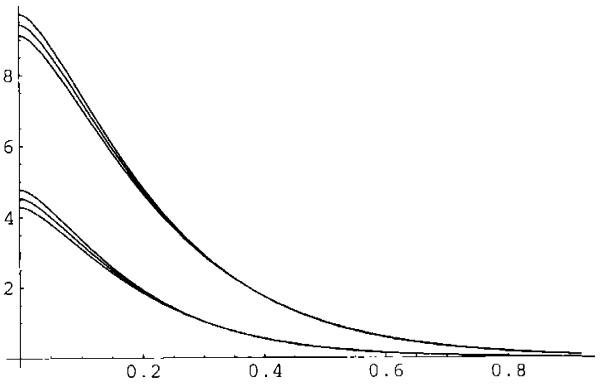

Figure 9-5: $q^f(\vec{b}_\perp)$ for $f = u - d$ and $u + d$, $m_\pi = 895$ MeV

in two dimensions gives rise to a distribution that is regular at the origin. This is in sharp contrast to the cusp that results from the three dimensional transform of a dipole as shown in Appendix O.18.

Assuming a dipole form for A_{10}^f for $f = u - d$ and $u + d$ and using the results from Appendices N and O.17, the transverse quark distributions are

$$q^f(\vec{b}_\perp) = \int d^2\Delta_\perp \, e^{-i\vec{b}_\perp \cdot \vec{\Delta}_\perp} \frac{A_f}{\left(1 + \frac{\vec{\Delta}_\perp^2}{m_f^2}\right)^2} = \pi \, A_f \, m_f^2 \, (m_f b_\perp) \, K_1(m_f b_\perp)$$

where $K_1(z)$ is a modified Bessel function, and the parameters A_f and m_f are given in Table G.1 for $f = u - d$ and $u + d$. The resulting $q^{u-d}(\vec{b}_\perp)$ and $q^{u+d}(\vec{b}_\perp)$ are shown in Figure 9-5 for the heaviest quark mass corresponding to $m_\pi = 895$ MeV. As indicated by the transverse radii in Table 9.6, the $u + d$ distribution is broader than the $u - d$ distribution. Furthermore, note that the $u + d$ distribution is the probability to find any quark, regardless of flavor, spin, or longitudinal momentum, at a displacement of $b_\perp$ from the center of the proton. Ignoring the disconnected diagrams, we now resolve the flavor structure of the total quark distribution q^{u+d}. To remain consistent with the results in Figure 9-5, we take $q^u = (q^{u+d} + q^{u-d})/2$ and $q^d = (q^{u+d} - q^{u-d})/2$. The resulting quark distributions are shown in Figure 9-6. We see that the u quark distribution dominates for smaller $b_\perp$, but as indicated by the transverse radii in Table G.1, the d quark distribution is ultimately broader. We note

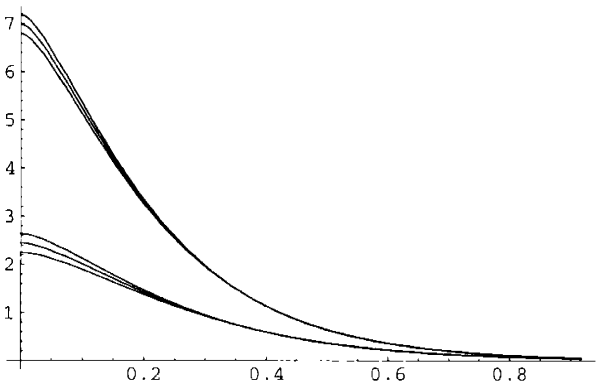

Figure 9-6: $q^f(\vec{b}_\perp)$ for $f = u$ and d, $m_\pi = 895$ MeV

that it is not visible with the resolution of Figure 9-6, but the u and d distributions cross at $b_\perp = 1.30$ fm, beyond which the d quark distribution dominates.

9.4.2 Polarized Transverse Quark Distributions

The polarized transverse quark distributions are related to $\tilde{A}^q_{10}$ and A^q_{10} as follows.

$$\begin{aligned} q^\uparrow(\vec{b}_\perp) &= \int_{-1}^{1} dx\, q^\uparrow(x,\vec{b}_\perp) = \int \tfrac{d^2\Delta_\perp}{(2\pi)^2}\, e^{-i\vec{b}_\perp\cdot\Delta_\perp}\, \tfrac{1}{2}\left[A^q_{10}(-\vec{\Delta}^2_\perp) + \tilde{A}^q_{10}(-\vec{\Delta}^2_\perp)\right] \\ q^\downarrow(\vec{b}_\perp) &= \int_{-1}^{1} dx\, q^\downarrow(x,\vec{b}_\perp) = \int \tfrac{d^2\Delta_\perp}{(2\pi)^2}\, e^{-i\vec{b}_\perp\cdot\Delta_\perp}\, \tfrac{1}{2}\left[A^q_{10}(-\vec{\Delta}^2_\perp) - \tilde{A}^q_{10}(-\vec{\Delta}^2_\perp)\right] \end{aligned}$$

The corresponding polarized transverse radii are

$$\begin{aligned} \langle b^2_\perp\rangle^{\uparrow q} &= \frac{\int d^2b_\perp b^2_\perp q^\uparrow(\vec{b}_\perp)}{\int d^2b_\perp q^\uparrow(\vec{b}_\perp)} = 4\left[\tfrac{d}{dt}A^q_{10}(t) + \tfrac{d}{dt}\tilde{A}^q_{10}(t)\right]_{t=0} \Big/ \left[A^q_{10}(0) + \tilde{A}^q_{10}(0)\right] \\ \langle b^2_\perp\rangle^{\downarrow q} &= \frac{\int d^2b_\perp b^2_\perp q^\downarrow(\vec{b}_\perp)}{\int d^2b_\perp b^2_\perp q^\downarrow(\vec{b}_\perp)} = 4\left[\tfrac{d}{dt}A^q_{10}(t) - \tfrac{d}{dt}\tilde{A}^q_{10}(t)\right]_{t=0} \Big/ \left[A^q_{10}(t) - \tilde{A}^q_{10}(t)\right], \end{aligned}$$

and the normalized spin fractions for each quark flavor are

$$\begin{aligned} \frac{\langle 1\rangle^{\uparrow q}}{\langle 1\rangle^q} &= \frac{1}{2}\left(\frac{A^q_{10}(0) + \tilde{A}^q_{10}(0)}{A^q_{10}(0)}\right) \\ \frac{\langle 1\rangle^{\downarrow q}}{\langle 1\rangle^q} &= \frac{1}{2}\left(\frac{A^q_{10}(0) - \tilde{A}^q_{10}(0)}{A^q_{10}(0)}\right). \end{aligned}$$

The polarized transverse quark distributions require the $\tilde{A}^f_{10}(t)$ as well as $A^f_{10}(t)$ form factors. Our lattice results for $A^f_{10}(t)$ are discussed carefully in Section 9.4.1.

m_π (MeV)	$\langle 1 \rangle^{\uparrow u - \uparrow d} / \langle 1 \rangle^{u-d}$	$\langle 1 \rangle^{\uparrow u + \uparrow d} / \langle 1 \rangle^{u+d}$	$\langle 1 \rangle^{\uparrow u} / \langle 1 \rangle^{u}$	$\langle 1 \rangle^{\uparrow d} / \langle 1 \rangle^{d}$
895	1.095(9)	0.614(3)	0.734(4)	0.373(5)

Table 9.7: Spin ↑ Fraction

m_π (MeV)	$\langle 1 \rangle^{\downarrow u - \downarrow d} / \langle 1 \rangle^{u-d}$	$\langle 1 \rangle^{\downarrow u + \downarrow d} / \langle 1 \rangle^{u+d}$	$\langle 1 \rangle^{\downarrow u} / \langle 1 \rangle^{u}$	$\langle 1 \rangle^{\downarrow d} / \langle 1 \rangle^{d}$
895	−0.095(9)	0.386(3)	0.266(4)	0.627(5)

Table 9.8: Spin ↓ Fraction

Briefly, we note that the results for $A_{10}^f(t)$ for $f = u - d$ and $u + d$ are shown for each quark mass in Appendix B. Each figure shows a dipole fit to $A_{10}^f(t)$, and the resulting parameters are given in Table G.1. Our lattice results for $\tilde{A}_{10}^f(t)$ are shown in Appendix E for $f = u-d$ and $u+d$ but only $m_\pi = 895$ MeV. The results for $\tilde{A}_{10}^f(t)$ are consistently fit with a dipole functional form in the range of t values considered in our work. The corresponding dipole parameters and errors are given in Table G.4. We repeat the comment from Section 9.4.1 that the use of a dipole form to determine the slopes of $A_{10}^f(t)$ and $\tilde{A}_{10}^f(t)$ is a rather mild assumption, and hence the values of the transverse radii given in this section are rather clean results. However, the use of the dipole form for all t is a stronger assumption and introduces a systematic error in the transverse distributions which is expected to be significant for the region $b_\perp < 0.11$ fm only.

The fraction of a flavor combination with spin parallel or anti-parallel to the proton spin is given in Tables 9.7 and 9.8 respectively for the usual flavor combinations $u-d$, $u+d$, u, and d. These values are calculated using only A_{10}^f and $\tilde{A}_{10}^f$ which can both be measured in the forward limit directly and are given in Tables F.1 and F.3 respectively. We note that the $u - d$ distribution is not positive definite. This is reflected in the larger than 1 and negative spin fractions for $u - d$ in Tables 9.7 and 9.8. Also, notice the striking difference between the u and d quarks. The u quark is nearly 2.8 times more likely to be polarized parallel to the nucleon than anti-parallel, whereas the d quark is almost 1.7 times more likely to be anti-parallel than parallel.

The polarized transverse radii are given in Tables 9.9 and 9.10. As mentioned

m_π (MeV)	$\sqrt{\langle b_\perp^2 \rangle^{\uparrow u - \uparrow d}}$ (fm)	$\sqrt{\langle b_\perp^2 \rangle^{\uparrow u + \uparrow d}}$ (fm)	$\sqrt{\langle b_\perp^2 \rangle^{\uparrow u}}$ (fm)	$\sqrt{\langle b_\perp^2 \rangle^{\uparrow d}}$ (fm)
895	0.336(10)	0.426(7)	0.395(7)	0.530(11)

Table 9.9: Spin ↑ Transverse Quark Radii

m_π (MeV)	$\sqrt{\langle b_\perp^2 \rangle^{\downarrow u - \downarrow d}}$ (fm)	$\sqrt{\langle b_\perp^2 \rangle^{\downarrow u + \downarrow d}}$ (fm)	$\sqrt{\langle b_\perp^2 \rangle^{\downarrow u}}$ (fm)	$\sqrt{\langle b_\perp^2 \rangle^{\downarrow d}}$ (fm)
895	$0.402(9) \cdot \sqrt{-1}$	0.487(8)	0.524(6)	0.453(10)

Table 9.10: Spin ↓ Transverse Quark Radii

above, these values depend only on the intercept and slope of $A_{10}^f(t)$ and $\tilde{A}_{10}^f(t)$. The forward limits of $A_{10}^f(t)$ and $\tilde{A}_{10}^f(t)$ are both directly calculable and are given in Tables F.1 and F.3 respectively. The slopes are determined from the dipole fits in Tables G.1 and G.4. Note that the $\downarrow u - \downarrow d$ distribution is not positive definite. As a consequence, the corresponding radii is negative, $\langle b_\perp^2 \rangle^{\downarrow u - \downarrow d} = -0.161(7)$ fm^2. This is indicate by the $\sqrt{-1}$ in the appropriate entry in Table 9.10. Furthermore, notice the parallels between the spin fraction and the transverse spin radius. The u quark is predominantly spin aligned, and the corresponding spin aligned radius is smaller then the spin anti-aligned radius. Whereas the d quark is predominantly spin anti-aligned, and the corresponding spin anti-aligned radius is smaller than the spin aligned radius. The same behavior occurs for the combination $u + d$ as well. Thus we see that the favored spin for a given quark flavor is more compactly distributed than the disfavored spin.

In an attempt to understand and visualize the above results we construct the polarized transverse quark distributions as a function of $b_\perp$. As discussed carefully in Section 9.4.1, we extend the established dipole pole behavior of A_{10}^f and $\tilde{A}_{10}^f$ beyond $-t = 3$ GeV^2. This assumption introduces some systematic or model dependent errors into our calculation of $q^\uparrow(\vec{b}_\perp)$ and $q^\downarrow(\vec{b}_\perp)$, though we expect the strongest effects to be limited to $b_\perp < 0.11$ fm. As discussed in Appendices N and O.17, the two dimensional Fourier transform of a dipole form factor results in a modified Bessel function. Applying the same results to the spin aligned and anti-aligned distributions gives linear combinations of the same Bessel function. The resulting polarized trans-

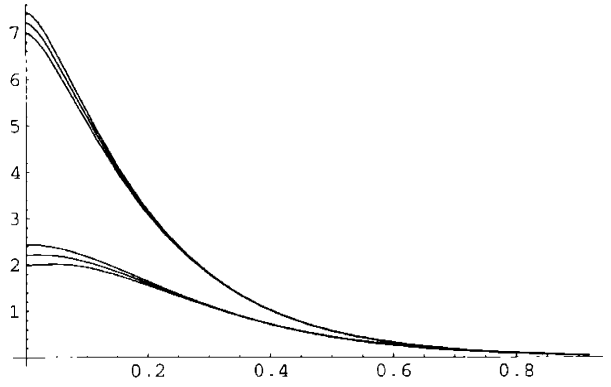

Figure 9-7: $q^{\uparrow u+\uparrow d}(\vec{b}_\perp)$ and $q^{\downarrow u+\downarrow d}(\vec{b}_\perp)$ for $m_\pi = 895$ MeV

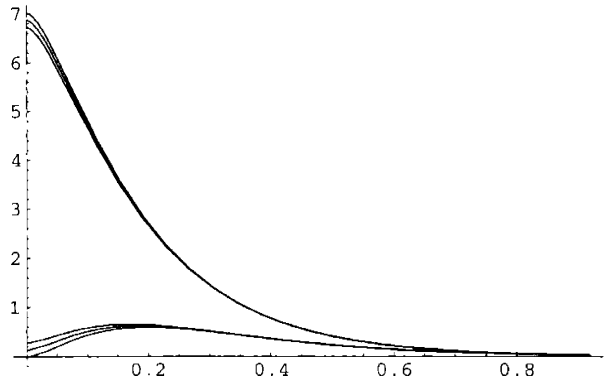

Figure 9-8: $q^{\uparrow u}(\vec{b}_\perp)$ and $q^{\downarrow u}(\vec{b}_\perp)$ for $m_\pi = 895$ MeV

verse quark distributions are given in Figures 9-7, 9-8 and 9-9 for $m_\pi = 895$ MeV. In Figure 9-7 we show the flavor combination $u + d$. This gives the net quark spin distribution regardless of the flavor. As remarked earlier, we see that the favored spin, in this case spin aligned, is more compactly distributed. Also notice that the spin anti-aligned distribution as a maximum at $b_\perp = 0.0174$ fm. This distance is sufficiently short that it is likely contaminated by systematic error due to the dipole assumption for $-t > 3$ GeV^2.

We also study the flavor structure of the transverse spin distributions. The $u^\uparrow(\vec{b}_\perp)$ and $u^\downarrow(\vec{b}_\perp)$ transverse spin distributions are shown in Figure 9-8 for $m_\pi = 895$ MeV, and the $d^\uparrow(\vec{b}_\perp)$ and $d^\downarrow(\vec{b}_\perp)$ distributions are shown in Figure 9-9 for the same pion mass. We see again that the disfavored spin is distributed more broadly than the

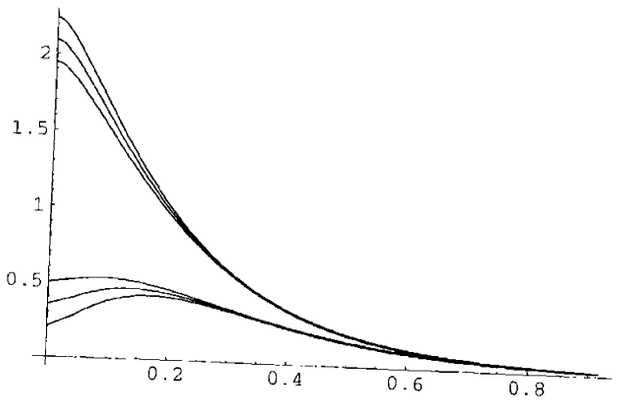

Figure 9-9: $q^{\uparrow d}(\vec{b}_\perp)$ and $q^{\downarrow d}(\vec{b}_\perp)$ for $m_\pi = 895$ MeV

favored spin. The $u^{\downarrow}(\vec{b}_\perp)$ distribution has a maximum at $b_\perp = 0.184$ fm, and the $d^{\uparrow}(\vec{b}_\perp)$ distribution has a maximum at $b_\perp = 0.134$ fm.

9.4.3 Transverse Charge Distributions

The transverse charge distributions are simple linear combinations of the unpolarized transverse quark distributions, hence all the information is already contained in Section 9.4.1. We choose to display these flavor combinations separately as they correspond directly to the form factors probed in experiment. Furthermore, the interpretation of, or lack thereof, the electromagnetic form factors has a long history. Therefore, we emphasis the idea that the F_1 form factor is the Fourier transform of the charge distribution in the transverse plane of a fast moving nucleon.

The flavor combinations corresponding to the proton and neutron charge distributions are

$$\rho^p(\vec{b}_\perp) = \frac{2}{3}u(\vec{b}_\perp) - \frac{1}{3}d(\vec{b}_\perp) = \int \frac{d^2\Delta_\perp}{(2\pi)^2}\, e^{-i\vec{b}_\perp\cdot\vec{\Delta}_\perp}\left[\frac{1}{6}A_{10}^{u+d}(-\vec{\Delta}_\perp^2) + \frac{1}{2}A_{10}^{u-d}(-\vec{\Delta}_\perp^2)\right]$$

$$\rho^n(\vec{b}_\perp) = -\frac{1}{3}u(\vec{b}_\perp) + \frac{2}{3}d(\vec{b}_\perp) = \int \frac{d^2\Delta_\perp}{(2\pi)^2}\, e^{-i\vec{b}_\perp\cdot\vec{\Delta}_\perp}\left[\frac{1}{6}A_{10}^{u+d}(-\vec{\Delta}_\perp^2) - \frac{1}{2}A_{10}^{u-d}(-\vec{\Delta}_\perp^2)\right]$$

m_π (MeV)	$\sqrt{\langle b_\perp^2 \rangle_\rho^p}$ (fm)	$\sqrt{\langle b_\perp^2 \rangle_\rho^n}$ (fm)
895	0.416(20)	0.177(20)
835	0.418(16)	0.171(16)
753	0.440(13)	0.189(13)

Table 9.11: Transverse Proton and Neutron Charge Radii

as given in Equation 3.3. The corresponding transverse charge radii are given as

$$\langle b_\perp^2 \rangle_\rho^p = \frac{1}{2}\langle b_\perp^2 \rangle^{u+d} + \frac{1}{2}\langle b_\perp^2 \rangle^{u-d} = \frac{2}{3}\frac{dA_{10}^{u+d}(0)}{dt} + 2\frac{dA_{10}^{u-d}(0)}{dt}$$

$$\langle b_\perp^2 \rangle_\rho^n = \frac{1}{2}\langle b_\perp^2 \rangle^{u+d} - \frac{1}{2}\langle b_\perp^2 \rangle^{u-d} = \frac{2}{3}\frac{dA_{10}^{u+d}(0)}{dt} - 2\frac{dA_{10}^{u-d}(0)}{dt}$$

where the apparent factor of 3 in front of $\langle b_\perp^2 \rangle^{u+d}$ is due to the difference in normalization of the $u+d$ distribution versus the charge distributions.

As we see from the above equations, the transverse charge radii depend on the slope of the A_{10}^f generalized form factors and the transverse charge distribution depends on the complete function $A_{10}^f(t)$. Our lattice results for $A_{10}^f(t)$ are discussed thoroughly in Section 9.4.1, therefore we simply summarize the results here. The lattice calculation of $A_{10}^f(t)$ is shown in Figures B-1 through B-6 for $f = u - d$ and $u + d$ and for each quark mass in our calculation. In each figure we show the resulting dipole fit. The parameters for each dipole fit are collected in Table G.1.

The proton and neutron charge radii are calculated for each quark mass and shown in Table 9.4.3. As discussed in Section 9.4.1, the transverse radii are not heavily dependent on the assumption of a dipole functional form. However, we remind the reader that the disconnected contributions are missing from the $u + d$ combination used above. The physical values for the proton and neutron transverse charge radii are $\sqrt{\langle b_\perp^2 \rangle_\rho^p} = 0.652(7)$ fm and $\sqrt{\langle b_\perp^2 \rangle_\rho^n} = 0.083(8)$ fm where we use the slopes of the F_1^p and F_1^n form factors as demonstrated in the Appendix I.[5] Note that our lattice results are essentially independent of m_π for the heavy quark masses in our calculations. Furthermore we note that the transverse proton charge radii, which

[5]We comment on the sign of the neutron transverse charge radius later in this section.

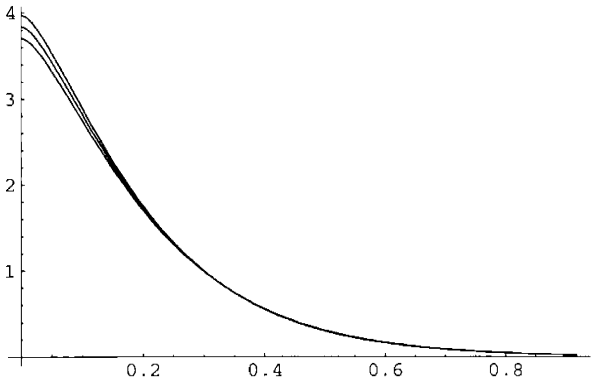

Figure 9-10: $\rho^p(\vec{b}_\perp)$ for $m_\pi = 895$ MeV

lie in the range $0.416 - 0.440$ fm, are all lower than the physical value of 0.652 fm, whereas the transverse neutron charge radii span the range $0.171 - 0.189$ fm, and are all higher than the rather small physical value of 0.083 fm.

In accordance with the previous two sections, we determine the transverse charge distributions based on the assumption of a dipole form factor. This is discussed thoroughly in Section 9.4.1. We remind the reader that the lattice results are consistent with a dipole functional form for $-t < 3$ GeV^2, and hence we expect the systematic errors associated with the assumption of a dipole form factor to be mostly limited to the region $b_\perp < 0.11$ fm. Our results for the proton transverse charge distribution for a pion mass of 895 MeV is shown in Figure 9.4.3. The charge radius from Table 9.4.3 for this pion mass is 0.416(20) fm, and is clearly the relevant scale for the proton charge distribution. Furthermore, we note that the proton charge distribution remains positive for all $b_\perp$. However, the neutron charge distribution must have regions of both positive and negative charge to give rise to an overall neutral object. The transverse charge distribution for the neutron at the same pion mass of 895 MeV is shown in Figure 9.4.3. The most striking feature of the neutron charge distribution is that the charge distribution is negative for small $b_\perp$ and positive for large $b_\perp$. This is clearly in accord with the sign of the transverse charge radii as calculated in Table 9.4.3, $\sqrt{\langle b_\perp^2 \rangle_\rho^n} = 0.177(20)$ fm, but is precisely the reverse of what is traditionally expected for the neutron. This traditional expectation is based on the result for the canonically

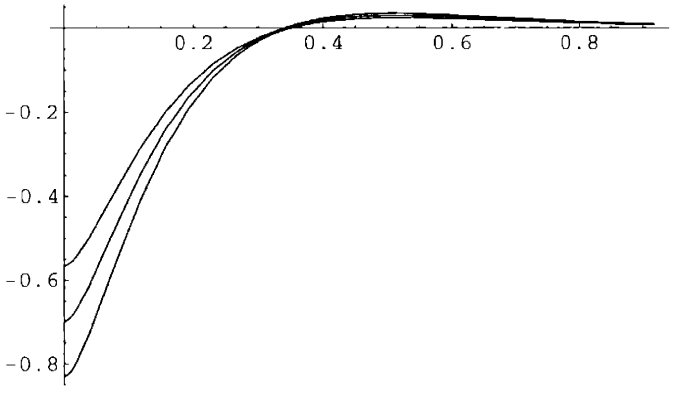

Figure 9-11: $\rho^n(\vec{b}_\perp)$ for $m_\pi = 895$ MeV

defined three dimensional charge radius, $\langle r^2 \rangle^n = 6G'_{En}(0) = -0.116$ fm^2. We point out that this definition is based on a non-relativistic argument and hence suffers from corrections controlled by $1/m_n^2 \approx 0.04$ fm. On the other hand, the transverse charge radius is given by $\langle b_\perp^2 \rangle_\rho^n = 4F'_{1n}(0) = 0.0069(14)$ fm^2, is based on an argument in the infinite momentum frame, and is not affected by relativistic corrections. Simply put, the slopes of G_{En} and F_{1n} have different signs, both in the natural world and in our lattice calculations. As a result the canonically defined charge distribution in the rest frame and the transverse charge distribution in the infinite momentum frame have different shapes.

9.4.4 Transverse Momentum Distributions

The transverse momentum distribution is determined by the $A_{20}^q(t)$ generalized form factor as given in Equation 3.4

$$\varepsilon^q(\vec{b}_\perp) = \int_{-1}^{1} dx\, xq(x, \vec{b}_\perp) = \int \frac{d^2\Delta_\perp}{(2\pi)^2} e^{-i\vec{b}_\perp \cdot \Delta_\perp} A_{20}^q(-\vec{\Delta}_\perp^2)$$

with transverse momentum radii given as

$$\langle b_\perp^2 \rangle_\varepsilon^q = \frac{\int d^2b_\perp b_\perp^2 \varepsilon^q(\vec{b}_\perp)}{\int d^2b_\perp \varepsilon^q(\vec{b}_\perp)} = 4\frac{d}{dt} A_{20}^q(t)\Big|_{t=0} / A_{20}^q(0).$$

m_π (MeV)	$\langle b_\perp^2 \rangle_\varepsilon^{u-d}$	$\langle b_\perp^2 \rangle_\varepsilon^{u+d}$	$\langle b_\perp^2 \rangle_\varepsilon^{u}$	$\langle b_\perp^2 \rangle_\varepsilon^{d}$
895	0.247(6)	0.675(6)	0.461(5)	0.214(4)
835	0.242(10)	0.656(10)	0.449(9)	0.207(4)
753	0.263(15)	0.677(15)	0.470(13)	0.207(8)

Table 9.12: Momentum Fractions

Furthermore, note that the fraction of the momentum carried by quark q is

$$\langle 1 \rangle_\varepsilon^q = \frac{\int d^2b_\perp \varepsilon^q(\vec{b}_\perp)}{\int d^2b_\perp \varepsilon^q(\vec{b}_\perp)} = A_{20}^q(0).$$

The above quantity is identically the momentum fraction for the quark q as well, that is, $\langle 1 \rangle_\varepsilon^q = \langle x \rangle^q$.

The momentum fraction carried by each quark is determined solely by $A_{20}^q(0)$ and, hence, is directly calculable. Our lattice results for $A_{20}^f(0)$ are given in Table F.2 for $f = u - d$ and $u + d$ and each quark mass. The transverse momentum radius is given by $A_{20}^q(0)$ and additionally the slope of $A_{20}^q(0)$. As discussed in the previous sections, in particular Section 9.4.1, the slope is determined by a dipole fit. The complete transverse momentum distribution depends on the functional form of $A_{20}^f(t)$. Our lattice results for $A_{20}^f(t)$ are shown in Appendix C for $f = u - d$ and $u + d$ and for each quark mass in our calculation. With each figure in Appendix C we show a dipole fit. As the figures show, the dipole form is a consistent fit. Phenomenologically, we know $A_{10}(t)$ and $B_{10}(t)$ are well described by a dipole form, therefore it is illuminating that this behavior continues to hold for the higher generalized form factors. The dipole parameters and errors are collected in Table G.2. We note that the individual quark and gluon transverse momentum distributions are renormalization scale dependent. Only the sum of all quark and gluon contributions is scale invariant. The renormalization scale used for the following results is $\mu = a^{-1}$ as given in Table 9.1. In particular, for the plotted distribution below at $m_\pi = 895$ MeV, the renormalization scale is $\mu = 2.01(1)$ GeV.

The momentum fractions are shown in Table 9.12. We note that this observable is evaluated directly on the lattice and requires no interpolation or extrapolation with

m_π (MeV)	$\langle b_\perp^2 \rangle_\varepsilon^{u-d}$ (fm^2)	$\langle b_\perp^2 \rangle_\varepsilon^{u+d}$ (fm^2)	$\langle b_\perp^2 \rangle_\varepsilon^{u}$ (fm^2)	$\langle b_\perp^2 \rangle_\varepsilon^{d}$ (fm^2)
895	0.324(9)	0.262(10)	0.309(8)	0.356(14)
835	0.324(8)	0.278(8)	0.313(6)	0.349(13)
753	0.362(14)	0.315(12)	0.350(11)	0.389(22)

Table 9.13: Transverse Momentum Radii

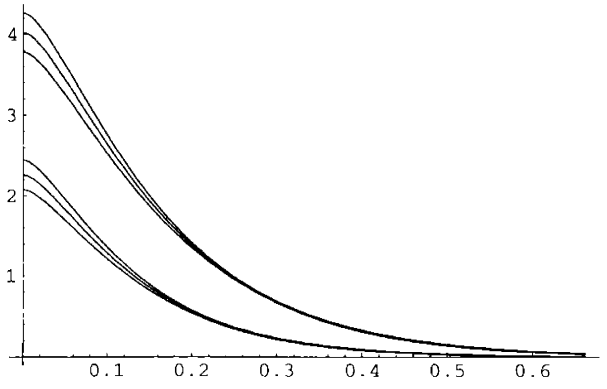

Figure 9-12: $\varepsilon^f(\vec{b}_\perp)$ for $f = u - d$ and $u + d$, $m_\pi = 895$ MeV

a dipole form. Hence, apart from disconnected contributions, these observables are sturdy results. The $u - d$ contribution is unaffected by disconnected diagrams and unambiguously determines that the u quark carries roughly 25 percent of the proton's momentum beyond that carried by the d quark.

In Table 9.13, we tabulate the transverse momentum radii. Notice that the transverse d quark momentum distribution is consistently broader than the u quark momentum distribution, whereas the u quark contributes more momentum to the proton that does the d quark. This is analogous to the spin distribution in which the favored spin alignment was narrower than the disfavored spin alignment.

The transverse momentum distributions are shown in Figures 9-12 and 9-13. The total quark transverse momentum distribution corresponds to the $u + d$ flavor combination shown in Figure 9-12. The flavor decomposition of the quark momentum combination is shown in Figure 9-13. Notice that the transverse d quark momentum distribution is broader than the u quark momentum distribution, despite contributing less than half the proton's momentum.

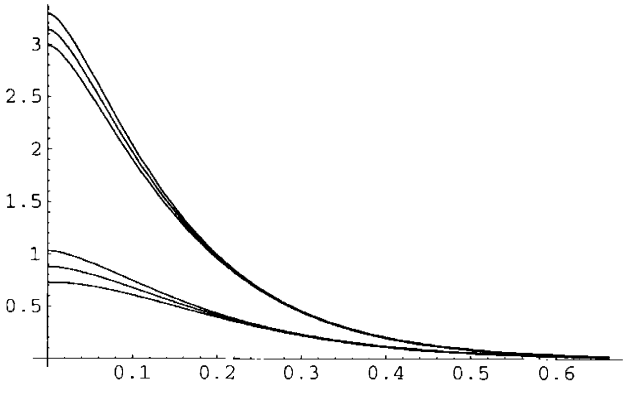

Figure 9-13: $\varepsilon^f(\vec{b}_\perp)$ for $f = u$ and d, $m_\pi = 895$ MeV

Appendix A

Conventions

Indices

The number of colors is $N_c = 3$, and color indices are denoted as lower case Latin letters: a, b, etc. The number of flavors is $N_f = 2$. Some results assume degenerate u and d quark masses. The dimension of the Dirac representation is denoted as $N_d = 4$, and Dirac indices are lower case greek letters: α, β, etc. The number of space-time dimensions is $D = 4$.

Gauge Links

The gauge links are defined so that $U_\mu^\dagger(x)$ parallel propagates a quark field from the point x to the point $x + \mu$. Some references use a different notation in which the parallel propagator from the point x to the point $x + \mu$ is denoted by $U(x + \mu, x)$. The mapping between the two notations is

$$U(x + \mu, x) = U_\mu^\dagger(x).$$

The backward gauge links are defined by

$$U_{-\mu}^\dagger(x) = U_\mu(x - \mu).$$

Dirac Matrices

The Minkowski Dirac matrices are denoted by $\gamma_{\rm M}^{\mu}$ with $\mu = 0$, 1, 2, or 3 and satisfy the Dirac algebra

$$\{\gamma_{\rm M}^{\mu}, \gamma_{\rm M}^{\nu}\} = 2g^{\mu\nu}$$

where g is a diagonal matrix given by $g^{\mu\nu} = \mathrm{diag}(1, -1, -1, -1)$. The Dirac matrices with lowered indices are defined as usual by $\gamma_{\mu}^{\rm M} = g_{\mu\nu}\gamma_{\rm M}^{\nu}$. The explicit representation used in our calculations is the *Bjorken and Drell* representation used in [3]. It is given in 2×2 block form as

$$\gamma^0 = \begin{pmatrix} 1 & 0 \\ 0 & -1 \end{pmatrix} \qquad \gamma^i = \begin{pmatrix} 0 & \sigma_i \\ -\sigma_i & 0 \end{pmatrix}$$

and explicitly in 4×4 form as

$$\gamma^0 = \begin{pmatrix} 1 & 0 & 0 & 0 \\ 0 & 1 & 0 & 0 \\ 0 & 0 & -1 & 0 \\ 0 & 0 & 0 & -1 \end{pmatrix} \quad \gamma^1 = \begin{pmatrix} 0 & 0 & 0 & 1 \\ 0 & 0 & 1 & 0 \\ 0 & -1 & 0 & 0 \\ -1 & 0 & 0 & 0 \end{pmatrix}$$

$$\gamma^2 = \begin{pmatrix} 0 & 0 & 0 & -i \\ 0 & 0 & i & 0 \\ 0 & i & 0 & 0 \\ -i & 0 & 0 & 0 \end{pmatrix} \quad \gamma^3 = \begin{pmatrix} 0 & 0 & 1 & 0 \\ 0 & 0 & 0 & -1 \\ -1 & 0 & 0 & 0 \\ 0 & 1 & 0 & 0 \end{pmatrix}.$$

The Dirac matrices for negative μ are defined by

$$\gamma_{\rm M}^{-\mu} = -\gamma_{\rm M}^{\mu}.$$

The charge conjugation matrix is

$$C = i\gamma_{\rm M}^2\gamma_{\rm M}^0$$

and γ^5 is

$$\gamma^5_{\rm M} = i\gamma^0_{\rm M}\gamma^1_{\rm M}\gamma^2_{\rm M}\gamma^3_{\rm M}.$$

The Euclidean Dirac matrices are

$$\begin{aligned}\gamma^{\rm E}_0 &= \gamma^0_{\rm M} \\ \gamma^{\rm E}_i &= -i\gamma^i_{\rm M}.\end{aligned}$$

Parton Distributions

The momentum fraction x used in ordinary, generalized, and transverse parton distributions is taken to be in the range $[-1, 1]$. With this convention the particle distributions are given by $q(x)$, $\Delta q(x)$, and $\delta q(x)$ for $x \geq 0$, and the anti-particle distributions are given by $\overline{q}(x) = -q(-x)$, $\Delta\overline{q}(x) = \Delta q(-x)$, and $\delta\overline{q}(x) = \delta q(-x)$ again for $x \geq 0$.

Appendix B

Figures of $A_{10}^{u-d}(t)$ and $A_{10}^{u+d}(t)$

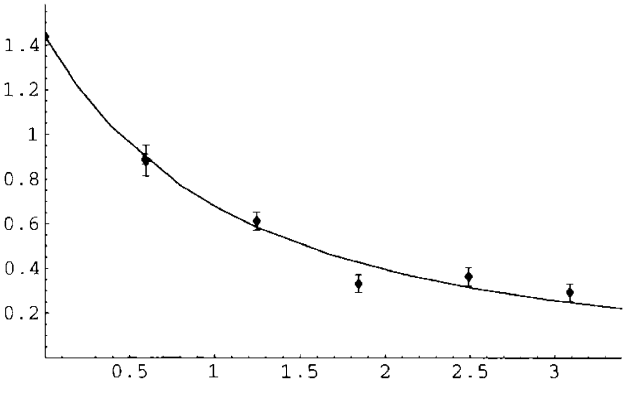

Figure B-1: A_{10}^{u-d} for $m_\pi = 895$ MeV

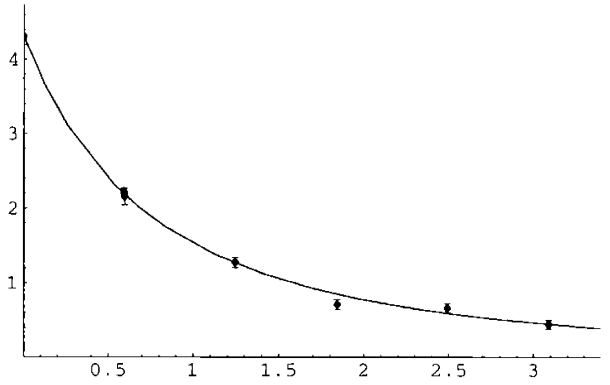

Figure B-2: A_{10}^{u+d} for $m_\pi = 895$ MeV

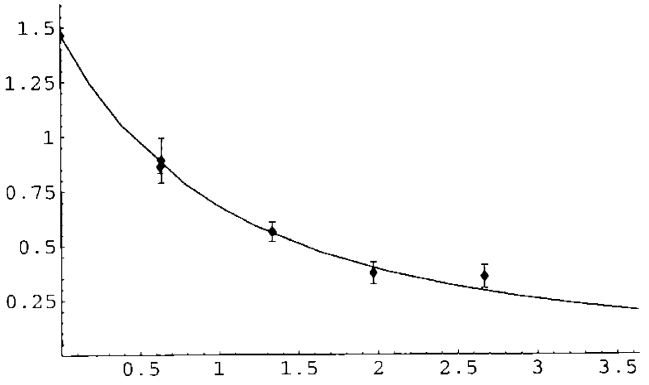

Figure B-3: A_{10}^{u-d} for $m_\pi = 835$ MeV

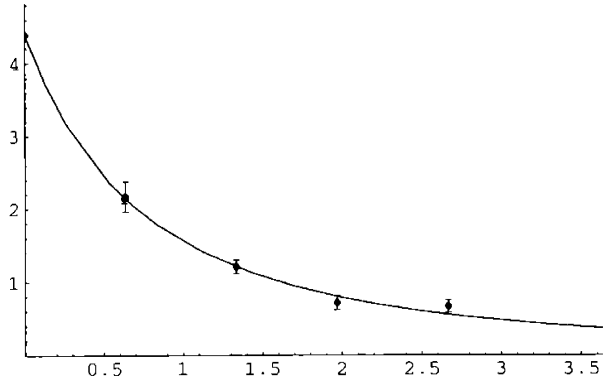

Figure B-4: A_{10}^{u+d} for $m_\pi = 835$ MeV

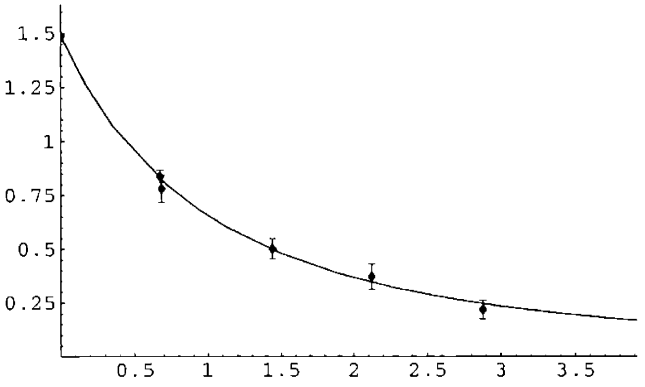

Figure B-5: A_{10}^{u-d} for $m_\pi = 753$ MeV

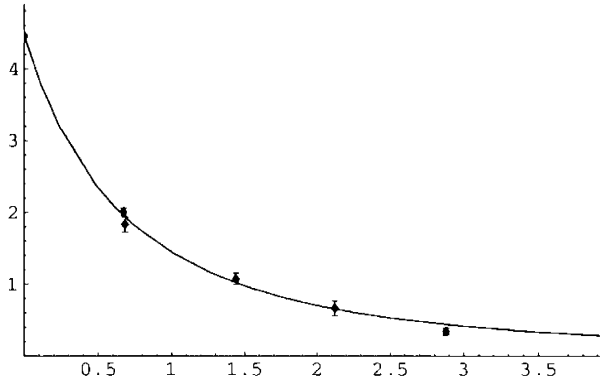

Figure B-6: A_{10}^{u+d} for $m_\pi = 753$ MeV

Appendix C

Figures of $A_{20}^{u-d}(t)$ and $A_{20}^{u+d}(t)$

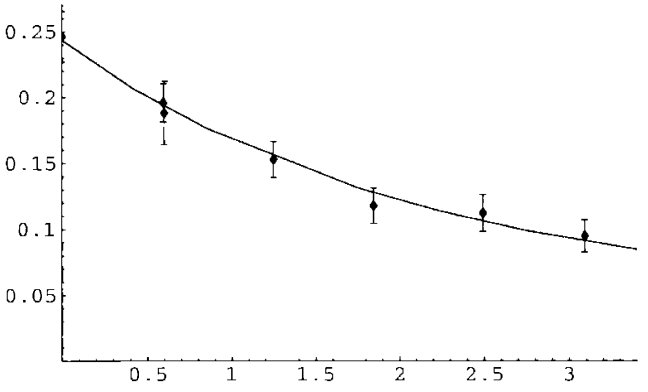

Figure C-1: A_{20}^{u-d} for $m_\pi = 895$ MeV

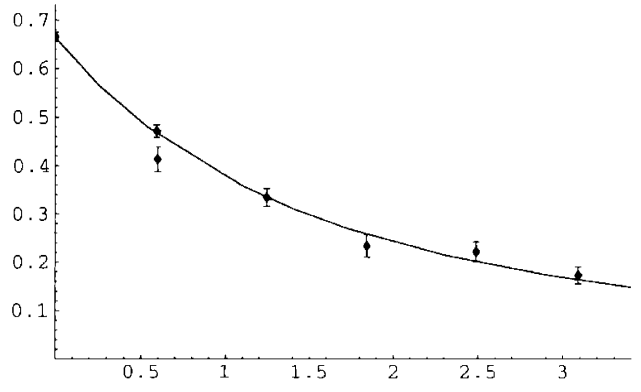

Figure C-2: A_{20}^{u+d} for $m_\pi = 895$ MeV

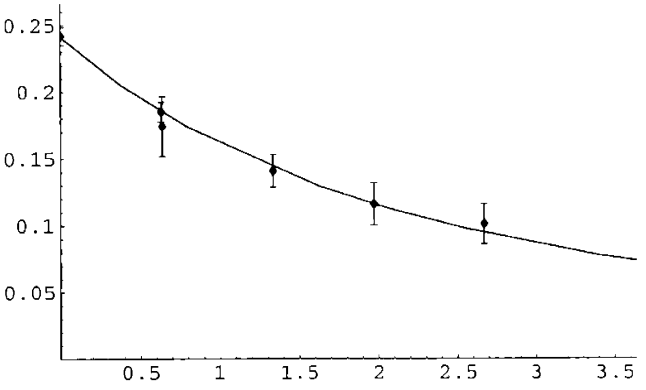

Figure C-3: A_{20}^{u-d} for $m_\pi = 835$ MeV

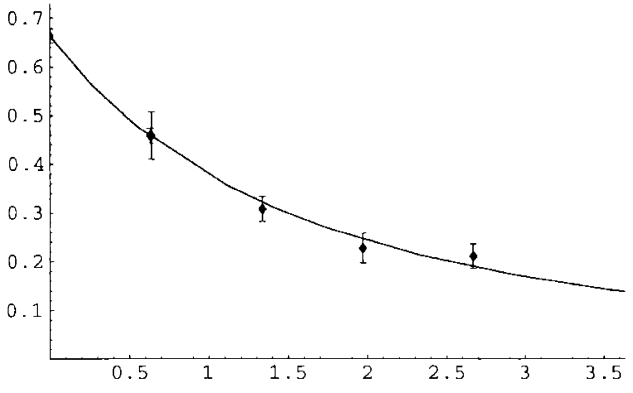

Figure C-4: A_{20}^{u+d} for $m_\pi = 835$ MeV

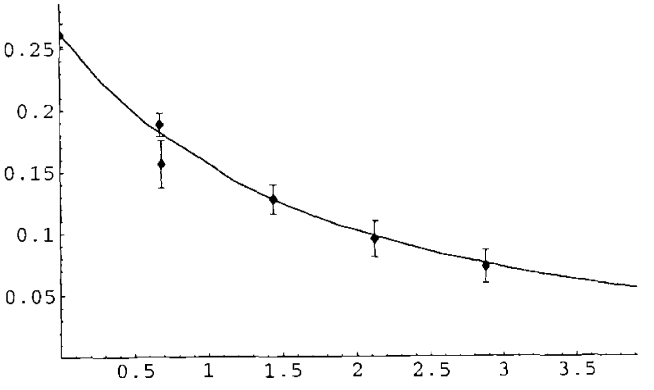

Figure C-5: A_{20}^{u-d} for $m_\pi = 753$ MeV

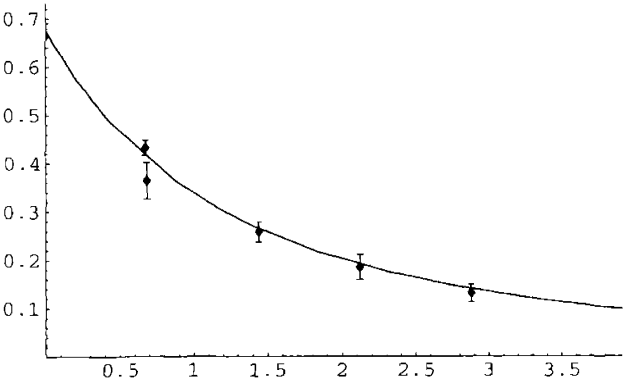

Figure C-6: A_{20}^{u+d} for $m_\pi = 753$ MeV

Appendix D

Figures of $B_{20}^{u-d}(t)$ and $B_{20}^{u+d}(t)$

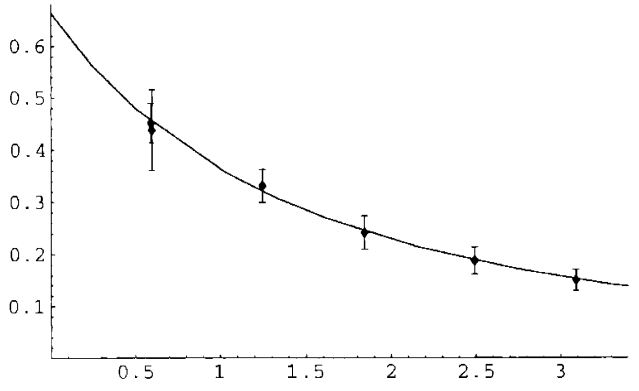

Figure D-1: B_{20}^{u-d} for $m_\pi = 895$ MeV

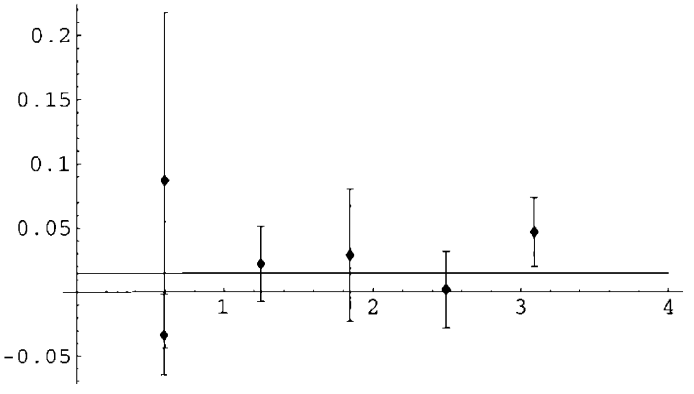

Figure D-2: B_{20}^{u+d} for $m_\pi = 895$ MeV

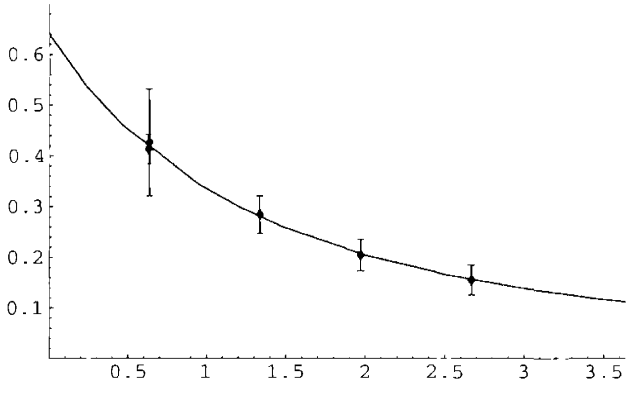

Figure D-3: B_{20}^{u-d} for $m_\pi = 835$ MeV

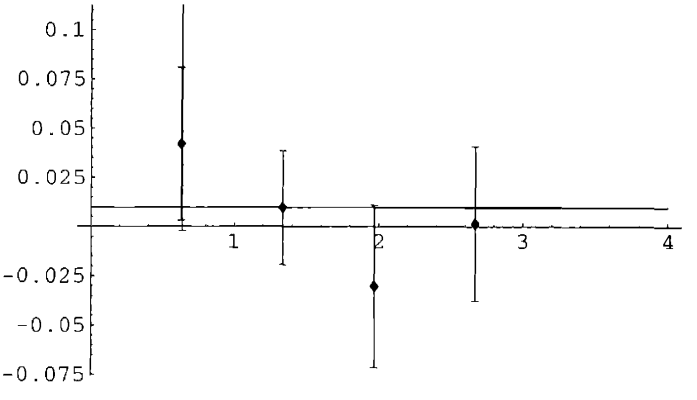

Figure D-4: B_{20}^{u+d} for $m_\pi = 835$ MeV

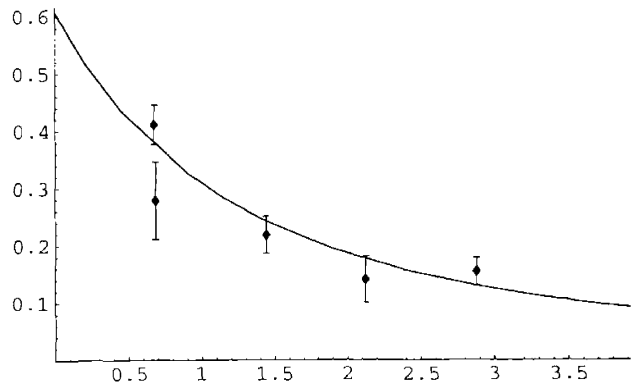

Figure D-5: B_{20}^{u-d} for $m_\pi = 753$ MeV

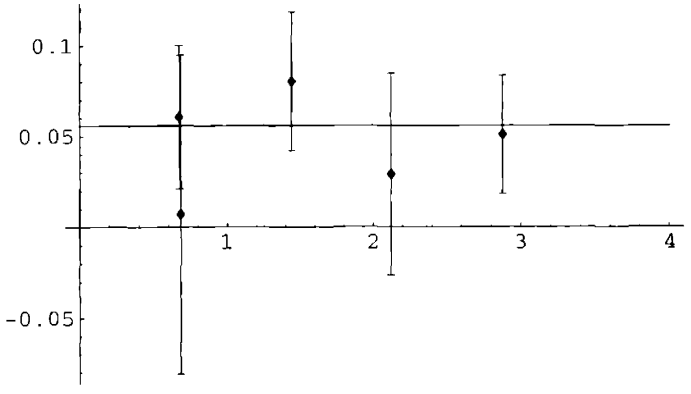

Figure D-6: B_{20}^{u+d} for $m_\pi = 753$ MeV

Appendix E

Figures of $\tilde{A}_{10}^{u-d}(t)$ and $\tilde{A}_{10}^{u+d}(t)$

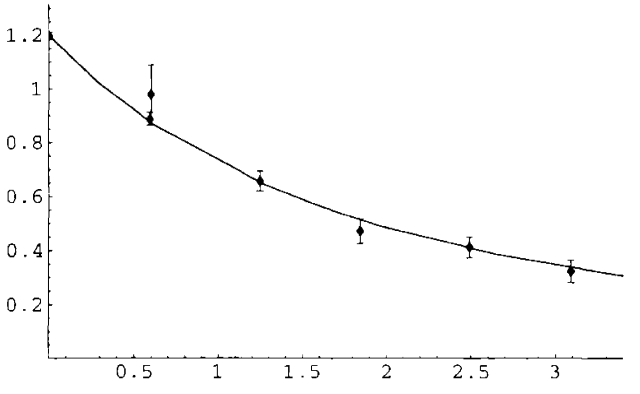

Figure E-1: $\tilde{A}_{10}^{u-d}$ for $m_\pi = 895$ MeV

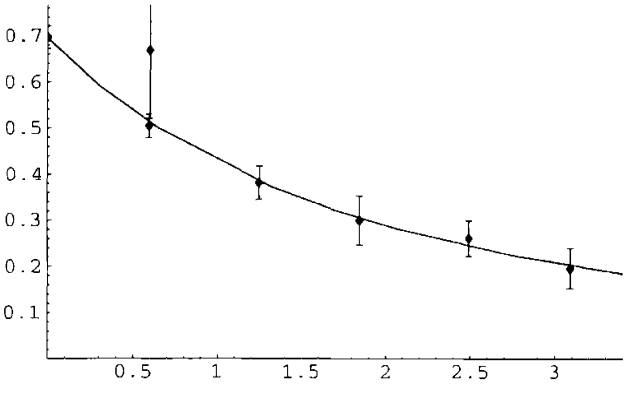

Figure E-2: $\tilde{A}_{10}^{u+d}$ for $m_\pi = 895$ MeV

Appendix F

Tables of Forward Moments

	m_π (MeV)	A
$u-d$	895	1.439(2)
$u+d$	895	4.310(4)
$u-d$	835	1.464(1)
$u+d$	835	4.387(3)
$u-d$	753	1.487(1)
$u+d$	753	4.454(5)

Table F.1: Forward Limit for A_{10}^{u-d} and A_{10}^{u+d} (unrenormalized)

	m_π (MeV)	A
$u-d$	895	0.247(6)
$u+d$	895	0.675(6)
$u-d$	835	0.242(10)
$u+d$	835	0.656(10)
$u-d$	753	0.263(15)
$u+d$	753	0.677(15)

Table F.2: Forward Limit for A_{20}^{u-d} and A_{20}^{u+d}

	m_π (MeV)	A
$u-d$	895	1.190(18)
$u+d$	895	0.682(18)
$u-d$	835	1.223(28)
$u+d$	835	0.727(28)
$u-d$	753	1.094(33)
$u+d$	753	0.666(33)

Table F.3: Forward Limit for $\tilde{A}_{10}^{u-d}$ and $\tilde{A}_{10}^{u+d}$

Appendix G

Tables of Dipole Fits

	m_π (MeV)	A	m (GeV)
$u-d$	895	1.439(2)	1.49(4)
$u+d$	895	4.310(4)	1.24(2)
$u-d$	835	1.464(1)	1.47(3)
$u+d$	835	4.387(3)	1.24(2)
$u-d$	753	1.487(1)	1.41(2)
$u+d$	753	4.454(5)	1.17(2)

Table G.1: Dipole Fits for A_{10}^{u-d} and A_{10}^{u+d} (unrenormalized)

	m_π (MeV)	A	m (GeV)
$u-d$	895	0.244(8)	2.13(8)
$u+d$	895	0.665(10)	1.72(5)
$u-d$	835	0.242(4)	2.01(6)
$u+d$	835	0.664(8)	1.72(4)
$u-d$	753	0.263(7)	1.77(7)
$u+d$	753	0.676(22)	1.54(6)

Table G.2: Dipole Fits for A_{20}^{u-d} and A_{20}^{u+d}

	m_π (MeV)	A	m (GeV)
$u-d$	895	0.56(6)	1.84(16)
$u-d$	835	0.60(4)	1.65(9)
$u-d$	753	0.58(14)	1.60(30)

Table G.3: Dipole Fits for B_{20}^{u-d}

	m_π (MeV)	A	m (GeV)
$u-d$	895	1.20(1)	1.86(3)
$u+d$	895	0.70(1)	1.87(6)

Table G.4: Dipole Fits for $\tilde{A}_{10}^{u-d}$ and $\tilde{A}_{10}^{u+d}$

Appendix H

Tables of Constant Fits

	m_π (MeV)	A	
$u+d$	895	0.015(13)	
$u+d$	835	0.010(14)	
$u+d$	753	0.056(10)	

Table H.1: Constant Fits for B_{20}^{u+d}

Appendix I

Experimentally Measured Slopes of A_{10}^f and $\tilde{A}_{10}^f$

The purpose of this appendix is to determine the slopes of the $F_1^f = A_{10}^f$ and $G_P^f = \tilde{A}_{10}^f$ form factors for a variety of flavor combinations from the experimentally measured values. Given that there are occasional confusions with the sign conventions, we give very explicit manipulations in this appendix to avoid any sign errors. In the following, q^2 is the invariant momentum transfer squared and is negative for electron nucleon scattering. The electric form factor $G_E(q^2)$ is given in terms of $F_1(q^2)$ and $F_2(q^2)$ as

$$G_E(q^2) = F_1(q^2) + \frac{q^2}{4m^2} F_2(q^2),$$

and hence the derivative at the origin is

$$\frac{d}{dq^2} G_E(q^2 = 0) = \frac{d}{dq^2} F_1(q^2 = 0) + \frac{F_2(0)}{4m^2}.$$

For simplicity we denote the above derivative with respect to q^2 with a prime, and we assume that all form factors are written as functions of q^2 and not $Q^2 = -q^2$. Now we solve for $F_1'(0)$ to give

$$F_1'(0) = G_E'(0) - \frac{F_2(0)}{4m^2}.$$

	p	n
$G'_E(0)$ GeV^{-2}	3.24(6)	-0.497(9)
$F'_1(0)$ GeV^{-2}	2.73(6)	0.044(9)

Table I.1: Slopes of G_E^p, G_E^n, F_1^p, and F_1^n

The slope of G_E is determined by the charge radius,

$$G'_E(0) = \frac{1}{6}\langle r^2\rangle_{\rm ch},$$

and $F_2(0)$ is given by the anomalous moment,

$$F_2(0) = \kappa.$$

The final result for the slope of F_1 in terms of physically determined quantities, $\langle r^2\rangle_{\rm ch}$, κ, and m, is

$$F'_1(0) = \frac{1}{6}\langle r^2\rangle_{\rm ch} - \frac{\kappa}{4m^2}.$$

In particular, the above holds for both the proton and neutron. The masses and anomalous magnetic moments are known very accurately, so we ignore their errors relative to those from the less well measured charge radii. For the proton we take $m_p = 938.3$ MeV, $\kappa_p = 1.793$, and $\sqrt{\langle r^2\rangle^p_{\rm ch}} = 0.870(8)$ fm [19]. For the neutron we use $m_n = 939.7$ MeV, $\kappa_n = -1.913$, and $\langle r^2\rangle^n_{\rm ch} = -0.1161(22)$ fm^2 [19]. The resulting slopes for G_E and F_1 for the proton and neutron are given in Table I.1. In particular notice that the slope of G_E^n is negative whereas the slope of F_1^n is positive.

The flavor combinations $u-d$, $u+d$, u, and d for F_1^f are related to F_1^p and F_1^n as follows.

$$\begin{aligned} F^{u-d} &= F_1^p - F_1^n \\ F^{u+d} &= 3F_1^p + 3F_1^n \\ F_1^u &= 2F_1^p + F_1^n \\ F_1^d &= F_1^p + 2F_1^n \end{aligned}$$

	$u-d$	$u+d$	u	d
$F_1'(0)$ GeV^{-2}	2.67(6)	8.3(2)	5.5(1)	2.82(6)

Table I.2: Slopes of F_1^f for $f = u-d$, $u+d$, u, and d

The slopes of F_1^f for these various flavor combinations are given in Table I.2. We note that, as always in this thesis, the flavor combinations $u-d$, $u+d$, u, and d refer to that flavor combination in the proton.

The neutral current couples to the iso-vector axial current and determines the G_A form factor. This form factor is conventionally parameterized as a dipole.

$$G_A(q^2) = \frac{g_A}{\left(1 - \frac{q^2}{m_A^2}\right)^2}$$

Using the value $g_A = 1.2670(35)$ and an average value for $m_A = 1.03(4)$, we can determine the slope of one flavor combination, $\tilde{A}_{10}^{u-d}$.

$$\tilde{A}_{10}^{u-d\prime}(0) = 2\frac{g_A}{m_A^2} = 2.4(2)$$

Appendix J

Euclidean Field Theory

The action for a general field theory in Minkowski space-time is

$$iS = i \int_{-\infty \cdot e^{-i\epsilon}}^{+\infty \cdot e^{-i\epsilon}} dt \int d^3x \; \mathcal{L}_{\rm M}(t, \vec{x})$$

where $\mathcal{L}_{\rm M}$ is the Minkowski Lagrangian and $\epsilon > 0$ is required to ensure that the corresponding functional integral is dominated by the appropriate vacuum to vacuum matrix element. The integral over t is a contour integral in a complex t plane. Performing an analytic continuation of $\mathcal{L}_{\rm M}$, we close the contour along the imaginary t axis. Assuming the fields in $\mathcal{L}_{\rm M}$ fall sufficiently fast, we ignore the contributions of the contour at large t. The resulting action in Euclidean space-time is

$$iS = i \int_{-\infty}^{+\infty} -id\tau \int d^3x \; \mathcal{L}_{\rm M}(-i\tau, \vec{x}) = \int_{-\infty}^{+\infty} d\tau \int d^3x \; \mathcal{L}_{\rm E}(\tau, \vec{x})$$

where $\mathcal{L}_{\rm E}(\tau, \vec{x}) = \mathcal{L}_{\rm M}(-i\tau, \vec{x})$ is the corresponding Euclidean Lagrangian. This is the origin of the simple rule $t \rightarrow -i\tau$. In the remainder of this appendix, we implement the analytic continuation for scalar, vector, and fermion fields to determine the corresponding Euclidean fields for each. Then, as a check, we briefly examine scalar and fermion gauge theories in Euclidean space-time.

First we consider a free scalar field theory. The Minkowski Lagrangian for a free

scalar field ϕ^a is

$$\begin{aligned}
&\mathcal{L}^S_{\rm M}(t,\vec{x}) = \\
&\quad = \partial^{\rm M}_\mu \phi^{a\,*}_{\rm M}\, \partial^\mu_{\rm M} \phi^a_{\rm M} - m^2 \phi^{a\,*}_{\rm M}\, \phi^a_{\rm M} \\
&\quad = \frac{\partial}{\partial t}\phi^{a\,*}_{\rm M}\, \frac{\partial}{\partial t}\phi^a_{\rm M} - \frac{\partial}{\partial x^i}\phi^{a\,*}_{\rm M}\, \frac{\partial}{\partial x^i}\phi^a_{\rm M} - m^2 \phi^{a\,*}_{\rm M}\, \phi^a_{\rm M}\,.
\end{aligned}$$

The corresponding Euclidean Lagrangian is

$$\begin{aligned}
&\mathcal{L}^S_{\rm E}(\tau,\vec{x}) = \\
&\quad = \frac{\partial}{\partial(-i\tau)}\phi^{a\,*}_{\rm E}\, \frac{\partial}{\partial(-i\tau)}\phi^a_{\rm E} - \frac{\partial}{\partial x^i}\phi^{a\,*}_{\rm E}\, \frac{\partial}{\partial x^i}\phi^a_{\rm E} - m^2 \phi^{a\,*}_{\rm E}\, \phi^a_{\rm E} \\
&\quad = -\frac{\partial}{\partial \tau}\phi^{a\,*}_{\rm E}\, \frac{\partial}{\partial \tau}\phi^a_{\rm E} - \frac{\partial}{\partial x^i}\phi^{a\,*}_{\rm E}\, \frac{\partial}{\partial x^i}\phi^a_{\rm E} - m^2 \phi^{a\,*}_{\rm E}\, \phi^a_{\rm E} \\
&\quad = -\partial^{\rm E}_\mu \phi^{a\,*}_{\rm E}\, \partial^{\rm E}_\mu \phi^a_{\rm E} - m^2 \phi^{a\,*}_{\rm E}\, \phi^a_{\rm E}
\end{aligned}$$

where the Euclidean scalar field is defined by

$$\phi^a_{\rm E}(\tau,\vec{x}) = \phi^a_{\rm M}(-i\tau,\vec{x}). \tag{J.1}$$

Notice this is the result one would expect from the simple rule $t \to -i\tau$.

Next we consider a vector field A^a_μ. The Lagrangian in Minkowski space-time is

$$\begin{aligned}
&\mathcal{L}^V_{\rm M}(t,\vec{x}) = \\
&\quad = -\frac{1}{4} F^{{\rm M}\,a}_{\mu\nu} F^{\mu\nu}_{{\rm M}\,a} \\
&\quad = -\frac{1}{2} F^{{\rm M}\,a}_{0i} F^{0i}_{{\rm M}\,a} - \frac{1}{4} F^{{\rm M}\,a}_{ij} F^{ij}_{{\rm M}\,a}
\end{aligned}$$

where

$$F^{{\rm M}\,a}_{\mu\nu} = \partial^{\rm M}_\mu A^{{\rm M}\,a}_\nu - \partial^{\rm M}_\nu A^{{\rm M}\,a}_\mu + g f^{abc} A^{{\rm M}\,b}_\mu A^{{\rm M}\,c}_\nu$$

and we use $F^{{\rm M}\,a}_{\nu\mu} = -F^{{\rm M}\,a}_{\mu\nu}$ in the third line. Now we consider each piece from the third line separately. The first piece is

$$F^{{\rm M}\,a}_{0i} F^{0i}_{{\rm M}\,a} =$$

$$
\begin{aligned}
&= \left(\frac{\partial}{\partial t}A_i^{\mathrm{M}a} - \frac{\partial}{\partial x^i}A_0^{\mathrm{M}a} + gf^{abc}A_0^{\mathrm{M}b}A_i^{\mathrm{M}c}\right) \\
&\quad \left(\frac{\partial}{\partial t}A^i_{\mathrm{M}a} - \frac{\partial}{\partial x_i}A^0_{\mathrm{M}a} + gf^{abc}A^0_{\mathrm{M}b}A^i_{\mathrm{M}c}\right) \\
&= \left(-\frac{\partial}{\partial t}A^i_{\mathrm{M}a} - \frac{\partial}{\partial x^i}A^0_{\mathrm{M}a} - gf^{abc}A^0_{\mathrm{M}b}A^i_{\mathrm{M}c}\right) \\
&\quad \left(\frac{\partial}{\partial t}A^i_{\mathrm{M}a} + \frac{\partial}{\partial x^i}A^0_{\mathrm{M}a} + gf^{abc}A^0_{\mathrm{M}b}A^i_{\mathrm{M}c}\right).
\end{aligned}
$$

The Euclidean counterpart is

$$
\begin{aligned}
&F_{0i}^{\mathrm{E}a}F_{0i}^{\mathrm{E}a} = \\
&= \left(-\frac{\partial}{\partial(-i\tau)}A^i_{\mathrm{M}a} - \frac{\partial}{\partial x^i}A^0_{\mathrm{M}a} - gf^{abc}A^0_{\mathrm{M}b}A^i_{\mathrm{M}c}\right) \\
&\quad \left(\frac{\partial}{\partial(-i\tau)}A^i_{\mathrm{M}a} + \frac{\partial}{\partial x^i}A^0_{\mathrm{M}a} + gf^{abc}A^0_{\mathrm{M}b}A^i_{\mathrm{M}c}\right) \\
&= \left(\frac{\partial}{\partial \tau}A^i_{\mathrm{M}a} - \frac{\partial}{\partial x^i}iA^0_{\mathrm{M}a} - gf^{abc}iA^0_{\mathrm{M}b}A^i_{\mathrm{M}c}\right) \\
&\quad \left(\frac{\partial}{\partial \tau}A^i_{\mathrm{M}a} - \frac{\partial}{\partial x^i}iA^0_{\mathrm{M}a} - gf^{abc}iA^0_{\mathrm{M}b}A^i_{\mathrm{M}c}\right) \\
&= \left(\partial_0^{\mathrm{E}}A_i^{\mathrm{E}a} - \partial_i^{\mathrm{E}}A_0^{\mathrm{E}a} - gf^{abc}A_0^{\mathrm{E}b}A_i^{\mathrm{M}c}\right) \\
&\quad \left(\partial_0^{\mathrm{E}}A_i^{\mathrm{E}a} - \partial_i^{\mathrm{E}}A_0^{\mathrm{E}a} - gf^{abc}A_0^{\mathrm{E}b}A_i^{\mathrm{E}c}\right),
\end{aligned}
$$

and we have tentatively defined the Euclidean vector field as

$$
\begin{aligned}
A_0^{\mathrm{E}a}(\tau,\vec{x}) &= iA^0_{\mathrm{M}a}(-i\tau,\vec{x}) \\
A_i^{\mathrm{E}a}(\tau,\vec{x}) &= A^i_{\mathrm{M}a}(-i\tau,\vec{x}).
\end{aligned}
\tag{J.2}
$$

Notice again the simple change $t \to -i\tau$. Additionally we include a factor of i in the definition of A_0^{E} to make the Euclidean invariance of the action manifest. Now we confirm this definition by examining the second piece of $F^{\mathrm{M}a}_{\mu\nu}F^{\mu\nu}_{\mathrm{M}a}$.

$$
\begin{aligned}
&F_{ij}^{\mathrm{M}a}F^{ij}_{\mathrm{M}a} = \\
&= \left(\frac{\partial}{\partial x^i}A_j^{\mathrm{M}a} - \frac{\partial}{\partial x^j}A_i^{\mathrm{M}a} + gf^{abc}A_i^{\mathrm{M}b}A_j^{\mathrm{M}c}\right)
\end{aligned}
$$

$$
\begin{aligned}
& \left(\frac{\partial}{\partial x_i} A^j_{\mathrm{M}a} - \frac{\partial}{\partial x_j} A^i_{\mathrm{M}a} + g f^{abc} A^i_{\mathrm{M}b} A^j_{\mathrm{M}c} \right) \\
= & \left(-\frac{\partial}{\partial x^i} A^j_{\mathrm{M}a} + \frac{\partial}{\partial x^j} A^i_{\mathrm{M}a} + g f^{abc} A^i_{\mathrm{M}b} A^j_{\mathrm{M}c} \right) \\
& \left(-\frac{\partial}{\partial x^i} A^j_{\mathrm{M}a} + \frac{\partial}{\partial x^j} A^i_{\mathrm{M}a} + g f^{abc} A^i_{\mathrm{M}b} A^j_{\mathrm{M}c} \right)
\end{aligned}
$$

The corresponding Euclidean piece is

$$
\begin{aligned}
& F^{\mathrm{E}a}_{ij} F^{\mathrm{E}a}_{ij} = \\
& = \left(-\partial^{\mathrm{E}}_i A^{\mathrm{E}a}_j + \partial^{\mathrm{E}}_j A^{\mathrm{E}a}_i + g f^{abc} A^{\mathrm{E}b}_i A^{\mathrm{E}c}_j \right) \\
& \quad \left(-\partial^{\mathrm{E}}_i A^{\mathrm{E}a}_j + \partial^{\mathrm{E}}_j A^{\mathrm{E}a}_i + g f^{abc} A^{\mathrm{E}b}_i A^{\mathrm{E}c}_j \right) \\
& = \left(\partial^{\mathrm{E}}_i A^{\mathrm{E}a}_j - \partial^{\mathrm{E}}_j A^{\mathrm{E}a}_i - g f^{abc} A^{\mathrm{E}b}_i A^{\mathrm{E}c}_j \right) \\
& \quad \left(\partial^{\mathrm{E}}_i A^{\mathrm{E}a}_j - \partial^{\mathrm{E}}_j A^{\mathrm{E}a}_i - g f^{abc} A^{\mathrm{E}b}_i A^{\mathrm{E}c}_j \right).
\end{aligned}
$$

This confirms the definition of the Euclidean vector fields in Equation J.2 above. The final result is

$$
\mathcal{L}^V_{\mathrm{E}}(t, \vec{x}) = -\frac{1}{4} F^{\mathrm{E}a}_{\mu\nu} F^{\mathrm{E}a}_{\mu\nu}
$$

where

$$
F^{\mathrm{E}a}_{\mu\nu} = \partial^{\mathrm{E}}_\mu A^{\mathrm{E}a}_\nu - \partial^{\mathrm{E}}_\nu A^{\mathrm{E}a}_\mu - g f^{abc} A^{\mathrm{E}b}_\mu A^{\mathrm{E}c}_\nu.
$$

Notice the change of sign of g. This change of sign relative to the Minkowski Lagrangian also occurs for the scalar and fermion gauge theories discussed below.

Now we examine a free fermion field ψ^a. The Minkowski Lagrangian is

$$
\begin{aligned}
& \mathcal{L}^F_{\mathrm{M}}(t, \vec{x}) = \\
& = \overline{\psi}^a_{\mathrm{M}} \, i \gamma^\mu_{\mathrm{M}} \partial^{\mathrm{M}}_\mu \, \psi^a_{\mathrm{M}} - m \, \overline{\psi}^a_{\mathrm{M}} \, \psi^a_{\mathrm{M}} \\
& = \overline{\psi}^a_{\mathrm{M}} \, i \left(\gamma^0_{\mathrm{M}} \frac{\partial}{\partial t} + \gamma^i_{\mathrm{M}} \frac{\partial}{\partial x^i} \right) \psi^a_{\mathrm{M}} - m \, \overline{\psi}^a_{\mathrm{M}} \, \psi^a_{\mathrm{M}}.
\end{aligned}
$$

The Lagrangian in Euclidean space-time is

$$
\mathcal{L}^F_{\mathrm{E}}(\tau, \vec{x}) =
$$

$$
\begin{aligned}
&= \overline{\psi}^a_{\rm E}\, i\left(\gamma^0_{\rm M}\frac{\partial}{\partial(-i\tau)} + \gamma^i_{\rm M}\frac{\partial}{\partial x^i}\right)\psi^a_{\rm E} - m\,\overline{\psi}^a_{\rm E}\,\psi^a_{\rm E} \\
&= -\overline{\psi}^a_{\rm E}\left(\gamma^0_{\rm M}\frac{\partial}{\partial\tau} - i\gamma^i_{\rm M}\frac{\partial}{\partial x^i}\right)\psi^a_{\rm E} - m\,\overline{\psi}^a_{\rm E}\,\psi^a_{\rm E} \\
&= -\overline{\psi}^a_{\rm E}\,\gamma^{\rm E}_\mu\partial^{\rm E}_\mu\,\psi^a_{\rm E} - m\,\overline{\psi}^a_{\rm E}\,\psi^a_{\rm E}
\end{aligned}
$$

where the Euclidean fermion field is

$$\psi^a_{\rm E}(\tau,\vec{x}) = \psi^a_{\rm E}(-i\tau,\vec{x}) \tag{J.3}$$

and the Euclidean Dirac matrices are

$$
\begin{aligned}
\gamma^{\rm E}_0 &= \gamma^0_{\rm M} \\
\gamma^{\rm E}_i &= -i\gamma^i_{\rm M}.
\end{aligned} \tag{J.4}
$$

We note that the Euclidean Dirac matrices are chosen to make the Euclidean invariance of the action easily visible, consequently they satisfy the Euclidean Dirac algebra $\{\gamma^{\rm E}_\mu,\gamma^{\rm E}_\nu\} = 2\delta^{\rm E}_{\mu\nu}$.

We check the consistency of the above results in Equations J.1, J.2, and J.3 by examining gauge theories for scalar and fermion fields. First we consider scalar gauge theories. The Minkowski Lagrangian for such theories is

$$
\begin{aligned}
&\mathcal{L}^{SG}_{\rm M}(t,\vec{x}) = \\
&= (D^{\rm M}_\mu\phi_{\rm M})^\dagger\,(D^\mu_{\rm M}\phi_{\rm M}) - m^2\phi^\dagger_{\rm M}\,\phi_{\rm M} \\
&= (\partial^{\rm M}_\mu\phi^\dagger_{\rm M} + igA^{{\rm M}\,a}_\mu\phi^\dagger_{\rm M}T^a)\,(\partial^\mu_{\rm M}\phi_{\rm M} - igA^\mu_{{\rm M}\,b}T^b\phi_{\rm M}) - m^2\phi^\dagger_{\rm M}\,\phi_{\rm M} \\
&= \mathcal{L}^S_{\rm M}(t,\vec{x}) - igA^\mu_{{\rm M}\,b}\partial^{\rm M}_\mu\phi^\dagger_{\rm M}T^b\phi_{\rm M} + igA^{{\rm M}\,a}_\mu\phi^\dagger_{\rm M}T^a\partial^\mu_{\rm M}\phi_{\rm M} + g^2A^{{\rm M}\,a}_\mu A^\mu_{{\rm M}\,b}\phi^\dagger_{\rm M}T^aT^b\phi_{\rm M}
\end{aligned}
$$

where we omit the pure gauge term since we examine it above and in line four we use the previous result for the scalar Minkowski action. Additionally, the covariant derivative in Minkowski space-time is given by

$$D^{\rm M}_\mu\phi_{\rm M} = (\partial^{\rm M}_\mu - igA^{{\rm M}\,a}_\mu T^a)\phi_{\rm M}.$$

The Euclidean scalar and gauge fields are already determine above in Equations J.1 and J.2. The resulting Euclidean action is

$$\begin{aligned}
&\mathcal{L}^{SG}_{\rm E}(\tau,\vec{x}) = \\
&\quad = \mathcal{L}^{S}_{\rm E}(t,\vec{x}) - igA^{{\rm E}\,b}_{\mu}\partial^{\rm E}_{\mu}\phi^{\dagger}_{\rm E}T^{b}\phi_{\rm E} + igA^{{\rm E}\,a}_{\mu}\phi^{\dagger}_{\rm E}T^{a}\partial^{\rm E}_{\mu}\phi_{\rm E} - g^{2}A^{{\rm E}\,a}_{\mu}A^{{\rm E}\,b}_{\mu}\phi^{\dagger}_{\rm E}T^{a}T^{b}\phi_{\rm E} \\
&\quad = -(\partial^{\rm E}_{\mu}\phi^{\dagger}_{\rm E} - igA^{{\rm E}\,a}_{\mu}\phi^{\dagger}_{\rm E}T^{a})\,(\partial^{\rm E}_{\mu}\phi_{\rm E} + igA^{{\rm E}\,b}_{\mu}T^{b}\phi_{\rm E}) - m^{2}\phi^{\dagger}_{\rm E}\,\phi_{\rm E} \\
&\quad = -(D^{\rm E}_{\mu}\phi_{\rm E})^{\dagger}\,(D^{\rm E}_{\mu}\phi_{\rm E}) - m^{2}\phi^{\dagger}_{\rm E}\,\phi_{\rm E}
\end{aligned}$$

where we use the easily verifiable results $A^{\mu}_{{\rm M}\,a}\partial^{\rm M}_{\mu} \rightarrow A^{{\rm E}\,a}_{\mu}\partial^{\rm E}_{\mu}$ and $A^{{\rm M}\,a}_{\mu}A^{\mu}_{{\rm M}\,b} \rightarrow -A^{{\rm E}\,a}_{\mu}A^{{\rm E}\,b}_{\mu}$ in the second line and the above result for the Euclidean scalar action in the third line. Additionally, we define the Euclidean covariant derivative as

$$D^{\rm E}_{\mu}\phi_{\rm E} = (\partial^{\rm E}_{\mu} + igA^{{\rm E}\,a}_{\mu}T^{a})\phi_{\rm E}\,.$$

Notice again the change in sign of g relative to the Minkowski covariant derivative.

We additionally check the above results for the Euclidean fields by considering fermion gauge theories. The Lagrangian in Minkowski space-time is given by

$$\begin{aligned}
&\mathcal{L}^{FG}_{\rm M}(\tau,\vec{x}) = \\
&\quad = \overline{\psi}_{\rm M}\,i\gamma^{\mu}_{\rm M}D^{\rm M}_{\mu}\,\psi_{\rm M} - m\,\overline{\psi}_{\rm M}\,\psi_{\rm M} \\
&\quad = \overline{\psi}_{\rm M}\,i\gamma^{\mu}_{\rm M}(\partial^{\rm M}_{\mu} - igA^{{\rm M}\,a}_{\mu}T^{a})\psi_{\rm M} - m\,\overline{\psi}_{\rm M}\,\psi_{\rm M} \\
&\quad = \mathcal{L}^{F}_{\rm M}(\tau,\vec{x}) + gA^{{\rm M}\,a}_{\mu}\overline{\psi}_{\rm M}\,\gamma^{\mu}_{\rm M}T^{a}\psi_{\rm M}
\end{aligned}$$

where the covariant derivative for fermions in Minkowski space-time is

$$D^{\rm M}_{\mu}\psi_{\rm M} = (\partial^{\rm M}_{\mu} - igA^{{\rm M}\,a}_{\mu}T^{a})\psi_{\rm M}\,.$$

Using the Euclidean fermion and gauge fields from Equations J.2 and J.3, we determine the resulting Euclidean action.

$$\mathcal{L}^{FG}_{\rm E}(\tau,\vec{x}) =$$

$$
\begin{aligned}
&= \mathcal{L}_{\mathrm{E}}^{I}(\tau,\vec{x}) - igA_{\mu}^{\mathrm{E}\,a}\overline{\psi}_{\mathrm{E}}\,\gamma_{\mu}^{\mathrm{E}}T^{a}\psi_{\mathrm{E}} \\
&= -\overline{\psi}_{\mathrm{E}}\,\gamma_{\mu}^{\mathrm{E}}(\partial_{\mu}^{\mathrm{E}} + igA_{\mu}^{\mathrm{E}\,a}T^{a})\psi_{\mathrm{E}} - m\,\overline{\psi}_{\mathrm{E}}\,\psi_{\mathrm{E}} \\
&= -\overline{\psi}_{\mathrm{E}}\,\gamma_{\mu}^{\mathrm{E}}D_{\mu}^{\mathrm{E}}\psi_{\mathrm{E}} - m\,\overline{\psi}_{\mathrm{E}}\,\psi_{\mathrm{E}}
\end{aligned}
$$

where in the second line we use the simple result $A_{\mu}^{\mathrm{M}}\gamma_{\mathrm{M}}^{\mu} \rightarrow -iA_{\mu}^{\mathrm{E}}\gamma_{\mu}^{\mathrm{E}}$. Additionally we define the Euclidean covariant derivative for fermions as

$$
D_{\mu}^{\mathrm{E}}\psi_{\mathrm{E}} = (\partial_{\mu}^{\mathrm{E}} + igA_{\mu}^{\mathrm{E}\,a}T^{a})\psi_{\mathrm{E}}
$$

where again there is change in sign of g relative to the Minkowski covariant derivative.

Appendix K

Symmetry Properties

In this appendix we collect the relevant symmetry properties of quarks and gluons and the Wilson actions for each. In particular, we examine the space-time symmetries associated with translations, Lorentz transformations, Euclidean rotations, parity, time reversal, and charge conjugation. We also examine the internal symmetries generated by isospin rotations and gauge transformations. We discuss these symmetries in both Minkowski and Euclidean continuum theories and also Euclidean lattice theories. As a suggestive short hand, we use an operator notation to denote each of the above symmetries as $U(\Delta)$, $U(\Lambda)$, $U(R)$, $U(P)$, $U(T)$, $U(C)$, $U(I)$, and $U(g)$ respectively. In the following we use common results which can be founded in any of many quantum field theory text books. In particular, we use results from [29] and [35] without explicit citation.

The operator notation applies to those actions for which a Hilbert space and hence a quantum mechanical description exist. [25] In such cases, the above transformations, except for time reversal, are implemented in Hilbert space as unitary operators. Time reversal, on the other hand, is implemented as an anti-unitary operator in Minkowski space and a unitary operator in Euclidean space. All operators, including those for time reversal, satisfy $U^{-1} = U^{\dagger}$. For those actions for which a Hilbert space does not exist for non-zero lattice spacing, these symmetries can still be implemented as field transformations of the functional integral. In such cases, an equation of the form $U\Phi_{\alpha}U^{\dagger} = M_{\alpha\beta}\Phi_{\beta}$ represents the field transformation given by $\Phi_{\alpha} \rightarrow \Phi'_{\alpha} = M_{\alpha\beta}\Phi_{\beta}$.

As remarked above, the symmetries we examine in this appendix are discussed thoroughly in many quantum field theory text books. The one exception is Euclidean time reversal. In a Euclidean theory, the improper Lorentz group is replaced by the group of four dimensional rotations, O(4). The improper Lorentz group has four disconnected components: the proper Lorentz group and three more components generated by $U(P)$, $U(T)$, and $U(T)\,U(P)$, whereas the improper group of four dimensional rotations has only two disconnected components: the proper group of four dimensional rotations SO(4) and one more component generated by $U(P)$. The reason for this distinction is that time reversal in a Euclidean theory is equivalent to parity modulo a proper four dimensional rotation. In particular, we have $T = R_{12}(\pi)\,R_{34}(-\pi)\,P$, where $R_{ij}(\theta)$ denotes a rotation in the i-j plane by an angle θ. The choice of $\pm\pi$ is irrelevant to the previous equation but gives rise to a simple phase convention for the time reversal of spin one-half fields.

Before discussing the specific representation of each of these symmetries for quarks and gluons, we note a few general remarks about these symmetries. In the following, lattice coordinates will be taken in the intervals

$$\begin{aligned} -N^\mu \leq x^\mu \leq N^\mu \quad & (\text{for } \mathrm{L}^\mu = 2\mathrm{N}^\mu + 1) \\ -N^\mu + 1 \leq x^\mu \leq N^\mu \quad & (\text{for } \mathrm{L}^\mu = 2\mathrm{N}^\mu) \end{aligned}$$

where L^μ is the extent of the lattice in the μ^{th} direction and N^μ and x^μ are integers. For the discussion of translations, Δ denotes a displacement in Minkowski or Euclidean space-time. Furthermore, for a lattice translation we require that each component Δ^μ is a multiple of the lattice spacing a and that arithmetic for space-time coordinates is performed as

$$\begin{aligned} (x+\Delta)^\mu &= (x^\mu + \Delta^\mu) \bmod (L^\mu) - N^\mu \qquad (\text{for } \mathrm{L}^\mu = 2\mathrm{N}^\mu + 1) \\ (x+\Delta)^\mu &= (x^\mu + \Delta^\mu) \bmod (L^\mu) - N^\mu + 1 \quad (\text{for } \mathrm{L}^\mu = 2\mathrm{N}^\mu) \end{aligned}$$

where the range of the mod function is given by $0 \leq x \bmod L < L$. The discussion of Lorentz transformations is clearly limited to Minkowski theories. The results regard-

ing Euclidean rotations apply to both three dimensional rotations in a Minkowski theory or four dimensional rotations in a Euclidean theory. For a lattice theory, we consider rotations about the points $(0,0,0)$ or $(0,0,0,0)$ for a three or four dimension rotation with $L^\mu = 2N^\mu + 1$ and the about the points $(1/2,1/2,1/2)$ or $(1/2,1/2,1/2,1/2)$ for three or four dimensional rotations with $L^\mu = 2N^\mu$. Rotations about points related to the above by translations are allowed, but the definition of such rotations must make appropriate use of the lattice arithmetic illustrated above. Parity and time reversal symmetries are applicable to both Minkowski and Euclidean theories. For a lattice theory the parity and time reversal transformations are defined with respect to $(0,0,0,0)$ for $L^\mu = 2N^\mu + 1$ or $(1/2,1/2,1/2,1/2)$ for $L^\mu = 2N^\mu$. Lattice inversions about other equivalent points are also possible, but, as for lattice rotations, this involves the proper use of a lattice translation and the ensuing modular arithmetic. The charge conjugation and isospin flavor symmetries are implemented the same way in Minkowski, Euclidean, and lattice theories. Whereas the gauge symmetry is implemented in the $\mathrm{su(N_c)}$ algebra for the Minkowski and Euclidean continuum theories but in the $\mathrm{SU(N_c)}$ group for the lattice theories.

K.1 Quarks

The translation of a quark field is given by

$$U(\Delta)\, q^a_\alpha(x)\, U^\dagger(\Delta) = q^a_\alpha(x+\Delta). \tag{K.1}$$

The Lorentz transformation of a quark field is

$$M_{\alpha\alpha'}(\Lambda)\, U(\Lambda)\, q^a_{\alpha'}(x)\, U^\dagger(\Lambda) = q^a_\alpha(\Lambda x) \tag{K.2}$$

where $M(\Lambda)$ denotes the Dirac spinor representation of the Lorentz group. This representation is given by

$$M(\Lambda(\omega)) = e^{-\frac{i}{2}\omega_{\mu\nu}S^{\mu\nu}_{\mathrm{M}}}$$

where $\omega_{\nu\mu} = -\omega_{\mu\nu}$ parameterizes the Lorentz transformation $\Lambda(\omega)$ and $S_{\rm M}^{\mu\nu}$ is given by

$$S_{\rm M}^{\mu\nu} = \frac{i}{4}\left[\gamma_{\rm M}^{\mu}, \gamma_{\rm M}^{\nu}\right].$$

Note that $M(\Lambda)$ is not unitary for Lorentz transformations containing a non-trivial boost. For Euclidean rotations Equation K.2 above holds with $\Lambda \rightarrow R$ as

$$M_{\alpha\alpha'}(R)\, U(R)\, q_{\alpha'}^{a}(x)\, U^{\dagger}(R) = q_{\alpha}^{a}(Rx) \tag{K.3}$$

with

$$M(R(\omega)) = e^{-\frac{i}{2}\omega_{\mu\nu}S_{\rm E}^{\mu\nu}}$$

where now $\omega_{\nu\mu} = -\omega_{\mu\nu}$ parameterizes the Euclidean rotation $R(\omega)$ and $S_{\rm E}^{\mu\nu}$ is given by

$$S_{\rm E}^{\mu\nu} = -\frac{i}{4}\left[\gamma_{\rm E}^{\mu}, \gamma_{\rm E}^{\nu}\right].$$

The extra minus sign above is chosen so that three dimensional Euclidean rotations are represented by the same matrix as the corresponding Lorentz transformation. For Euclidean rotations, $S_{\rm E}^{\mu\nu}$ is Hermitian and consequently $M(R)$ is unitary. The parity transformation of a quark field is

$$M(P)_{\alpha\alpha'}\, U(P)\, q_{\alpha'}^{a}(x)\, U^{\dagger}(P) = q_{\alpha}^{a}(Px) \tag{K.4}$$

where $M(P) = \gamma_{\rm M}^{0} = \gamma_{0}^{\rm E}$ and we explicitly take the intrinsic parity of the quark to be positive. The charge conjugation transformation of a quark field is

$$M(C)_{\alpha\alpha'}\, U(C)\, q_{\alpha'}^{a}(x)\, U^{\dagger}(C) = (q_{\alpha}^{a}(x))^{\dagger} \tag{K.5}$$

where $M(C) = \gamma_{\rm M}^{0} C$ and $C = i\gamma_{\rm M}^{2}\gamma_{\rm M}^{0}$ is the charge conjugation matrix. Using this form for C gives $M(C) = -i\gamma_{\rm M}^{2} = \gamma_{2}^{\rm E}$. The time reversal transformation of a quark field in Minkowski space-time is

$$M(T_{\rm M})_{\alpha\alpha'}\, U(T_{\rm M})\, q_{\alpha'}^{a}(x)\, U^{-1}(T_{\rm M}) = q_{\alpha}^{a}(Tx) \tag{K.6}$$

where $M(T_{\rm M}) = -\gamma_{\rm M}^5 C$. Using the explicit form for C gives $M(T_{\rm M}) = \gamma_{\rm M}^1\gamma_{\rm M}^3 = -\gamma_1^{\rm E}\gamma_3^{\rm E}$. The time reversal transformation of a quark field in Euclidean space-time is

$$M(T_{\rm E})_{\alpha\alpha'}\, U(T_{\rm E})\, q^a_{\alpha'}(x)\, U^{-1}(T_{\rm E}) = q^a_\alpha(Tx) \tag{K.7}$$

where $M(T_{\rm E}) = M(R_{01}(\pi))\, M(R_{23}(\pi))\, M(P)$. Using the matrices given above for $M(R)$ and $M(P)$ gives $M(T_{\rm E}) = -\gamma_{\rm M}^1\, \gamma_{\rm M}^2\, \gamma_{\rm M}^3 = i\gamma_1^{\rm E}\, \gamma_2^{\rm E}\, \gamma_3^{\rm E}$. The isospin transformation of a quark doublet q_i is

$$M_{ij}(I)\, U(I)\, q^a_{j\alpha}\, U^\dagger(I) = q^a_{i\alpha} \tag{K.8}$$

where $q_1 = u$ and $q_2 = d$ and $M(I)$ is the spin one-half representation of SU(2) given by

$$M(I(\vec{\omega})) = e^{-i\frac{\vec{\omega}\cdot\vec{\sigma}}{2}}$$

where $\vec{\omega}$ parameterizes the isospin rotation $I(\vec{\omega})$. The gauge transformation of a quark field is given in Equation 4.2 as

$$\begin{aligned} {}^g q_\alpha(x) &= g(x)\, q_\alpha(x) \\ {}^g \overline{q}_\alpha(x) &= \overline{q}_\alpha(x) g^\dagger(x). \end{aligned}$$

The matrices $M(P)$, $M(T_{\rm M})$, and $M(C)$ satisfy identities relevant to the square of P, T, and C transformations.

$$\begin{aligned} M(P)\, M(P) &= 1 \\ M(T_{\rm M})\, M(T_{\rm M}) &= -1 \\ M(T_{\rm M})\, M(T_{\rm M})^* &= 1 \\ M(C)\, M(C) &= 1 \end{aligned}$$

Additionally, the charge conjugation matrix, C, satisfies several useful properties.

$$C^2 = -1$$

$$
\begin{aligned}
C^\dagger &= -C \\
C^T &= -C \\
C\gamma^\mu C &= \gamma^{\mu T}
\end{aligned}
$$

The Equations K.2, K.4, K.5, K.7 and K.6 are essentially definitions of each symmetry. We note here a few properties following from these equations. First it is convenient to express Equations K.2, K.4, K.5, and K.6 as follows.

$$U(\Lambda)\, q^a_\alpha(x)\, U^\dagger(\Lambda) = M^{-1}_{\alpha\alpha'}(\Lambda)\, q^a_{\alpha'}(\Lambda x) = M_{\alpha\alpha'}(\Lambda^{-1})\, q^a_{\alpha'}(\Lambda x)$$

$$U(P)\, q^a_\alpha(x)\, U^\dagger(P) = \gamma^0_{\alpha\alpha'}\, q^a_{\alpha'}(Px)$$

$$U(C)\, q^a_\alpha(x)\, U^\dagger(C) = \left(\gamma^0 C\right)_{\alpha\alpha'}\, (q^a_{\alpha'}(x))^\dagger = (-C)_{\alpha\alpha'}\, \overline{q}^a_{\alpha'}(x)$$

$$U(T)\, q^a_\alpha(x)\, U^{-1}(T) = \left(\gamma^5 C\right)_{\alpha\alpha'}\, q^a_{\alpha'}(Tx)$$

The adjoint of each of these equations is given below.

$$U(\Lambda)\, \overline{q}^a_\alpha(x)\, U^\dagger(\Lambda) = q^a_{\alpha'}(\Lambda x)\, M_{\alpha\alpha'}(\Lambda)$$

$$U(P)\, \overline{q}^a_\alpha(x)\, U^\dagger(P) = \overline{q}^a_{\alpha'}(Px)\, \gamma^0_{\alpha'\alpha}$$

$$U(C)\, \overline{q}^a_\alpha(x)\, U^\dagger(C) = q^a_{\alpha'}(x)\, (-C)_{\alpha'\alpha}$$

$$U(T)\, \overline{q}^a_\alpha(x)\, U^{-1}(T) = \overline{q}^a_{\alpha'}(Tx)\, \left(-C\gamma^5\right)_{\alpha\alpha'}$$

K.2 Gluons

The Lorentz transformation of a gluon is

$$\Lambda^\mu_\nu\, U(\Lambda)\, A^\nu_i(x)\, U^\dagger(\Lambda) = A^\mu_i(\Lambda x). \tag{K.9}$$

The parity transformation of a gluon is

$$P^\mu_\nu\, U(P)\, A^\nu_i(x)\, U^\dagger(P) = A^\mu_i(Px). \tag{K.10}$$

This follows from demanding that $U(P)\,\overline{q}(x)\gamma_\mu \overleftrightarrow{D}^\mu q(x)\, U^\dagger(P) = \overline{q}(Px)\gamma_\mu \overleftrightarrow{D}^\mu q(Px)$ as shown in the following.

$$\begin{aligned}
&U(P)\,\overline{q}^a_\alpha(x)\,\gamma^{\alpha\beta}_\mu \overleftrightarrow{D}^\mu_{ab}\, q^b_\beta(x)\, U^\dagger(P) = \\
&\quad = \overline{q}^a_{\alpha'}(Px)\,\gamma^0_{\alpha'\alpha}\,\gamma^{\alpha\beta}_\mu\,(P^\mu_\nu \overleftrightarrow{\delta}^\nu \delta_{ab} + igP^\mu_\nu A^\nu_i \lambda^i_{ab})\,\gamma^0_{\beta\beta'}\, q^b_{\beta'}(Px) \\
&\quad = \overline{q}^a_{\alpha'}(Px)\,\gamma^{\dagger\alpha'\beta'}_\mu P^\mu_\nu\,(\overleftrightarrow{\delta}^\nu \delta_{ab} + igA^\nu_i \lambda^i_{ab})\, q^b_{\beta'}(Px) \\
&\quad = \overline{q}^a_{\alpha'}(Px)\,\gamma^{\alpha'\beta'}_\mu(\overleftrightarrow{\delta}^\mu \delta_{ab} + igA^\mu_i \lambda^i_{ab})\, q^b_{\beta'}(Px) \\
&\quad = \overline{q}^a_{\alpha'}(Px)\,\gamma^{\alpha'\beta'}_\mu \overleftrightarrow{D}^\mu_{ab}\, q^b_{\beta'}(Px)
\end{aligned}$$

Note from the second line on the derivatives are with respect to Px. The charge conjugation transformation of a gluon is

$$-U(C)\, A^\mu_i(x)\lambda^i_{ab}\, U^\dagger(C) \;= A^\mu_i(x)\lambda^{iT}_{ab}. \tag{K.11}$$

This follows from demanding that $U(C)\,\overline{q}\gamma_\mu \overleftrightarrow{D}^\mu q\, U^\dagger(C) = \overline{q}\gamma_\mu \overleftrightarrow{D}^\mu q$ as shown in the following sequence of manipulations.

$$\begin{aligned}
&U(C)\,\overline{q}^a_\alpha(x)\,\gamma^{\alpha\beta}_\mu \overleftrightarrow{D}^\mu_{ab}\, q^b_\beta(x)\, U^\dagger(C) = \\
&\quad = U(C)\,\overline{q}^a_\alpha(x)\, U^\dagger(C)\,\gamma^{\alpha\beta}_\mu(\overleftrightarrow{\delta}^\mu \delta_{ab} + igU(C)\, A^\mu_i \lambda^i_{ab}\, U^\dagger(C))\, U(C)\, q^b_\beta(x)\, U^\dagger(C) \\
&\quad = q^a_{\alpha'}(x)\,(-C)_{\alpha'\alpha}\,\gamma^{\alpha\beta}_\mu\,(\overleftrightarrow{\delta}^\mu \delta_{ab} - igA^\mu_i \lambda^i_{ba})\,(-C)_{\beta\beta'}\,\overline{q}^b_{\beta'}(x) \\
&\quad = q^a_{\alpha'}(x)\,\gamma^{T\alpha'\beta'}_\mu(\overleftrightarrow{\delta}^\mu \delta_{ab} - igA^\mu_i \lambda^i_{ba})\,\overline{q}^b_{\beta'}(x) \\
&\quad = -\,\overline{q}^b_{\beta'}(x)\,\gamma^{\beta'\alpha'}_\mu(-\overleftrightarrow{\delta}^\mu \delta_{ba} - igA^\mu_i \lambda^i_{ba})\, q^a_{\alpha'}(x) \\
&\quad = \overline{q}^b_{\beta'}(x)\,\gamma^{\beta'\alpha'}_\mu(\overleftrightarrow{\delta}^\mu \delta_{ba} + igA^\mu_i \lambda^i_{ba})\, q^a_{\alpha'}(x) \\
&\quad = \overline{q}^b_\beta(x)\,\gamma^{\beta\alpha}_\mu \overleftrightarrow{D}^\mu_{ba}\, q^a_\alpha(x)
\end{aligned}$$

The overall sign in the fifth line comes from interchanging the Grassmann fields. The sign in front of $\overleftrightarrow{\delta}$ comes from the interchange of $\overrightarrow{\delta}$ and $\overleftarrow{\delta}$ that occurs while interchanging $\overline{q}$ and q. The time reversal transformation of a gluon is

$$-T^{\mu}_{\nu}\, U(T)\, A^{\mu}_{i}(x)\lambda^{i}_{ab}\, U^{\dagger}(T) = A^{\mu}_{i}(Tx)\lambda^{i}_{ab}. \tag{K.12}$$

This follows from demanding that $U(T)\,\overline{q}(x)i\gamma_{\mu}\overleftrightarrow{D}^{\mu} q(x)\,U^{\dagger}(T) = \overline{q}(Tx)i\gamma_{\mu}\overleftrightarrow{D}^{\mu} q(Tx)$ as shown by the following

$$\begin{aligned}
&U(T)\,\overline{q}^{a}_{\alpha}(x)\,i\gamma^{\alpha\beta}_{\mu}\overleftrightarrow{D}^{\mu}_{ab}\, q^{b}_{\beta}(x)\,U^{\dagger}(T) = \\
&= U(T)\,\overline{q}^{a}_{\alpha}(x)\,U^{\dagger}(T)\,U(T)\,i\gamma^{\alpha\beta}_{\mu}(\overleftrightarrow{\delta}^{\mu}\,\delta_{ab} + igA^{\mu}_{i}\lambda^{i}_{ab})\,U^{\dagger}(T)\,U(T)\,q^{b}_{\beta}(x)\,U^{\dagger}(T) \\
&= \overline{q}^{a}_{\alpha'}(Tx)\,(-\gamma^{5}C)_{\alpha'\alpha}\,(-i)\gamma^{\alpha\beta *}_{\mu}\,(T^{\mu}_{\nu}\overleftrightarrow{\delta}^{\nu}\,\delta_{ab} - ig(-T)^{\mu}_{\nu}\,A^{\mu}_{i}\lambda^{i}_{ab})\,(\gamma^{5}C)_{\beta\beta'}\,q^{b}_{\beta'}(Tx) \\
&= -\overline{q}^{a}_{\alpha'}(Tx)\,(C)_{\alpha'\alpha}\,i\gamma^{\alpha\beta *}_{\mu}\,(T^{\mu}_{\nu}\overleftrightarrow{\delta}^{\nu}\,\delta_{ab} + igT^{\mu}_{\nu}\,A^{\nu}_{i}\lambda^{i}_{ab})\,(C)_{\beta\beta'}\,q^{b}_{\beta'}(Tx) \\
&= -\overline{q}^{a}_{\alpha'}(Tx)\,i\gamma^{\dagger\alpha'\beta'}_{\mu}\,T^{\mu}_{\nu}\,(\overleftrightarrow{\delta}^{\nu}\,\delta_{ab} + igA^{\nu}_{i}\lambda^{i}_{ab})\,q^{b}_{\beta'}(Tx) \\
&= \overline{q}^{a}_{\alpha'}(Tx)\,i\gamma^{\alpha'\beta'}_{\mu}(\overleftrightarrow{\delta}^{\mu}\,\delta_{ab} + igA^{\mu}_{i}\lambda^{i}_{ab})\,q^{b}_{\beta'}(Tx) \\
&= \overline{q}^{a}_{\alpha'}(Tx)\,i\gamma^{\alpha'\beta'}_{\mu}\,\overleftrightarrow{D}^{\mu}_{ab}\,q^{b}_{\beta'}(Tx)
\end{aligned}$$

where from the third line on the derivative is with respect to Tx.

K.3 Wilson Lines

The Wilson line corresponding to a path $z(\tau)$ parameterized for $\tau \in [0,1]$ is

$$U[z(\tau)] = \mathcal{P}e^{i\int_{z(0)}^{z(1)} A^{i}_{\mu}(z)\lambda^{i}dz^{\mu}} = \mathcal{P}e^{i\int_{0}^{1} A^{i}_{\mu}(z(\tau))\lambda^{i}\frac{dz^{\mu}}{d\tau}d\tau}.$$

The Lorentz transformation (or Euclidean rotation) of a Wilson line is

$$U(\Lambda)\,U[z(\tau)]\,U^{\dagger}(\Lambda) = U[\Lambda z(\tau)]. \tag{K.13}$$

The parity transformation of a Wilson line is

$$U(P)\,U[z(\tau)]\,U^\dagger(P) = U[z^P(\tau)]. \tag{K.14}$$

The charge conjugation transformation of a Wilson line is

$$U(C)\,U[z(\tau)]\,U^\dagger(C) = U^*[z(\tau)]. \tag{K.15}$$

The time reversal transformation of a Wilson line is

$$U(T)\,U[z(\tau)]\,U^\dagger(T) = U[Tz(\tau)]. \tag{K.16}$$

K.4 Gauge Links

The transformation properties of a gauge link follow easily from those of a general Wilson line using the simple relationship

$$U_\mu^\dagger(x) = U[x + \mu\tau].$$

The Lorentz transformation (or Euclidean rotation) of a gauge link is

$$U(\Lambda)\,U_\mu^\dagger(x)\,U^\dagger(\Lambda) = U_{\Lambda\mu}^\dagger(\Lambda x). \tag{K.17}$$

The parity transformation of a gauge link is

$$U(P)\,U_\mu^\dagger(x)\,U^\dagger(P) = U_{P\mu}^\dagger(Px). \tag{K.18}$$

The charge conjugation transformation of a gauge link is

$$U(C)\,U_\mu^\dagger(x)\,U^\dagger(C) = U_\mu^*(x). \tag{K.19}$$

The time reversal transformation of a gauge link is

$$U(T)\,U_\mu^\dagger(x)\,U^\dagger(T) = U_{T\mu}^\dagger(Tx). \tag{K.20}$$

Appendix L

Wick's Theorem for Extended Quarks

Wick's theorem is simply a statement about Grassmann Gaussian integrals. We consider a quadratic fermion action of the form $S_F[\psi, \overline{\psi}, U_\mu] = \overline{\psi}\, M[U_\mu]\, \psi$. Additionally, we assume that the action is flavor diagonal, $S_F[\psi, \overline{\psi}, U_\mu] = \sum_q \overline{q}\, M[U_\mu; q]\, q$. For such an action Wick's theorem is

$$\begin{aligned} &\int D\psi D\overline{\psi}\; e^{-S_F[\psi,\overline{\psi},U_\mu]}\; \psi_1 \cdots \psi_N\, \overline{\psi}_N \cdots \overline{\psi}_1 = \\ &= \det(M[U_\mu])\, \sum_\pi (-1)^\pi\, M[U_\mu]^{-1}_{1\pi_1} \cdots M[U_\mu]^{-1}_{N\pi_N} \end{aligned}$$

where $\psi_i = \psi^{a_i}_{f_i\alpha_i}(x_i)$, $\overline{\psi}_i = \overline{\psi}^{b_i}_{g_i\beta_i}(y_i)$, and $M[U_\mu]^{-1}_{i\pi_i} = (M^{-1})^{a_i b_{\pi_i}}_{\alpha_i\beta_{\pi_i}}(x_i, y_{\pi_i}; f_i)\, \delta_{f_i g_{\pi_i}}$. We generalize this result to the case of the extended quark fields discussed in Chapter 6. Consider the integral

$$\int D\psi D\overline{\psi}\; e^{-S_F[\psi,\overline{\psi},U_\mu]}\; Q_1 \cdots Q_N\, \overline{Q}_N \cdots \overline{Q}_1$$

where $Q_i = Q^{a_i}_{\alpha_i}(x_i; A_i, f_i)$ and $\overline{Q}_i = \overline{Q}^{b_i}_{\beta_i}(y_i; B_i, g_i)$ are smeared quark fields. The indices A_i and B_i describe the smearing and f_i and g_i denote the flavor of Q_i and $\overline{Q}_i$

respectively. As given in Equations 6.7 and 6.9, the smeared quark fields are

$$\begin{aligned} Q^{a_i}_{\alpha_i}(x_i; A_i, f_i) &= S^{a_i a'_i}_{\alpha_i \alpha'_i}(x_i, x'_i; A_i)\; q^{a'_i}_{\alpha'_i}(x'_i, f_i) \\ \overline{Q}^{b_i}_{\beta_i}(y_i; B_i, g_i) &= \overline{q}^{b'_i}_{\beta'_i}(y'_i; g_i)\; \overline{S}^{b'_i b_i}_{\beta'_i \beta_i}(y'_i, y_i; B_i). \end{aligned}$$

Substituting these expressions for the smeared quarks into the integral above gives

$$\begin{gathered} S^{a_1 a'_1}_{\alpha_1 \alpha'_1}(x_1, x'_1; A_1) \cdots S^{a_N a'_N}_{\alpha_N \alpha'_N}(x_N, x'_N; A_N) \\ \int D\psi D\overline{\psi}\; e^{-S_F[\psi, \overline{\psi}, U_\mu]}\; q^{a'_1}_{\alpha'_1}(x'_1, f_1) \cdots q^{a'_N}_{\alpha'_N}(x'_N, f_N)\; \overline{q}^{b'_N}_{\beta'_N}(y'_N; g_N) \cdots \overline{q}^{b'_1}_{\beta'_1}(y'_1; g_1) \\ \overline{S}^{b'_N b_N}_{\beta'_N \beta_N}(y'_N, y_N; B_N) \cdots \overline{S}^{b'_1 b_1}_{\beta'_1 \beta_1}(y'_1, y_1; B_1). \end{gathered}$$

The smearing matrices S and $\overline{S}$ depend on the gauge field U_μ but, as written above, can be moved outside the fermion integral. Now use Wick's theorem for point quarks to evaluate this integral. The result is

$$\begin{gathered} S^{a_1 a'_1}_{\alpha_1 \alpha'_1}(x_1, x'_1; A_1) \cdots S^{a_N a'_N}_{\alpha_N \alpha'_N}(x_N, x'_N; A_N) \\ \det(M[U_\mu])\; \textstyle\sum_\pi (-1)^\pi \\ (M^{-1})^{a'_1 b'_{\pi_1}}_{\alpha'_1 \beta'_{\pi_1}}(x'_1, y'_{\pi_1}; f_1)\, \delta_{f_1 g_{\pi_1}} \cdots (M^{-1})^{a'_N b'_{\pi_N}}_{\alpha'_N \beta'_{\pi_N}}(x'_N, y'_{\pi_N}; f_N)\, \delta_{f_N g_{\pi_N}} \\ \overline{S}^{b'_N b_N}_{\beta'_N \beta_N}(y'_N, y_N; B_N) \cdots \overline{S}^{b'_1 b_1}_{\beta'_1 \beta_1}(y'_1, y_1; B_1). \end{gathered}$$

Next, for each factor of M^{-1} combine the corresponding factors of S and $\overline{S}$ to give the following.

$$\begin{gathered} \det(M[U_\mu])\; \textstyle\sum_\pi (-1)^\pi\, (S(A_1) M^{-1} \overline{S}(B_{\pi_1}))^{a_1 b_{\pi_1}}_{\alpha_1 \beta_{\pi_1}}(x_1, y_{\pi_1}; f_1)\, \delta_{f_1 g_{\pi_1}} \cdots \\ (S(A_N) M^{-1} \overline{S}(B_{\pi_N}))^{a_N b_{\pi_N}}_{\alpha_N \beta_{\pi_N}}(x_N, y_{\pi_N}; f_N)\, \delta_{f_N g_{\pi_N}} \end{gathered}$$

The combination $F_{i\pi_i} = S(A_i) M^{-1} \overline{S}(B_{\pi_i})$ is the smeared-to-smeared forward propagator introduced in Equation 7.9. Using this gives the generalization of Wick's theorem to extended quarks

$$\int D\psi D\overline{\psi}\; e^{-S_F[\psi, \overline{\psi}, U_\mu]}\; Q_1 \cdots Q_N\, \overline{Q}_N \cdots \overline{Q}_1 = \tag{L.1}$$

$$= \det(M[U_\mu]) \sum_\pi (-1)^\pi F[U_\mu]_{1\pi_1} \cdots F[U_\mu]_{N\pi_N}$$

where again $Q_i = Q^{a_i}_{\alpha_i}(x_i; A_i, f_i)$ and $\overline{Q}_j = \overline{Q}^{b_j}_{\beta_j}(y_j; B_j, g_j)$ are smeared quark and adjoint quark fields and $F[U_\mu]_{ij}$ is the corresponding smeared-to-smeared forward propagator. Thus, Wick's theorem holds for smeared quarks if we replace all quark propagators with the appropriate smeared-to-smeared propagators.

Appendix M

Twist Two Operators

The purpose of this appendix is to demonstrate the construction of the twist two operators. In particular, we illustrate the origins of the two-sided derivatives as well as the projection of the symmetric traceless piece used to define the twist two operators. Rigorous derivations are available in several quantum field theory textbooks, hence we are a bit cavalier with the following manipulations

The integrands of the light cone operators in Equation 2.1 are of the form

$$\overline{q}(-\lambda n/2)\,\Gamma_n\,\mathcal{P}e^{-ig\int_{\lambda n/2}^{-\lambda n/2}dz\,n\cdot A(z)}\,q(\lambda n/2)$$

where $\Gamma_n = n_\mu\gamma^\mu$, $n_\mu\gamma^\mu\gamma^5$, or $in_\mu\sigma^{\mu\nu}$ and n is a light like vector conventionally choosen to be $(1,0,0,-1)/\sqrt{2}$. Choosing light cone gauge given by $n\cdot A = 0$, the above becomes

$$\overline{q}(-\lambda n/2)\,\Gamma_n\,q(\lambda n/2).$$

Now simply Taylor expand in λ as follows.

$$\begin{aligned}
&\overline{q}(-\lambda n/2)\,\Gamma_n\,q(\lambda n/2) = \\
&= \overline{q}(-\lambda n/2)\sum_{k=0}^{\infty}\frac{1}{k!}\left(-\frac{\lambda}{2}n\cdot\overleftarrow{\delta}\right)^k\Bigg|_{x=0}\Gamma_n\sum_{l=0}^{\infty}\frac{1}{l!}\left(\frac{\lambda}{2}n\cdot\overrightarrow{\delta}\right)^l q(x)\Bigg|_{x=0} = \\
&= \overline{q}\,e^{-\frac{\lambda}{2}n\cdot\overleftarrow{\delta}}\,\Gamma_n\,e^{\frac{\lambda}{2}n\cdot\overrightarrow{\delta}}\,q
\end{aligned}$$

$$
\begin{aligned}
&= \overline{q}\,\Gamma_n\, e^{\lambda n\cdot\left(\frac{\overrightarrow{\delta}-\overleftarrow{\delta}}{2}\right)} q \\
&= \overline{q}\,\Gamma_n\, e^{\lambda n\cdot\overleftrightarrow{\delta}}\, q \\
&= \sum_{l=0}^{\infty}\frac{1}{l!}\,\overline{q}\,\Gamma_n\left(\lambda n\cdot\overleftrightarrow{\delta}\right)^l q
\end{aligned}
$$

Notice that the double sided derivative comes from the Taylor expansion of both q and $\overline{q}$. Now in light cone gauge, $n\cdot\overleftrightarrow{D}= n\cdot\overleftrightarrow{\delta}$, so the above becomes

$$
\begin{aligned}
&\overline{q}(-\lambda n/2)\,\Gamma_n\, q(\lambda n/2) = \\
&\quad = \sum_{l=0}^{\infty}\frac{\lambda^l}{l!}\, n_{\mu_2}\cdots n_{\mu_{l+1}}\,\overline{q}\,\Gamma_n\,\overleftrightarrow{D}^{\mu_2}\cdots\overleftrightarrow{D}^{\mu_{l+1}} q.
\end{aligned}
$$

Remember, the operators are of the form $\Gamma_n = n_\mu\gamma^\mu$, $n_\mu\gamma^\mu\gamma^5$, or $in_\mu\sigma^{\mu\nu}$ which can all be written as $n_{\mu_1}\Gamma^{\mu_1}$ for $\Gamma^{\mu_1} = \gamma^{\mu_1}$, $\gamma^{\mu_1}\gamma^5$, or $i\sigma^{\mu_1\nu}$. Therefore the last line above becomes

$$
\begin{aligned}
&\overline{q}(-\lambda n/2)\,\Gamma_n\, q(\lambda n/2) = \\
&\quad = \sum_{l=0}^{\infty}\frac{\lambda^l}{l!}\, n_{\mu_1}n_{\mu_2}\cdots n_{\mu_{l+1}}\,\overline{q}\,\Gamma^{\mu_1}\,\overleftrightarrow{D}^{\mu_2}\cdots\overleftrightarrow{D}^{\mu_{l+1}} q \\
&\quad = \sum_{l=0}^{\infty}\frac{\lambda^l}{l!}\, n_{\mu_1}\cdots n_{\mu_{l+1}}\, O^{\mu_1\cdots\mu_{l+1}}
\end{aligned}
$$

where $O^{\mu_1\cdots\mu_{l+1}}$ is the appropriate twist two operator. Note that the tensors $n_{\mu_1}\cdots n_{\mu_l}$ are manifestly symmetric. Additionally, since $n^2 = 0$, these tensors are also traceless. Therefore in the above we can take the symmetric traceless piece of $\overleftrightarrow{D}^{\mu_1}\cdots\overleftrightarrow{D}^{\mu_l}$ as is done in defining the twist two operators. The advantage is that this piece can be shown to transform as an irreducible representation of the Lorentz group.

Appendix N

Transverse Phenomenology of Dipole Form Factors

The transverse quark, charge, and momentum distributions as well as the transverse distributions of higher moments of parton distributions are all related to generalized form factors through equations of the following form

$$\rho(\vec{b}_\perp) = \int d^2\Delta_\perp \; e^{-i\vec{b}_\perp \cdot \vec{\Delta}_\perp} A(-\vec{\Delta}_\perp^2)$$

where $\rho(\vec{b}_\perp)$ is any of the transverse distributions and $A(-\vec{\Delta}_\perp^2)$ is the appropriate generalized form factor. In this appendix we examine the consequences of assuming the following dipole form for $A(-\vec{\Delta}_\perp^2)$.

$$A(-\vec{\Delta}_\perp^2) = \frac{A}{\left(1 + \frac{\vec{\Delta}_\perp^2}{m^2}\right)^2}$$

The resulting transverse distribution is

$$\rho(\vec{b}_\perp) = \int d^2\Delta_\perp \; e^{-i\vec{b}_\perp \cdot \vec{\Delta}_\perp} \frac{A}{\left(1 + \frac{\vec{\Delta}_\perp^2}{m^2}\right)^2} = \pi A m^2 (mb_\perp) K_1(mb_\perp)$$

where the integral and a few properties of the modified Bessel functions $K_\nu(z)$ are discussed in Appendix O.17. The resulting transverse radius of this distribution is

$$\langle \vec{b}_\perp^2 \rangle = \frac{\int d^2b_\perp \vec{b}_\perp^2 \rho(\vec{b}_\perp)}{\int d^2b_\perp \rho(\vec{b}_\perp)} = \frac{8}{m^2}.$$

Assuming uncorrelated errors σ_A and σ_m in A and m respectively, the resulting error in $\rho(\vec{b}_\_)$ is

$$\sigma^2_{\rho(\vec{b}_\perp)} = \left(\frac{d\rho(\vec{b}_\perp)}{dA}\right)^2 \sigma_A^2 + \left(\frac{d\rho(\vec{b}_\perp)}{dm}\right)^2 \sigma_m^2.$$

The required derivatives are

$$\frac{d\rho(\vec{b}_\perp)}{dA} = \pi m^2 (mb_\perp) K_1(mb_\perp)$$

and

$$\frac{d\rho(\vec{b}_\perp)}{dm} = \pi A m (mb_\perp) \left(-\frac{mb_\perp}{2} K_0(mb_\perp) + 3K_1(mb_\perp) - \frac{mb_\perp}{2} K_2(mb_\perp)\right)$$

where again the necessary details of the Bessel functions are given in Appendix O.17. We use this error analysis in all plots of transverse distributions. Additionally, we note that the point b_c at which $\rho(\vec{b}_\perp)$ falls to 1% is the solution of the following equation

$$\frac{\rho(b_c)}{\rho(0)} = mb_c K_1(mb_c) = 0.01$$

which is numerically $mb_c = 5.76714(3)$.

Appendix O

Details

O.1 Transverse Limits

The normalization condition for the wave packets in Equation 3.1 follows from the following.

$$\begin{aligned}
&\langle \psi, s | \psi, s \rangle = \\
&= \int \frac{d^3p'}{\sqrt{(2\pi)^3}} \frac{\psi(\vec{p}')}{\sqrt{2E_{\vec{p}'}}} \int \frac{d^3p}{\sqrt{(2\pi)^3}} \frac{\psi(\vec{p})}{\sqrt{2E_{\vec{p}}}} \langle \vec{p}', s | \vec{p}, s \rangle \\
&= \int \frac{d^3p' d^3p}{(2\pi)^3 2\sqrt{E_{\vec{p}'} E_{\vec{p}}}} \psi(\vec{p}')\, \psi(\vec{p})\, 2E_{\vec{p}}\, (2\pi)^3 \delta^3(\vec{p}' - \vec{p}) \\
&= \int d^3p\, |\psi(\vec{p})|^2
\end{aligned} \tag{O.1}$$

To take the transverse limits of various spinor matrix elements, we use the explicit representation of Dirac matrices, γ^μ, given here,

$$\gamma^0 = \begin{pmatrix} 1 & 0 \\ 0 & -1 \end{pmatrix} \quad \text{and} \quad \gamma^i = \begin{pmatrix} 0 & \sigma^i \\ -\sigma^i & 0 \end{pmatrix},$$

where the σ^i are the Pauli matrices,

$$\sigma^1 = \begin{pmatrix} 0 & 1 \\ 1 & 0 \end{pmatrix} \quad \sigma^2 = \begin{pmatrix} 0 & -i \\ i & 0 \end{pmatrix} \quad \sigma^3 = \begin{pmatrix} 1 & 0 \\ 0 & -1 \end{pmatrix}.$$

The resulting $\gamma^5 = i\gamma^0\gamma^1\gamma^2\gamma^3$ matrix is

$$\gamma^5 = \begin{pmatrix} 0 & 1 \\ 1 & 0 \end{pmatrix}.$$

The explicit solutions of Dirac's equation are

$$u(\vec{p}, \hat{s}) = \sqrt{E+m} \begin{pmatrix} \chi_{\hat{s}} \\ \frac{\vec{p}\cdot\vec{\sigma}}{E+m}\chi_{\hat{s}} \end{pmatrix},$$

and the adjoint solutions are

$$\overline{u}(\vec{p}', \hat{s}) = \sqrt{E'+m} \begin{pmatrix} \chi^\dagger_{\hat{s}} & -\chi^\dagger_{\hat{s}} \frac{\vec{p}'\cdot\vec{\sigma}}{E'+m} \end{pmatrix}.$$

We are interested in the following limit

$$\begin{aligned} \vec{p}' &= \vec{k} + \frac{1}{2}\vec{q}_\perp \\ \vec{p} &= \vec{k} - \frac{1}{2}\vec{q}_\perp \end{aligned}$$

where $k_z = K_z \to \infty$. Consequently, we see that in this limit $E' = E = K_z$. Additionally, we assume $\hat{s} = s\hat{z}$ where $s = \pm 1$.

Now we consider several spinor matrix elements. In the following we simply denote various lines as being equal if they are equal in the above limit. First consider the scalar matrix element.

$$\begin{aligned} &\frac{1}{2E}\,\overline{u}(\vec{p}', \hat{s})\, u(\vec{p}, \hat{s}) = \\ &= \frac{1}{2E}\sqrt{E'+m}\,\sqrt{E+m}\,\chi^\dagger_{\hat{s}} \left(1 - \frac{\vec{p}'\cdot\vec{\sigma}}{E'+m}\,\frac{\vec{p}\cdot\vec{\sigma}}{E+m}\right)\chi_{\hat{s}} \end{aligned} \tag{O.2}$$

$$
\begin{aligned}
&= \frac{1}{2}\chi^{\dagger}_{\hat{s}}\left(1-\frac{\vec{p}'\cdot\vec{p}+i\vec{p}'\times\vec{p}\cdot\vec{\sigma}}{E^2}\right)\chi_{\hat{s}} \\
&= \frac{1}{2}\left(1-\frac{\vec{p}'\cdot\vec{p}+i\vec{p}'\times\vec{p}\cdot\hat{s}}{E^2}\right) \\
&= \frac{1}{2}\left(1-\frac{K_z^2+k_\perp^2-\frac{1}{4}q_\perp^2+i\vec{q}_\perp\times\vec{k}_\perp\cdot\hat{s}}{E^2}\right) \\
&= \frac{1}{2}\left(1-\frac{K_z^2}{E^2}\right) \\
&= 0
\end{aligned}
$$

Therefore the final result is simply

$$
\lim_{K_z\to\infty}\frac{1}{2E}\,\overline{u}(\vec{p}',\hat{s})\,u(\vec{p},\hat{s})=0. \tag{O.3}
$$

Second consider the pseudo scalar matrix element.

$$
\begin{aligned}
&\frac{1}{2E}\,\overline{u}(\vec{p}',\hat{s})\,\gamma^5\,u(\vec{p},\hat{s}) = \qquad\qquad (O.4)\\
&= \frac{1}{2E}\sqrt{E'+m}\,\sqrt{E+m}\,\chi^{\dagger}_{\hat{s}}\left(\frac{\vec{p}\cdot\vec{\sigma}}{E+m}-\frac{\vec{p}'\cdot\vec{\sigma}}{E'+m}\right)\chi_{\hat{s}} \\
&= \frac{1}{2E}\left(\vec{p}\cdot\hat{s}-\vec{p}'\cdot\hat{s}\right) \\
&= -\frac{\vec{q}_\perp\cdot\hat{s}}{2E} \\
&= 0
\end{aligned}
$$

Therefore the final result is simply

$$
\lim_{K_z\to\infty}\frac{1}{2E}\,\overline{u}(\vec{p}',\hat{s})\,\gamma^5\,u(\vec{p},\hat{s})=0. \tag{O.5}
$$

Now consider the vector matrix element. First examine the $\mu=0$ component.

$$
\begin{aligned}
&\frac{1}{2E}\,\overline{u}(\vec{p}',\hat{s})\,\gamma^0\,u(\vec{p},\hat{s}) = \qquad\qquad (O.6)\\
&= \frac{1}{2E}\sqrt{E'+m}\,\sqrt{E+m}\,\chi^{\dagger}_{\hat{s}}\left(1+\frac{\vec{p}'\cdot\vec{\sigma}}{E'+m}\frac{\vec{p}\cdot\vec{\sigma}}{E+m}\right)\chi_{\hat{s}}
\end{aligned}
$$

$$
\begin{aligned}
&= \frac{1}{2}\chi^\dagger_{\hat{s}}\left(1+\frac{\vec{p}'\cdot\vec{p}+i\vec{p}'\times\vec{p}\cdot\vec{\sigma}}{E^2}\right)\chi_{\hat{s}} \\
&= \frac{1}{2}\left(1+\frac{\vec{p}'\cdot\vec{p}+i\vec{p}'\times\vec{p}\cdot\hat{s}}{E^2}\right) \\
&= \frac{1}{2}\left(1+\frac{K_z^2+k_\perp^2-\frac{1}{4}q_\perp^2+i\vec{q}_\perp\times\vec{k}_\perp\cdot\hat{s}}{E^2}\right) \\
&= \frac{1}{2}\left(1+\frac{K_z^2}{E^2}\right) \\
&= 1
\end{aligned}
$$

Next examine the $\mu = i$ components.

$$
\begin{aligned}
&\frac{1}{2E}\,\overline{u}(\vec{p}',\hat{s})\,\gamma^i\,u(\vec{p},\hat{s}) = \qquad\qquad (O.7)\\
&= \frac{1}{2E}\sqrt{E'+m}\sqrt{E+m}\,\chi^\dagger_{\hat{s}}\left(\frac{\vec{p}'\cdot\vec{\sigma}}{E'+m}\sigma^i+\sigma^i\frac{\vec{p}\cdot\vec{\sigma}}{E+m}\right)\chi_{\hat{s}} \\
&= \frac{1}{2E}\,\chi^\dagger_{\hat{s}}\left(\vec{p}'\cdot\vec{\sigma}\sigma^i+\sigma^i\vec{p}\cdot\vec{\sigma}\right)\chi_{\hat{s}} \\
&= \frac{1}{2E}\,\chi^\dagger_{\hat{s}}\left(p'_i+p_i-i(\vec{p}'\times\vec{\sigma})_i+i(\vec{p}\times\vec{\sigma})_i\right)\chi_{\hat{s}} \\
&= \frac{1}{2E}\left(p'_i+p_i-i(\vec{p}'\times\hat{s})_i+i(\vec{p}\times\hat{s})_i\right) \\
&= \frac{1}{2E}\left(2k_i-i(\vec{q}_\perp\times\hat{s})_i\right) \\
&= \frac{k_i}{E} \\
&= \delta_{i3}
\end{aligned}
$$

Combining the result for $\mu = 0$ with this result for $\mu = i$ gives the final result

$$
\lim_{K_z\to\infty}\frac{1}{2E}\,\overline{u}(\vec{p}',\hat{s})\,\gamma^\mu\,u(\vec{p},\hat{s}) = n_+^\mu \qquad (O.8)
$$

where $n_+ = (1,0,0,1)$. Next consider the axial vector matrix element. Again, we examine the $\mu = 0$ component first.

$$
\begin{aligned}
&\frac{1}{2E}\,\overline{u}(\vec{p}',\hat{s})\,\gamma^0\gamma^5\,u(\vec{p},\hat{s}) = \qquad\qquad (O.9)\\
&= \frac{1}{2E}\sqrt{E'+m}\sqrt{E+m}\,\chi^\dagger_{\hat{s}}\left(\frac{\vec{p}\cdot\vec{\sigma}}{E+m}+\frac{\vec{p}'\cdot\vec{\sigma}}{E'+m}\right)\chi_{\hat{s}}
\end{aligned}
$$

$$
\begin{aligned}
&= \frac{1}{2E}\,\chi^\dagger_{\hat{s}}\,(\vec{p}\cdot\vec{\sigma}+\vec{p}'\cdot\vec{\sigma})\,\chi_{\hat{s}} \\
&= \frac{1}{2E}\,(\vec{p}\cdot\hat{s}+\vec{p}'\cdot\hat{s}) \\
&= \frac{K_z}{E} \\
&= 1
\end{aligned}
$$

Next consider the $\mu = i$ components.

$$
\begin{aligned}
&\frac{1}{2E}\,\overline{u}(\vec{p}',\hat{s})\,\gamma^i\gamma^5\,u(\vec{p},\hat{s}) = \qquad\qquad (O.10)\\
&= \frac{1}{2E}\,\sqrt{E'+m}\,\sqrt{E+m}\,\chi^\dagger_{\hat{s}}\left(\sigma_i+\frac{\vec{p}'\cdot\vec{\sigma}}{E'+m}\sigma_i\frac{\vec{p}\cdot\vec{\sigma}}{E+m}\right)\chi_{\hat{s}} \\
&= \frac{1}{2}\,\chi^\dagger_{\hat{s}}\left(\sigma_i+\frac{1}{E^2}\vec{p}'\cdot\vec{\sigma}\sigma_i\vec{p}\cdot\vec{\sigma}\right)\chi_{\hat{s}} \\
&= \frac{1}{2}\,\chi^\dagger_{\hat{s}}\left(\sigma_i+\frac{1}{E^2}\,(p'_i\vec{p}\cdot\vec{\sigma}+p_i\vec{p}'\cdot\vec{\sigma}-i(\vec{p}'\times\vec{p})_i-\vec{p}'\cdot\vec{p}\sigma_i)\right)\chi_{\hat{s}} \\
&= \frac{1}{2}\left(\hat{s}_i+\frac{1}{E^2}\,(p'_i\vec{p}\cdot\hat{s}+p_i\vec{p}'\cdot\hat{s}-i(\vec{p}'\times\vec{p})_i-\vec{p}'\cdot\vec{p}\hat{s}_i)\right) \\
&= \frac{1}{2}\left(\hat{s}_i+\frac{1}{E^2}\left(2k_iK_z+i(\vec{q}_\perp\times\vec{k}_\perp)_i-(K_z^2+k_\perp^2-\frac{1}{4}q_\perp^2)\hat{s}_i\right)\right) \\
&= \frac{k_i}{E} \\
&= \delta_{i3}
\end{aligned}
$$

Using the result for $\mu = 0$ with this result for $\mu = i$ gives the final result

$$
\lim_{K_z\to\infty}\frac{1}{2E}\,\overline{u}(\vec{p}',\hat{s})\,\gamma^\mu\gamma^5\,u(\vec{p},\hat{s}) = n_+^\mu \qquad (O.11)
$$

where again $n_+ = (1,0,0,1)$. Now last we consider the tensor matrix elements. First examine the $\mu = 0$, $\nu = i$ case.

$$
\begin{aligned}
&\frac{1}{2E}\,\overline{u}(\vec{p}',\hat{s})\,\sigma^{0i}\,u(\vec{p},\hat{s}) = \qquad\qquad (O.12)\\
&= \frac{i}{2E}\,\sqrt{E'+m}\,\sqrt{E+m}\,\chi^\dagger_{\hat{s}}\left(-\frac{\vec{p}'\cdot\vec{\sigma}}{E'+m}\sigma_i+\sigma_i\frac{\vec{p}\cdot\vec{\sigma}}{E+m}\right)\chi_{\hat{s}} \\
&= \frac{i}{2E}\,\chi^\dagger_{\hat{s}}\,(-\vec{p}'\cdot\vec{\sigma}\sigma_i+\sigma_i\vec{p}\cdot\vec{\sigma})\,\chi_{\hat{s}}
\end{aligned}
$$

$$
\begin{aligned}
&= \frac{i}{2E}\left(-p'_i + p_i - i(\vec{p}' \times \hat{s})_i + i(\vec{p} \times \hat{s})_i\right) \\
&= -\frac{iq^i_\perp}{2E} \\
&= 0
\end{aligned}
$$

Now we do the same for $\mu = i$, $\nu = j$.

$$
\begin{aligned}
&\frac{1}{2E}\,\overline{u}(\vec{p}', \hat{s})\,\sigma^{ij}\,u(\vec{p}, \hat{s}) = \qquad (O.13) \\
&= -\frac{i}{2E}\sqrt{E'+m}\sqrt{E+m}\,\chi^\dagger_{\hat{s}}\left(\sigma_i\sigma_j - \frac{\vec{p}'\cdot\vec{\sigma}}{E'+m}\sigma_i\sigma_j\frac{\vec{p}\cdot\vec{\sigma}}{E+m}\right)\chi_{\hat{s}} \\
&= -\frac{i}{2}\,\chi^\dagger_{\hat{s}}\left(\sigma_i\sigma_j - \frac{1}{E^2}\vec{p}'\cdot\vec{\sigma}\sigma_i\sigma_j\vec{p}\cdot\vec{\sigma}\right)\chi_{\hat{s}} \\
&= -\frac{i\epsilon_{ijk}}{2}\,\chi^\dagger_{\hat{s}}\left(\sigma_k - \frac{1}{E^2}(p'_k\vec{p}\cdot\vec{\sigma} + p_k\vec{p}'\cdot\vec{\sigma} - \vec{p}'\cdot\vec{p}\sigma_k - i(\vec{p}'\times\vec{p})_k)\right)\chi_{\hat{s}} \\
&= -\frac{i\epsilon_{ijk}}{2}\left(\hat{s}_k - \frac{1}{E^2}(p'_k\vec{p}\cdot\hat{s} + p_k\vec{p}'\cdot\hat{s} - \vec{p}'\cdot\vec{p}\hat{s}_k - i(\vec{p}'\times\vec{p})_k)\right) \\
&= -\frac{i\epsilon_{ijk}}{2}\left(\hat{s}_k - \frac{1}{E^2}\left(2k_kK_z - (K_z^2 + K_\perp^2 + \frac{1}{4}q_\perp^2)\hat{s}_k - i(\vec{q}_\perp\times\vec{k})_k\right)\right) \\
&= -\frac{i\epsilon_{ijk}}{2}\left(\hat{s}_k - \frac{1}{E^2}\left(2k_kK_z - (K_z^2 + K_\perp^2 + \frac{1}{4}q_\perp^2)\hat{s}_k - i(\vec{q}_\perp\times\vec{k})_k\right)\right) \\
&= -\frac{i\epsilon_{ijk}}{2}\left(\hat{s}_k - \frac{2k_k}{E} + \hat{s}_k\right) \\
&= -i\epsilon_{ijk}\left(\hat{s}_k - \frac{k_k}{E}\right) \\
&= -i\epsilon_{ijk}\left(\delta_{k3} - \delta_{k3}\right) \\
&= 0
\end{aligned}
$$

Collecting the $\mu = 0$, $\nu = i$ results with the $\mu = i$, $\nu = j$ results gives

$$
\lim_{K_z\to\infty}\frac{1}{2E}\,\overline{u}(\vec{p}', \hat{s})\,\sigma^{\mu\nu}\,u(\vec{p}, \hat{s}) = 0. \qquad (O.14)
$$

O.2 Neutron Field

To determine the neutron field, N, corresponding to the proton field, P, in Equation 5.1, we demand that the pair (P, N) transform as an isospin doublet. The isospin

transformation for a doublet Q_i is given in Equation K.8 as

$$M_{ij}(I)\,U(I)\,Q_j\,U^\dagger(I) = Q_i.$$

Now we choose $I = I_y(\pi)$. The corresponding transformation matrix $M(I_y(\pi))$ is

$$M(I_y(\pi)) = \cos\left(\frac{\pi}{2}\right) - i\sin\left(\frac{\pi}{2}\right)\sigma_y = \begin{pmatrix} 0 & -1 \\ 1 & 0 \end{pmatrix}.$$

The resulting transformations for the the nucleon doublet (P, N) and quark doublet (U, D) are

$$U(I_y(\pi)) \begin{pmatrix} P \\ N \end{pmatrix} U^\dagger(I_y(\pi)) = M^\dagger(I_y(\pi)) \begin{pmatrix} P \\ N \end{pmatrix} = \begin{pmatrix} N \\ -P \end{pmatrix}$$

and

$$U(I_y(\pi)) \begin{pmatrix} U \\ D \end{pmatrix} U^\dagger(I_y(\pi)) = M^\dagger(I_y(\pi)) \begin{pmatrix} U \\ D \end{pmatrix} = \begin{pmatrix} D \\ -U \end{pmatrix}.$$

Given the proton field from Equation 5.1,

$$P_\alpha(x) = f_{\alpha\beta\gamma\delta}\,\epsilon_{bcd}\,U^b_\beta(x)\,U^c_\gamma(x)\,D^d_\delta(x),$$

the corresponding neutron field is

$$\begin{aligned} N_\alpha(x) &= U(I_y(\pi))\,P_\alpha(x)\,U^\dagger(I_y(\pi)) \qquad \text{(O.15)} \\ &= U(I_y(\pi))\,f_{\alpha\beta\gamma\delta}\,\epsilon_{bcd}\,U^b_\beta(x)\,U^c_\gamma(x)\,D^d_\delta(x)\,U^\dagger(I_y(\pi)) \\ &= f_{\alpha\beta\gamma\delta}\,\epsilon_{bcd}\,U(I_y(\pi))\,U^b_\beta(x)\,U^\dagger(I_y(\pi))\,U(I_y(\pi))\,U^c_\gamma(x)\,U^\dagger(I_y(\pi)) \\ &\quad U(I_y(\pi))\,D^d_\delta(x)\,U^\dagger(I_y(\pi)) \\ &= f_{\alpha\beta\gamma\delta}\,\epsilon_{bcd}\,D^b_\beta(x)\,D^c_\gamma(x)\,(-1)U^d_\delta(x) \\ &= -f_{\alpha\beta\gamma\delta}\,\epsilon_{bcd}\,D^b_\beta(x)\,D^c_\gamma(x)\,U^d_\delta(x). \end{aligned}$$

We use $U(I)\,U^{\dagger}(I) = 1$ in the third line and Equation K.8 for the isospin transformation of the quark doublet in fourth line. This result is first used in Equation 5.2.

O.3 Adjoint of Nucleon Fields

Our general form for the nucleon field is given in Equation 5.1. For convenience we change the dummy indices slightly and write the nucleon field as

$$P_{\alpha'}(x) = f_{\alpha'\beta'\gamma'\delta'}\,\epsilon_{bcd}\,U^{b}_{\beta'}(x)\,U^{c}_{\gamma'}(x)\,D^{d}_{\delta'}(x).$$

The adjoint of the above equation is

$$\begin{aligned}
\overline{P}_{\alpha}(x) &= P^{\dagger}_{\alpha'}(x)\,\gamma^{0}_{\alpha'\alpha} \qquad\qquad (O.16)\\
&= D^{d\,\dagger}_{\delta'}(x)\,U^{c\,\dagger}_{\gamma'}(x)\,U^{b\,\dagger}_{\beta'}(x)\,\epsilon_{bcd}\,f^{*}_{\alpha'\beta'\gamma'\delta'}\,\gamma^{0}_{\alpha'\alpha}\\
&= \overline{D}^{d}_{\delta}(x)\,\gamma^{0}_{\delta\delta'}\,\overline{U}^{c}_{\gamma}(x)\,\gamma^{0}_{\gamma\gamma'}\,\overline{U}^{b}_{\beta}(x)\,\gamma^{0}_{\beta\beta'}\,\epsilon_{bcd}\,f^{*}_{\alpha'\beta'\gamma'\delta'}\,\gamma^{0}_{\alpha'\alpha}\\
&= \overline{D}^{d}_{\delta}(x)\,\overline{U}^{c}_{\gamma}(x)\,\overline{U}^{b}_{\beta}(x)\,\epsilon_{bcd}\,\gamma^{0}_{\delta\delta'}\,\gamma^{0}_{\gamma\gamma'}\,\gamma^{0}_{\beta\beta'}\,f^{*}_{\alpha'\beta'\gamma'\delta'}\,\gamma^{0}_{\alpha'\alpha}\\
&= \overline{D}^{d}_{\delta}(x)\,\overline{U}^{c}_{\gamma}(x)\,\overline{U}^{b}_{\beta}(x)\,\overline{\epsilon}_{dcb}\,\overline{f}_{\delta\gamma\beta\alpha}
\end{aligned}$$

where

$$\overline{f}_{\delta\gamma\beta\alpha} = \gamma^{0}_{\delta\delta'}\,\gamma^{0}_{\gamma\gamma'}\,\gamma^{0}_{\beta\beta'}\,f^{*}_{\alpha'\beta'\gamma'\delta'}\,\gamma^{0}_{\alpha'\alpha} \qquad (O.17)$$

and

$$\overline{\epsilon}_{dcb} = \epsilon_{bcd}. \qquad (O.18)$$

The $\overline{f}$ and $\overline{\epsilon}$ symbols are defined so that the order of indices matches the order of quark fields in the adjoint nucleon field. These results are first used in Equations 5.3, 5.4, and 5.5.

O.4 Translational Covariance of Nucleon Fields

In this section we demonstrate that the nucleon field $P_\alpha(x)$ has the correct transformation under a translation. The expected translation of the proton field is

$$U(\Delta)P_\alpha(x)U^\dagger(\Delta) = P_\alpha(x+\Delta).$$

As a reminder, the proton field from Equation 5.1 is

$$P_\alpha(x) = f_{\alpha\beta\gamma\delta}\,\epsilon_{bcd}\,U^b_\beta(x)\,U^c_\gamma(x)\,D^d_\delta(x).$$

The translation of the proton field is determined in the following.

$$\begin{aligned} U(\Delta)\,P_\alpha(x)\,U^\dagger(\Delta) = & \qquad \text{(O.19)} \\ = \;& U(\Delta)\,f_{\alpha\beta\gamma\delta}\,\epsilon_{bcd}\,U^b_\beta(x)\,U^c_\gamma(x)\,D^d_\delta(x)\,U^\dagger(\Delta) \\ = \;& f_{\alpha\beta\gamma\delta}\,\epsilon_{bcd}\,U(\Delta)\,U^b_\beta(x)\,U^\dagger(\Delta)\,U(\Delta)\,U^c_\gamma(x)\,U^\dagger(\Delta)\,U(\Delta)\,D^d_\delta(x)\,U^\dagger(\Delta) \\ = \;& f_{\alpha\beta\gamma\delta}\,\epsilon_{bcd}\,U^b_\beta(x+\Delta)\,U^c_\gamma(x+\Delta)\,D^d_\delta(x+\Delta) \\ = \;& P_\alpha(x+\Delta) \end{aligned}$$

Note, in the third line we use $U(\Delta)\,U^\dagger(\Delta) = 1$, and in the fourth we use Equation K.1 for the translation of a quark field. This demonstrates that the nucleon field in Equation 5.1 has the correct behavior under translations regardless of the choice of $f_{\alpha\beta\gamma\delta}$.

O.5 Rotational Covariance of Nucleon Fields

In this section we determine the constraints on the proton field $P_\alpha(x)$ required by rotational covariance. In particular we determine the constraints on $f_{\alpha\beta\gamma\delta}$, as given in Equation 5.6, required to ensure that the nucleon has spin one-half. The rotation of a spin one-half field is given in Equation K.2 for quarks and is written here for the

case of the proton.

$$M_{\alpha'\alpha}(R)\, U(R)\, P_\alpha(x)\, U^\dagger(R) = P_{\alpha'}(Rx).$$

To determine the constraints imposed by the above equation, we first relabel the dummy indices and write the proton field, given in Equation 5.1, as

$$P_\alpha(x) = f_{\alpha\beta\gamma\delta}\, \epsilon_{b'c'd'}\, U^{b'}_\beta(x)\, U^{c'}_\gamma(x)\, D^{d'}_\delta(x).$$

The desired result is shown in the following lines.

$$\begin{aligned}
&M_{\alpha\alpha'}(R)\, U(R)\, P_{\alpha'}(x)\, U^\dagger(R) = \qquad\qquad (O.20)\\
&= M_{\alpha\alpha'}(R)\, U(R)\, f_{\alpha\beta\gamma\delta}\, \epsilon_{b'c'd'}\, U^{b'}_\beta(x)\, U^{c'}_\gamma(x)\, D^{d'}_\delta(x)\, U^\dagger(R)\\
&= M_{\alpha\alpha'}(R)\, f_{\alpha\beta\gamma\delta}\, \epsilon_{b'c'd'}\, U(R)\, U^{b'}_\beta(x)\, U^\dagger(R)\, U(R)\, U^{c'}_\gamma(x)\, U^\dagger(R)\, U(R)\, D^{d'}_\delta(x)\, U^\dagger(R)\\
&= M_{\alpha\alpha'}(R)\, f_{\alpha\beta\gamma\delta}\, \epsilon_{b'c'd'}\, M^\dagger_{\beta\beta'}(R)\, U^{b'}_{\beta'}(Rx)\, M^\dagger_{\gamma\gamma'}(R)\, U^{c'}_{\gamma'}(Rx)\, M^\dagger_{\delta\delta'}(R)\, D^{d'}_{\delta'}(Rx)\\
&= M_{\alpha\alpha'}(R)\, f_{\alpha\beta\gamma\delta}\, M^\dagger_{\beta\beta'}(R)\, M^\dagger_{\gamma\gamma'}(R)\, M^\dagger_{\delta\delta'}(R)\, \epsilon_{b'c'd'}\, U^{b'}_{\beta'}(Rx)\, U^{c'}_{\gamma'}(Rx)\, D^{d'}_{\delta'}(Rx)\\
&= f_{\alpha'\beta'\gamma'\delta'}\, \epsilon_{b'c'd'}\, U^{b'}_{\beta'}(Rx)\, U^{c'}_{\gamma'}(Rx)\, D^{d'}_{\delta'}(Rx)\\
&= P_{\alpha'}(Rx)
\end{aligned}$$

In the third line we use $U(R)\, U^\dagger(R) = 1$. In the fourth line we use Equation K.2 for the rotation of quark fields, and in the sixth line we use the constraint on $f_{\alpha\beta\gamma\delta}$ given in Equation 5.6 as

$$M_{\alpha\alpha'}(R)\, f_{\alpha\beta\gamma\delta}\, M^\dagger_{\beta\beta'}(R)\, M^\dagger_{\gamma\gamma'}(R)\, M^\dagger_{\delta\delta'}(R) = f_{\alpha'\beta'\gamma'\delta'}.$$

This constraint ensures that the proton field $P_\alpha(x)$ transforms in the spin one-half representation of the rotation group. The argument uses the continuum description of rotations, but the spin one-half representation, restricted to cubic lattice rotations, is an irreducible representation of the group of three dimensional lattice rotations. Hence the above constraint guarantees that the proton field $P_\alpha(x)$ transforms in the

irreducible spin one-half representation of the group of cubic lattice rotations.

O.6 Parity Covariance of Nucleon Fields

In this section we determine the constraints on the proton field $P_\alpha(x)$ required by parity. This in turn results in the constraints on $f_{\alpha\beta\gamma\delta}$ given in Equation 5.7. We require that the proton field transform under parity as follows.

$$\gamma^0_{\alpha'\alpha}\, U(P)\, P_\alpha(x)\, U^\dagger(P) = P_{\alpha'}(Px).$$

This transformation is the same as the parity transformation of a quark field as given in Equation K.4. Next, with a change in the dummy indices, the proton field from Equation 5.1 is

$$P_\alpha(x) = f_{\alpha\beta\gamma\delta}\, \epsilon_{b'c'd'}\, U^{b'}_\beta(x)\, U^{c'}_\gamma(x)\, D^{d'}_\delta(x).$$

Now we determine the conditions on $f_{\alpha\beta\gamma\delta}$ required to satisfy the above parity transformation.

$$\begin{aligned}
&\gamma^0_{\alpha'\alpha}\, U(P)\, P_\alpha(x)\, U^\dagger(P) = \qquad\qquad (O.21)\\
&= \gamma^0_{\alpha'\alpha}\, U(P)\, f_{\alpha\beta\gamma\delta}\, \epsilon_{b'c'd'}\, U^{b'}_\beta(x)\, U^{c'}_\gamma(x)\, D^{d'}_\delta(x)\, U^\dagger(P)\\
&= \gamma^0_{\alpha'\alpha}\, f_{\alpha\beta\gamma\delta}\, \epsilon_{b'c'd'}\, U(P)\, U^{b'}_\beta(x)\, U^\dagger(P)\, U(P)\, U^{c'}_\gamma(x)\, U^\dagger(P)\, U(P)\, D^{d'}_\delta(x)\, U^\dagger(P)\\
&= \gamma^0_{\alpha'\alpha}\, f_{\alpha\beta\gamma\delta}\, \epsilon_{b'c'd'}\, \gamma^0_{\beta\beta'}\, U^{b'}_{\beta'}(Px)\, \gamma^0_{\gamma\gamma'}\, U^{c'}_{\gamma'}(Px)\, \gamma^0_{\delta\delta'}\, D^{d'}_{\delta'}(Px)\\
&= \gamma^0_{\alpha'\alpha}\, f_{\alpha\beta\gamma\delta}\, \gamma^0_{\beta\beta'}\, \gamma^0_{\gamma\gamma'}\, \gamma^0_{\delta\delta'}\, \epsilon_{b'c'd'}\, U^{b'}_{\beta'}(Px)\, U^{c'}_{\gamma'}(Px)\, D^{d'}_{\delta'}(Px)\\
&= f_{\alpha'\beta'\gamma'\delta'}\, \epsilon_{b'c'd'}\, U^{b'}_{\beta'}(Px)\, U^{c'}_{\gamma'}(Px)\, D^{d'}_{\delta'}(Px)\\
&= P_{\alpha'}(Px)
\end{aligned}$$

In the third line we use the unitarity relation $U(P)\, U^\dagger(P) = 1$, and in the fourth line we use Equation K.4 for the parity transformation of a quark. Then in the sixth line we use the constraint on $f_{\alpha\beta\gamma\delta}$ from Equation 5.7 which gives

$$\gamma^0_{\alpha'\alpha}\, f_{\alpha\beta\gamma\delta}\, \gamma^0_{\beta\beta'}\, \gamma^0_{\gamma\gamma'}\, \gamma^0_{\delta\delta'} = f_{\alpha'\beta'\gamma'\delta'}.$$

O.7 Charge Conjugation Covariance of Nucleon Fields

In this section we calculate the charge conjugation of the nucleon field $P_\alpha(x)$ and determine the resulting constraint on $f_{\alpha\beta\gamma\delta}$. The charge conjugation of the proton field is required to be the same as that of a quark field which is given in Equation K.5 and is given here for the proton.

$$C_{\alpha'\alpha}\, U(C)\, P_\alpha(x)\, U^\dagger(C) = \overline{P}_{\alpha'}(x)$$

Relabelling the dummy indices of the proton field in Equation 5.1 gives

$$P_\alpha(x) = f_{\alpha\beta\gamma\delta}\, \epsilon_{b'c'd'}\, U^{b'}_\beta(x)\, U^{c'}_\gamma(x)\, D^{d'}_\delta(x).$$

Next, in the following lines we determine the conditions on $f_{\alpha\beta\gamma\delta}$ needed to ensure the correct charge conjugation of $P_\alpha(x)$.

$$\begin{aligned}
&C_{\alpha'\alpha}\, U(C)\, P_\alpha(x)\, U^\dagger(C) = \qquad\qquad (O.22)\\
&= C_{\alpha'\alpha}\, U(C)\, f_{\alpha\beta\gamma\delta}\, \epsilon_{b'c'd'}\, U^{b'}_\beta(x)\, U^{c'}_\gamma(x)\, D^{d'}_\delta(x)\, U^\dagger(C)\\
&= C_{\alpha'\alpha}\, f_{\alpha\beta\gamma\delta}\, \epsilon_{b'c'd'}\, U(C)\, U^{b'}_\beta(x)\, U^\dagger(C)\, U(C)\, U^{c'}_\gamma(x)\, U^\dagger(C)\, U(C)\, D^{d'}_\delta(x)\, U^\dagger(C)\\
&= C_{\alpha'\alpha}\, f_{\alpha\beta\gamma\delta}\, \epsilon_{b'c'd'}\, (-C_{\beta\beta'})\, \overline{U}^{b'}_{\beta'}(x)\, (-C_{\gamma\gamma'})\, \overline{U}^{c'}_{\gamma'}(x)\, (-C_{\delta\delta'})\, \overline{D}^{d'}_{\delta'}(x)\\
&= -\, C_{\alpha'\alpha}\, f_{\alpha\beta\gamma\delta}\, C_{\beta\beta'}\, C_{\gamma\gamma'}\, C_{\delta\delta'}\, \epsilon_{b'c'd'}\, \overline{U}^{b'}_{\beta'}(x)\, \overline{U}^{c'}_{\gamma'}(x)\, \overline{D}^{d'}_{\delta'}(x)\\
&= C_{\alpha'\alpha}\, f_{\alpha\beta\gamma\delta}\, C_{\beta\beta'}\, C_{\gamma\gamma'}\, C_{\delta\delta'}\, \epsilon_{b'c'd'}\, \overline{D}^{d'}_{\delta'}(x)\, \overline{U}^{c'}_{\gamma'}(x)\, \overline{U}^{b'}_{\beta'}(x)\\
&= \overline{f}_{\delta'\gamma'\beta'\alpha'}\, \overline{\epsilon}_{d'c'b'}\, \overline{D}^{d'}_{\delta'}(x)\, \overline{U}^{c'}_{\gamma'}(x)\, \overline{U}^{b'}_{\beta'}(x)\\
&= \overline{P}_{\alpha'}(x)
\end{aligned}$$

In the third line we use the relation $U(C)\, U^\dagger(C) = 1$. In the fourth line we use Equation K.5 for the charge conjugation of a quark field, and in the sixth line we anti-commute the quark fields. Then in the seventh line we use Equation 5.5 for $\overline{\epsilon}$

and the constraint on $f_{\alpha\beta\gamma\delta}$ given by Equation 5.8 as

$$C_{\alpha'\alpha}\, f_{\alpha\beta\gamma\delta}\, C_{\beta\beta'}\, C_{\gamma\gamma'}\, C_{\delta\delta'} = \overline{f}_{\delta'\gamma'\beta'\alpha'}.$$

And finally in the eighth line we use Equation 5.3 for the adjoint of the proton field.

O.8 Gauge Invariance of Nucleon Fields

Here we show that the nucleon field $P_\alpha(x)$ is gauge invariant. Precisely we require that

$${}^{g}P_\alpha(x) = P_\alpha(x).$$

Relabelling the dummy indices for convenience gives the proton field from Equation 5.1 as

$$P_\alpha(x) = f_{\alpha\beta\gamma\delta}\, \epsilon_{b'c'd'}\, U^{b'}_{\beta}(x)\, U^{c'}_{\gamma}(x)\, D^{d'}_{\delta}(x).$$

We now show that $P_\alpha(x)$ is gauge invariant.

$$\begin{aligned}
{}^{g}P_\alpha(x) = & \qquad\qquad (O.23)\\
&= f_{\alpha\beta\gamma\delta}\, \epsilon_{b'c'd'}\, {}^{g}U^{b'}_{\beta}(x)\, {}^{g}U^{c'}_{\gamma}(x)\, {}^{g}D^{d'}_{\delta}(x)\\
&= f_{\alpha\beta\gamma\delta}\, \epsilon_{b'c'd'}\, g^{b'b}(x)\, U^{b}_{\beta}(x)\, g^{c'c}(x)\, U^{c}_{\gamma}(x)\, g^{d'd}(x)\, D^{d}_{\delta}(x)\\
&= f_{\alpha\beta\gamma\delta}\, \epsilon_{b'c'd'}\, g^{b'b}(x)\, g^{c'c}(x)\, g^{d'd}(x)\, U^{b}_{\beta}(x)\, U^{c}_{\gamma}(x)\, D^{d}_{\delta}(x)\\
&= f_{\alpha\beta\gamma\delta}\, \epsilon_{bcd}\, \det(g(x))\, U^{b}_{\beta}(x)\, U^{c}_{\gamma}(x)\, D^{d}_{\delta}(x)\\
&= f_{\alpha\beta\gamma\delta}\, \epsilon_{bcd}\, U^{b}_{\beta}(x)\, U^{c}_{\gamma}(x)\, D^{d}_{\delta}(x)\\
&= P_\alpha(x)
\end{aligned}$$

In the third line we use Equation 4.2 for the gauge transformation of a quark field. Then in the fifth line we simply use the definition of the determinant, and in the sixth line we use $\det(g) = 1$ for $\mathrm{SU(N_c)}$ gauge transformations. The result is that the proton field from Equation 5.1 is gauge invariant.

O.9 Parity Projection

The hadronic level parity projected field corresponding to $P_\alpha(x)$ is

$$P^{\pm}_{\alpha}(x) = \left(\frac{1 \pm \gamma^0}{2}\right)_{\alpha\alpha'} P_{\alpha'}(x).$$

The resulting field satisfies

$$U(P)\, P^{\pm}_{\alpha}(x)\, U^{\dagger}(P) = \pm\, P^{\pm}_{\alpha}(Px)$$

as seen from the following.

$$\begin{aligned} & U(P)\, P^{\pm}_{\alpha}(x)\, U^{\dagger}(P) = \\ &= U(P) \left(\frac{1 \pm \gamma^0}{2}\right)_{\alpha\alpha'} P_{\alpha'}(x)\, U^{\dagger}(P) \\ &= \left(\frac{1 \pm \gamma^0}{2}\right)_{\alpha\alpha'} U(P)\, P_{\alpha'}(x)\, U^{\dagger}(P) \\ &= \left(\frac{1 \pm \gamma^0}{2}\right)_{\alpha\alpha'} \gamma^0_{\alpha'\alpha''}\, P_{\alpha''}(Px) \\ &= \pm \left(\frac{1 \pm \gamma^0}{2}\right)_{\alpha\alpha'} P_{\alpha'}(Px) \\ &= \pm\, P^{\pm}_{\alpha}(x) \end{aligned} \tag{O.24}$$

The quark level parity projected field for $P_\alpha(x)$ is

$$P^{\pm}_{\alpha}(x) = f_{\alpha\beta\gamma\delta}\, \epsilon_{bcd}\, P^{\pm}_{\beta\beta'}\, U^{b}_{\beta'}(x)\, P^{\pm}_{\gamma\gamma'}\, U^{c}_{\gamma'}(x)\, P^{\pm}_{\delta\delta'}\, D^{d}_{\delta'}(x).$$

Again this field satisfies

$$U(P)\, P^{\pm}_{\alpha}(x)\, U^{\dagger}(P) = \pm\, P^{\pm}_{\alpha}(Px)$$

as indicated in the following.

$$U(P)\, P^{\pm}_{\alpha}(x)\, U^{\dagger}(P) = \tag{O.25}$$

$$
\begin{aligned}
&= U(P)\, f_{\alpha\beta\gamma\delta}\, \epsilon_{bcd}\, P^{\pm}_{\beta\beta'}\, U^{b}_{\beta'}(x)\, P^{\pm}_{\gamma\gamma'}\, U^{c}_{\gamma'}(x)\, P^{\pm}_{\delta\delta'}\, D^{d}_{\delta'}(x)\, U^{\dagger}(P) \\
&= f_{\alpha\beta\gamma\delta}\, \epsilon_{bcd}\, P^{\pm}_{\beta\beta'}\, U(P)\, U^{b}_{\beta'}(x)\, U^{\dagger}(P)\, P^{\pm}_{\gamma\gamma'}\, U(P)\, U^{c}_{\gamma'}(x)\, U^{\dagger}(P)\, P^{\pm}_{\delta\delta'}\, U(P)\, D^{d}_{\delta'}(x)\, U^{\dagger}(P) \\
&= f_{\alpha\beta\gamma\delta}\, \epsilon_{bcd}\, P^{\pm}_{\beta\beta'}\, \gamma^{0}_{\beta'\beta''}\, U^{b}_{\beta''}(Px)\, P^{\pm}_{\gamma\gamma'}\, \gamma^{0}_{\gamma'\gamma''}\, U^{c}_{\gamma''}(Px)\, P^{\pm}_{\delta\delta'}\, \gamma^{0}_{\delta'\delta''}\, D^{d}_{\delta''}(Px) \\
&= f_{\alpha\beta\gamma\delta}\, \epsilon_{bcd}\, (\pm 1)\, P^{\pm}_{\beta\beta'}\, U^{b}_{\beta'}(Px)\, (\pm 1)\, P^{\pm}_{\gamma\gamma'}\, U^{c}_{\gamma'}(Px)\, (\pm 1)\, P^{\pm}_{\delta\delta'}\, D^{d}_{\delta'}(Px) \\
&= (\pm 1)\, f_{\alpha\beta\gamma\delta}\, \epsilon_{bcd}\, P^{\pm}_{\beta\beta'}\, U^{b}_{\beta'}(Px)\, P^{\pm}_{\gamma\gamma'}\, U^{c}_{\gamma'}(Px)\, P^{\pm}_{\delta\delta'}\, D^{d}_{\delta'}(Px) \\
&= \pm P^{\pm}_{\alpha}(Px)
\end{aligned}
$$

O.10 Lorentz Covariance of Extended Quark Fields

In this appendix we prove that various extended quarks constructed in Chapter 6 are Lorentz covariant. In other words, we demonstrate that the extended quark fields transform under Lorentz transformations just as point quarks do. To start, we verify that the gauge field independent smearing in Equation 6.1,

$$Q^{a}_{\alpha}(x) = \int d^4y\ f((x-y)^2)\, q^{a}_{\alpha}(y),$$

is indeed Lorentz covariant. The statement of Lorentz covariance for point quarks is given in Equation K.2. The following sequence of steps show that the extended quarks fields in Equation 6.1 are also Lorentz covariant.

$$
\begin{aligned}
&M_{\alpha\beta}(\Lambda)\, U(\Lambda)\, Q^{a}_{\beta}(x)\, U^{\dagger}(\Lambda) = \qquad\qquad (O.26) \\
&\quad = \int d^4y\ f((x-y)^2)\, M_{\alpha\beta}(\Lambda)\, U(\Lambda)\, q^{a}_{\beta}(y)\, U^{\dagger}(\Lambda) \\
&\quad = \int d^4y\ f((x-y)^2)\, q^{a}_{\alpha}(\Lambda y) \\
&\quad = \int d^4y\ f((x-\Lambda^{-1}y)^2)\, q^{a}_{\alpha}(y) \\
&\quad = \int d^4y\ f((\Lambda x-y)^2)\, q^{a}_{\alpha}(y) \\
&\quad = Q^{a}_{\alpha}(\Lambda x)
\end{aligned}
$$

In the third line we use Equation K.2 for the Lorentz transformation of a point quark. In the fourth line we make the change of variables $y \rightarrow \Lambda^{-1}y$, and in the fifth line we

use the Lorentz invariance of the smearing function f.

Next we consider the simple example of gauge covariant smearing given in Equation 6.2 as

$$Q^a_\alpha(x) = \int d^4y \; U^{ab}(x,y)\, q^b_\alpha(y)\, f((x-y)^2).$$

A nearly identical sequence of steps shows that this extended quark field has the proper Lorentz transformation property as well.

$$\begin{aligned} & M^{\alpha\beta}(\Lambda)\, U(\Lambda)\, Q^a_\beta(x)\, U^\dagger(\Lambda) = \\ &= \int d^4y \; U(\Lambda)\, U^{ab}(x,y)\, U^\dagger(\Lambda)\, M^{\alpha\beta}(\Lambda)\, U(\Lambda)\, q^b_\beta(y)\, U^\dagger(\Lambda)\, f((x-y)^2) \\ &= \int d^4y \; U^{ab}(\Lambda x, \Lambda y)\, q^b_\alpha(\Lambda y)\, f((x-y)^2) \\ &= \int d^4y \; U^{ab}(\Lambda x, y)\, q^b_\alpha(y)\, f((x-\Lambda^{-1}y)^2) \\ &= \int d^4y \; U^{ab}(\Lambda x, y)\, q^b_\alpha(y)\, f((\Lambda x-y)^2) \\ &= Q^a_\alpha(\Lambda x) \end{aligned} \tag{O.27}$$

In addition to the basic steps used to derive Equation O.26 above, we now use $U^\dagger(\Lambda)U(\Lambda) = 1$ in the second line and the Lorentz transformation of the Wilson line $U^{ab}(x,y)$ in the third line. The Lorentz transformation of $U^{ab}(x,y)$ can be derived from the Lorentz transformation of a general Wilson line given in Equation K.13. The Lorentz transformation of the straight line Wilson path $U^{ab}(x,y)$ is determined in the following lines.

$$\begin{aligned} & U(\Lambda)\, U(x,y)\, U^\dagger(\Lambda) \\ &= U(\Lambda)\, U[(1-\tau)x + \tau y]\, U^\dagger(\Lambda) \\ &= U[\Lambda((1-\tau)x + \tau y)] \\ &= U[(1-\tau)\Lambda x + \tau \Lambda y)] \\ &= U(\Lambda x, \Lambda y) \end{aligned} \tag{O.28}$$

In line two we use the definition of $U(x,y)$ given as $U(x,y) = U[(1-\tau)x + \tau y]$, and in line three we use the Lorentz transformation of an arbitrary Wilson path given in

Equation K.13. Thus we find that $U(x,y)$ is a scalar function of each argument.

Now we examine the general form for gauge covariant extended quarks. The general form is given in Equation 6.3 and written here.

$$Q^a_\alpha(x) = \int Dz(\tau)_{z(0)=x}\; F[z(\tau)]\, U^{ab}[z(\tau)]\, q^b_\alpha(z(1))$$

The discussion for the general case is almost an identical copy of the example above. The one exception is that instead of a Lorentz invariant function f we have a Lorentz invariant functional integral $D\Lambda z(\tau) = Dz(\tau)$ and a Lorentz invariant functional $F[\Lambda z(\tau)] = F[z(\tau)]$. Using these two statements, we demonstrate the Lorentz covariance of the general gauge covariant extended quark field in the following lines.

$$\begin{aligned}
&M^{\alpha\beta}(\Lambda)\, U(\Lambda)\, Q^a_\beta(x)\, U^\dagger(\Lambda) = \qquad\qquad (O.29)\\
&= \int Dz(\tau)_{z(0)=x}\; F[z(\tau)]\, U(\Lambda)\, U^{ab}[z(\tau)]\, U^\dagger(\Lambda)\, M^{\alpha\beta}(\Lambda)\, U(\Lambda)\, q^b_\beta(z(1))\, U^\dagger(\Lambda)\\
&= \int Dz(\tau)_{z(0)=x}\; F[z(\tau)]\, U^{ab}[\Lambda z(\tau)]\, q^b_\alpha(\Lambda z(1))\\
&= \int Dz(\tau)_{z(0)=\Lambda x}\; F[\Lambda^{-1} z(\tau)]\, U^{ab}[z(\tau)]\, q^b_\alpha(z(1))\\
&= \int Dz(\tau)_{z(0)=\Lambda x}\; F[z(\tau)]\, U^{ab}[z(\tau)]\, q^b_\alpha(z(1))\\
&= Q^a_\alpha(\Lambda x)
\end{aligned}$$

In the third line we use the Lorentz transformation of a Wilson path given in Equation K.13. Additionally, the change of variables in the fourth line is now $z(\tau) \rightarrow \lambda^{-1} z(\tau)$, and we use the Lorentz invariance of the measure $Dz(\tau)$ and the functional $F[z(\tau)]$ in the fifth line.

O.11 Gauge Covariance of Extended Quark Fields

In this appendix we verify the gauge covariance of the appropriate extended quark fields defined in Chapter 6. The gauge transformation of a point quark is given in Equation 4.2, and in the following equations, we show that the extended quarks, with the exception of the gauge fixed quark fields, also transform just as a point

quark under gauge transformations. First we consider the simple example for gauge covariant smearing given in Equation 6.2 as

$$Q^a_\alpha(x) = \int d^4y\ U^{ab}(x,y)\, q^b_\alpha(y)\, f((x-y)^2).$$

In the following lines we demonstrate that this extended quark field has the correct gauge transformation.

$$\begin{aligned} {}^gQ^a_\alpha(x) = & \qquad (O.30)\\ &= \int d^4y\ {}^gU^{ab}(x,y)\, {}^gq^b_\alpha(y)\, f((x-y)^2) \\ &= \int d^4y\ g^{ac}(x) U^{cd}(x,y)\, (g^\dagger)^{db}(y)\, g^{be}(y)\, q^e_\alpha(y)\, f((x-y)^2) \\ &= g^{ac}(x) \int d^4y\ U^{cd}(x,y)\, q^d_\alpha(y)\, f((x-y)^2) \\ &= g^{ab}(x)\, Q^b_\alpha(x) \end{aligned}$$

In the third line we use the gauge transformations of quark and link fields given in Equation 4.2, and in the fourth line we use the unitarity of the gauge transformation $g^\dagger(y)g(y) = 1$.

Now we repeat the argument above for the case of the general extended quark field given in Equation 6.3 as

$$Q^a_\alpha(x) = \int Dz(\tau)_{z(0)=x}\ F[z(\tau)]\, U^{ab}[z(\tau)]\, q^b_\alpha(z(1)).$$

The gauge covariance of the general extended quark fields is demonstrated in the following lines. The required sequence of steps is essentially identical to those in the above example.

$$\begin{aligned} {}^gQ^a_\alpha(x) = & \qquad (O.31)\\ &= \int Dz(\tau)_{z(0)=x}\ F[z(\tau)]\, {}^gU^{ab}[z(\tau)]\, {}^gq^b_\alpha(z(1)) \\ &= \int Dz(\tau)_{z(0)=x}\ F[z(\tau)]\, g^{ac}(x) U^{cd}[z(\tau)]\, (g^\dagger)^{db}(z(1))\, g^{be}(z(1))\, q^e_\alpha(z(1)) \\ &= g^{ac}(x) \int Dz(\tau)_{z(0)=x}\ F[z(\tau)]\, U^{cd}[z(\tau)]\, q^d_\alpha(z(1)) \end{aligned}$$

$$= \; g^{ab}(x)\, Q^{b}_{\alpha}(x)$$

The final conclusion is that extended quark fields of Equation 6.3 have the same gauge transformation properties as point quarks.

O.12 Adjoint of Extended Quark Fields

The general form for an extended quark field is given in Equation 6.7 as

$$Q^{a}_{\beta}(x) = S^{aa'}_{\beta\beta'}(x, x')\, q^{a'}_{\beta'}(x')$$

where we make a small change in the dummy indices. The adjoint field is determined in the following

$$\begin{aligned} \overline{Q}^{a}_{\alpha}(x) &= \\ &= Q^{a\dagger}_{\beta}(x)\, \gamma^{0}_{\beta\alpha} \\ &= q^{a'\dagger}_{\beta'}(x')\, S^{aa'*}_{\beta\beta'}(x, x')\, \gamma^{0}_{\beta\alpha} \\ &= q^{a'\dagger}_{\gamma}(x')\, \gamma^{0}_{\gamma\alpha'}\, \gamma^{0}_{\alpha'\beta'}\, S^{aa'*}_{\beta\beta'}(x, x')\, \gamma^{0}_{\beta\alpha} \\ &= \overline{q}^{a'}_{\alpha'}(x')\, \gamma^{0}_{\alpha'\beta'}\, S^{aa'*}_{\beta\beta'}(x, x')\, \gamma^{0}_{\beta\alpha} \\ &= \overline{q}^{a'}_{\alpha'}(x')\, \overline{S}^{a'a}_{\alpha'\alpha}(x', x), \end{aligned} \tag{O.32}$$

where in the fourth line we use $\gamma^0\gamma^0 = 1$ and in the last line we define $\overline{S}$ as

$$\overline{S}^{a'a}_{\alpha'\alpha}(x', x) = \gamma^{0}_{\alpha'\beta'}\, S^{aa'*}_{\beta\beta'}(x, x')\, \gamma^{0}_{\beta\alpha}.$$

O.13 γ^5 Hermiticity for Forward Propagators

In this section we demonstrate that the basic relationship $\gamma^{\rm E}_5 M^{\dagger} \gamma^{\rm E}_5 = M$, which holds for the Wilson-Dirac matrix M, applies to the smeared-to-smeared forward propagator F_{QQ} as well. First we present the argument for M. The Wilson-Dirac

matrix M is given in Equation 4.9 as

$$M(x,x') = \delta(x-x') - \frac{1}{\kappa}\sum_{\mu=\pm 1}^{\pm D}(r+\gamma_\mu^{\mathrm{E}})U_\mu^\dagger(x-\mu)\delta(x'-(x-\mu))$$

where we use a matrix notation for the color and Dirac indices but leave the lattice indices, x and x', explicit. We demonstrate the γ^5 Hermiticity of M in the following sequence of steps.

$$\begin{aligned}
&\left(\gamma_5^{\mathrm{E}} M^\dagger \gamma_5^{\mathrm{E}}\right)(x,x') = \qquad\qquad (O.33)\\
&= \gamma_5^{\mathrm{E}} M^\dagger(x',x)\gamma_5^{\mathrm{E}}\\
&= \gamma_5^{\mathrm{E}}\left(\delta(x'-x) - \frac{1}{\kappa}\sum_{\mu=\pm 1}^{\pm D}(r+\gamma_\mu^{\mathrm{E}})U_\mu(x'-\mu)\delta(x-(x'-\mu))\right)\gamma_5^{\mathrm{E}}\\
&= \delta(x'-x) - \frac{1}{\kappa}\sum_{\mu=\pm 1}^{\pm D}(r-\gamma_\mu^{\mathrm{E}})U_{-\mu}^\dagger(x')\delta(x-(x'-\mu))\\
&= \delta(x-x') - \frac{1}{\kappa}\sum_{\mu=\pm 1}^{\pm D}(r+\gamma_{-\mu}^{\mathrm{E}})U_{-\mu}^\dagger(x+\mu)\delta(x'-(x+\mu))\\
&= \delta(x-x') - \frac{1}{\kappa}\sum_{\mu=\pm 1}^{\pm D}(r+\gamma_\mu^{\mathrm{E}})U_\mu^\dagger(x-\mu)\delta(x'-(x-\mu))\\
&= M(x,x')
\end{aligned}$$

In the previous lines, the meaning of † depends on the context. In particular, in the first line the † applies to all the indices of M: the color, Dirac, and lattice indices. In the remaining lines, † applies to only the color and Dirac indices. Additionally, to go from the fifth to sixth lines we make a change in the summation index, $\mu \to -\mu$.

Next we examine the Hermiticity properties of the forward propagators, both point-to-point and smeared-to-smeared. The point-to-point forward propagator is given in Equation 7.8 as $F_{qq} = M^{-1}$. This satisfies

$$\begin{aligned}
&\gamma_5^{\mathrm{E}} F_{qq}^\dagger \gamma_5^{\mathrm{E}} =\\
&= \gamma_5^{\mathrm{E}}\left(M^{-1}\right)^\dagger \gamma_5^{\mathrm{E}}\\
&= \left(\gamma_5^{\mathrm{E}} M^\dagger \gamma_5^{\mathrm{E}}\right)^{-1}
\end{aligned}$$

$$= M^{-1}$$
$$= F_{qq}.$$

Hence the γ^5 Hermiticity holds for F_{qq} as well. Next, the smeared-to-smeared forward propagator is given in Equation 7.10 as

$$F_{Q'Q} = S' F_{qq} \overline{S}$$

where $\overline{S} = S^\dagger$. The generalization of the γ^5 Hermiticity for $F_{Q'Q}$ is determined in the following.

$$\begin{aligned} \gamma_5^{\mathrm{E}} F^\dagger_{Q'Q} \gamma_5^{\mathrm{E}} = & \qquad (O.34) \\ &= \gamma_5^{\mathrm{E}} \left(S' F_{qq} S^\dagger \right)^\dagger \gamma_5^{\mathrm{E}} \\ &= \gamma_5^{\mathrm{E}} S F^\dagger_{qq} S'^\dagger \gamma_5^{\mathrm{E}} \\ &= S \gamma_5^{\mathrm{E}} F^\dagger_{qq} \gamma_5^{\mathrm{E}} S'^\dagger \\ &= S F_{qq} \overline{S'} \\ &= F_{QQ'} \end{aligned}$$

Thus we find the generalized Hermiticity relation $\gamma_5^{\mathrm{E}} F^\dagger_{Q'Q} \gamma_5^{\mathrm{E}} = F_{QQ'}$. In particular, we note that for the case of identical smearing in the source and sink, we have $\gamma_5^{\mathrm{E}} F^\dagger_{QQ} \gamma_5^{\mathrm{E}} = F_{QQ}$ which is precisely the same Hermiticity condition as for the point-to-point propagator F_{qq} and the Wilson-Dirac matrix M.

O.14 Momentum Projection for Two Point Functions

In the following sequence of steps we extract the momentum conserving δ function from the momentum projected nucleon two point function defined in Equation 7.14.

$$\langle P'_{\alpha'}(t', \vec{p}') \overline{P}_\alpha(t, \vec{p}) \rangle = \qquad (O.35)$$

$$
\begin{aligned}
&= \int d^3\vec{x}' \int d^3\vec{x}\; e^{-i\vec{p}'\cdot\vec{x}}\, e^{i\vec{p}\cdot\vec{x}}\, \langle\, P'_{\alpha'}(t',\vec{x}')\, \overline{P}_{\alpha}(t,\vec{x})\,\rangle \\
&= \int d^3\vec{x}' \int d^3\vec{x}\; e^{-i\vec{p}'\cdot\vec{x}'}\, e^{i\vec{p}\cdot\vec{x}}\, \langle\, P'_{\alpha'}(t',\vec{x}'-\vec{x})\, \overline{P}_{\alpha}(t,\vec{0})\,\rangle \\
&= \int d^3\vec{R} \int d^3\vec{r}\; e^{-i\vec{p}'\cdot\left(\vec{R}+\frac{1}{2}\vec{r}\right)}\, e^{i\vec{p}\cdot\left(\vec{R}-\frac{1}{2}\vec{r}\right)}\, \langle\, P'_{\alpha'}(t',\vec{r})\, \overline{P}_{\alpha}(t,\vec{0})\,\rangle \\
&= \int d^3\vec{R}\; e^{-i\vec{R}\cdot(\vec{p}'-\vec{p})} \int d^3\vec{r}\; e^{-i\left(\frac{\vec{p}'+\vec{p}}{2}\right)\cdot\vec{r}}\, \langle\, P'_{\alpha'}(t',\vec{r})\, \overline{P}_{\alpha}(t,\vec{0})\,\rangle \\
&= (2\pi)^3\, \delta^3\,(\vec{p}'-\vec{p}) \int d^3\vec{x}'\; e^{-i\vec{p}'\cdot\vec{x}'}\, \langle\, P'_{\alpha'}(t',\vec{x}')\, \overline{P}_{\alpha}(t,\vec{0})\,\rangle \\
&= (2\pi)^3\, \delta^3\,(\vec{p}'-\vec{p})\; \langle\, P'_{\alpha'}(t',\vec{p}')\, \overline{P}_{\alpha}(t,\vec{x}=\vec{0})\,\rangle
\end{aligned}
$$

We use translational invariance in the third line, introduce relative and center of mass coordinates, $\vec{r} = \vec{x}' - \vec{x}$ and $R = (\vec{x}' + \vec{x})/2$, in the fourth line, and reintroduce $\vec{x}'$ in the sixth line. To be explicitly clear, in the last line P' is a momentum projected proton field whereas $\overline{P}$ is a proton field in position space.

O.15 Spectral Representation for Two Point Functions

The momentum projected proton two point correlation functions $C^{(2)}_{\alpha'\alpha}$ and $C^{(2)}_{\Gamma}$ are given in Equations 7.16 and 7.17 respectively. In the following sequence of steps we derive the spectral representation for the $C^{(2)}_{\alpha'\alpha}$ correlation function.

$$
\begin{aligned}
&C^{(2)}_{\alpha'\alpha}(t',\vec{p}';t,\vec{x}) = \qquad\qquad (O.36)\\
&= \int d^3\vec{x}'\, e^{-i\vec{p}'\cdot\vec{x}'}\, \langle\, P_{\alpha'}(t',\vec{x}')\, \overline{P}_{\alpha}(t,\vec{x})\,\rangle \\
&= \int d^3\vec{x}'\, e^{-i\vec{p}'\cdot\vec{x}'}\, \langle\Omega|\, \mathcal{T}\left\{P_{\alpha'}(t',\vec{x}')\, \overline{P}_{\alpha}(t,\vec{x})\right\}\, |\Omega\rangle \\
&= \int d^3\vec{x}'\, e^{-i\vec{p}'\cdot\vec{x}'}\, \langle\Omega|\, e^{Ht'}\, e^{-i\vec{P}\cdot\vec{x}'}\, P_{\alpha'}(0)\, e^{-Ht'}\, e^{i\vec{P}\cdot\vec{x}'}\, e^{Ht}\, e^{-i\vec{P}\cdot\vec{x}}\, \overline{P}_{\alpha}(0)\, e^{-Ht}\, e^{i\vec{P}\cdot\vec{x}}\, |\Omega\rangle \\
&= \int d^3\vec{x}'\, e^{-i\vec{p}'\cdot\vec{x}'}\, \langle\Omega|\, P_{\alpha'}(0)\, e^{-H(t'-t)}\, e^{i\vec{P}\cdot(\vec{x}'-\vec{x})}\, \overline{P}_{\alpha}(0)\, |\Omega\rangle \\
&= \int d^3\vec{x}'\, e^{-i\vec{p}'\cdot\vec{x}'}\, \langle\Omega|\, P_{\alpha'}(0)\, e^{-H(t'-t)}\, e^{i\vec{P}\cdot(\vec{x}'-\vec{x})} \sum_{H,s} \int \frac{d^3\vec{k}}{(2\pi)^3} \frac{|H,s,\vec{k}\rangle\langle H,s,\vec{k}|}{2E^H_{\vec{k}}}\, \overline{P}_{\alpha}(0)\, |\Omega\rangle \\
&= \sum_{N,s} \int \frac{d^3\vec{k}}{(2\pi)^3} \frac{1}{2E^N_{\vec{k}}} \int d^3\vec{x}'\, e^{-i\vec{p}'\cdot\vec{x}'}\, e^{-E^N_{\vec{k}}(t'-t)}\, e^{i\vec{k}\cdot(\vec{x}'-\vec{x})}
\end{aligned}
$$

$$
\begin{aligned}
& \langle\Omega|\, P_{\alpha'}(0)\,|N,s,\vec{k}\rangle\langle N,s,\vec{k}|\overline{P}_\alpha(0)\,|\Omega\rangle \\
= & \sum_{N,s}\int\frac{d^3\vec{k}}{(2\pi)^3}\frac{1}{2E^N_{\vec{k}}}\, e^{-E^N_{\vec{k}}(t'-t)}\, e^{-i\vec{k}\cdot\vec{x}}\,(2\pi)^3\delta^3\left(\vec{p}\,'-\vec{k}\right) \\
& \langle\Omega|\, P_{\alpha'}(0)\,|N,s,\vec{k}\rangle\langle N,s,\vec{k}|\overline{P}_\alpha(0)\,|\Omega\rangle \\
= & \sum_{N,s}\frac{1}{2E^N_{\vec{p}\,'}}\, e^{-E^N_{\vec{p}\,'}(t'-t)}\, e^{-i\vec{p}\,'\cdot\vec{x}}\,\langle\Omega|\, P_{\alpha'}(0)\,|N,s,\vec{p}\,'\rangle\langle N,s,\vec{p}\,'|\overline{P}_\alpha(0)\,|\Omega\rangle \\
= & \sum_{N,s}\frac{1}{2E^N_{\vec{p}\,'}}\, e^{-E^N_{\vec{p}\,'}(t'-t)}\, e^{-i\vec{p}\,'\cdot\vec{x}}\, Z_N\, U_{\alpha'}(p'_N,s)\, Z^*_N\,\overline{U}_{\alpha'}(p'_N,s) \\
= & \sum_{N}\frac{|Z_N|^2}{2E^N_{\vec{p}\,'}}\, e^{-E^N_{\vec{p}\,'}(t'-t)}\, e^{-i\vec{p}\,'\cdot\vec{x}}\,\left(p'_N\cdot\gamma+m_N\right)_{\alpha'\alpha}
\end{aligned}
$$

In the third line we use the results from the transfer matrix formalism in Section 4.4. In particular we use Equation 4.17 in which we assume the $T\to\infty$ limit. In the fourth line we assume $t'>t$ and use the translation covariance of the proton fields. Then in the sixth line we insert a complete set of states. Actually, we insert only a complete set of single particle states labelled by the hadron H and spin s. Given that we are interested in the ground state within the proton channel, we ignore the missing multiparticle states from the completeness relation. In the seventh line we consider all hadrons with the quantum numbers of the proton which we label with an N. Then in the tenth line we use the continuum relation

$$
\langle\Omega|\, P_{\alpha'}(0)\,|N,s,\vec{p}\,'\rangle = Z_N\, U_{\alpha'}(p'_N,s)
$$

where p'_N is the on-shell four momentum for the N^{th} state. Finally, in the last line we use the spinor completeness relation

$$
\sum_s U_{\alpha'}(p,s)\overline{U}_\alpha(p,s) = (p\cdot\gamma+m)_{\alpha'\alpha}\,.
$$

The spectral representation for $C^{(2)}_\Gamma$ is now straight forward.

$$
\begin{aligned}
& C^{(2)}_\Gamma(t',\vec{p}\,';t,\vec{x}) = \\
= & \ \Gamma^{\alpha\alpha'}C^{(2)}_{\alpha'\alpha}(t',\vec{p}\,';t,\vec{x})
\end{aligned}
\qquad (O.37)
$$

$$
\begin{aligned}
&= \Gamma^{\alpha\alpha'} \sum_N \frac{|Z_N|^2}{2E^N_{\vec{p}'}} e^{-E^N_{\vec{p}'}(t'-t)} e^{-i\vec{p}'\cdot\vec{x}} \left(p'_N \cdot \gamma + m_N\right)_{\alpha'\alpha} \\
&= \sum_N \frac{|Z_N|^2}{2E^N_{\vec{p}'}} e^{-E^N_{\vec{p}'}(t'-t)} e^{-i\vec{p}'\cdot\vec{x}} \operatorname{tr}\left(\Gamma \left(p'_N \cdot \gamma + m_N\right)\right)
\end{aligned}
$$

The trace in the final line above ensures that such correlation functions are independent of the choice of basis for the Dirac matrices.

O.16 Spectral Representation for Three Point Functions

The three point correlation function $C^{(3)}_{\alpha'\alpha}$ is given in Equation 8.24. The spectral representation of $C^{(3)}_{\alpha'\alpha}$ is determined in the following lines.

$$
\begin{aligned}
&C^{(3)}_{\alpha'\alpha}\left((t',\vec{p}');(\tau,\vec{q});x\right) = \qquad\qquad (O.38)\\
&= \int d^3\vec{x}'\; e^{-i\vec{p}'\cdot\vec{x}'} \int d^3\vec{y}\; e^{i\vec{q}\cdot\vec{y}} \left\langle\, P'_{\alpha'}(t',\vec{x}')\right. \\
&\quad \left. \overline{q}^{e'}_{\epsilon'}(y'(\tau,\vec{y}))\, O^{e'e}_{\epsilon'\epsilon}(y'(\tau,\vec{y}),(\tau,\vec{y}))\, q^e_\epsilon(\tau,\vec{y})\, \overline{P}_\alpha(x)\,\right\rangle_{\mathrm{qc}} \\
&= \int d^3\vec{x}'\; e^{-i\vec{p}'\cdot\vec{x}'} \int d^3\vec{y}\; e^{i\vec{q}\cdot\vec{y}} \left\langle\Omega\right| \mathcal{T}\left\{P'_{\alpha'}(t',\vec{x}')\right. \\
&\quad \left. \overline{q}^{e'}_{\epsilon'}(y'(\tau,\vec{y}))\, O^{e'e}_{\epsilon'\epsilon}(y'(\tau,\vec{y}),(\tau,\vec{y}))\, q^e_\epsilon(\tau,\vec{y})\, \overline{P}_\alpha(x)\right\} \left|\Omega\right\rangle \\
&= \int d^3\vec{x}'\; e^{-i\vec{p}'\cdot\vec{x}'} \int d^3\vec{y}\; e^{i\vec{q}\cdot\vec{y}} \left\langle\Omega\right| e^{Ht'}\, e^{-i\vec{P}\cdot\vec{x}'}\, P'_{\alpha'}(0)\, e^{-Ht'}\, e^{i\vec{P}\cdot\vec{x}'}\, e^{H\tau}\, e^{-i\vec{P}\cdot\vec{y}} \\
&\quad \overline{q}^{e'}_{\epsilon'}(0)\, O^{e'e}_{\epsilon'\epsilon}(0,0)\, q^e_\epsilon(0)\, e^{-H\tau}\, e^{i\vec{P}\cdot\vec{y}}\, e^{Ht}\, e^{-i\vec{P}\cdot\vec{x}}\, \overline{P}_\alpha(0)\, e^{-Ht}\, e^{i\vec{P}\cdot\vec{x}} \left|\Omega\right\rangle \\
&= \int d^3\vec{x}'\; e^{-i\vec{p}'\cdot\vec{x}'} \int d^3\vec{y}\; e^{i\vec{q}\cdot\vec{y}} \left\langle\Omega\right| P'_{\alpha'}(0)\, e^{-H(t'-\tau)}\, e^{i\vec{P}\cdot(\vec{x}'-\vec{y})} \\
&\quad \overline{q}^{e'}_{\epsilon'}(0)\, O^{e'e}_{\epsilon'\epsilon}(0,0)\, q^e_\epsilon(0)\, e^{-H(\tau-t)}\, e^{i\vec{P}\cdot(\vec{y}-\vec{x})}\, \overline{P}_\alpha(0) \left|\Omega\right\rangle \\
&= \int d^3\vec{x}'\; e^{-i\vec{p}'\cdot\vec{x}'} \int d^3\vec{y}\; e^{i\vec{q}\cdot\vec{y}} \left\langle\Omega\right| P'_{\alpha'}(0)\, e^{-H(t'-\tau)}\, e^{i\vec{P}\cdot(\vec{x}'-\vec{y})} \\
&\quad \sum_{H',s'} \int \frac{d^3\vec{k}'}{(2\pi)^3} \frac{|H',s',\vec{k}'\rangle\langle H',s',\vec{k}'|}{2E^{H'}_{\vec{k}'}}\, \overline{q}^{e'}_{\epsilon'}(0)\, O^{e'e}_{\epsilon'\epsilon}(0,0)\, q^e_\epsilon(0) \\
&\quad \sum_{H,s} \int \frac{d^3\vec{k}}{(2\pi)^3} \frac{|H,s,\vec{k}\rangle\langle H,s,\vec{k}|}{2E^H_{\vec{k}}}\, e^{-H(\tau-t)}\, e^{i\vec{P}\cdot(\vec{y}-\vec{x})}\, \overline{P}_\alpha(0) \left|\Omega\right\rangle \\
&= \sum_{N',s'} \int \frac{d^3\vec{k}'}{(2\pi)^3} \frac{e^{-E^{N'}_{\vec{k}'}(t'-\tau)}}{2E^{N'}_{\vec{k}'}} \sum_{N,s} \int \frac{d^3\vec{k}}{(2\pi)^3} \frac{e^{-E^N_{\vec{k}}(\tau-t)}}{2E^N_{\vec{k}}}
\end{aligned}
$$

$$
\begin{aligned}
& \int d^3\vec{x}' \; e^{-i\vec{p}'\cdot\vec{x}'} \int d^3\vec{y} \; e^{i\vec{q}\cdot\vec{y}} \, e^{i\vec{k}'\cdot(\vec{x}'-\vec{y})} \, e^{i\vec{k}\cdot(\vec{y}-\vec{x})} \\
& \langle\Omega| \, P'_{\alpha'}(0) \, |N', s', \vec{k}'\rangle \, \langle N', s', \vec{k}'| \, \overline{q}^{e'}_{\epsilon'}(0) \, O^{e'e}_{\epsilon'\epsilon}(0,0) \, q^{e}_{\epsilon}(0) \, |N, s, \vec{k}\rangle \\
& \langle N, s, \vec{k}| \, \overline{P}_{\alpha}(0) \, |\Omega\rangle \\
= & \sum_{N',s'} \int \frac{d^3\vec{k}'}{(2\pi)^3} \frac{e^{-E^{N'}_{\vec{k}'}(t'-\tau)}}{2E^{N'}_{\vec{k}'}} \sum_{N,s} \int \frac{d^3\vec{k}}{(2\pi)^3} \frac{e^{-E^{N}_{\vec{k}}(\tau-t)}}{2E^{N}_{\vec{k}}} \\
& (2\pi)^3\delta^3\left(\vec{p}' - \vec{k}'\right) (2\pi)^3\delta^3\left(\vec{q} - \vec{k}' + \vec{k}\right) \, e^{-i\vec{k}\cdot\vec{x}} \\
& \langle\Omega| \, P'_{\alpha'}(0) \, |N', s', \vec{k}'\rangle \, \langle N', s', \vec{k}'| \, \overline{q}^{e'}_{\epsilon'}(0) \, O^{e'e}_{\epsilon'\epsilon}(0,0) \, q^{e}_{\epsilon}(0) \, |N, s, \vec{k}\rangle \\
& \langle N, s, \vec{k}| \, \overline{P}_{\alpha}(0) \, |\Omega\rangle \\
= & \sum_{N',s'} \frac{e^{-E^{N'}_{\vec{p}'}(t'-\tau)}}{2E^{N'}_{\vec{p}'}} \sum_{N,s} \frac{e^{-E^{N}_{\vec{p}}(\tau-t)}}{2E^{N}_{\vec{p}}} \, e^{-i\vec{p}\cdot\vec{x}} \, \langle\Omega| \, P'_{\alpha'}(0) \, |N', s', \vec{p}'\rangle \\
& \langle N', s', \vec{p}'| \, \overline{q}^{e'}_{\epsilon'}(0) \, O^{e'e}_{\epsilon'\epsilon}(0,0) \, q^{e}_{\epsilon}(0) \, |N, s, \vec{p}\rangle \, \langle N, s, \vec{p}| \, \overline{P}_{\alpha}(0) \, |\Omega\rangle \\
= & \sum_{N',s'} \frac{e^{-E^{N'}_{\vec{p}'}(t'-\tau)}}{2E^{N'}_{\vec{p}'}} \sum_{N,s} \frac{e^{-E^{N}_{\vec{p}}(\tau-t)}}{2E^{N}_{\vec{p}}} \, e^{-i\vec{p}\cdot\vec{x}} \, Z'_{N'} \, U_{\alpha'}(p'_{N'}, s) \\
& \overline{U}(p'_{N'}, s') \, \mathcal{O}_{N'N} \, U(p_N, s) \, Z^*_N \, \overline{U}_{\alpha}(p_N, s) \\
= & \sum_{N',s'} \frac{Z'_{N'} \, e^{-E^{N'}_{\vec{p}'}(t'-\tau)}}{2E^{N'}_{\vec{p}'}} \sum_{N,s} \frac{Z^*_N \, e^{-E^{N}_{\vec{p}}(\tau-t)}}{2E^{N}_{\vec{p}}} \, e^{-i\vec{p}\cdot\vec{x}} \\
& \left(\left(p'_{N'} \cdot \gamma + m_{N'} \right) \mathcal{O}_{N'N} \left(p_N \cdot \gamma + m_N \right) \right)_{\alpha'\alpha}
\end{aligned}
$$

In line three we use the transfer matrix results from Section 4.4. We assume $t' > \tau > t$ in line four. Additionally, we assume $\tau' = \tau$ for the remainder of this argument. This is true in the continuum limit, and hence assuming $\tau' = \tau$ only changes the $O(a)$ corrections to the above result. In line six we insert a complete set of states. (See the comments regarding the corresponding step in Section O.15 for the spectral representation of the two point functions.) In line seven we restrict the sum over hadrons H and H' to the contributions from the nucleon states N and N' only. Then in line nine we define $\vec{p} = \vec{p}' - \vec{q}$. In line ten we use the continuum relations

$$\langle\Omega| \, P'_{\alpha'}(0) \, |N, s, \vec{p}'\rangle = Z'_N \, U_{\alpha'}(p'_{N'}, s)$$

and

$$\langle N, s, \vec{p}| \, \overline{P}_{\alpha}(0) \, |\Omega = Z^*_N \, \overline{U}_{\alpha}(p_N, s)$$

where $p'^2_{N'} = m^2_{N'}$ and $p^2_N = m^2_N$. Additionally we introduce a continuum form factor decomposition for the operator $\overline{q}^{\epsilon'}_{\epsilon'}(0)\, O^{\epsilon' \epsilon}_{\epsilon' \epsilon}(0,0)\, q^{\epsilon}_{\epsilon}(0)$ as given by

$$\langle N', s', \vec{p}' |\, O\, | N, s, \vec{p} \rangle = \overline{U}(p'_{N'}, s')\, \mathcal{O}_{N'N}\, U(p_N, s).$$

Then in the last line we use the spin sum

$$\sum_s U_{\alpha'}(p,s) \overline{U}_{\alpha}(p,s) = (p \cdot \gamma + m)_{\alpha' \alpha}\,.$$

Using the spectral representation above for $C^{(3)}_{\alpha' \alpha}$ we now determine the corresponding spectral representation for $C^{(3)}_{\Gamma}$.

$$\begin{aligned} & C^{(3)}_{\Gamma}\left((t', \vec{p}'); (\tau, \vec{q}); x\right) = \qquad\qquad (O.39) \\ & = \Gamma^{\alpha \alpha'} C^{(3)}_{\alpha' \alpha}\left((t', \vec{p}'); (\tau, \vec{q}); x\right) \\ & = \Gamma^{\alpha \alpha'} \sum_{N', s'} \frac{Z'_{N'}\, e^{-E^{N'}_{\vec{p}'}(t' - \tau)}}{2 E^{N'}_{\vec{p}'}} \sum_{N, s} \frac{Z^*_N\, e^{-E^N_{\vec{p}}(\tau - t)}}{2 E^N_{\vec{p}}} \\ & \quad \left((\, p'_{N'} \cdot \gamma + m_{N'})\, \mathcal{O}_{N'N}\, (\, p_N \cdot \gamma + m_N) \right)_{\alpha' \alpha} \\ & = \sum_{N', s'} \frac{Z'_{N'}\, e^{-E^{N'}_{\vec{p}'}(t' - \tau)}}{2 E^{N'}_{\vec{p}'}} \sum_{N, s} \frac{Z^*_N\, e^{-E^N_{\vec{p}}(\tau - t)}}{2 E^N_{\vec{p}}} \\ & \quad \mathrm{tr}\left(\Gamma\, (\, p'_{N'} \cdot \gamma + m_{N'})\, \mathcal{O}_{N'N}\, (\, p_N \cdot \gamma + m_N) \right) \end{aligned}$$

O.17 Two Dimensional Fourier Transform of a Dipole Form Factor

In this section we calculate the Fourier transform of a dipole form factor in two dimensions. The Fourier transform is

$$\int d^2 q\, \frac{e^{i \vec{q} \cdot \vec{r}}}{(q^2 + m^2)^2}.$$

First scale out the mass using $\vec{q} = m\vec{k}$.

$$\frac{1}{m^2}\int d^2k\ \frac{e^{i\vec{k}\cdot m\vec{r}}}{(k^2+1)^2}$$

Now choose $\vec{r} = r\hat{x}$, scale the radius using $\overline{r} = mr$, and introduce Cartesian coordinates.

$$\frac{1}{m^2}\int_{-\infty}^{\infty} dk_x e^{ik_x\overline{r}} \int_{-\infty}^{\infty} dk_y \frac{1}{(k_x^2+k_y^2+1)^2}$$

Now let $k_y = \sqrt{1+k_x^2}\, l_y$.

$$\frac{1}{m^2}\int_{-\infty}^{\infty} dk_x \frac{e^{ik_x\overline{r}}}{(k_x^2+1)^{3/2}} \int_{-\infty}^{\infty} dl_y \frac{1}{(l_y^2+1)^2}$$

Use

$$\int_{-\infty}^{\infty} dl_y \frac{1}{(l_y^2+1)^2} = \frac{\pi}{2}$$

and let $l_x = k_x\overline{r}$.

$$\frac{\pi}{2}\frac{\overline{r}^2}{m^2}\int_{-\infty}^{\infty} dl_x \frac{e^{il_x}}{(l_x^2+\overline{r}^2)^{3/2}}$$

By averaging over l_x we get

$$\frac{\pi\overline{r}^2}{m^2}\int_0^{\infty} dl_x \frac{\cos(l_x)}{(l_x^2+\overline{r}^2)^{3/2}}.$$

This is nearly of the form of a modified Bessel function $K_\nu(z)$ given by

$$K_\nu(z) = \frac{\Gamma(\nu+1/2)(2z)^\nu}{\sqrt{\pi}}\int_0^{\infty} dt \frac{\cos(t)}{(t^2+z^2)^{\nu+1/2}}.$$

For $\nu = 1$ and using $\Gamma(3/2) = \sqrt{\pi}/2$, we have

$$K_1(z) = z\int_0^{\infty} dt \frac{\cos(t)}{(t^2+z^2)^{3/2}}.$$

Therefore, comparing with the integral over l_x above, we finally have

$$\int d^2q\ \frac{e^{i\vec{q}\cdot\vec{r}}}{(q^2+m^2)^2} = \frac{\pi}{m^2}(mr)K_1(mr).$$

Multiplying the above by m^4 gives the common form for the dipole.

$$\int d^2q \, \frac{e^{i\vec{q}\cdot\vec{r}}}{(1+\frac{q^2}{m^2})^2} = \pi m^2 (mr) K_1(mr). \tag{O.40}$$

The behavior of $K_\nu(z)$ for small z is

$$K_\nu(z) \to \frac{\Gamma(\nu)}{2}\left(\frac{z}{2}\right)^{-\nu}$$

and for large z is

$$K_\nu(z) \to \sqrt{\frac{\pi}{2z}} e^{-z}.$$

We note that there are general formulas for the derivatives. The one derivative of interest to us is

$$\frac{dK_1(z)}{dz} = -\frac{1}{2}\left(K_0(z) + K_2(z)\right).$$

O.18 Three Dimensional Fourier Transform of a Dipole Form Factor

In this section we calculate the Fourier transform of a dipole form factor in three dimensions. The Fourier transform is

$$\int d^3q \, \frac{e^{i\vec{q}\cdot\vec{r}}}{(q^2+m^2)^2}.$$

First notice that

$$\int d^3q \, \frac{e^{i\vec{q}\cdot\vec{r}}}{(q^2+m^2)^2} = -\frac{1}{2m}\frac{d}{dm}\int d^3q \, \frac{e^{i\vec{q}\cdot\vec{r}}}{(q^2+m^2)}.$$

Now calculate this second integral in spherical coordinates.

$$\int d^3q \, \frac{e^{i\vec{q}\cdot\vec{r}}}{(q^2+m^2)} = \int_0^{2\pi} d\phi \int_{-1}^{1} d(\cos\theta) \int_0^{\infty} dq \; q^2 \frac{e^{iqr\cos\theta}}{q^2+m^2}$$

The $d\phi$ and $d(\cos\theta)$ integrals are straightforward and give

$$\frac{2\pi}{ir}\int_0^\infty dq\ q\frac{e^{iqr}-e^{-iqr}}{q^2+m^2}.$$

Now symmetrize the integral in q and factorize the denominator to give

$$\frac{2\pi}{ir}\int_{-\infty}^\infty dq\ q\frac{e^{iqr}}{(q+im)(q-im)}.$$

Now complete the integral in the upper half plane picking up the pole at $q = im$. The result is

$$\frac{2\pi^2}{r}e^{-mr}.$$

Finally, taking the appropriate derivative indicated above gives the result

$$\int d^3q\ \frac{e^{i\vec{q}\cdot\vec{r}}}{(q^2+m^2)^2} = \frac{\pi^2}{m}e^{-mr}.$$

Bibliography

[1] Gunnar S. Bali et al. Quark mass effects on the topological susceptibility in qcd. *Phys. Rev.*, D64:054502, 2001.

[2] Claude W. Bernard, T. Draper, G. Hockney, and A. Soni. Calculation of weak matrix elements: Some technical aspects. In *Wuppertal 1985, Proceedings, Lattice Gauge Theory*, 199-207.

[3] J. D. Bjorken and S. D. Drell. Relativistic quantum field theory. (german translation). Bibliograph.Inst./mannheim 1967, 409 P.(B.i.-hochschultaschenbuecher, Band 101).

[4] J. Blumlein and H. Bottcher. Qcd analysis of polarized deep inelastic scattering data and parton distributions. *Nucl. Phys.*, B636:225–263, 2002.

[5] Matthias Burkardt. Impact parameter dependent parton distributions and off-forward parton distributions for $\zeta \to 0$. *Phys. Rev.*, D62:071503, 2000. Erratum-ibid. D66, 119903 (2002).

[6] Matthias Burkardt. Impact parameter space interpretation for generalized parton distributions. *Int. J. Mod. Phys.*, A18:173–208, 2003.

[7] M. Creutz. Quarks, gluons and lattices. Cambridge, UK: University Press (1983) 169 p. (Cambridge Monographs On Mathematical Physics).

[8] W. Detmold, W. Melnitchouk, J. W. Negele, D. B. Renner, and Anthony W. Thomas. Chiral extrapolation of lattice moments of proton quark distributions. *Phys. Rev. Lett.*, 87:172001, 2001.

[9] M. Diehl. Generalized parton distributions in impact parameter space. *Eur. Phys. J.*, C25:223–232, 2002.

[10] M. Diehl. Generalized parton distributions. *Phys. Rept.*, 388:41–277, 2003.

[11] D. Dolgov et al. Moments of structure functions in full qcd. *Nucl. Phys. Proc. Suppl.*, 94:303 306, 2001.

[12] D. Dolgov et al. Moments of nucleon light cone quark distributions calculated in full lattice qcd. *Phys. Rev.*, D66:034506, 2002.

[13] P. Dreher et al. Continuum extrapolation of moments of nucleon quark distributions in full qcd. *Nucl. Phys. Proc. Suppl.*, 119:392–394, 2003.

[14] U. Glassner et al. Qcd with dynamical wilson fermions - first results from sesam. *Nucl. Phys. Proc. Suppl.*, 47:386–393, 1996.

[15] M. Gockeler et al. A preliminary lattice study of the glue in the nucleon. *Nucl. Phys. Proc. Suppl.*, 53:324 326, 1997.

[16] K. Goeke, Maxim V. Polyakov, and M. Vanderhaeghen. Hard exclusive reactions and the structure of hadrons. *Prog. Part. Nucl. Phys.*, 47:401–515, 2001.

[17] V. N. Gribov. Quantization of non-abelian gauge theories. *Nucl. Phys.*, B139:1, 1978.

[18] S. Gusken. A study of smearing techniques for hadron correlation functions. *Nucl. Phys. Proc. Suppl.*, 17:361–364, 1990.

[19] K. Hagiwara et al. Review of particle physics. *Phys. Rev.*, D66:010001, 2002.

[20] Ph. Hagler. Form factor decomposition of generalized parton distributions at leading twist. 2004.

[21] Philipp Hagler et al. Moments of nucleon generalized parton distributions in lattice qcd. *Phys. Rev.*, D68:034505, 2003.

[22] Xiang-Dong Ji. Gauge invariant decomposition of nucleon spin. *Phys. Rev. Lett.*, 78:610–613, 1997.

[23] Xiang-Dong Ji. Off-forward parton distributions. *J. Phys.*, G24:1181–1205, 1998.

[24] LHPC et al. Transverse structure of nucleon parton distributions from lattice qcd. 2003.

[25] M. Luscher. Construction of a selfadjoint, strictly positive transfer matrix for euclidean lattice gauge theories. *Commun. Math. Phys.*, 54:283, 1977.

[26] I. Montvay and G. Munster. Quantum fields on a lattice. Cambridge, UK: University Press (1994) 491 p. (Cambridge monographs on mathematical physics).

[27] J. W. Negele et al. Insight into nucleon structure from generalized parton distributions. 2003.

[28] J. W. Negele et al. Insight into nucleon structure from lattice calculations of moments of parton and generalized parton distributions. 2004.

[29] Michael E. Peskin and D. V. Schroeder. An introduction to quantum field theory. Reading, USA: Addison-Wesley (1995) 842 p.

[30] A. V. Radyushkin. Generalized parton distributions. 2000.

[31] D. B. Renner et al. Calculation of nucleon electromagnetic form factors. *Nucl. Phys. Proc. Suppl.*, 119:395–397, 2003.

[32] H. J. Rothe. Lattice gauge theories: An introduction. *World Sci. Lect. Notes Phys.*, 59:1–512, 1997.

[33] W. Schroers et al. Moments of nucleon spin-dependent generalized parton distributions. 2003.

[34] J. Smit. Introduction to quantum fields on a lattice: A robust mate. *Cambridge Lect. Notes Phys.*, 15:1–271, 2002.

[35] Steven Weinberg. The quantum theory of fields. vol. 1: Foundations. Cambridge, UK: Univ. Pr. (1995) 609 p.

[36] Kenneth G. Wilson. Quarks and strings on a lattice. New Phenomena In Subnuclear Physics. Part A. Proceedings of the First Half of the 1975 International School of Subnuclear Physics, Erice, Sicily, July 11 - August 1, 1975, ed. A. Zichichi, Plenum Press, New York, 1977, p. 69, CLNS-321.

[37] Kenneth G. Wilson. Confinement of quarks. *Phys. Rev.*, D10:2445–2459, 1974.